Multimodal nano-theranostic systems targeting tumour biomarkers

Richard Young

A thesis submitted to
the University of Birmingham
for the degree of
Doctor of Philosophy

PSIBS Doctoral Training Centre
School of Chemistry
University of Birmingham
September 2018

Abstract

Folate receptor overexpression is a confirmed cancer biomarker which has been relatively underutilised within the literature in the application of targeted cellular delivery of therapeutics and diagnostics to date.

A folate receptor targeting theranostic nanoparticle system has been developed and its ability to track nanoparticle uptake and deliver a novel Pt(IV) pro drug to human cancer cell lines measured. This system comprises folate capped gold nanoparticles for the targeted delivery of a fluourescent ruthenium based polypyridyl probe and a novel Pt(IV) pro drug to folate receptor positive cell lines. The ability of the system to display selective uptake in folate receptor positive cell lines was probed through comparative uptake of a citrate capped gold nanoparticle system, comprising the same theranostic agents as that of the folate capped system. This difference in uptake was investigated through the use of folate receptor blocking and simulating flow of particles within a cellular suspension, comparing uptake of respective particles with confocal microscopy, flow cytometry and ICPMS.

The novel Pt(IV) agent has been fully characterised and its anti-cancer efficacy investigated, presenting with improved toxicity over cisplatin in cisplatin resistant A549 cells. Cisplatin-DNA adducts have been identified through employment of a commercially available antibody, where the Pt(IV) agent displayed increased adducts over cisplatin alone. This adduct formation and imparted toxicity was investigated by confocal microscopy, flow cytometry, ICPMS and MTT assays in A549 cells.

Acknowledgements

I would like to thank my wife for her support, encouragement and tolerance throughout my academic and life endeavours. Without her I would be a fraction of myself and have accomplished an even smaller fraction of my achievements. People always say that without you I would have achieved nothing…. I still largely disagree.

A further thank you to my parents for their attempts at understanding what I have researched. Your interest in what I have done, irrespective of how much of it you can follow, has certainly helped me maintain my focus! I hope that you enjoy attempting to read this on one of your many holidays at the Monti…. Now get back to work.

On a more serious note, I would like to thank Professors Mike Hannon and Zoe Pikramenou, Dr Nik Hodges and Dr Hamid Dehghani for their continued guidance throughout my research. This thank you is especially extended to Mike and Nik who have helped me with my transition into the challenging world of cellular biology. A thank you to past and present members of the Hannon, Pikramenou and Hodges groups and all those associated with the PSIBS / Sci Phy DTC for making my time at the university less stressful than it otherwise would have been. Again, an extended thank you to Alessio Perotti and Lucia Cardo for their help in my transition towards biology and cell research. An additional thank you to the PSIBS DTC, the University of Birmingham and the EPSRC for funding.

Abbreviations

ADC – Acetonedicarboxylate

A549 – Human lung cancer cell line

CRISPR - Clustered Regularly Interspaced Short Palindromic Repeats

cDNA – Complementary DeoxyriboNucleic Acid

DLS – Dynamic Light Scattering

DMEM – Dulbecco's Modified Eagle Media

DNA – DeoxyriboNucleic Acid

dNTP - DeoxyriboNucleotide TriPhosphate

EDTA – EthyleneDiamineTetraaceticAcid

FACS – Fluorescence Activated Cell Sorting

FOLR1 – Folate receptor gene responsible for folate receptor α

FOLR2 - Folate receptor gene responsible for folate receptor β

FOLR3 - Folate receptor gene responsible for folate receptor γ

GPI – Glycosylphosphatidylinositol

GNP-Cit – Citrate capped gold nanoparticles

GNP-Fol – Folate capped gold nanoparticles

GNP-GSH-Fol – Citrate capped gold nanoparticles with folate tethered via glutathione

GNP-Cit-Theranos - Citrate capped gold nanoparticles loaded with RuPhen and YoungPt(IV)

GNP-Fol-Theranos - Folate capped gold nanoparticles loaded with RuPhen and YoungPt(IV)

HeLa – Cancerous human cervical cell line

MLCT – Metal Ligand Charge Transfer

MSC – Mesenchymal Stem Cells

PDI – PolyDispersity Index

PBS – Phosphate Buffered Saline

PCR – Polymerase Chain Reaction

RPMI – Gibco cell culture media

RNA – RiboNucleic Acid

StDev – Standard Deviation

SPR – Surface Plasmon Reference

TEM - Transition Electron Microscopy

λ_{max} – Wavelength with maximum absorbance

λ_{min} – Wavelength with minimum absorbance

16HBE140(-) – Human bronchial epithelial cell line

Contents

Chapter 1: Introduction

1.1. Folate Receptors

It has been a consistent objective of cancer research to develop targeted, patient specific therapeutic agents so as to maximise anti-tumour efficacy whilst minimising non-target cell damage and inherent toxicity to the patient. In this regard, there is an omnipresent demand for research to identify and explore potential means of targeting specific cancer sub-types with chemotherapeutic agents. Combining such targeted therapeutics with innovative and accurate diagnostic measures should therefore pave the way to truly personalised anti-cancer treatments, significantly improving the prospects for the prospective patients. One such form of potential cancer cell targeting vector is that of folate receptors.

Since the early 1990's, research has found that folate receptors are significantly over expressed on the surface of a variety of cancer cell lines and tissues whilst maintaining a comparably low expression in healthy cell lines[1]. These receptors have a high binding affinity and specificity for folic acid and its structural derivatives and have since been established as a scientifically acknowledged cancer biomarker[2, 3, 4]. The structure of folic acid is represented below in Figure 101.

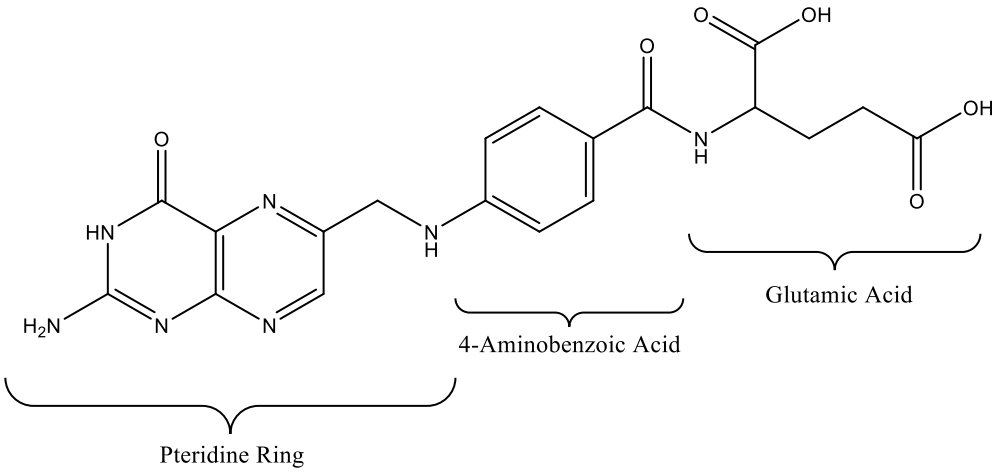

Figure 101: Structure of folic acid.

This overexpression and confirmation as a cancer biomarker establishes folate receptors as an exciting prospect within anticancer research and may present with serious potential within the field.

1.1.1. Receptor Type and Function

Folate receptors are present in a wide variety of healthy cell lines throughout the human body and are believed to offer a key role in the maintenance of these cells through enabling influx and efflux of folic acid and folate based derivatives [5]. In this regard, it is believed that these folate based entities assist with a number of cellular processes, including assisting in the recycling of ADP back to ATP for cellular processes and mitosis, through a number of different pathways and metabolites[6, 7]. Why folate receptors are not expressed in all healthy cell tissues is a contentious area of the literature and one that is not fully understood on account of the positive role they may play and the potential benefits to the cells. However, it appears that the general consensus is that folic acid and folates are still able to be taken up into cells that are folate receptor negative through other active uptake proteins as well as passive uptake mechanisms. In particular, there are three proposed folate active uptake methods[8, 9]:

1. Reduced Folate Carrier SLC19A1 – an organic anion exchanger;
2. Proton Coupled Folate Transporter SLC46A1 - a unidirectional folate transporter which primarily operates at acidic pH; and
3. Folate Receptors α and β – folate receptor influx proteins via receptor-mediated endocytosis.

Whilst there are three confirmed active uptake means for cellular uptake of folates, folate receptors α and β display the highest binding affinity and selectivity for folates and so are considered to be the primary means of uptake, where more than one system is presented.

1.1.2. Folate Receptor Expression

Whilst folate receptors α and β are cited above as the primary folate receptors responsible for folate uptake into cells, there are a total of four types of folate receptor (α, β, γ and δ)[7, 11]. Folate receptors α and β are both surface localised cellular proteins, however, α is typically expressed on the surface of the epithelial cells of the lungs and kidneys, and β is typically expressed on the surface of activated myeloid cells[11-14]. Folate receptors γ and δ are far less prominent than α and β, where folate receptor γ is primarily an excretory protein and is found in the blood, whilst folate receptor δ is expressed on regulatory T-Cells and its function is yet to be ascertained[11, 15, 16]. It is therefore evident in the literature that these receptors operate somewhat independently from one another within healthy tissues, however, in some tissues there is a degree of co-localisation. Levels of expression of these receptors within healthy cells and tissues that are receptor positive do vary, however, they are not typically expressed in large quantities.

In contrast, folate receptor expression varies significantly in different cancer cell lines, with some cell lines being receptor negative (zero expression) and some displaying large levels of expression for a multitude of these receptors. Most interestingly, and opportunistically, there are certain cancer cell types which not only express folate receptors α and / or β (the primary influx proteins), but they overexpress said receptors with levels significantly beyond those of healthy cells. In particular, as reported in Elnakat *et al.*[7] and Shen *et al.*[11], folate receptor α is known to be overexpressed in cancers of the ovary, breast, head & neck, endometrium, lung, bladder, pancreas, colon and kidney[17-25]. As further reported by Shen *et al.*[11], folate receptor β is known to typically be overexpressed in cancers of the lung, breast, liver, brain, uterus, thyroid, stomach, ovary, head & neck, skin, kidney, pancreas, bladder, cervix, oesophagus,

prostate, testis, and colon[26, 27]. Accordingly, it is evident that there are cancerous tissues which display a high level of overexpression of both of these folate receptors.

It is hypothesised that this overexpression of folate receptors α and β in cancer cell lines is as a result of their increased metabolic needs, stemming from their rapid multiplication. Accordingly, it is assumed within the literature that the bulk of folic acid transportation is via receptor mediated endocytosis as it offers the most selective and efficient means for folate uptake[28]. At present, the exact mechanics of folate receptor mediated binding and uptake of folic acid conjugates is not completely understood, however, as above, there is little debate surrounding the proposed mechanism of receptor mediated endocytosis.

1.1.3. Utilisation within Research

The above research all in effect stem from the pioneering research of Leamon and Low, who identified folic acid's ability to transfer large proteins into plant cells as a result of the folic acid – folate receptor interaction, forming the first establishment of folate receptor mediated endocytosis of agents into cells[29]. Shortly after, research conducted by Coney *et al.*[2] and Weitman *et al.*[30] reported that several monoclonal antibodies which were typically used to identify cancer cells in tissue biopsies were also able to selectively bind to folate receptors[28]. Subsequently, folate receptor targeted delivery of chemotherapeutics and imaging agents was a developing field of research.

An early research contribution in this regard is that of Leamon *et al.,* whose subsequent research into folate based cytotoxics employed the use of folate-tethered protein toxins for tumour targeting[28, 31]. These protein based studies included the use of folate-momordin and folate-pseudomonas exotoxin, the latter possessing an IC_{50} of $\sim 10^{-11}$ M. significantly, this

research also demonstrated that the nature of the bond linking the folate to the protein directly affects the toxicity of the system. Specifically, when linked by a reducible disulfide bond, an IC_{50} of ~10^{-11} M was achieved. In contrast, when linked via a thioether bond, potency was reduced by four orders of magnitude[31]. These results therefore displayed an early indication of increased cellular uptake of anticancer agents when folate receptors were targeted and the importance of designing folate targeting anticancer treatments with a cleavable linker for improved drug delivery[32].

Figure 102 below is a diagrammatical representation produced by Leamon *et al.*[28] that gives an overview of the proposed folate receptor mediated uptake of folic acid drug conjugates (whilst the specifics for this overview are targeted to their conjugates, the overview of the mechanism of uptake is identical to that proposed for all folic acid conjugates).

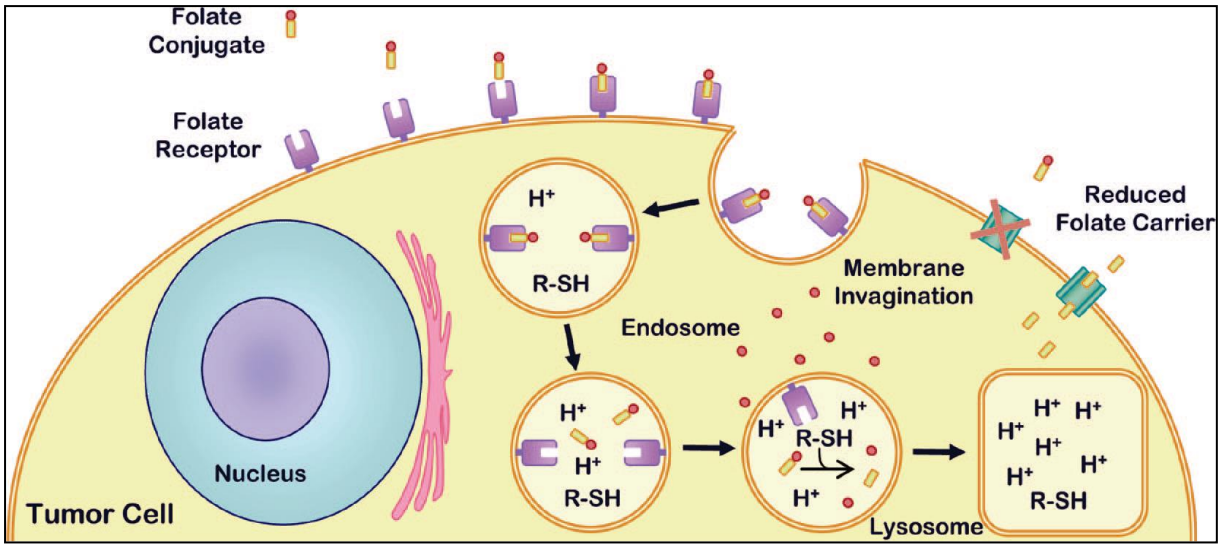

Figure 102: Image and text directly sourced from Leamon *et al.*[28]

"Folate Receptor (FR) mediated endocytosis of a folic acid drug conjugate. Folate conjugates bind to FR's with high affinity and are subsequently internalized into endosomes that can reduce disulfide bonds. Within the endosome, a folate–disulfide–drug

conjugate is released from the FR and the prodrug is reduced to liberate the parent drug cargo. Because the pH of FR-containing endosomes is only mildly acidic, acid-labile linkers do not release the attached drug as efficiently".

Folate Targeted Therapeutics

A number of folate targeted chemotherapeutics have been investigated in the literature, some of which have subsequently entered into clinical trials[11]. One such example is that of Naumann *et al*, who developed the folate receptor targeting anticancer agent Vintafolide (EC145)[33]. Vintafolide is a folic acid–desacetylvinblastine conjugate that Naumann *et al*. have progressed through phases one to three of clinical trials to ascertain its potential as a targeted chemotherapeutic when utilised in combination therapy with Pegylated Liposomal Doxorubicin (PLD)[33-135]. The structure of Vintafolide is provided in Figure 103.

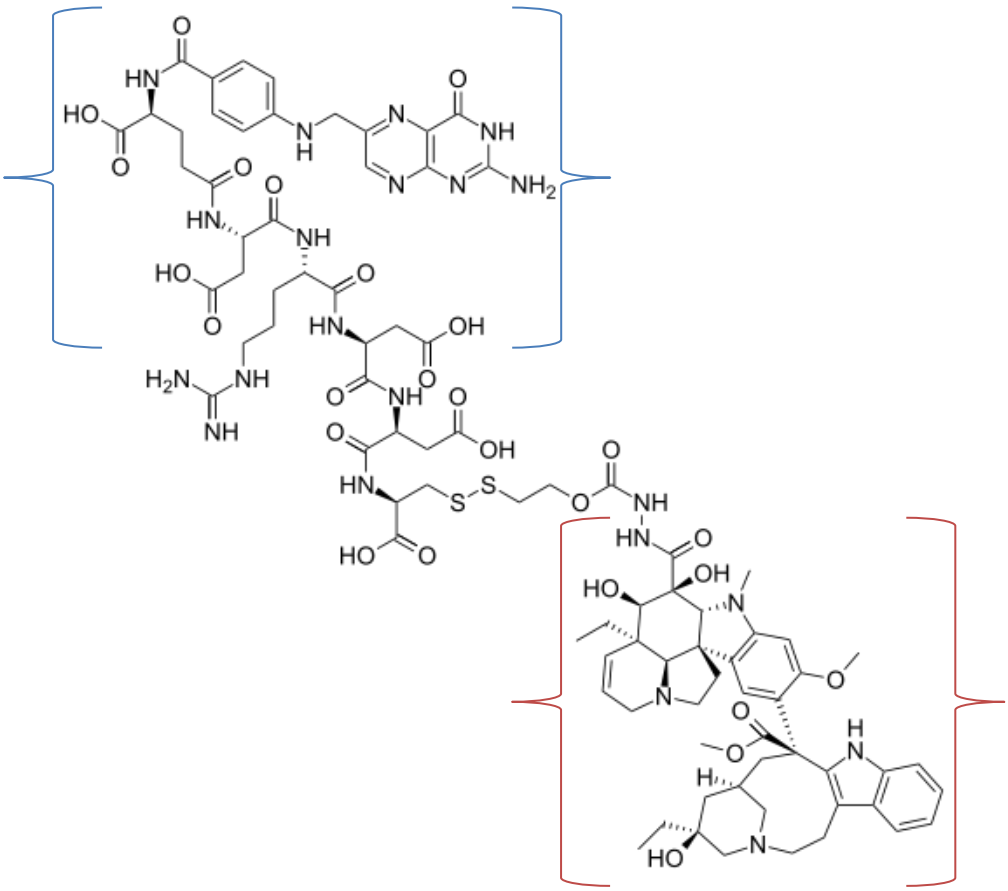

Figure 103: Chemical structure of Vintafolide[36].

As can be seen in Figure 103, Vintafolide comprises a folic acid unit (circled in blue) that is connected to a desacetylvinblastine monohydrazide (DAVLBH, circled in red) conjugate by way of a disulphide linker[37]. DAVLBH is an agent which prevents microtubule formation within the cells during mitosis, thus preventing cellular replication and leading to apoptosis.

These studies looked at the survival rates of women who presented with recurring platinum agent resistant ovarian cancer and looked to compare the progression-free survival of the patients. Where a combination of Vintafolide and PLD were used, the median survival rate was 5 months, whereas PLD alone was 2.7 months. Additionally, the patients subjected to the combination therapy presented with no additional symptoms or side-effects over those experienced by the PLD group only, further supporting that Vintafolide was indeed highly targeting[33].

Folate Targeted Diagnostics

In addition to the utilisation of folate as a means for targeted therapeutics, there are also examples in the literature of folate targeted imaging agents. A more recent example of such research includes that of Okusanya *et al*, who developed a fluorescently labelled folate receptor α targeting molecular contrast agent[38]. This folate receptor targeting contrast agent comprised a folate-fluorescein-isothiocyanate (FITC) conjugated folic acid unit, displaying fluorescence within the green region of the visible spectrum (λ_{ex} 465-490nm, λ_{em} 520-530nm). This contrast agent was utilised intra-operatively to identify folate receptor α positive lung adenocarcinoma cells via real-time optical imaging. Sample images collected and reported by Okusanya *et al* are represented below as depicted in their article[38].

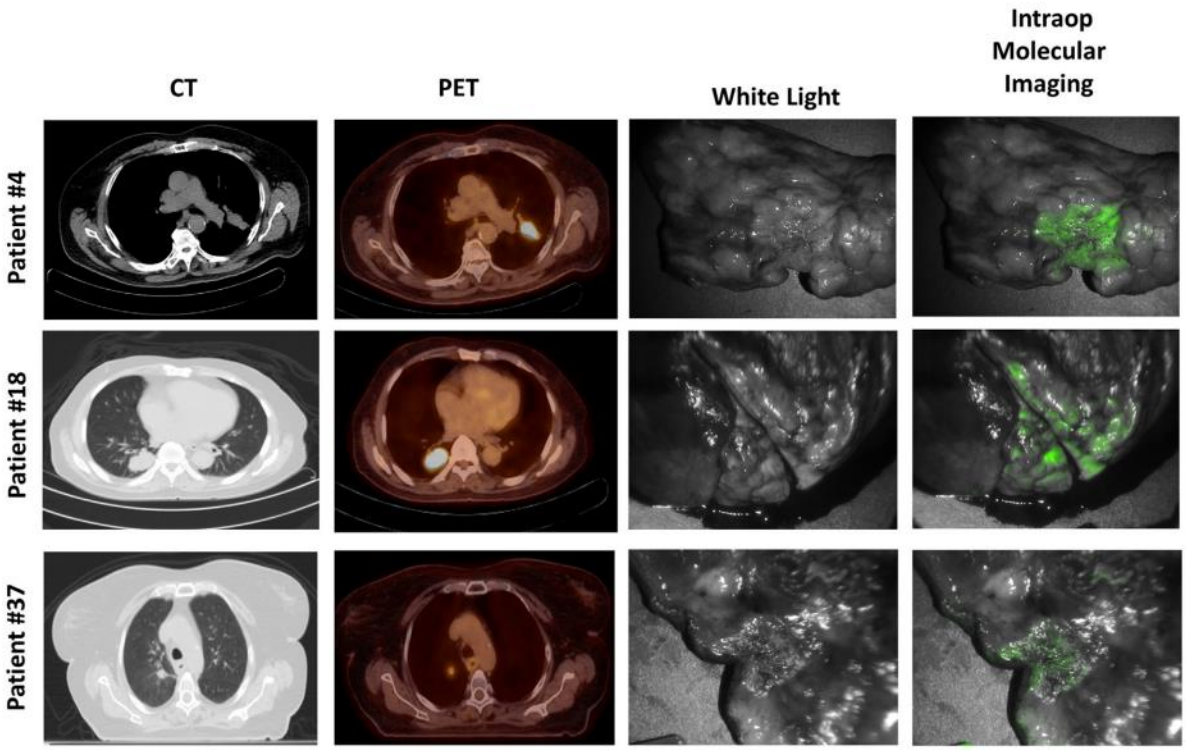

Figure 104: Image and text were sourced as per Okusanya *et al*[38].

"Lung adenocarcinomas can be detected using intraoperative molecular imaging. Three representative patients diagnosed with lung adenocarcinoma by preoperative CT, PET, and optical molecular imaging".

This research reported that 92% of the lung adenocarcinomas studied presented with FITC fluorescence, with no false positives or non-selective binding of the contrast agent. Of the 8% that were not fluorescent, postoperative immunohistochemistry confirmed that there were no α folate receptors expressed. Patient bisection was required for the majority of cases in order to attain sufficient probe signal[38].

1.1.4. Conclusions

It is evident from the literature that folate receptor expression appears to be a viable mechanism for targeted delivery of chemotherapeutics and diagnostic agents. There are a number of established and promising agents within the field directed toward either a folate receptor targeting therapeutic or diagnostic system. However, there does not yet appear to be a folate receptor targeting agent which displays the potential to act as both a therapeutic and diagnostic (theranostic) system. Accordingly, utilisation of theranostic agents which exhibit folate receptor targeting might present with notable research outcomes, given that cellular delivery of such agents by way of folate receptor mediated endocytosis appears to have not yet been established in the literature.

1.2. Gold Nanoparticles

1.2.1. Nanoparticles and their Properties

Nanoparticles of varying forms have been utilised within research in a broad spectrum of applications, from the use of Multi-Walled Carbon Nanotubes (MWCNTs) and Single-Walled Carbon Nanotubes (SWCNTs) as nano-carriers of chemotherapeutic agents[39-42], to the use of colloidal quantum dots for solar cells[43] (examples of such SWCNT and MWCNT systems are depicted in Figure 105 as drawn from the literature)[44].

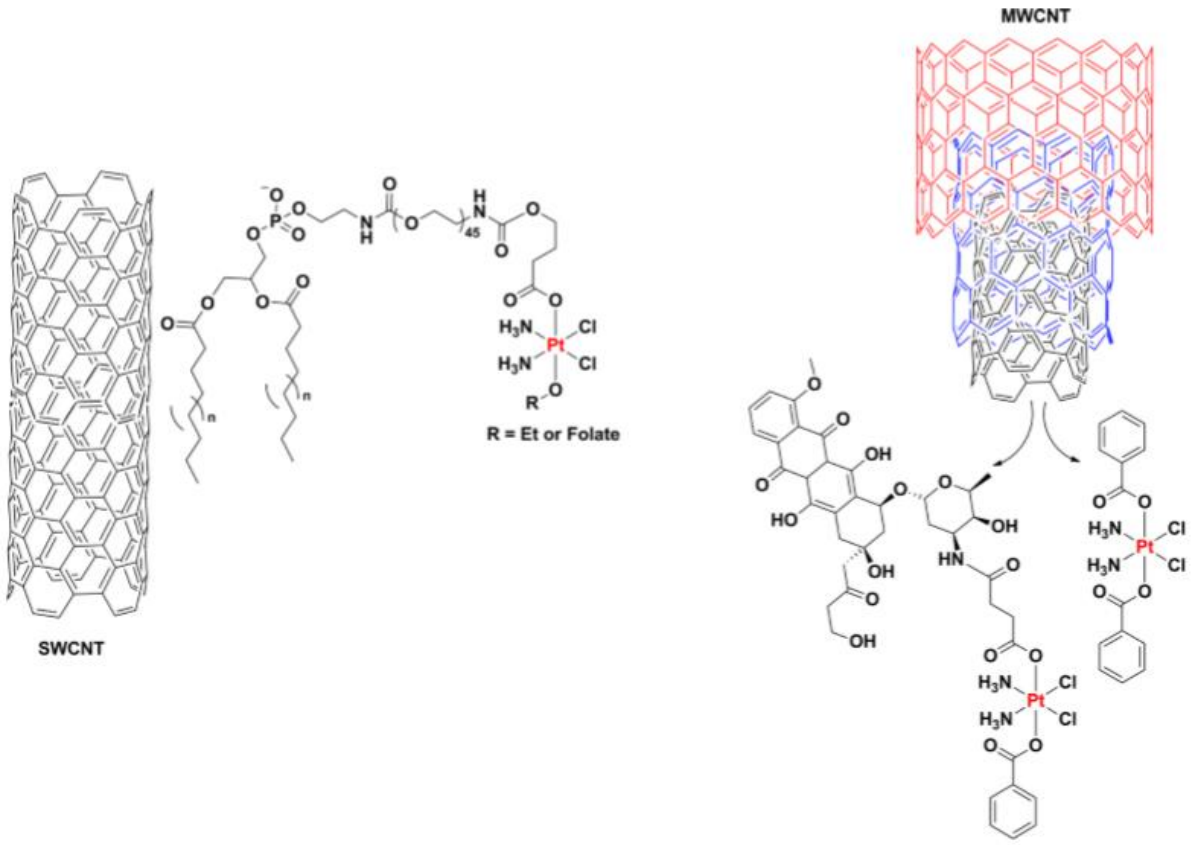

Figure 105: Diagrammatic representation of Single-Walled Carbon Nanotube (SWCNTs) and Multi-Walled Carbon Nanotube (MWCNTs) delivery systems for platinum(IV) prodrugs. Figure sourced and amended from Chart 18 of Johnstone, Suntharalingam and Lippard[44].

Polymer based nanoparticles are also commonly employed within the literature. An example of which is that of Zhe Wang *et al.*, who demonstrated RGD peptide targeted delivery of anti-angiogenesis (combretastatin A4) and anticancer (Paclitaxel) agents to Human Umbilical Vein Endothelial Cells (HUVECs) through utilisation of Poly-Lactic-co-Glycolic Acid (PLGA) nanoparticular system[45].

Of the various nanoparticular systems of the literature, one particular form which has been used extensively in research is that of gold nanoparticles. Gold nanoparticles can be readily synthesised as spherical particles (which are more commonly utilised within therapeutic and

diagnostic applications), or as nano-rods, for varying uses such as contrast agents, bacterial separation agents and therapeutics[46-49]. These spherical gold nanoparticles have been used extensively within the literature in the delivery of large payloads of therapeutic compounds and / or imaging agents to cancerous tissues. Gold nanoparticles have been utilised to this end as a result of a number of favourable properties, which include:

- a passive tumour targeting effect;
- ability to be surface functionalised with a wide variety of compounds;
- a large loading capacity; and
- limited cellular toxicity.

As above, nanoparticles have been proven to exhibit a passive tumour targeting effect as a result of their extended circulation time in the bloodstream and accumulation within tumour regions and micro-environments[50]. This inherently useful quality of nanoparticles is depicted in Figure 106 as produced by Loureiro *et al*[51]. In brief, the tumour vasculature presents with large pores which facilitate extravasation of nanoparticles from the blood stream into the tumour micro-environment. The nanoparticles then typically accumulate within these tissues as they are not readily flushed out. This retention is largely as a result of poor lymphatic drainage of the tissue. This is known as the "Enhanced Permeability and Retention "(EPR) effect[51]. Accordingly, gold nanoparticles that are in the 10-200nm range and surface functionalised with anti-cancer compounds may significantly increase the effectively delivered dose of such compounds to the tumour environment through their EPR effect[44].

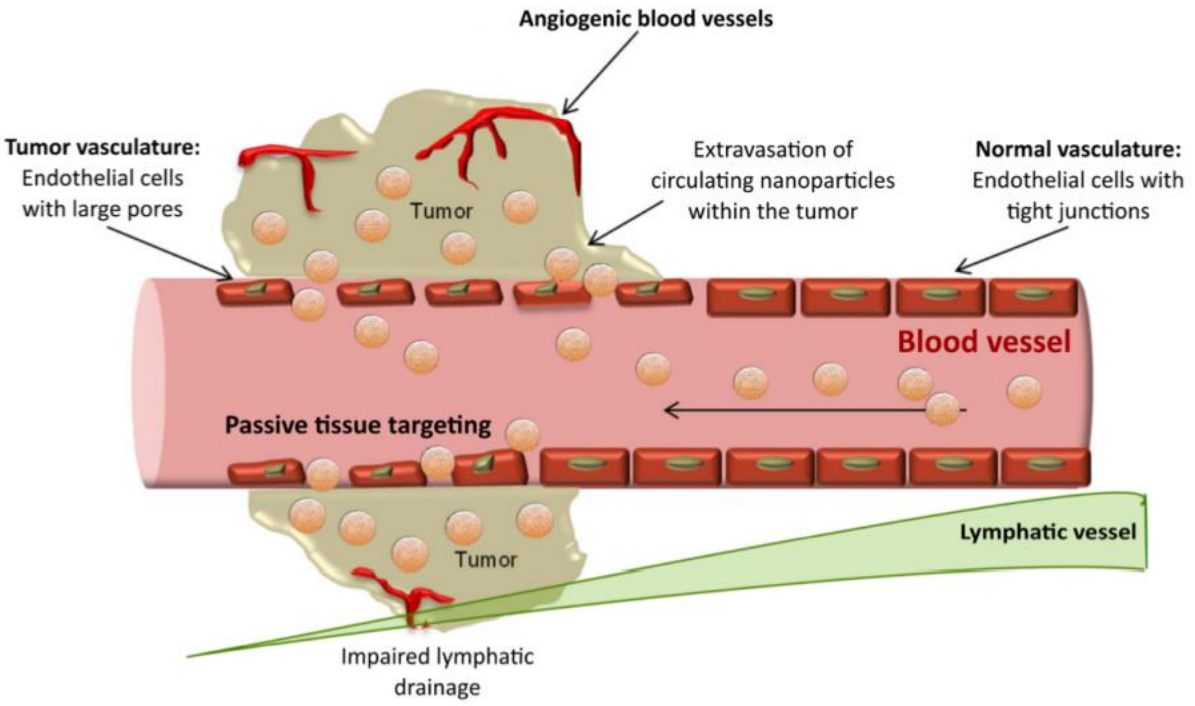

Figure 106: Diagrammatical representation of passive tumour targeting of nanoparticles as produced by Loureiro *et al*[51].

The loading capacity, cellular toxicity and surface functionalisation of these gold nanoparticles are largely dependent on the size of the particles and their surface properties. The size and surface properties of these nanoparticles are in turn largely dictated by the method employed in their synthesis and the reagents employed in their composition.

1.2.2. Citrate Capped Gold Nanoparticles

All spherical nanoparticles may be synthesised by way of either a "top-down" or "bottom-up" methodology, through laser ablation of bulk materials or reduction of a gold salt respectively[52-54]. The "bottom-up" gold salt reduction method is most commonly utilised within the literature and also forms the most commonly utilised gold nanoparticle system in that of citrate capped gold nanoparticles GNP-Cit.

This bottom-up method was first reported by Turkevich *et al.* who developed a consistent batch method for formation of citrate capped / stabilised gold nanoparticles[54]. This fundamental protocol was then further developed within the field by Vossmeyer *et al*, whose adaptation of the Turkevich method allows for batch production of consistently sized and monodisperse GNP-Cit[55]. This research demonstrates the highly tuneable characteristics of the GNP-Cit through variation of the gold salt to citrate ion ratio, reaction temperature and orders of addition. Moreover, the article offers an in depth analysis of the physical principles of gold salt reduction and particle formation, as depicted in Figure 107 (adapted from the literature)[55].

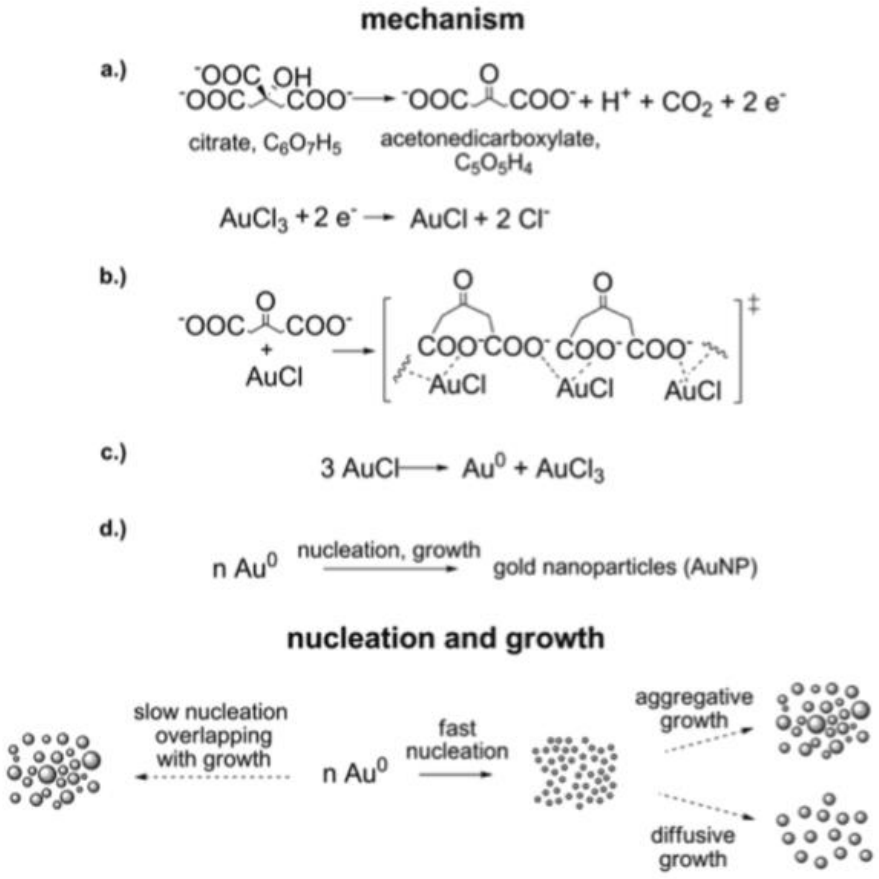

Figure 107: Representation of gold salt reduction and particle nucleation and growth as set forth by Vossmeyer *et al.* Figure and text are sourced and adapted from the literature[55].

(a) Redox reaction of citrate and Au(III) to form Au(I) ions and acetonedicarboxylate (ADC). (b) ADC organizes Au(I) to form areas of high Au(I) concentration, facilitating (c) disproportionation of Au(I) to Au(0) and Au(III), leading to (d) nucleation and growth of Au(0)

to form GNP-Cit. Fast nucleation and good stabilization give a narrow size distribution of the particles. Conversely, slow nucleation and low stabilization give a broad size distribution of the particles[55].

This research further demonstrates that batches of 13nm GNP-Cit may be utilised for consistent production of 25nm GNP-Cit as a starting block which is compounded on. These 25nm particles may then be carried forward in the same manner for consistent production of 50nm and 100nm particles. Thus, the production and characteristics of GNP-Cit are well explored and understood within the literature.

1.2.3. Folate Capped Gold Nanoparticles

Another example of a gold nanoparticular system is that of folate capped gold nanoparticles (GNP-Fol). In contrast to the well understood citrate capped gold nanoparticular preparation as above, folate capped gold nanoparticles have been comparatively under-utilised within the literature and hence, protocols for their preparation are equally unexplored. In this regard, one prominent example of the direct bottom-up synthesis of GNP-Fol is that of Wang *et al*[56]. By comparison to the Vossmeyer GNP-Cit protocol, this GNP-Fol protocol utilises folic acid and sodium folate in coordination with gold salt, employing the use of less conventional microwave reactor heating. Whilst this is one of the more prominent examples of direct synthesis of GNP-Fol within the literature, the quality of the particles are comparatively poor with respect to Vossmeyer GNP-Cit. More particularly, it appears that there has not been development of a GNP-Fol protocol which produces particles of a consistent size, which are monodisperse and are largely spherical. For comparison, and to emphasis the difference in particle quality of the literature, TEM images of the Vossmeyer GNP-Cit and Wang GNP-Fol

systems are represented in Figure 108 (as drawn from the respective articles of the authors[55 & 56]).

a) b)

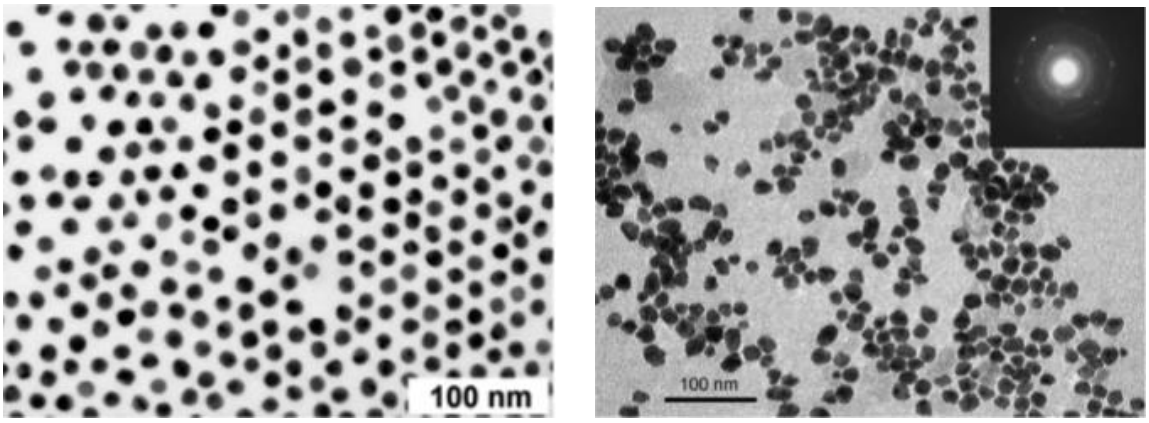

Figure 108: TEM images drawn from the literature for comparison of particle qualities of the: a) Vossmeyer *et al.* GNP-Cit system[55]; and b) Wang *et al.* GNP-Fol system[56]

Whilst these particles therefore seemingly present with poorer physical properties than the GNP-Cit system, they have still been used within the literature for a broad range of studies on account of their intrinsic potential as a folate receptor targeting nanoparticular system. More particularly, given that their surface is capped / stabilised by folate moieties, it has been shown in the literature that these particles may be readily taken up by folate receptor positive cell lines.

1.2.4. Utilisation within Research

As discussed above, there are broad ranges of utilisation of gold nanoparticular systems within the literature. However, of primary concern in the present research is the utilisation of citrate and folate capped gold nanoparticles for delivery of diagnostic and therapeutic agents to cancer cells. In this regard, and as noted, a significant advantage of using nanoparticles as a delivery system of such agents is the inherently reduced systemic dose and maximised delivery

of large payloads of the agents to the target cancer cells[44]. This benefit can be further enhanced through surface functionalisation of nanoparticles with a ligand that may selectively bind to receptors that are explicitly expressed on the surface of specific cancer cells, thus facilitating receptor mediated endocytosis[44, 57].

Applications of GNP-Cit

An example of a GNP-Cit system which exhibits targeted delivery of chemotherapeutic agents is that of Yang *et al*[58]. In this research Yang *et al* synthesised GNP-Cit via utilisation of the Vossmeyer protocol and subsequently functionalised the surface of the particles with an RGD peptide (cancer tissue targeting agent) and the anticancer agent Bleomycin (the structure of Bleomycin is shown in Figure 109). Yang *et al* demonstrated the increased uptake and anticancer efficacy of this targeted anticancer GNP-Cit system within human breast cancer cells (MDA-MB-231) in comparison to a non-RGD labelled (non-targeting) GNP-Cit system.

Moreover, the research found that the labelled GNP-Cit system outperformed the non-labelled system when combined with radiation therapy, showing a 38% increase in cellular uptake and 32% decrease in cell viability. In this regard, it is known within the literature that gold nanoparticles may enhance the photo-induced DNA damage of radiotherapy through localized amplification of said radiation dose[58-60]. Accordingly, the RGD targeted GNP-Cit system affords increased cellular uptake and localisation of the particles bearing the anticancer agent Bleomycin within the MDA cells. This then subsequently leads to a localised delivery of a large payload of Bleomycin and the localised amplification of photo-induced DNA damage. The Yang *et al* system therefore represents a targeted GNP-Cit combination therapy system (chemotherapy and radiotherapy).

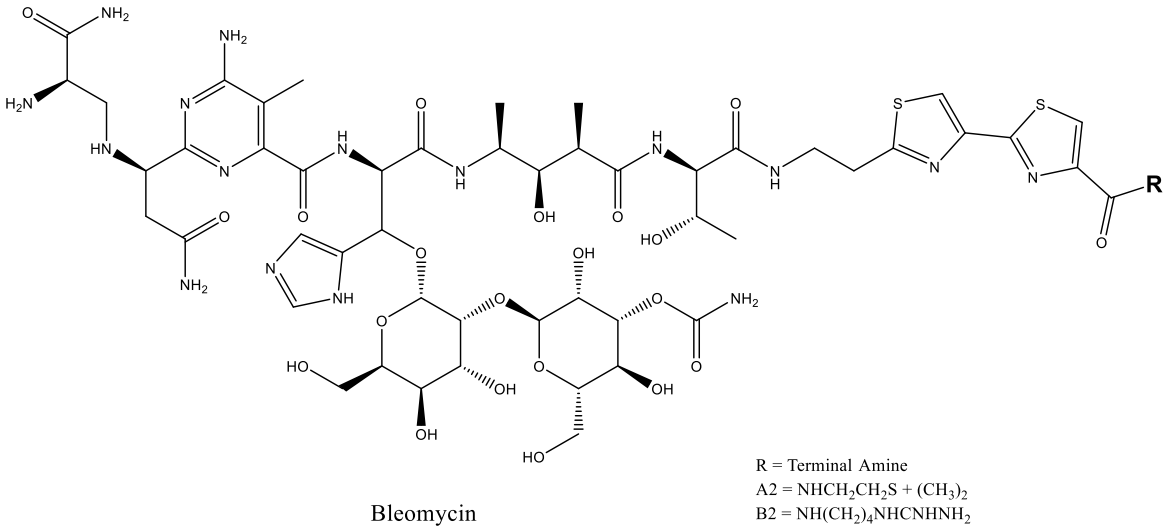

Figure 109: Unaltered representation of the chemical structure of Bleomycin as reported by Galba *et al*[61] (figure 1 of the cited article).

Another application of GNP-Cit is that of the targeted multi-modal imaging particles developed and reported by Schooneveld *et al*[62]. Schooneveld et al utilised a GNP-Cit core coated with a poly(ethylene glycol), paramagnetic and fluorescent lipid coating. These particles were then utilised as a trimodal contrast agent in macrophage cells via in vitro magnetic resonance imaging (MRI), X-ray computed tomography (CT) and fluorescence imaging (FI). The general structure of these particles is represented in Figure 110 as drawn from the literature[62].

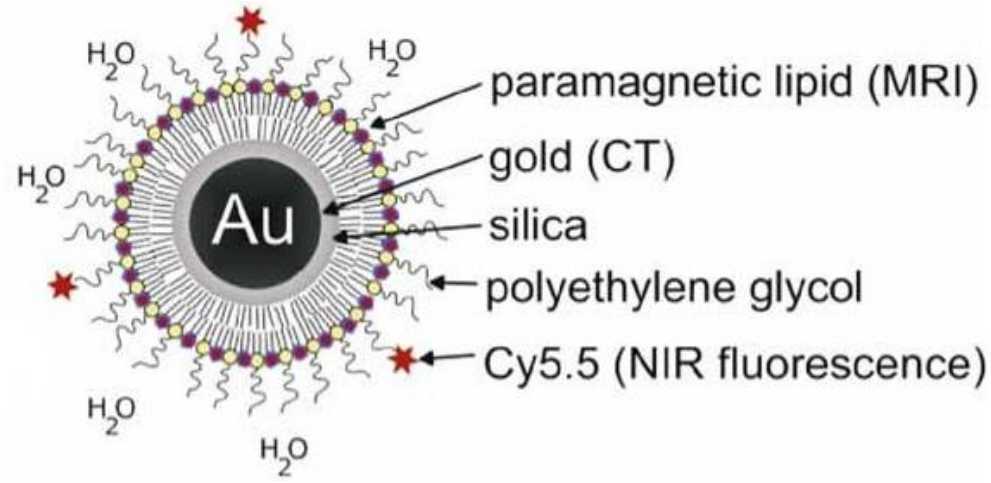

Figure 110: Schematic representation of the Schooneveld tri-modal contrast agent particle as reported in the literature[62].

As can be seen in Figure 110, the Schooneveld particles comprise a citrate capped gold nanoparticle core (capable of imaging via CT), a silica sub-layer and an outer PEG layer. The outer PEG layer further comprises fluorescently labelled PEG molecules for FI applications (Cyanine5.5 conjugated PEG) and paramagnetic labelled lipids (Gadolinium conjugated diethylene triamine pentaacetic acid di(stearylamide)). The research found that these tri-modal particles were successfully taken up by phagocytotic cells and generated contrast in MRI, CT and FI applications with approximately nanomolar (MRI/CT) and ~100 pM (FI) detection limits[62].

Applications of GNP-Fol

As previously noted, whilst there is an abundance of research into the use of citrate capped GNPs that have had their surface subsequently functionalised with folate, there appears to be a lack of research into the use of folate capped GNPs[63-66]. As hypothesised, this likely stems from the seemingly under-developed synthetic protocol for such particles. However, one notable application of folate capped gold nanoparticles within the literature is that of J.Ai *et al*[67]. J.Ai *et al*. utilised the synthetic protocol of Wang *et al.* to synthesise GNP-Fol, which they subsequently labelled with a functionalised FITC dye by way of a thiol linker. These FITC labelled folate capped GNPs showed elevated uptake and emission in folate receptor positive HeLa cells (cervical cancer cell line) over folate receptor negative CCRF-CEM cells (a T lymphoblastoid cell line), as represented in confocal microscopy and flow cytometry studies. One key criticism of this research however is the utilisation of different cell lines as the folate receptor positive vs negative measure, as they likely present with significantly different physical characteristics, which will inherently have an impact on the levels of cellular uptake.

Another example of the literature is the more recently published works of Jesna et al[68]. Jesna reports an alternative protocol for the direct synthesis of GNP-Fol, adapted from the Wang protocol[56]. Jesna utilises these folate capped GNPs to target folate receptor positive A549 cells (lung carcinoma), conjugating a thionene dye to the surface of the particles for cellular tracking applications. These folate targeted particles showed elevated levels of cellular uptake over non-folate capped particles, displaying their potential as a targeted diagnostic system. The particles also exhibit therapeutic applications when irradiated, inducing localised cytotoxicity in vitro[68]. This research demonstrates the ability to track the surface binding of reagents to nanoparticles through the utilisation of Dynamic Light Scattering (DLS) and measuring changes in the Surface Plasmon Resonance of the particles.

More particularly, it is known in the literature that gold nanoparticles present with a localised SPR as a result of oscillating surface electrons. Thus, the oscillating surface electrons interact with light waves and polarise one surface of the particle. Accordingly, the SPR induces an electromagnetic field[52 & 69-72]. A generalised representation of the GNP SPR / electromagnetic field interaction is depicted in Figure 111 below, as drawn from the literature[72]. As reported in the literature, the SPR band of a nanoparticle suspension can be monitored by UV-Vis spectroscopy and typically presents with a λ_{max} between 500-750nm dependant on the size and shape of the particles[71]. Accordingly, as GNPs are surface functionalised, their shape and diameter change, thus inducing a shift in the density of the electric field and therefore a shift in the SPR λ_{max}[72]. Therefore, UV-Vis observations of the SPR band of a nanoparticle suspension can be indicative of surface functionalisation with appropriate reagents.

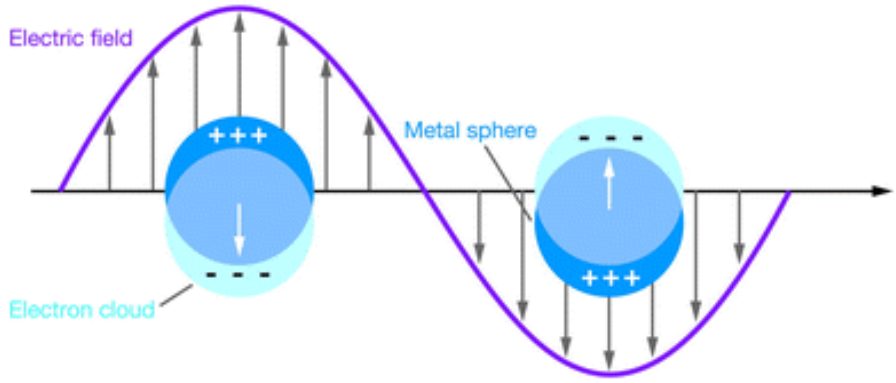

Figure 111: Localised SPR band of GNPs, as reported by Willets and Doyne[72].

1.2.5. Conclusions

There is a wealth of research in the literature in the targeted delivery of citrate capped gold nanoparticles to cancer cells for the purposes of diagnostics and therapeutics. There is also a broad spectrum of research into the functionalisation of nanoparticles with folic acid for folate receptor targeting. However, there appears to be a substantial gap in the literature for the utilisation of directly folate capped gold nanoparticles for targeted delivery of agents to cancer cell lines. Accordingly, utilisation of folate capped gold nanoparticles for delivery of either imaging or therapeutic agents might present with reasonably unexplored research outcomes.

1.3. Platinum Anticancer Agents

1.3.1. Platinum(II) Complexes and Cisplatin Activity

Platinum complexes remain one of the most widely utilised anticancer chemotherapeutics worldwide. At present, three platinum based anticancer agents are clinically approved worldwide for the treatment of cancer (cisplatin, carboplatin and oxaliplatin), whilst an additional three are approved for use in select countries only (nedaplatin, lobaplatin and

heptaplatin)[44]. The chemical structures for these complexes are depicted in Figure 112 as directly sourced from the literature.

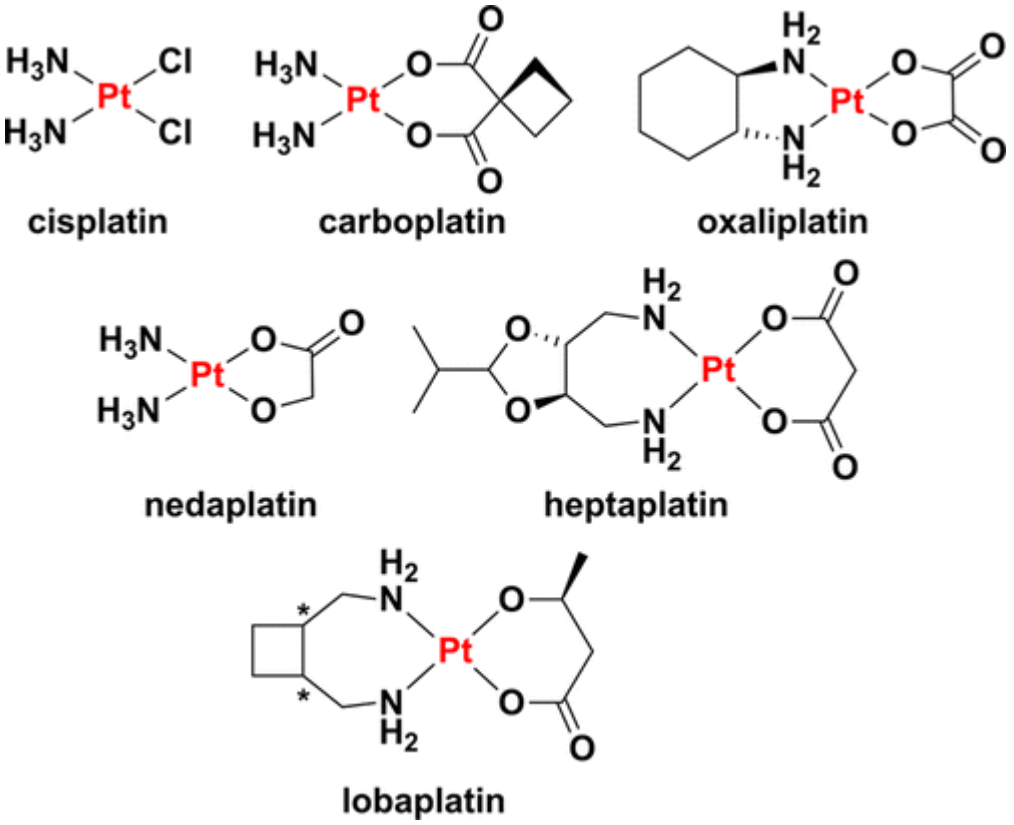

Figure 112: Chemical structures for clinically approved Pt based anticancer agents, as sourced from Lippard *et al*[44].

Perhaps the most notable application and success of these clinically approved Pt agents is that of the platinum(II) drug cisplatin in the treatment of testicular cancer, which now presents with cure rates which exceed 95%[44, 73]. Cisplatin's mode of action is to form intra-strand covalent bonds to adjacent Guanine residues of the DNA helix within the nucleus of cancer cells. As a result of these covalent bonds, a 'kink' is formed in the structure which prevents replication and transcription, ultimately leading to apoptosis[74]. The mechanism of action of cisplatin is a result of intracellular activation by the aquation of one of the two chloride ligands, which subsequently enables cisplatin to covalently bind to DNA, forming DNA adducts[75]. This process is dependent on local Cl^- concentration; where low concentrations allow these chloride

ligands to be more easily replaced with OH or OH_2 ligands. It is thought that the active species of cisplatin is that shown in Figure 4 below:

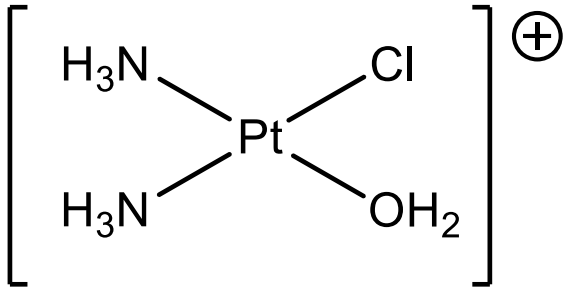

Figure 113: Structure of Active Cisplatin

Whilst cisplatin is especially effective at treating testicular cancer, it has a significantly reduced anticancer efficacy in a number of other types of cancer. In this regard, the efficacy of treatment with cisplatin is determined by a number of factors. However, the most significant limiting factors in the broad utilisation of cisplatin are its lack of specificity for target cancer cells (i.e. uptake of cisplatin into non target cells) and the degree of resistance that the cancer cells possess towards cisplatin[76]. With regards to cisplatin resistance, this resistance can be split into two key categories; inherent resistance and developed resistance.

Inherent Resistance refers to where cells seemingly have a significantly reduced uptake of cisplatin. Some research suggests that this may be as a result of a lack of copper membrane transporters (CTR1 and ATP7A/B) and / or Organic Cationic Transporters (OCT1-3) which are theorised to help transport cisplatin into the cells[44, 74 & 77]. Other research suggests that cisplatin may still enter the cells via passive diffusion, thus stipulating that these copper and OCT transporters play no significant role in cisplatin uptake[78-80]. Despite this latter point, it is still largely perceived within the literature that these active uptake proteins play a significant role in the uptake of platinum based chemotherapeutic agents.

Developed cisplatin resistance arises during the cycles of chemotherapy, where cancers progressively display a lack of response to cisplatin and therefore an increased dose is required each cycle[81]. This developed resistance could be as a result of a number of key resistance mechanisms, which include:

- down regulation of copper pumps (CTR1 and ATP7A) and / or Organic Cationic Transporters (OCT1-3), thus reducing cisplatin uptake;
- increased efflux of cisplatin by upregulation of ATP7B, typically as a result of increased inactivation of cisplatin by naturally occurring cytosolic agents (glutathione (GSH) and methionine (MT)); and
- increased DNA repair or increased DNA damage tolerance.

An overview of cisplatin uptake, inactivation, activation, efficacy and efflux are depicted in Figure 114 as sourced from the literature[44, 82].

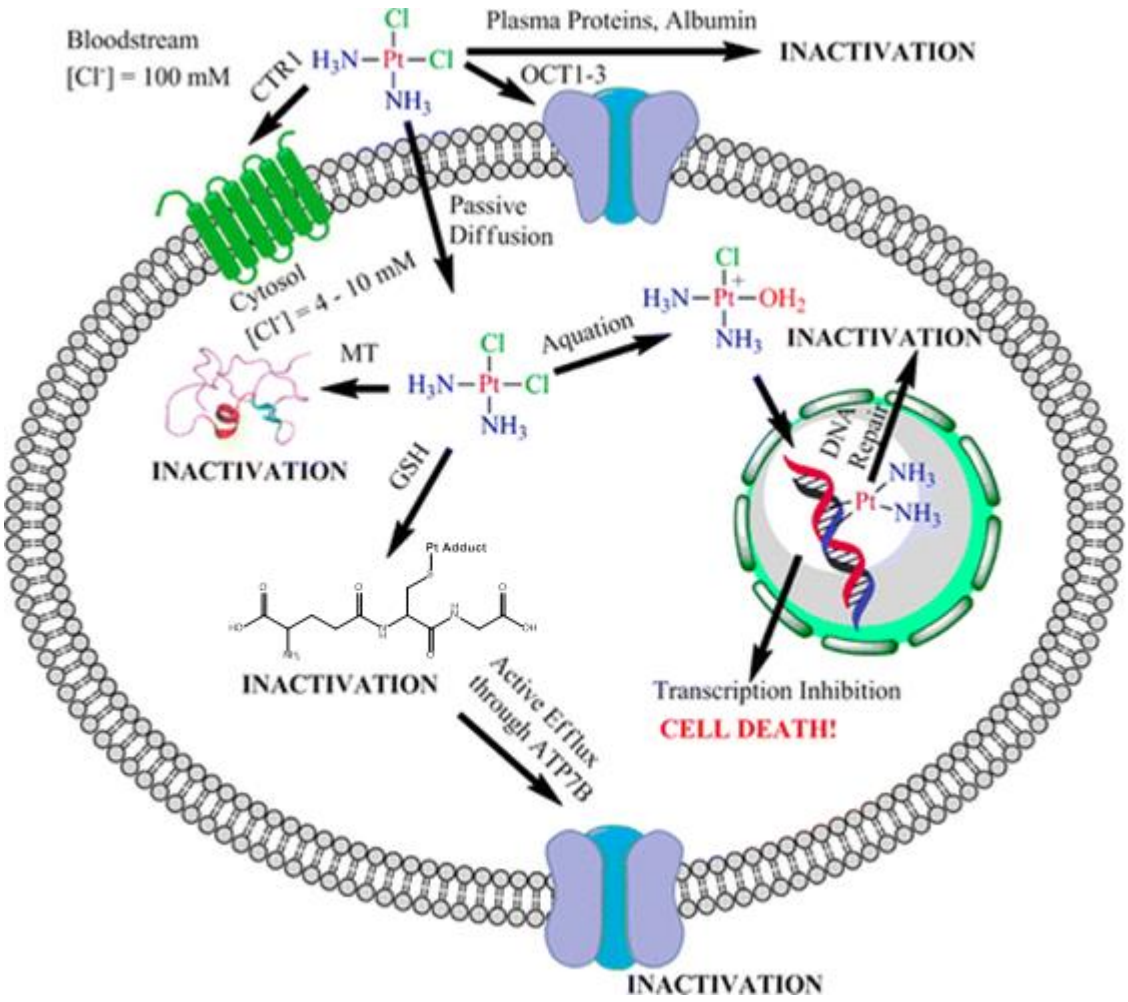

Figure 114: Overview of potential uptake, activity of and tumour resistance to cisplatin as sourced from Lippard *et al*. and originally produced by Johnstone *et al*[44, 82], with minor amendments.

1.3.2. Utilisation of Platinum(II) agents within Research

Leading on from the wealth of research into the utilisation of cisplatin (which of course led to its clinical approval and use) there have been a number of novel Pt(II) complexes developed in the literature in pursuit of an alternative Pt based anticancer agent whose structure loosely imitates that of clinically approved Pt(II) drugs. In this regard, it has been an objective of the field to develop Pt(II) agents which present with improved physical characteristics such as improved solubility, stability and targeting, whilst either maintaining the activity of the

founding drug or presenting with entirely new models of anticancer activity. These research goals are largely in the pursuit of anticancer agents that are more effective within select cell lines and / or display efficacy in typically Pt(II) drug (such as cisplatin) resistant cell lines.

As per the thorough literature review of Lippard *et al.* there are a number of Pt(II) agents which incorporate targeting modalities into the structure of the complex[44]. Examples of such targeting include sugar receptors (such as glucose receptors)[83], steroidal receptors (such as oestrogen receptors α and β)[84] and peptide receptors (such as CD13)[185]. In addition to these targeting vectors, a number of folate receptor targeting Pt(II) agents have been developed in the literature. One notable example of such a complex is that developed by Aronov *et al.*, whose Pt(II) complex comprised a PEG linked folic acid motif and mimicked the structure of carboplatin[86]. The structure of Aronov *et al*'s Pt(II) complex is represented in Figure 115 as drawn from the literature[44, 86].

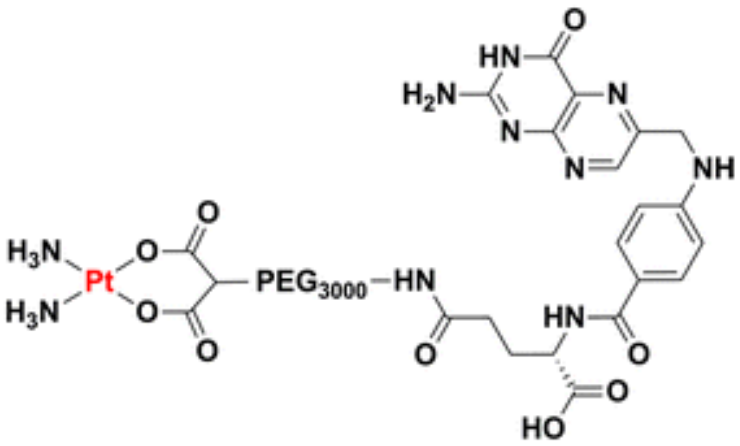

Figure 115: Structure of Aronov *et al*'s carboplatin based folate receptor targeting Pt(II) agent, taken from Lippard *et al*[44, 86].

The Aronov *et al.* Pt(II) complex comprises a PEG spacer between the dicarboxylate chelating ligand and a folic acid unit, thus enhancing the water solubility of the complex over that of

carboplatin. Their research investigated the levels of uptake of various Pt(II) agents in folate receptor positive and negative cell lines, with the above complex displaying enhanced uptake and cytotoxicity in receptor positive lines. This enhanced uptake and efficacy was assumed to be as a result of folate receptor mediated endocytosis of the complex. Unfortunately, the complex was less cytotoxic than carboplatin, which was assumed to be as a result of fewer Pt-DNA adducts being formed[86].

1.3.3. Platinum(IV) Chemotherapeutic Alternatives

An alternative to the targeted Pt(II) agents of the literature is that of the more recently explored Pt(IV) pro-drugs. In this regard, whilst Pt(II) agents typically vary one or two of the ligands to present with novel structures loosely associated to clinically approved Pt(II) agents, Pt(IV) agents comprise octahedral structures, which thus afford the opportunity to incorporate and vary axial ligands. The general structure of Pt(IV) complexes is represented in Figure 116, as drawn from the literature[87].

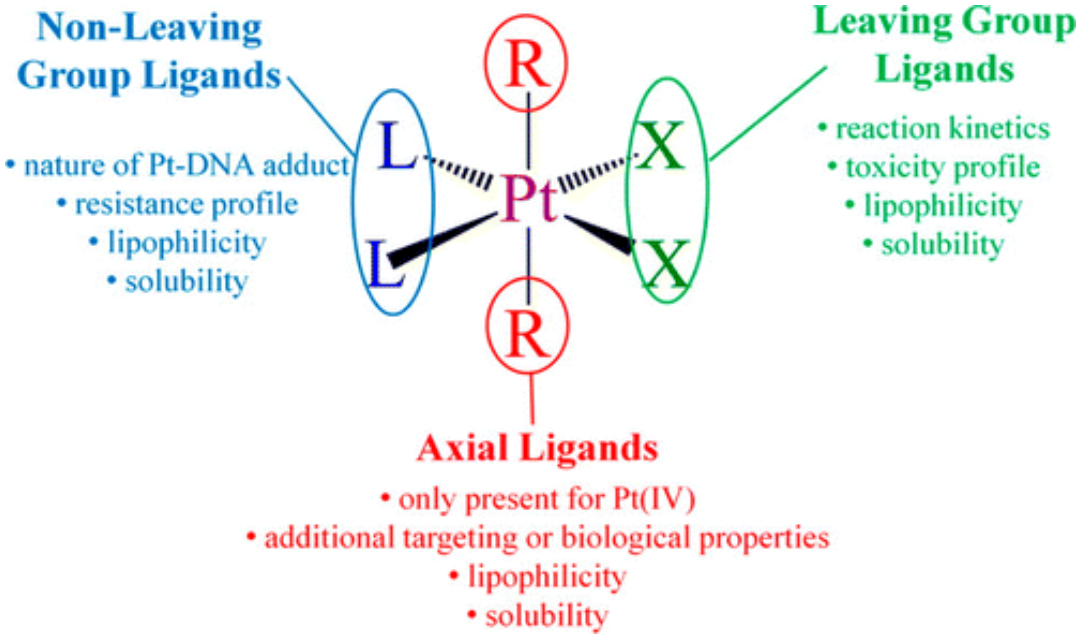

Figure 116: General structure of Pt(IV) complexes and the opportunities afforded in alteration of the equatorial or axial ligands, taken from Wilson and Lippard[87].

As a result of the octahedral geometry these complexes are typically much more kinetically inert than their square planar Pt(II) counterparts. As a result, Pt(IV) complexes are typically more resistant to ligand substitution reactions, which in turn inherently presents the complexes with enhanced resistance to unwanted side-reactions with biomolecules prior to DNA binding[87]. Perhaps the most beneficial aspect of Pt(IV) agents though is the additional two coordination sites (axial), which allows for further incorporation of ligands for alteration of the complex's properties, such as; water solubility, lipophilicity, stability and additional targeting motifs[44, 87]. A number of key examples exist within the literature which presented with promising results, only to be ultimately ruled out through clinical trials. These complexes include satraplatin, ormaplatin, LA-12 and iproplatin, whose structures are given in Figure 117 as taken from the literature[44].

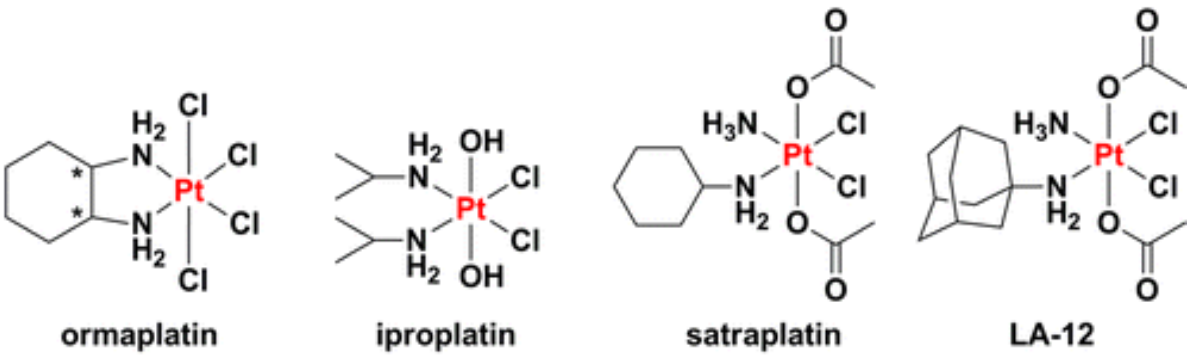

Figure 117: Chemical structures of Pt(IV) complexes that have undergone clinical trials, taken from Lippard *et al*[44].

Each of the complexes presented in Figure 117 are examples of Pt(IV) pro-drugs. A pro-drug is a compound that originally enters the organism in an inactive form and is subsequently metabolised to form the active compound. Whilst there is a vast wealth of research into the use of Pt(IV) pro-drugs for anti-cancer purposes, there is still some debate surrounding the proposed mechanism of reduction of the Pt(IV) centre to give the desired Pt(II) drug at the target location. That being said, it is largely believed that this reduction is the result of the

hypoxic environment of the tumour and / or the presence of reductive species within endosomes[88].

Of the notable Pt(IV) complexes in Figure 117, satraplatin presented with the most promising results, displaying oral activity, increased cytotoxicity over cisplatin and efficacy in cisplatin resistant cell lines. Unfortunately the complex did not progress through stage three clinical trials as it was found that the complex negatively affected the efficacy of prednisone when used in combination therapy[44, 89 – 91]. Pt(IV) structures remain a prominent area of interest within the literature, with a number of promising pro-drug candidates. One example is that reported by Dabrowiak *et al*, who developed a Pt(IV) pro-drug which may be reduced in situ to form the active drug cisplatin and may also be tethered to the surface of citrate capped gold nanoparticles for targeted cellular uptake[92]. The chemical structure of this Pt(IV) pro-drug is represented in Figure 118.

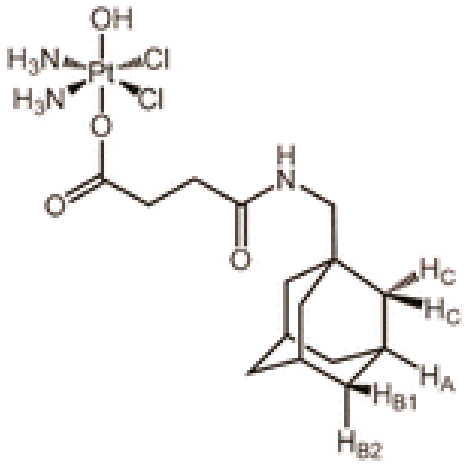

Figure 118: Chemical structure of the Pt(IV) pro drug developed by Dabrowiak *et al*, taken from Dabrowiak *et al*[92].

The surface of the citrate capped gold nanoparticles was loaded with the above Pt(IV) compound and subsequently further functionalised with a thiolate modified β-cyclodextrin for incorporation of receptor targeting. Unfortunately, this pro drug was found to be less cytotoxic

than cisplatin when administered to neuroblastoma SK-N-SH cells, irrespective of nanoparticular loading[92].

1.3.4. Conclusions

A number of platinum anticancer agents have been developed within the literature as Pt(II) and Pt(IV) complexes. Despite a wealth of research efforts, traditional Pt(II) complexes such as cisplatin and carboplatin remain as the most clinically viable models. Despite the promising opportunities which might be afforded to Pt(IV) complexes, there are still no clinically approved Pt(IV) agents to date. Research into the use of Pt(IV) agents has also investigated their potential as therapeutic agents within nanoparticle systems. Pt(IV) agents remain a promising prospect within chemotherapeutics and may yet form the clinically approved Pt drugs of the near future.

1.4. Transition Metal Imaging Agents

1.4.1. Ru(II) polypyridyl complexes and their properties

Inorganic imaging agents present with a number of favourable physical properties and have thus been utilised across a broad range of applications within the literature. Of these agents, transition metal based polypyridyl complexes have been of particular interest and use on account of their strong fluorescence within the visible region, long excitation state lifetimes (typically in the nano-seconds), comparatively high photostability and facilitation of photo-induced energy transfer processes[52, 93, 94].

Ruthenium(II) based polypyridyl complexes in particular present with characteristic absorption bands in the blue range (typically around 290 and 460nm), corresponding to the $1(\pi-\pi^*)$ and singlet metal-to-ligand charge transfer (^{1}MLCT) bands respectively[95]. These complexes also

typically present with a ^{3}MLCT based broad emission band centred in the red field (~620-680nm). These complexes therefore typically present with large stokes shifts, in the region of ~200nm, thus significantly reduces the amount of emission that might otherwise be re-absorbed by the very same probe. The origin of MLCT and the formation of the different states (singlet (^{1}MLCT) and triplet (^{3}MLCT)) are depicted in Figures 119 and 120 and are briefly discussed below.

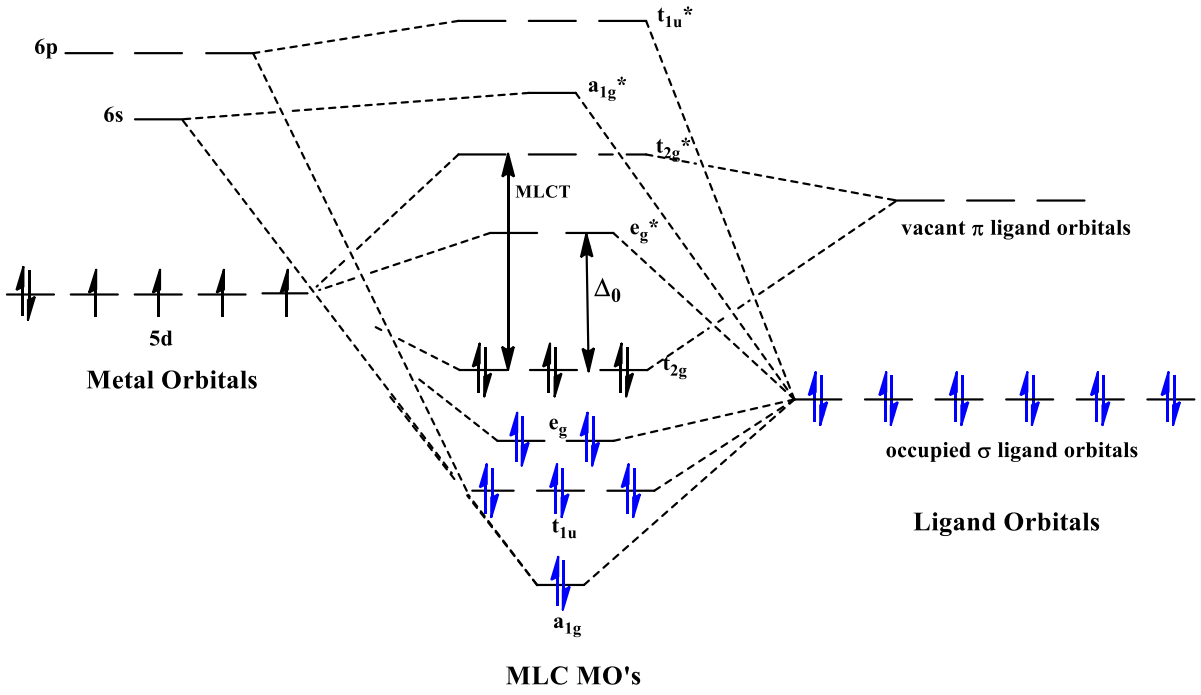

Figure 119: MLCT for a typical d^6 transition metal complex, such as those of Ru(II) polypyridyl complexes. MLCT is the result of electrons being excited from lower lying metal based orbitals (*d* orbitals) to higher in energy vacant orbitals provided by ligands as a result of absorption of energy from photons, serving as the origin of the fluorescence found in fluorescence active transition metal complexes.

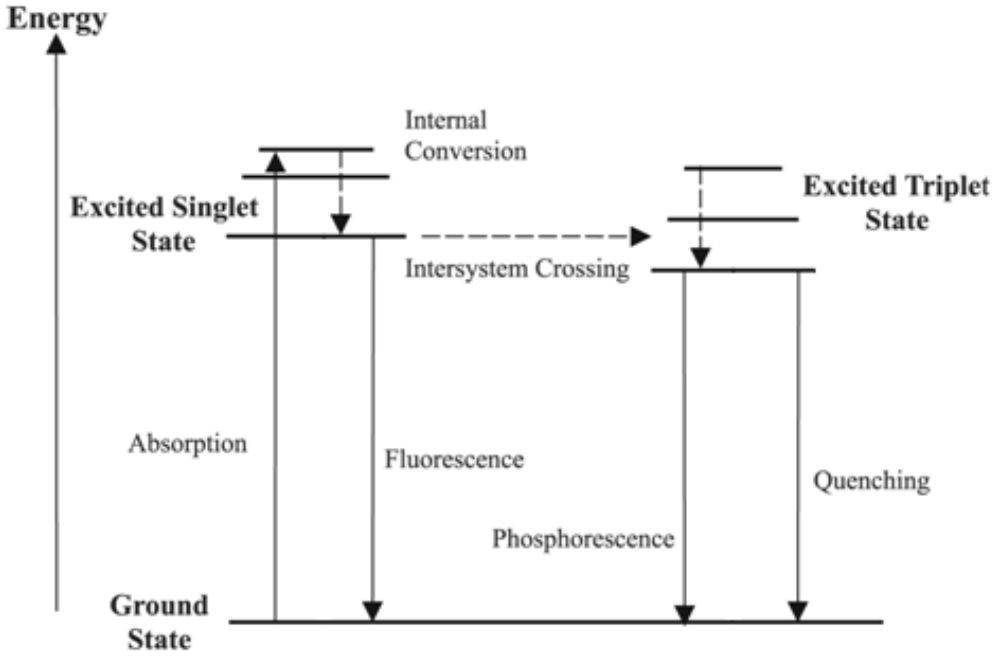

Figure 120: Jablonski Diagram, showing the typical energy state of Ru(II) polypyridyl complexes and the associated pathways for release of energy absorbed from photons[95].

Upon excitation of an electron to one of the vacant π^* ligand based orbitals, the electron is said to be in an excited singlet state or ^{1}MLCT. From this excited singlet state, the electron can relax back down to its ground state and give fluorescent emission, or it can undergo a process known as intersystem crossing (ISC). Intersystem crossing is the non-radiative transition of an electron from its singlet state multiplicity to a triplet state multiplicity or ^{3}MLCT. From this excited triplet state, the electron can relax back to its original ground state and in turn give phosphorescent emission. This phosphorescent emission is typically saught after for emissive probes as it is spin-forbidden and therefore presents with longer emissive lifetimes[96].

Due to the restricted depth penetration of the excitation and emission wavelengths for these imaging probes they are typically limited to utilisation as cellular tracking agents within cells by way of confocal microscopy and flow cytometry.

1.4.2. Utilisation within Research

One of the most prominent examples of a Ru(II) polypyridyl complex in the literature is that of $[Ru(bpy)_3]^{2+}$, as originally developed by Cook *et al*[52, 97]. $[Ru(bpy)_3]^{2+}$ is a low spin d^6 complex that is typically stabilised by cl^- counter ions, displaying water solubility and stability as a result of its slow rate of ligand exchange. This complex possesses a strong ^{1}MLCT absorption at 450nm (ε13000 mol^{-1} cm^{-1}), a relatively strong ^{3}MLCT emission at 650nm, a quantum yield of 3% and typical lifetimes of ~370-400 nano-seconds. Examples of the absorption and emission spectra of this complex are represented below in Figure 121, as sourced from the literature.

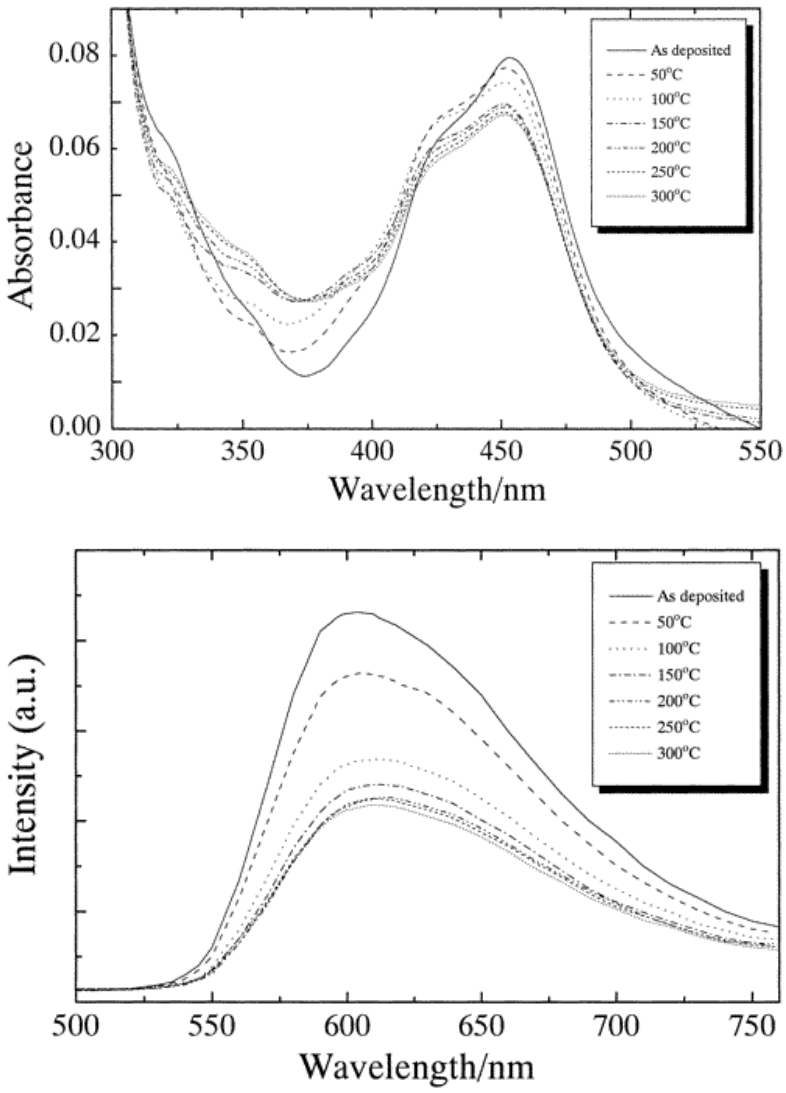

Figure 121: A) absorance and B) emission spectra of $[Ru(bpy)_3]^{2+}$ taken from Yoko *et al*[98].

Stemming from the conceptualisation and broad utilisation of $[Ru(bpy)_3]^{2+}$, a number of Ru(II) polypyridyl based imaging agents have been developed. Of particular interest are those that have been utilised within cellular imaging application. In this regard, one notable application of the literature is that of Turro *et al*, who synthesised $[(Ru(bpy)_2)_2(tpphz)]^{4+}$, whose structure is depicted in Figure 122[99, 100].

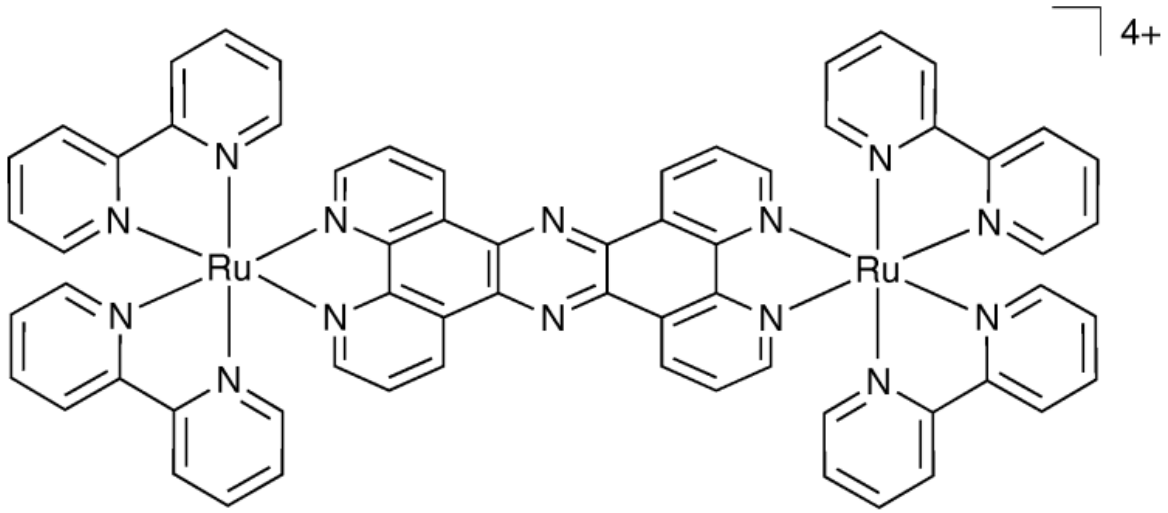

Figure 122: Chemical structure of Turro *et al*'s Ru(II) polypyridyl complex[100], taken from Gill and Thomas[99].

The Turro Ru(II) imaging agent was found to selectively bind within the major groove of the DNA helix. Upon major groove binding, the photophysical properties of the probe are changed and a substantial shift in the emission wavelength is observed. Accordingly, these imaging probes inherently present with a positive means of differentiating between bound and unbound molecular probe, thus making them a potent cellular tracking agent.

Alternative Ru(II) polypyridyl imaging agents have also been utilised within research as nanoparticle tracking agents. In this regard, Osborne *et al* synthesised and investigated a number of novel Ru(II) polypyridyl based imaging probes comprising variable ligands for

surface functionalisation of citrate capped gold nanoparticles[101]. Some of these structures are represented in Figure 123 below, as drawn from the literature.

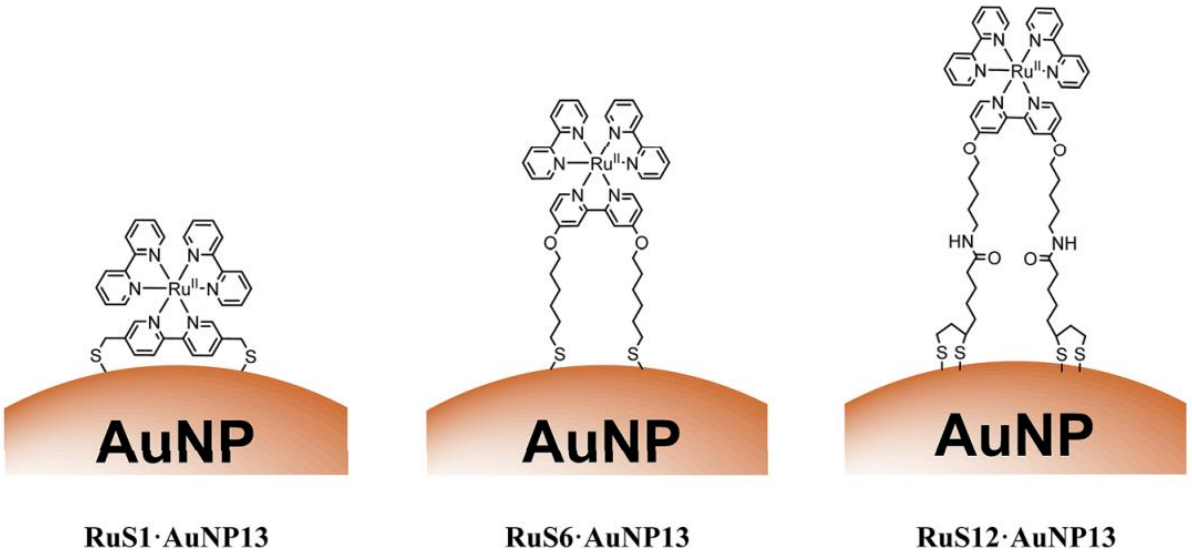

Figure 123: Diagrammatic representation of three novel Ru(II) polypyridyl based imaging agents as developed by Osborne *et al*. Taken from Osborne *et al*[101].

Osborne *et al* utilised the above structures to investigate the effect of Ruthenium core distance from the nanoparticle surface and what effect this might have on the probes emissive properties. It was found that a combination of the probe distance from the particle surface, the nature of the nanoparticle surface and any surface stabilising agents (such as the surfactant Zonyl FSA) lead to varying degrees of quenching. Optimal emissive conditions were found for Ru(II) probes with longer surface tethering linkers, such as that of RuS12 as depicted in Figure 123.

1.4.3. Conclusions

There is a wealth of research into the photo-physical properties of Ru(II) polypyridyl imaging agents within the literature. These ligands have been utilised in cellular imaging and present with different methods of action, including DNA major groove binding and nanoparticle tracking studies. The number of desirable physical and photo-physical properties

make Ru(II) polypyridyl complexes desirable cellular imaging agents within confocal microscopy and flow cytometry studies. Accordingly, utilisation of such complexes within a theranostic imaging agent may present with favourable nanoparticle tracking capabilities.

1.5. Thesis Aims

This thesis focusses on the development of a folate receptor targeting theranostic gold nanoparticle system. Accordingly, chapter 2 addresses the development of a new protocol for the synthesis of folate capped gold nanoparticles. This new protocol was developed to address the lack of a robust and reliable method for the production of such particles, as has been discussed in the above literature review.

Chapter 3 addresses the loading of both citrate and folate capped gold nanoparticle systems with a ruthenium based polypyridyl probe that has been previously synthesised by the Pikramenou group. These fluorescent gold nanoparticle systems were then subjected to in vitro cellular studies and their uptake in folate receptor positive and negative cells investigated. In particular, different methods of adjusting the levels of folate receptors within a single cell line were investigated, so as to give a more representative measure of folate receptor mediated uptake only.

Chapter 4 investigates the development of a novel Pt(IV) pro drug that has the potential to be administered on its own or as part of a surface functionalised agent on citrate or folate capped gold nanoparticles for targeted delivery. Its potential as a chemotherapeutic agent was investigated via MTT assays, ICPMS studies and immunocytochemical analysis utilising a commercial antibody for cisplatin-DNA adduct recognition.

Chapter 5 investigates the utilisation of the ruthenium based polypyridyl probe and novel Pt(IV) agents as part of surface functionalised citrate and folate capped gold nanoparticle systems. These theranostic particles were investigated within folate receptor positive A549 cells.

References

1 - Leamon C. P, Low P. S. Cytotoxicity of momordin–folate conjugates in cultured human cells. Journal of Biological Chemistry (1992). 267, 24966–24971.

2 - Coney LR, Tomassetti and Carayannopoulos L. Cloning of a tumor-associated antigen: MOv18 and MOv19 antibodies recognize a folate-binding protein. Cancer Research (1991). 51 (22): 6125–6132.

3 - Weitman SD, Frazier KM, Kamen BA. The folate receptor in central nervous system malignancies of childhood. Journal of Neurooncology (1994). 21 (2): 107–112.

4 - Campbell IG, Jones TA, Foulkes WD, Trowsdale J. Folate-binding protein is a marker for ovarian cancer. Cancer Research (1991). 51 (19): 5329–5338.

5 - O'Shannessy DJ, Somers EB, Wang L, Wang H and Hsu R. Expression of folate receptors alpha and beta in normal and cancerous gynecologic tissues: correlation of expression of the beta isoform with macrophage markers. Journal of Ovarian Research (2015). 8:29, 1-9.

6 - Boyles AL, Yetley EA, Thayer KA, and Coates PM. Safe use of high intakes of folic acid: research challenges and paths forward. Nutrition Reviews (2016). 74(7): 469–474.

7 –Elnakat H and Ratnam M. Distribution, functionality and gene regulation of folate receptor isoforms: implications of targeted therapy. Advanced Drug Delivery Reviews (2004). 1067-1084.

8 - Smith D, Hornstra J, Rocha M, Jansen G, Assaraf Y, Lasry I, Blom H and Smulders YM. Folic Acid Impairs the Uptake of 5-Methyltetrahydrofolate in Human Umbilical Vascular Endothelial Cells. Journal of Cardiovasc Pharmacol (2017). 271-275.

9 - Zhao R, Diop-Bove N, Visentin M and Goldman ID. Mechanisms of membrane transport of folates into cells and across epithelia. Annual Review of Nutrition (2011). 177–201.

10 - Ross JF, Chaudhuri PK, Ratnam M. Differential regulation of folate receptor isoforms in normal and malignant tissues in vivo and in established cell lines. Physiologic and clinical implications, Cancer (1994). 2432 – 2443.

11 – Shen J, Hu Y, Putt KS, Singhal S, Han H, Visscher DW, Murphy LM and Low PS. Assessment of folate receptor alpha and beta expression in selection of lung and pancreatic cancer patients for receptor targeted therapies. Oncotarget (2018). 4485-4495.

12 – Zhao R, Diop-Bove N, Visentin M, and Goldman ID. Mechanisms of Membrane Transport of Folates into Cells and Across Epithelia. Annual Review of Nutrition (2011). 177-201.

13 – Assaraf YG, Rothem L, Hooijberg JH, Stark and M, Ifergan I. Loss of multidrug resistance protein 1 expression and folate efflux activity results in a highly concentrative folate transport in human leukemia cells. Journal of Biological Chemistry (2003). 6680–6686.

14 – Puig-Kroger A, Sierra-Filardi E, Dominguez-Soto A, Samaniego R, Corcuera MT, Gomez-Aguado F, Ratnam M, Sanchez-Mateos P, Corbi AL. Folate receptor beta is expressed by tumor-associated macrophages and constitutes a marker for M2 anti-inflammatory/regulatory macrophages. Cancer Research (2009). 9395–9403.

15 – Ifergan I and Assaraf YG. Molecular mechanisms of adaptation to folate deficiency. Vitamins and Hormones (2008). 99–143.

16 – Tian Y, Wu G, Xing JC, Tang J, Zhang Y, Huang ZM, Jia ZC, Zhao R, Tian ZQ, Wang SF, Chen XL, Wang L and Wu YZ. A novel splice variant of the folate receptor 4 predominantly expressed in regulatory T cells. BMC Immunology (2012). 13-30.

17 - Wu M, Gunning W, Ratnam M. Expression of folate receptor type alpha in relation to cell type, malignancy, and differentiation in ovary, uterus, and cervix, Cancer Epidemiological. Biomarkers Previews (1999). 775 – 782.

18 - Bueno R, Appasani K, Mercer H, Lester S, Sugarbaker D. The alpha folate receptor is highly activated in malignant pleural mesothelioma. Journal of Thoracic and Cardiovascular Surgery (2001). 225 – 233.

19 - Evans CO, Young AN, Brown MR, Brat DJ, Parks JS, Neish AS and Oyesiku NM. Novel patterns of gene expression in pituitary adenomas identified by complementary deoxyribonucleic acid microarrays and quantitative reverse transcription-polymerase chain reaction. Journal of Clinical Endocrinology and Metabolism (2001). 3097 – 3107.

20 - Yuan Y, Nymoen DA, Dong HP, Bjørang O, Shih IM, Low PS, Trope' CG and Davidson B. Expression of the folate receptor genes FOLR1 and FOLR3 differentiates ovarian carcinoma from breast carcinoma and malignant mesothelioma in serous effusions. Human Pathology (2009). 1453–1460.

21 – O'Shannessy DJ, Yu G, Smale R, Fu YS, Singhal S, Thiel RP, Somers EB, Vachari A. Folate receptor alpha expression in lung cancer: diagnostic and prognostic significance. Oncotarget (2012). 414–425.

22 – Christoph DC, Reyna-Asuncion B, Hassan B, Tran C, Maltzman JD, O'Shannessy DJ, Gauler TC, Wohlsclaeger J, Schuler M, Eberhardt WE, Hirsch FR. Assessment of folate receptor-α and epidermal growth factor receptor expression in pemetrexed-treated non-small-cell lung cancer patients. Clinical Lung Cancer (2014). 320–330.

23 - Köbel M, Madore J, Ramus SJ, Clarke BA, Pharoah PD, Deen S, Bowtell DD, Odunsi K, Menon U, Morrison C, Lele S, Bshara W, Sucheston L, "Evidence for a timedependent association between FOLR1 expression and survival from ovarian carcinoma: implications for clinical testing. An ovarian tumor tissue analysis consortium study", British Journal of Cancer (2014), 2297–2307.

24 – Zhang Z, Wang J, Tacha DE, Li P, Bremer RE, Chen H, Wei B, Xiao X, Da J, Skinner K, Hicks DG, Bu H and Tang P. Folate receptor α associated with triple-negative breast cancer and poor prognosis. Archives of Pathology & Laboratory Medicine (2014). 890–895.

25 – Iwakiri S, Sonobe M, Nagai S, Hirata T, Wada H and Miyahara R. Expression status of folate receptor alpha is significantly correlated with prognosis in non-small-cell lung cancer. Annals of Surgical Oncology (2008). 889–899.

26 - Kurahara H, Takao S, Kuwahata T, Nagai T, Ding Q, Maeda K, Shinchi H, Mataki Y, Maemura K, Matsuyama T and Natsugoe S. Clinical significance of folate receptor β-expressing tumor-associated macrophages in pancreatic cancer. Annals Surgical Oncology (2012). 2264–2271.

27 - Shen J, Putt KS, Visscher DW, Murphy L, Cohen C, Singhal S, Sandusky G, Feng Y, Dimitrov DS and Low PS. Assessment of folate receptor-β expression in human neoplastic tissues. Oncotarget (2015). 14700–14709.

28 - Leamon C. P and Low P. S. Cytotoxicity of momordin–folate conjugates in cultured human cells. Journal of Biological Chemistry (1992). 267, 24966–24971.

29 - Leamon, C. P and Low, P. S. Delivery of macromolecules into living cells: A method that exploits folate receptor endocytosis. Proceedings of the National Acadamy of Sciences Of the U.S.A. (1991). 88, 5572–5576.

30 – Weitman, S. D, Lark, R. H, Coney, L. R, Fort, D. W, Frasca, V, Zurawski, V. R., Jr and Kamen, B. A. Distribution of the folate receptor GP38 in normal and malignant cell lines and tissues. Cancer Research (1992). 52, 3396–3401.

31 - Leamon C. P, Pastan I and Low P. S. Cytotoxicity of folate–Pseudomonas exotoxin conjugates toward tumor cells. Contribution of translocation domain. Journal of Biological Chemistry (1993) 268, 24847–24854.

32 - Low PS, Henne WA and Doorneweerd DD. Discovery and Development of Folic-Acid-Based Receptor Targeting for Imaging and Therapy of Cancer and Inflammatory Diseases. Accounts of Chemical Research. (2008) Vol. 41, No. 1, 120-129.

33 –LoRusso PM, Edelman PM, Bever SL, Forman KM, Pilat M, Quinn MF, Li J, Heath EI, Malburg LM, Klein PJ, Leamon CP, Messmann RA, and Sausville EA. Phase I Study of Folate Conjugate EC145 (Vintafolide) in Patients With Refractory Solid Tumors. American Society of Clinical Oncology. 2012. 4011-4016.

34 - Naumann RW, Coleman RL, Burger RA, Sausville EA, Kutarska E, Ghamande SA, Gabrail NY, Depasquale SE, Nowara E, Gilbert L, Gersh RH, Teneriello MG and Harb WA. PRECEDENT: a randomized phase II trial comparing vintafolide (EC145) and pegylated liposomal doxorubicin (PLD) in combination versus PLD alone in patients with platinum-resistant ovarian cancer. Journal of Clinical Oncology. 2013. 4400–4406.

35 - Oza AM, Vergoteb IB, Gilbert LG, Ghatage LP, Lisyankaya A, Ghamande S, Chambers SK, Arranz JA, Provencher DM, Bessette P, Amnon A, Symanowski J, Penson RT, Naumann RW and Clark R. A randomized double-blind phase III trial comparing vintafolide (EC145) and pegylated liposomal doxorubicin (PLD/Doxil®/Caelyx®) in combination versus PLD in participants with platinum-resistant ovarian cancer (PROCEED) (NCT01170650). Gynecologic Oncology 137 (2015) 2–91.

36 – The Chemical structure of Vintafolide was sourced on 09th September 2018 at 15:30 from https://en.wikipedia.org/wiki/Vintafolide#/media/File:Vintafolide.svg.

37 - Luyckx M, Votino R, Squifflet JL and Baurain JF. Profile of vintafolide (EC145) and its use in the treatment of platinum-resistant ovarian cancer. International Journal of Womens Health. 2014. 351–358.

38 - Okusanya OT, DeJesus EM, Jiang JX, Judy RP, Venegas OG, Deshpande CG, Heitjan DF, Nie S, Low PS, Singhal S. Intraoperative molecular imaging can identify lung adenocarcinomas during pulmonary resection. Journal of Thoracic & Cardiovascular Surgery. 2015. 28–35.

39 – Wong, B. S, Yoong, S. L, Jagusiak, A, Panczyk, T, Ho, H. K, Ang, W. H, and Pastorin, G. Carbon Nanotubes for Delivery of Small Molecule Drugs. Advanced Drug Delivery Reviews. 2013, 65, 1964−2015.

40 – Muzi, L, Ménard-Moyon, C, Russier, J, Li, J, Chin, C. F, Ang, W. H, Pastorin, G, Risuleo, G and Bianco, A. Diameter-Dependent Release of a Cisplatin Pro-Drug from Small and Large Functionalized Carbon Nanotubes. Nanoscale 2015, 7, 5383−5394.

41 –Sobh RA, Nasr HE, Moustafa AB and Mohamed WS. Tailoring of anticancer drugs loaded in MWCNT/Poly(MMA-co-HEMA) nanosphere composite by using in situ microemulsion polymerization. Journal of Pharmaceutical Investigations. (2018). 1-11.

42 –Chen Z, Zhang A, Wang X, Zhu J, Fan Y, Yu H, and Yang Z. The Advances of Carbon Nanotubes in Cancer Diagnostics and Therapeutics. Journal of Nanomaterials (2013), 1-13.

43 –Yang Z, Fan JZ, Proppe AH, Pelayo García de Arquer F, Rossouw D, Voznyy O, Lan X, Liu M, Walters G, Quintero-Bermudez R, Sun B, Hoogland S, Botton GA, Kelley SO and Sargent EH. Mixed-quantum-dot solar cells. Nature Communications (2017). 8: 1325, 1-17.

44 – Johnstone TC, Suntharalingam K and Lippard SJ. The Next Generation of Platinum Drugs: Targeted Pt(II) Agents, Nanoparticle Delivery, and Pt(IV) Prodrugs. Chemical Reviews. (2016). 3436−3486.

45 - Wang Z & Chui WK and Ho PC. Nanoparticulate Delivery System Targeted to Tumor Neovasculature for Combined Anticancer and Antiangiogenesis. Therapeutic & Pharmaceutical Research. (2011) 28:585–596.

46 –Kang X, Guo X, Niu X, An W, Li S, Liu Z, Yang Y, Wang N, Jiang Q, Yan C, Wang H and Zhang Q. Photothermal therapeutic application of gold nanorodsporphyrin-trastuzumab complexes in HER2-positive breast cancer. Nature Scientific Reports (2017). Article number: 42069.

47 –Ding H, Yong KT, Roy I, Pudavar HE, Law WC, Bergey EJ, and Prasad PN. Gold Nanorods Coated with Multilayer Polyelectrolyte as Contrast Agents for Multimodal Imaging. Journal of Physical Chemistry. 12552-12557.

48 –Ramzannezhad A, Gill P and Bahari A. Fabrication of magnetic nanorods and their applications in medicine. De Gruyter Impact Factors (2017). 1-31.

49 –Yi GC, Wang C and Park WI. ZnO Nanorods: Synthesis, Characterization and Applications. Semiconductor Science and Technology (2005) 20(20): 22-34.

50 -Farokhzad OC, Cheng JJ, Teply BA, Sherifi I, Jon S and Kantoff PW. Targeted nanoparticle-aptamer bioconjugates for cancer chemotherapy in vivo. Proceedings of the National Academy of Sciences of the USA. (2006) 103:6315-6320.

51 –Loureiro A, Azoia NG, Gomes AC and Cavaco-Paulo A. Albumin-Based Nanodevices as Drug Carriers. Current Pharmaceutical Design. 2016. 22, 1-21.

52 – Osborne SAM. Luminescent Ruthenium Nanoprobes for Applications in dye Sensitized Solar Cells. PhD Thesis (2017), Department of Chemistry, University of Birmingham.

53 –Xu X, Duan G, Li Y, Liu G, Wang J, Zhang H, Dai Z and Cai W. Fabrication of Gold Nanoparticles by Laser Ablation in Liquid and Their Application for Simultaneous Electrochemical Detection of Cd2+, Pb2+, Cu2+, Hg2+. ACS Applied Materiels and Interfaces (2014). 6, 65-71.

54 – Turkevich J, Stevenson PC and Hillier J. A study of the nucleation and growth processes in the synthesis of colloidal gold. Faraday Discussions. (1951). 11, 55-75.

55 - Schulz F, Homolka T, Bastús NG, Puntes V, Weller H and Vossmeyer T, "Little Adjustments Significantly Improve the Turkevich Synthesis of Gold Nanoparticles", Langmuir, 2014, 30, 10779-10784.

56 - Li G, Li D, Zhang L, Zhai J and Wang E. One-Step Synthesis of Folic Acid Protected Gold Nanoparticles and Their Receptor-Mediated Intracellular Uptake. Chemical European Journal. (2009). 15, 9868–9873.

57 - Iversen, T.G, Skotland, T and Sandvig, K. Endocytosis and Intracellular Transport of Nanoparticles: Present Knowledge and Need for Future Studies. Nano Today (2011). 6, 176−185.

58 - Yang C, Bromma K, Ciano-Oliveira CD, Zafarana G, Prooijen MV and Chithrani DB. Gold nanoparticle mediated combined cancer therapy. Cancer Nanotechnology (2018) 9:4, 1-14.

59 - Yohan D and Chithrani BD. Applications of nanoparticles in nanomedicine. Journal of Biomedical Nanotechnology (2014). 10:2371–2392.

60 - Yang C, Uertz J and Chithrani DB. Colloidal gold-mediated delivery of bleomycin for improved outcome in chemotherapy. Nanomaterials (2016). 6:48.

61 –Galba J, Piestansky LVJ, Mego M, Novotny L, Dokupilova S, Kova KM, Nek HV and Mikus P. HPLC-QTOF-MS Method for Identification and Determination of Bleomycin A2 and B2 Fractions. Journal of Liquid Chromatography & Related Technologies (2015). 38: 294–302.

62 - Schooneveld MM, Cormode DP, Koole R, Wijngaarden JT, Calcagno C, Skajaa T, Hilhorst J, Hart DC, Fayad ZA, Mulder WJM and Meijerink A. A fluorescent, paramagnetic and PEGylated gold/silica nanoparticle for MRI, CT and fluorescence imaging. Contrast Media Mololecular Imaging (2010). 5(4): 231–236.

63 – Kumar SSD, Mahesh A, Antoniraj MG, Rathore HS, Houreld NN and Kandasamy R. Cellular imaging and folate receptor targeting delivery of gum kondagogu capped gold nanoparticles in cancer cells. International Journal of Biological Macromolecules (2018). 220-230.

64 –Devendiran RM, Chinnaiyan SK, Yadav NK, Moorthy GK, Ramanathan G, Singaravelu S, Sivagnanam UT and Perumal PT. Green synthesis of folic acid-conjugated gold nanoparticles with pectin as reducing/stabilizing agent for cancer theranostics. RSC Advances (2016). 6, 29757-29768.

65 –Samadian H, Hosseini-Nami S, Kamrava SK, Ghaznavi H and Shakeri-Zadeh A. Folate-conjugated gold nanoparticle as a new nanoplatform for targeted cancer therapy. Journal of Cancer Research and Clinical Oncology (2016). 142(11), 2217-2229

66 - Mansoori GA, Brandenburg KS and Shakeri-Zadeth A. A Comparative Study of Two Folate-Conjugated Gold Nanoparticles for Cancer Nanotechnology Applications. Cancers (2010). 2, 1911-1928.

67 - Ai J, Xu Y, Li D, Liu Z and Wang E. Folic acid as delivery vehicles: targeting folate conjugated fluorescent nanoparticles to tumors imaging. Talanta (2012). 101: 32–37.

68 - Jesna KK and Ilanchelian M. Photophysical changes of thionine dye with folic acid capped gold nanoparticles by spectroscopic approach and its in vitro cytotoxicity towards A-549 lung cancer cells. Journal of Molecular Liquids (2017). 242: 1042–1051.

69 –Link S and El-Sayed MA. Spectral Properties and Relaxation Dynamics of Surface Plasmon Electronic Oscillations in Gold and Silver Nanodots and Nanorods. Journal of Physical Chemistry (1999). 103, 8410-8426.

70 –Daniel MC and Astruc D. Gold Nanoparticles: Assembly, Supramolecular Chemistry, Quantum-Size-Related Properties, and Applications toward Biology, Catalysis, and Nanotechnology. Chemical Reviews (2004). 104, 293-346.

71 –Eustis S and El Sayed MA. Why gold nanoparticles are more precious than pretty gold: Noble metal surface plasmon resonance and its enhancement of the radiative and nonradiative properties of nanocrystals of different shapes. Chemical Society Reviews (2006). 35, 209-217

72 –Willets KA and Van Duyne RP. Localized surface plasmon resonance spectroscopy and sensing. Annual Reviews. Phys. Chem (2007). 58, 267-297.

73 - Noone HN, Krapcho AM, Neyman M, Aminou N, Waldron R, Altekruse W, Kosary SF, Ruhl CL, Tatalovich J, Cho Z, Mariotto H, Eisner A, Lewis MP, Chen DR, Feuer HS, Cronin EJ and *S*eer KA. Cancer Statistics Review, 1975−2009; National Cancer Institute: Bethesda, MD, 2012.

74 - Kelland L. The resurgence of platinum based cancer chemotherapy. Nature Reviews (2007). 7, 573-583.

75 - Johnstone, T. C, Suntharalingam, K and Lippard, S. J. Third Row Transition Metals for the Treatment of Cancer. Philosophical Transactions of the Royal Society (2015). 373.

76 - Rabik, C. A and Dolan, M. E. Molecular Mechanisms of Resistance and Toxicity Associated with Platinating Agents. Cancer Treatment Reviews (2007). 33: 9 −23.

77 - Lovejoy, K. S, Todd, R. C, Zhang, S, McCormick, M. S, D'Aquino, J. A, Reardon, J. T, Sancar, A, Giacomini, K. M and Lippard, S. J. cis-Diammine(pyridine)chloroplatinum(II), a

Monofunctional Platinum(II) Antitumor Agent: Uptake, Structure, Function, and Prospects. Proceedings of the National Academy of Sciences of the U. S. A (2008). 105, 8902−8907.

78 –Ishida S, Lee J, Thiele DJ and Herskowitz I. Uptake of the anticancer drug cisplatin mediated by the copper transporter Ctr1 in yeast and mammals. Proceedings of the National Academy of Sciences of the U. S. A (2002). 99 (22): 14298-14302

79 –Ishida S, McCormick F, Smith-McCuneK and Hanahan D. Enhancing tumor-specific uptake of the anticancer drug cisplatin with a copper chelator. Cancer Cell (2010). 17(6): 574–583.

80 –Franke RM, Kosloske AM, Lancaster CS, Filipski KK, Hu C, Zolk O, Mathijssen RH and Sparreboom A. Influence of Oct1/Oct2-Deficiency on Cisplatin-Induced Changes in Urinary N-Acetyl-β-D-Glucosaminidase. Clinical Cancer Research (2010). 16(16): 4198–4206.

81 - Shen DW, Pouliot LM, Hall MD, and Gottesman MM. Cisplatin Resistance: A Cellular Self-Defense Mechanism Resulting from Multiple Epigenetic and Genetic Changes. Pharmacological Reviews (2012). 64(3): 706–721.

82 - Johnstone, T. C, Wilson, J. J and Lippard, S. J. Monofunctional and Higher-Valent Platinum Anticancer Agents. Inorganic Chemistry (2013). 52, 12234−12249.

83 - Chen, Y, Heeg, M. J, Braunschweiger, P. G, Xie, W and Wang, P. G. A Carbohydrate-Linked Cisplatin Analogue Having Antitumor Activity. Angewandte Chemie International Edition. (1999). 38, 1768−1769.

84 – Provencher-Mandeville, J, Descôteaux, C, Mandal, S. K, Leblanc, V, Asselin, É and Bérubé, G. Synthesis of 17β-EstradiolPlatinum(II) Hybrid Molecules Showing Cytotoxic Activity on Breast Cancer Cell Lines. Bioorganic & Medicinal Chemistry Letters (2008). 18, 2282−2287.

85 – Ndinguri, M. W, Solipuram, R, Gambrell, R., Aggarwal, S and Hammer, R. P. Peptide Targeting of Platinum Anti-Cancer Drugs. Bioconjugate Chemistry (2009). 20, 1869−1878.

86 - Aronov, O, Horowitz, A. T, Gabizon, A and Gibson, D. FolateTargeted PEG as a Potential Carrier for Carboplatin Analogs. Synthesis and in Vitro Studies. Bioconjugate Chemistry (2003). 14, 563−574.

87 - Wilson, J. J and Lippard, S. J. Synthetic Methods for the Preparation of Platinum Anticancer Complexes. Chemical Reviews (2014). 114, 4470−4495.

88 – Wilson, W and Hay, M. Targeting hypoxia in cancer therapy. Nature Reviews Cancer (2011). 11: 393-410.

89 - Squibb BM Report. “A Randomized Phase II Study of Satraplatin (JM216) or Standard Platinum Therapy in Patients with Late Relapses of Epithelial Ovarian Cancer (CA 142-006)”, Jun 9, 1998. Accession no. 910068667.

90 - Trudeau, M, Stuart, G, Hirte, H, Drouin, P, Plante, M, Bessette, P, Dulude, H, Lebwohl, D, Fisher, B and Seymour, L. A Phase II Trial of JM-216 in Cervical Cancer: An NCIC CTG Study. Gynecologic Oncology (2002). 84, 327−331.

91 - Sternberg, C. N, Whelan, P, Hetherington, J, Paluchowska, B, Slee, P. H. Th. J, Vekemans, K, Van Erps, P, Theodore, C, Koriakine, O, Oliver, T, Lebwohl, D, Debois, M, Zurlo, A and Collette, L. Phase III Trial of Satraplatin, an Oral Platinum Plus Prednisone vs. Prednisone Alone in Patients with Hormone-Refractory Prostate Cancer. Oncology (2005). 68: 2−9.

92 - Shi, Y, Goodisman, J and Dabrowiak, J. C. Cyclodextrin Capped Gold Nanoparticles as a Delivery Vehicle for a Prodrug of Cisplatin. Inorganic Chemistry (2013). 52: 9418−9426.

93 - Juris A, Balzani V, Barigelletti F, Campagna S, Belser P and Von Zelewsky A, Ru(II) polypyridine complexes: photophysics, photochemistry, electrochemistry and chemiluminescence. Coordination Chemistry Reviews (1988). 84: 85-277.

94 - Leung MY, Leung SYL, Wu D, Yu T and Yam VWW. Synthesis, Electrochemistry, and Photophysical Studies of Ruthenium(II) Polypyridine Complexes with D–π–A–π–D Type Ligands and Their Application Studies as Organic Memories. Chemistry a European Journal (2016). 22: 14013 – 14021.

95 - Adams SJ, Lewis DJ, Preece JA and Pikramenou Z. Luminescent Gold Surfaces for Sensing and Imaging: Patterning of Transition Metal Probes. ACS Applied Mater Interfaces (2014). 6: 11598−11608.

96 - Campagna S, Puntoriero F, Nastasi F, Bergamini G and Balzani V. Photochemistry and Photophysics of Coordination Compounds I. Photochemistry and Photophysics of Coordination Compounds I, eds. V. Balzani and S. Campagna, Springer Berlin Heidelberg, 2007.

97 - Cook MJ, Lewis AP, McAuliffe GSG, Skarda V, Thomson AJ, Glasper JL and Robbins DJ. Luminescent metal complexes. Part 1. Tris-chelates of substituted 2,2′-bipyridyls with ruthenium (II) as dyes for luminescent solar collectors. Journal of the Chemical. Society., Perkin Transactions. 2, 1984, 1293-1301.

98 - Innocenzi P, Kozuka H and Yoko T. Fluorescence Properties of the $Ru(bpy)_3^{2+}$ Complex Incorporated in Sol-Gel-Derived Silica Coating Films. Journal of Physical Chemistry. B (1997). 101: 2285-2291.

99 –Gill MR and Thomas JA. Ruthenium(II) polypyridyl complexes and DNA—from structural probes to cellular imaging and therapeutics. Chemical Society Reviews (2012). 41: 3179–3192

100 - Lutterman DA, Chouai A, Liu Y, Sun Y, Stewart CD, Dunbar KR and Turro C. Intercalation is not required for DNA light-switch behavior. J. American Chemical Society (2008). 130: 1163.

101 - Osborne SAM and Pikramenou Z. Highly luminescent gold nanoparticles: effect of ruthenium distance for nanoprobes with enhanced lifetimes. Faraday Discussions (2015). 185: 219-231.

Chapter 2 – GNP Preparation & Probe Development

2.1. Nanoparticle Development

2.1.1. GNP-Cit and GNP-GSH-Folate

Nanoparticles have been used extensively in the literature for the delivery of payloads, be it therapeutic compounds and / or imaging agents, to cancer cells and tissues (see section 1.2.4). One of the most common gold nanoparticle systems to be utilised for the delivery of imaging agents or therapeutics is citrate capped gold nanoparticles. There are well-established synthetic protocols for the development of specific size batches of these GNPs, displaying little standard deviation (5-8%) and polydispersity (average <3%)[1]. An example of such a protocol is that of the Turkevich method[2], or the more frequently used, advanced Turkevich method developed by Vossmeyer *et al*[3]. An adaptation of this method was used in the present research for the development of 13nm citrate capped gold nanoparticles, said adaptation was published in the works of Osborne *et al*[4]. This nanoparticle preparation protocol allows for the development of 13nm, 25nm, 50nm and 100nm citrate capped gold nanoparticles batches sequentially through the implementation of a simple batch method, delivering improved batch uniformity (over the literature) and consistently reproducible results.

Whilst the development of specific sized citrate capped gold nanoparticles is well established within the field, a method for the preparation of consistently sized, low polydispersity folate capped gold nanoparticles is yet to be documented. As previously stated, there is ongoing research and indeed published works into the development of such a protocol. Therefore, initial efforts in the present research were made towards the synthesis of consistently sized folate capped gold nanoparticles through methods reported in the literature.

One such example of a folate capped gold nanoparticle preparation is that developed by Zhang *et al*[5]. This method utilises 13nm citrate capped gold nanoparticles with folic acid tethered to their surface via a glutathione linker. An overview of this surface adaptation is depicted in Figure 201.

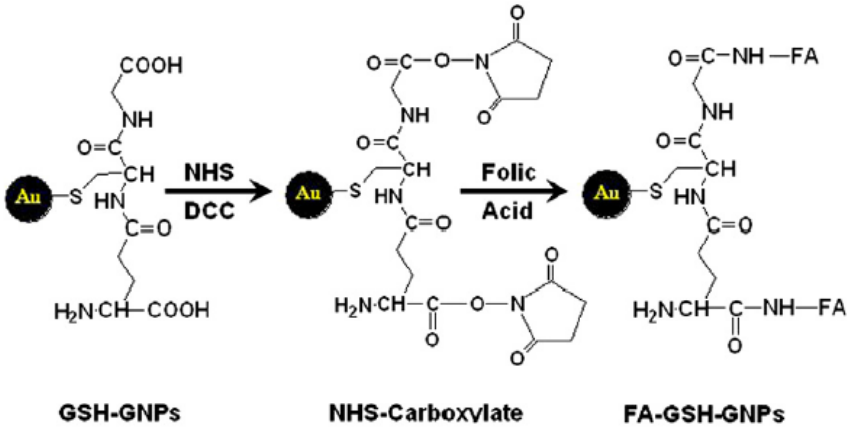

Figure 201: Schematic representation of surface modification of citrate capped gold nanoparticles for the tethering of folic acid via glutathione[5].

GSH = Glutathione. FA = Folic Acid. Au = GNP surface.

A batch of 13nm citrate capped gold nanoparticles (GNP-CIT) was prepared as per the improved Turkevich method (see experimental section 2.3.2 for full details) and their size characterised by DLS (see Figure 202). The surface of the citrate capped GNPs were then functionalised with glutathione molecules via thiol tethering. The carboxylic acid moieties at the distal ends of said glutathione tethers were functionalised to the NHS ester and then subsequently formed amide linkages to the amino groups of folic acid as per the schematic representation in Figure 201 (see experimental section 2.3.2 for full details). It should be noted, given that folic acid comprises only one primary amine group, there is theoretically little purification required and no side reactions (as reported by Zhang *et al*[5]).

a)

		Size (d.nm):	% Intensity:	St Dev (d.nm):
Z-Average (d.nm): 19.29	Peak 1:	23.50	100.0	8.976
PdI: 0.200	Peak 2:	0.000	0.0	0.000
Intercept: 0.850	Peak 3:	0.000	0.0	0.000
Result quality : Good				

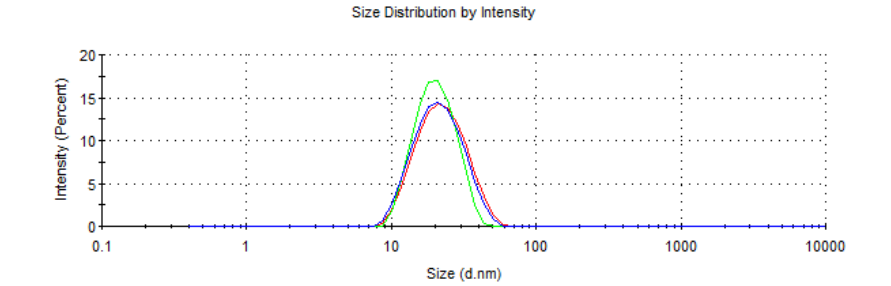

b)

		Size (d.nm):	% Number:	St Dev (d.nm):
Z-Average (d.nm): 19.29	Peak 1:	12.52	100.0	3.575
PdI: 0.200	Peak 2:	0.000	0.0	0.000
Intercept: 0.850	Peak 3:	0.000	0.0	0.000
Result quality : Good				

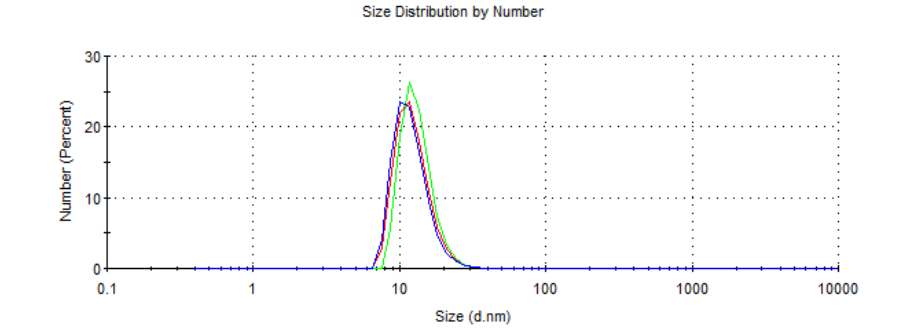

Figure 202: a) Size by intensity of GNP-Cit as prepared by Turkevich method, showing monodisperse sample with good PDI and standard deviation, b) Size by number of the same GNP-Cit batch, giving a more accurate representation of the actual nanoparticle size range.

Theoretically, this glutathione tethering method gives a good loading potential as it allows for two units of folic acid per unit of glutathione. However, in practice, this method proves to make the nanoparticles unstable, with the literature noting that the nanoparticles “may” aggregate and crash out of solution. The scientist invested efforts to vary many of the conditions (pH,

loading volume, nanoparticle concentration) in order to improve stability and it was their optimal reported conditions that were employed in the present research.

Despite using the optimal conditions as reported in the literature, the present research observed the same instability, with aggregation seemingly occurring more frequently than reported. The resulting GNP-GSH-Folate particles displayed a typical stability of 24 hours, after which, aggregation was evident by colour change and DLS (large peak ~1µm, size by intensity). The large polydispersity (PDI - 0.522) and standard deviation (StDev - 20.03) of the GNP-GSH-Folate particles (as can be seen in Figure 203) prevented an accurate calculation of the mean size of the particles as it was not possible to obtain clean TEM data. It was anticipated that the particles would be further de-stabilised upon loading with imaging and therapeutic agents in subsequent research and therefore this protocol was not pursued any further.

a)

		Size (d.nm):	% Intensity:	St Dev (d.nm):
Z-Average (d.nm): 80.92	Peak 1:	139.7	100.0	83.61
PdI: 0.482	Peak 2:	0.000	0.0	0.000
Intercept: 0.858	Peak 3:	0.000	0.0	0.000

Result quality : Refer to quality report

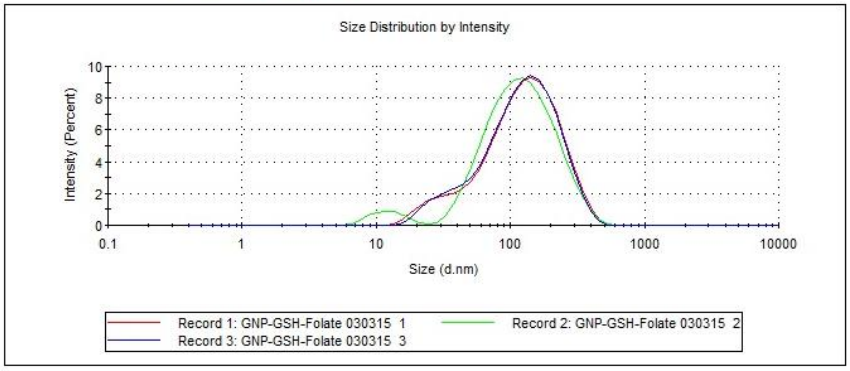

b)

		Size (d.nm):	% Number:	St Dev (d.nm):
Z-Average (d.nm): 114.9	Peak 1:	41.71	100.0	20.03
PdI: 0.522	Peak 2:	0.000	0.0	0.000
Intercept: 0.828	Peak 3:	0.000	0.0	0.000

Result quality : Refer to quality report

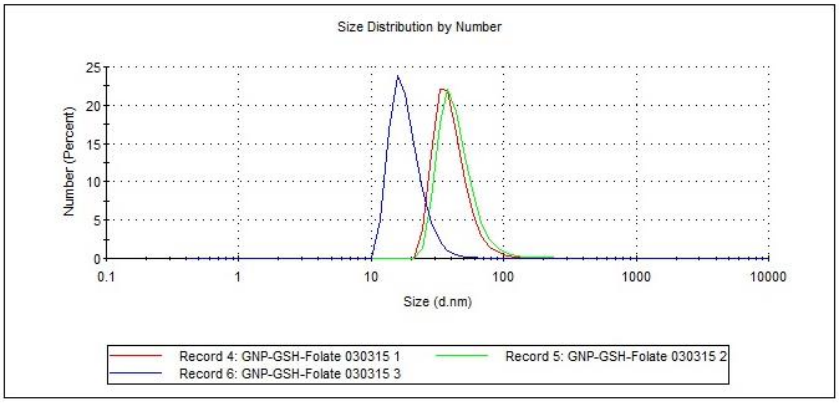

Figure 203: a) Size by intensity for GNP-GSH-Folate, showing highly polydisperse nature of the sample, with a high PDI and standard deviation, b) Size by number for the same sample of GNP-GSH-Folate, showing the variation in computed size as a result of the highly polydisperse nature of the sample.

2.1.2. GNP-Folate

Subsequent investigations were made into the direct synthesis of folate capped gold nanoparticles (GNP-Fol). Zhang *et al.*[6] utilised a microwave reactor as opposed to a heating mantle, which is significant in that the latter is typically employed in the majority of the GNP

methods, including that of the Turkevich method. Heating mantles are typically utilised in GNP research as they allow for a more progressive heating and cooling method of the GNP solution. This progressive heating and cooling is believed to be significant in the literature for assisting with polydispersity and batch consistency.

The Zhang *et al* microwave method does afford a somewhat consistent method for the production of GNP-Fol. However, it does still suffer from poor overall yield of particles (~10mL, 0.5nM), unused starting materials that must be dialysed out of solution and a varying degree of polydispersity. However, it was this preparation that was optimised by former Hannon Group Post-Doctoral researcher Ana Caballero and formed the scope for initial GNP-Fol protocol studies within the present research.

Caballero's method maintained the use of the microwave reactor whilst adjusting the ratios, concentrations, volumes and order of addition of the reagents employed (see experimental section 2.3.2 for full details). Through these preparation amendments the Caballero method increased the yield of the reaction to ~15ml (a 50% increase) whilst maintaining a comparable size, polydispersity and batch consistency to that of the originating Zhang method. As aforementioned, the Caballero method was employed for much of the foundation work on folate capped gold nanoparticles within this research, however, it still lacked sufficient batch consistency, with the nanoparticles ranging anything from 10nm to 30nm (see Figure 204 for typical DLS data). Furthermore, this 15mL batch protocol affords GNP-Fol with a concentration of ~0.3nM that is quite frequently polydisperse. To emphasise the batch variability of the Caballero method, Table 201 presents a range of the nanoparticle data gathered from a selection of the experiments run.

a)

		Size (d.nm):	% Number:	St Dev (d.nm):
Z-Average (d.nm): 26.53	Peak 1:	17.62	100.0	4.701
PdI: 0.182	Peak 2:	0.000	0.0	0.000
Intercept: 0.918	Peak 3:	0.000	0.0	0.000

Result quality : Good

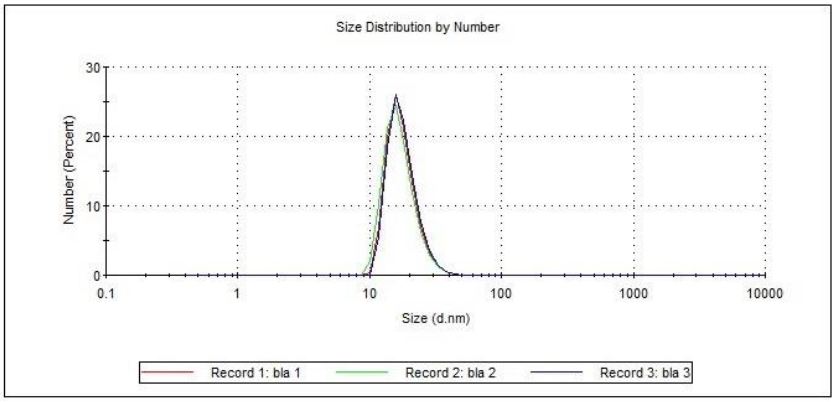

b)

		Size (d.nm):	% Intensity:	St Dev (d.nm):
Z-Average (d.nm): 26.53	Peak 1:	30.40	100.0	10.97
PdI: 0.182	Peak 2:	0.000	0.0	0.000
Intercept: 0.918	Peak 3:	0.000	0.0	0.000

Result quality : Good

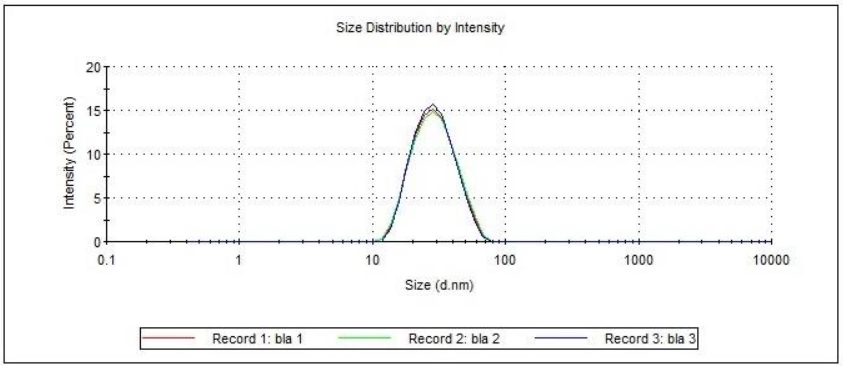

Figure 204: Typical sizing data for GNP-Fol as prepared by the Caballero method, recorded by DLS. a) Size by number for GNP-Fol, with an acceptable PDI (0.182) and relatively broad standard deviation (4.701), b) Size by intensity for the same sample of GNP-Fol, showing the variation in computed size as a result of the broad distribution of nanoparticle size, with the same PDI (0.182) but expectedly much larger standard deviation (10.97).

Experiment	Average Nanoparticle Size by Number (nm)	Average Nanoparticle Size by Intensity (nm)	Average PDI	StDev (nm)
1	13.23	21.48	0.253	3.425
2	28.76	35.87	0.513	6.78
3	17.70	27.88	0.208	4.525
4	17.95	28.55	0.197	4.650
5	24.45	33.27	0.44	7.23

Table 201: Tabulated key experimental data to exemplify the variation in batch consistency for the Caballero GNP-Fol synthesis. Experiments 1) – N) were run under identical conditions with the same protocol.

From Figure 204 and Table 201, the batch variation for the Caballero method is rather significant. From the tabulated data alone, it is evident that there is a spread in the average size by number of the batches of 15.53nm, with a PDI as high as 0.513, which is a measure of significant polydispersity within the system. With regard to the latter, it can be seen in figure 201, the size by intensity plot (Figure 204, b)) shows a typical peak broadness, signifying an acceptable degree of polydispersity, for which, the PDI value was 0.182. It is generally known amongst users of such DLS instrumentation, a PDI above 0.24 is tending toward being quite polydisperse.

Given that one of the key research goals was to draw comparisons on cellular uptake of GNP-Cit and GNP-Fol the size range and batch consistency of GNP-Fol is of utmost importance. Given that the improved Turkevich preparation yields GNP-Cit that are ~13nm (±2nm), monodisperse and with a concentration of ~1nM consistently. GNP-Fol must be of a

comparable size, polydispersity and concentration to the GNP-Cit system. Accordingly, a new preparation for GNP-Fol was developed and utilised throughout the present research.

2.1.3. Young GNP-Fol Preparation

Initial efforts utilised the lessons of both the Caballero and Turkevich methods. It was assumed that the polydispersity issues of the Caballero method were likely stemming from the use of the microwave reactor over the conventional heating mantle. It was noted that upon completion of the heating stage in the microwave reactor of the Caballero method (see experimental section 2.3.2 for full details), the reactor not only cooled the solution rapidly, but it also appeared to stop stirring the nanoparticle solution. Therefore, whilst the nanoparticles were still being produced / growing, the solution was being cooled and no longer stirred, which could potentially account for the inconsistent and abnormal nanoparticle growth within the solution. By comparison, in the Turkevich method, the nanoparticles are allowed to gradually cool down to room temperature whilst being constantly stirred, which is believed to be a key contributing factor to the development of monodisperse and significantly spherical nanoparticles.

As a result of these hypotheses, early adaptations looked to utilise the apparatus of the Turkevich method, along with the orders of addition and reaction times, whilst replacing like for like reagents and maintaining ratios and concentrations of the respective reagents.

Variation 1

The first variation (Variation 1) toward the development of a new protocol for GNP-Fol sought to mimic the exact method of the improved Turkevich method[3]. Trisodium citrate and citric acid were replaced with sodium folate and folic acid respectively, maintaining their molar equivalents and ratios. EDTA was also utilised as the literature cited this compound as playing

a key (yet, not fully understood) role in the production of more spherical GNP-Cit. Variation 1 did not successfully synthesise gold nanoparticles and no changes were observed to the colour or composition of the solution were observed.

This result was not overly unexpected as there were a significant number of changes made to the original Caballero protocol and furthermore, no protocol of the literature (for GNP-Fol synthesis) featured concurrent use of folic acid and sodium folate, or the use of EDTA. Additional efforts were made into adjusting the ratios of the reagents employed and the overall volume of the reaction, however, there was still no successful production of nanoparticles. Given that no nanoparticles were being formed the most likely conclusion was that the gold salt was not successfully being reduced in solution and therefore no nanoparticles were being seeded for growth.

pH Dependent Reduction

It was hypothesised that the pH of the solution may have been a key factor in the lack of reduction events, noting that Caballero emphasised substantial efforts into optimising the amount of sodium hydroxide titrated post addition of sodium folate to the stirring solution of gold salt (see experimental section 2.3.2), indicating that a specific pH range was essential. Furthermore, Vossmeyer *et al.*[3] emphasise that a pH of 5.6 is optimal for the improved Turkevich synthesis, indicating a potentially fundamental reliance on pH. Accordingly, the pH was recorded for the optimised Caballero method at four time points; 1) primed reaction solution, 2) post reagent addition, 3) post sodium hydroxide addition and 4) end of the reaction. Once these key pH points were established, the pH of Variation 1 and the Turkevich protocol at points 1), 2) and 4) were measured (point 3 could not be measured as there is no additional sodium hydroxide addition step or equivalent). These measurements were taken so as to allow

for a more complete overview of the pH range and to potentially allude to the reason for the lack of production of GNP-Fol (these pH's can be seen in Table 202).

	Measured pH at Respective Time Point			
Method	1	2	3	4
Caballero	5.1	8.5	11.2	10.5
Variation 1	5.8	5.5	-	5.6
Turkevich	5.6	5.3	-	5.5

Table 202: Tabulated pH measurements associated with various stages of the Caballero protocol, Variation 1 and the Turkevich protocol, at various time point equivalents, which include; 1) primed reaction solution, 2) post reagent addition, 3) post sodium hydroxide addition and 4) end of the reaction. The data showing the significantly basic pH range of the Caballero protocol by comparison to the mildly acidic pH range of the improved Turkevich protocol, with Variation 1 expectedly showing a pH range toward that of improved Turkevich.

It is evident from the data of Table 202 that the Caballero protocol operates under severely basic conditions, exhibiting a pH of 8.5 post the addition of sodium folate and a pH of 11.2 post the addition of sodium hydroxide, and exhibiting a final pH of 10.5. By comparison, the Turkevich protocol operates under somewhat acidic conditions, exhibiting a pH of 5.3 post the addition of gold salt and a final pH of 5.5. It was therefore hypothesised that no nanoparticles were successfully formed in Variation 1 as a result of the difference in pH and, more specifically, fundamental differences in the mechanism for reduction of the gold salt between the citrate and the folate systems. The hypothetical mechanism for gold salt reduction in the citrate nanoparticle method as set forth by Vossmeyer *et al* is highlighted in Figure 205, whilst

the structure of folic acid and potential equivalent redox reaction sites is depicted in Figure 206.

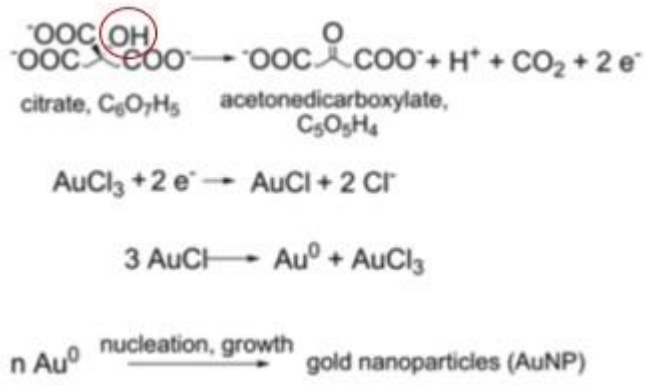

Figure 205: Adaptation of Figure 1 from Vossmeyer *et al.*[3] paper on the advanced Turkevich method, reporting the proposed mechanism of the Turkevich synthesis. Redox reaction of citrate and the gold salt (Au(III) precursor) produces Au(I) ions and acetonedicarboxylate. Disproportionation of Au(I) produces Au(0) and Au(III), with the former initiating nucleation and growth to form citrate coated gold nanoparticles.

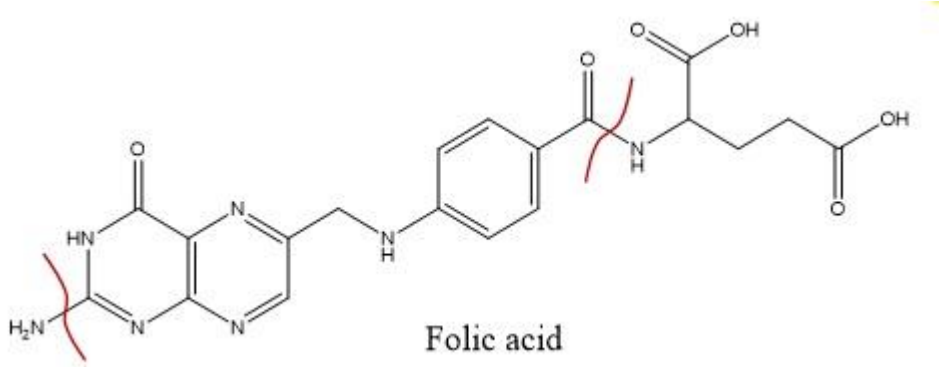

Figure 206: Proposed sites capable of being oxidised to produce electrons which can subsequently partake in a redox reaction with gold salt, reducing Au(III) to form Au(I), which may then subsequently go on to form Au(0) and undergo nucleation / growth of folate capped gold nanoparticles, much in the same way as proposed by Vossmeyer *et al*[3].

As taught by Vossmeyer, and therefore, in the case of citrate capped gold nanoparticle formation, there is a hydroxyl group bound to the same carbon as a carboxylic acid (see Figure 205) and it is oxidation at this site which produces the electrons required to then reduce the gold salt (Au(III)) to Au(I) and go on to initiate nanoparticle formation (see introduction section 1.2.2 for full details)[3]. In contrast, there is no comparable hydroxyl group available in folic acid and therefore the gold salt must be reduced via the formation of some other intermediate. It is proposed that this may be at either of the amide / amine bonds highlighted in Figure 206. Such species could theoretically mimic the function of acetonedicarboxylate, organizing Au(I) into polymolecular complexes, whilst also facilitating the production of the electrons required for gold salt reduction, the combination of which ultimately leads to the nucleation and growth of Au(0) to Au NP's. However, this hypothesis requires much further experimentation and deliberation. In particular, the intermediate structure responsible for subsequent gold salt reduction must be identified so as to better understand the process. A potential experiment for this might be to take samples at different time points of the experiment and analyse them via IR Spectroscopy so as to analyse the functional groups present. Additionally, mass spectrometry and NMR studies of said samples would hopefully help to better identify any intermediate structures.

Variation 2

In light of these pH investigations, and upon review of the literature regarding the aforementioned mechanism for the production of citrate capped gold nanoparticles, the pH of the system was systematically adjusted across a series of reactions. Accordingly, to reduce the pH of the reaction mixture that was heated prior to the addition of the gold salt (see experiment section 2.3.2) the ratio of sodium folate to folic acid was adjusted. Incremental increases in the ratio of sodium folate to folic acid were investigated, maintaining the ratio of folic moieties to

gold salt moieties, effectively lowering the pH of the system whilst maintaining other key parameters. These pH dependent experimental studies are not tabulated, however, it is noteworthy that GNP-Fol formation was unsuccessful until a minimum pH of 10.5 was attained, whereupon GNP-Fol formation was feasible, but with poor resulting nanoparticle suspensions (Variation 2).

Variation 2 required overnight refluxing of the reaction mixture before nanoparticles were successfully formed. It is believed that the point of nanoparticle seeding and subsequent growth was after approximately 12 hours of reflux. It is believed that this very slow rate of gold salt reduction led to an uneven rate and distribution of nanoparticle seeding events, which subsequently gave batches of GNP-Fol that were of a high polydispersity (PDI 0.4), highly non spherical and inconsistent in concentration (1-2nM) and average size (16nm – 25nm, characterized only by DLS, size by Number and Intensity). This theory is supported by the literature, with Vossmeyer *et al* emphasising the importance of rapid reductive events in the GNP-Cit method, which is believed to facilitate a nanoparticle system where the majority of nanoparticle growth events are initiated largely simultaneously[3]. Simultaneous nanoparticle seeding and rate of growth gives a significantly greater chance of monodisperse and uniform nanoparticles, the kind of which are of course sought after for the GNP-Fol system so as to afford a comparable platform for nanoparticle investigations.

Variation 3

Further investigation of GNP-Fol synthesis utilising the core methodology of Vossmeyer was conducted, systematically altering further parameters including temperature (80-150°C), volume (50-125mL), molar ratios, heat source (mantle vs oil bath) and reaction time (10 mins to overnight). None of these alternative parameters afforded a GNP-Fol system with

comparable polydispersity, size, shape, concentration and batch consistency of the Turkevich GNP-Cit method. Subsequent efforts therefore reverted to the system and parameters of the Caballero method.

Whilst the Caballero method gave poor parameters for GNP-Fol (batch consistency, polydispersity, concentration etc), it was re-visited as it was at the very least able to produce GNP-Fol within a comparable reaction time to that of GNP-Cit (Osborne / Vossmeyer)[3/4]. As such, the reductive events of the reaction must also have been occurring within a significantly shorter timeframe than that of the aforementioned GNP-Fol experiments and therefore, is a step closer to nanoparticle uniformity and batch consistency. It was previously postulated that the resulting poor polydispersity and batch consistency of the Caballero method may be as a result of the microwave reactor employed, with aggressive heating and cooling windows and non-continuous stirring of the reaction mixture. Accordingly, efforts leading on from this research utilised alternative heat sources such as a heating mantle or a stirrer hotplate with an oil bath.

Variation 3 utilised a stirrer hotplate and oil bath as an alternative heat source so that the reaction may be gradually heated and cooled and the solution stirred at all times. For this first deviation from the Caballero method, the entirety of the method was maintained, only the heat source was replaced. Initial efforts were unsuccessful, however, after amending the order of addition of sodium folate and sodium hydroxide, Variation 3 successfully formed GNP-Fol. However, with a PDI of 0.3 and a particle size range of ±10, it was evident that polydispersity and batch consistency issues still remained. Moreover, it was noted that the reduction of the gold salt still took significantly longer than that of the literature (~10 minutes) and therefore this may have resulted in the aforementioned poor nanoparticle uniformity.

In addition to the slow rate of gold salt reduction, it was theorised that these poor metrics were potentially the result of the difference in the "charged reaction mixture" of the method[3]. That is to say, the improved Turkevich method effectively primes the reaction before adding the gold salt, heating a solution of citric acid, trisodium citrate and EDTA, thus priming the system with the reductive species required prior to adding the gold salt. The Caballero method on the other hand primes a gold salt solution and then relies on uniformity of the incurred reductive events upon addition of the sodium folate and sodium hydroxide. It was therefore hypothesised that the poor nanoparticle uniformity may be as a result of an effective lag in the production of the reductive species as opposed to having the system primed with these in the first instance.

Variation 4

Accordingly, the subsequent reaction, Variation 4, saw almost the inverse of the charged mixture of Caballero, with a solution of sodium folate refluxed prior to the addition of the gold salt, followed by sodium hydroxide to keep the pH of the solution within the 10.5 – 12 range believed to be required. Variation 4 achieved gold salt reduction within 15 seconds and was the first successful adaptation of the Caballero method in view of the teachings of Vossmeyer *et al*.

The metrics for GNP-Fol produced by Variation 4 were an improvement over those of the Caballero method, with a PDI of 0.16 and a StDev of ±8, however, they were considered to still be too far removed from those of GNP-Cit[3, 4].

Variation 5

Further experiments varied reagent volumes (for nanoparticle uniformity and for scale up), reagent concentrations (for nanoparticle yield) and reaction conditions (for rate of reduction and nanoparticle uniformity). In relation to reagent volume, a first adaptation utilised a significantly more concentrated solution of gold salt, dissolving the same quantity in 1mL of deionised water, as opposed to 18mL in the Caballero method and 25mL in the improved Turkevich method. This adaptation allowed the gold salt to be added in a single movement, directly and rapidly into the vortex of the stirring reaction mixture via a 1000µL Gilson pipette. The effect of which was a significantly improved polydispersity index and standard deviation of nanoparticles formed. It is believed that this is as a result of a more homogenised solution of reductive events, with a significantly improved proportion of the gold salt being converted to Au(0) simultaneously and thus, the majority of the nanoparticles being formed at a similar rate and from a similar time point. Variation 5 yielded a 20mL suspension of ~1nM GNP-Fol, with an average size of ~15nm ±3nm.

Variation 6

A second adaptation scaled up the volumes of all reagents employed, looking to increase the yield of the protocol to comparable volumes of the improved Turkevich method. Unlike previous scale up attempts, Variation 6 utilised the methodology of Variation 5 and merely scaled up the reaction with the exception of the volume of gold salt, which was maintained at 1mL in water and had its concentration altered. This scale up successfully a GNP-Fol suspension, however, the metrics for this method were significantly poorer than required, with hgh polydispersity, standard deviation and a weak particle concentration (~0.2nM). The most significant metric perhaps is the concentration of the reaction, which, despite using 10 times more gold salt and more sodium folate, the effective nanoparticle yield the reaction only

increased by 70%. Thus, the protocol was successfully scaled up in volume, but was significantly less efficient at nanoparticle formation, yielding a dilute suspension with a significant proportion of starting materials or undesired side reactions.

Summary of Findings

Extensive efforts were invested in the development of a novel direct synthetic protocol for the production of folate capped gold nanoparticles. All key reaction parameters were varied, including equipment used, order of addition of reagents, volumes, and concentration etc. Variation 5 was the most successful protocol, representing an adaptation of the Caballero method with teachings drawn from the Osborne and Vossmeyer protocols[3, 4]. Variation 5 presents a protocol for the production of GNP-Fol in a comparable timeframe to Caballero, with significantly improved metrics of the system into a comparable range to those afforded by the Osborne method for GNP-Cit. Variation 5 was therefore utilised for all nanoparticle studies reported hereafter and is termed the "Young Protocol".

2.2. Imaging Agent Development

2.2.1. Transition Metal Based Probes

Ruthenium and Iridium based transition metal imaging agents have been studied within the Pikramenou group for a significant period of time and, accordingly, extensive research efforts have been invested into novel agent development and full characterisation of the emissive capabilities of the probes both on their own and when loaded onto GNP-Cit (see introduction section 1.4.2 for full details). As such, no efforts were made in the present research into the development of novel probes, nor into ascertaining the emissive parameters of such agents. Instead, the loading capacity of a selection of established probes was investigated when loaded onto the surface of GNP-Fol as prepared by the Young protocol. The probes of interest

were RuBpySS, IrBpySS and RuPhenSS, affording a comparison to be drawn between the metal core employed and the nature of the ligands facilitating MLCT (see introduction section 1.4.1). These transition metal based probes are well established within the literature by both Adams[7] and Osborne[4] and their structures can be seen in Figure 207. The associated synthetic pathways to the production of RuBpySS and IrBpySS are represented in Figure 208. It shall be appreciated that the pathway to RuPhenSS varies only in the production of [$RuPhen_2Cl_2$] as the intermediary complex as opposed to [$RuBpy_2Cl_2$], the tethering ligand remains the same (full details in experimental section 2.3.3).

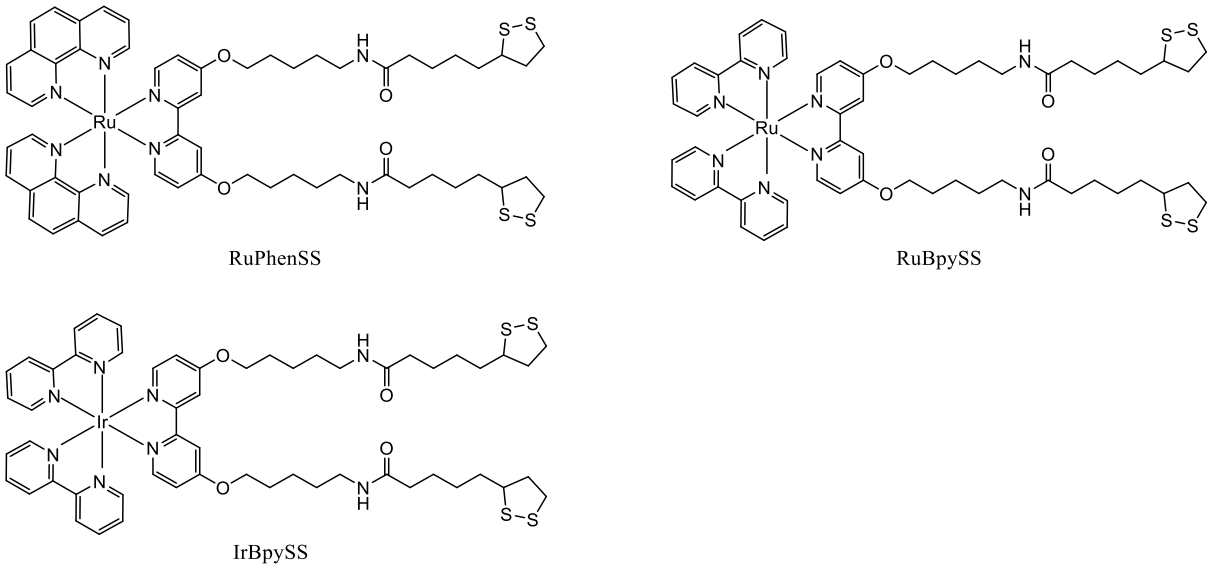

Figure 207: Chemical structures of the transition metal based imaging agents employed within nanoparticle loading and emissive capability studies. A) RuBypSS, B) IrBpySS and C) RuPhenSS.

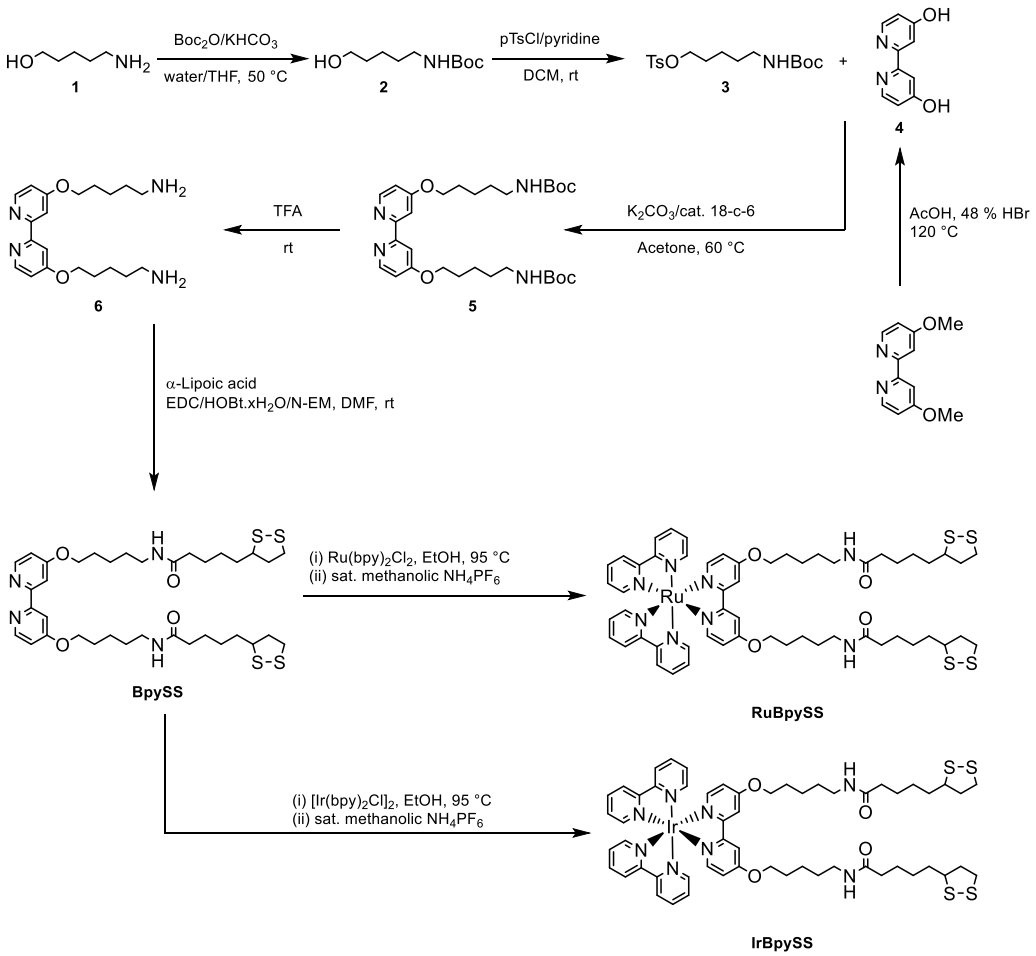

Figure 208: Synthetic route to RuBpySS and IrBpySS as outlined by Adams *et al.*[7].

In addition to the benefit of the established nature of the aforementioned probes within the research group, such transition metal probes typically exhibit numerous favourable properties, which include; a good stokes shift and relatively strong emissions (outlined in more depth in section 1.4.1 of the introduction), hence justifying their utilisation.

2.2.2. GNP Folate Loading Studies

The degree of stability of a nanoparticle system is a somewhat speculative and qualitative measure. As previously discussed (see introduction section 1.2), the most common parameters for ascertaining the stability of a nanoparticle system are:

- the degree of shift and broadening of the SPR (Surface Plasmon Resonance) band of the UV-Vis absorption spectrum;

- any induced polydispersity or general aggregation of the nanoparticles; and
- change in colour of the solution.

The binding of structures to the surface of gold nanoparticles induces a shift in the SPR band of the system. Upon binding, the SPR band will generally broaden and shift, with the latter being an increase or decrease in the absorption intensity and / or peak wavelength (λ_{max}). Therefore, the UV-Vis absorbance spectrum of each nanoparticle system was measured after incremental titrations with the respective fluorescent probe, with the degree of SPR band broadening and shifting recorded accordingly. With regards to induced polydispersity and aggregation, the polydispersity and average nanoparticle size of the systems were ascertained via DLS measurements at selective titration points. Any potential colour change of the respective nanoparticle suspension was qualitatively noted after each titration of the respective transition metal probe. The UV-Vis absorption spectra for these titration experiments are represented in Figure 208, whilst the associated SPR peak shifts are recorded in Table 203.

a)

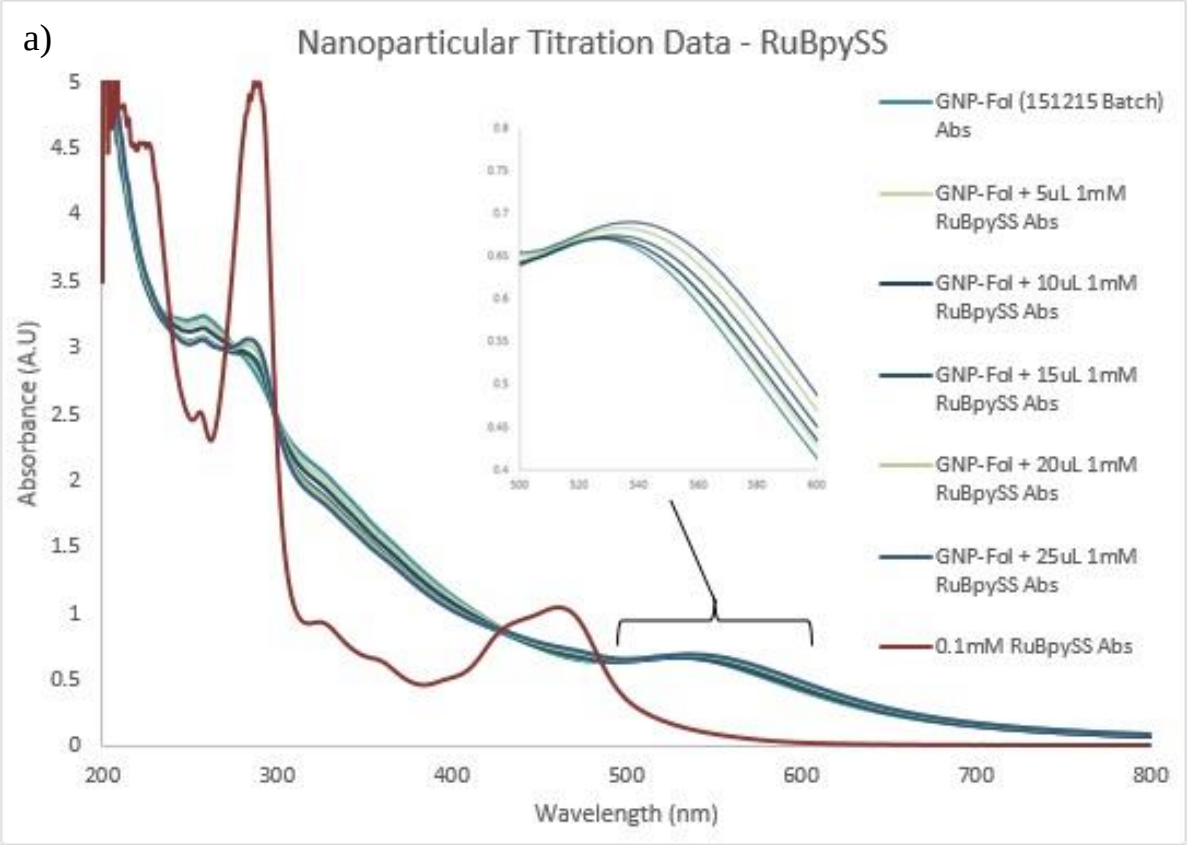
Nanoparticular Titration Data - RuBpySS
Absorbance (A.U)
Wavelength (nm)
GNP-Fol (151215 Batch) Abs
GNP-Fol + 5uL 1mM RuBpySS Abs
GNP-Fol + 10uL 1mM RuBpySS Abs
GNP-Fol + 15uL 1mM RuBpySS Abs
GNP-Fol + 20uL 1mM RuBpySS Abs
GNP-Fol + 25uL 1mM RuBpySS Abs
0.1mM RuBpySS Abs

b)

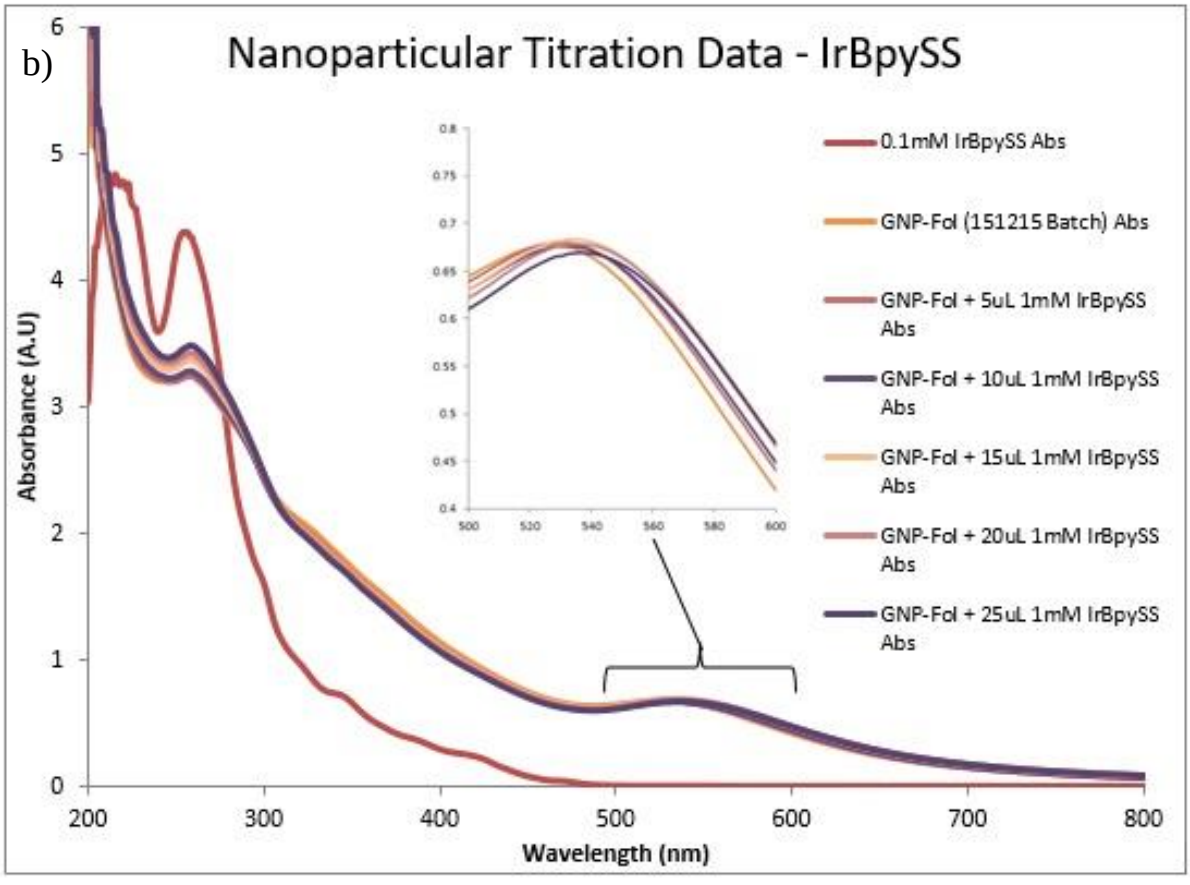
Nanoparticular Titration Data - IrBpySS
Absorbance (A.U)
Wavelength (nm)
0.1mM IrBpySS Abs
GNP-Fol (151215 Batch) Abs
GNP-Fol + 5uL 1mM IrBpySS Abs
GNP-Fol + 10uL 1mM IrBpySS Abs
GNP-Fol + 15uL 1mM IrBpySS Abs
GNP-Fol + 20uL 1mM IrBpySS Abs
GNP-Fol + 25uL 1mM IrBpySS Abs

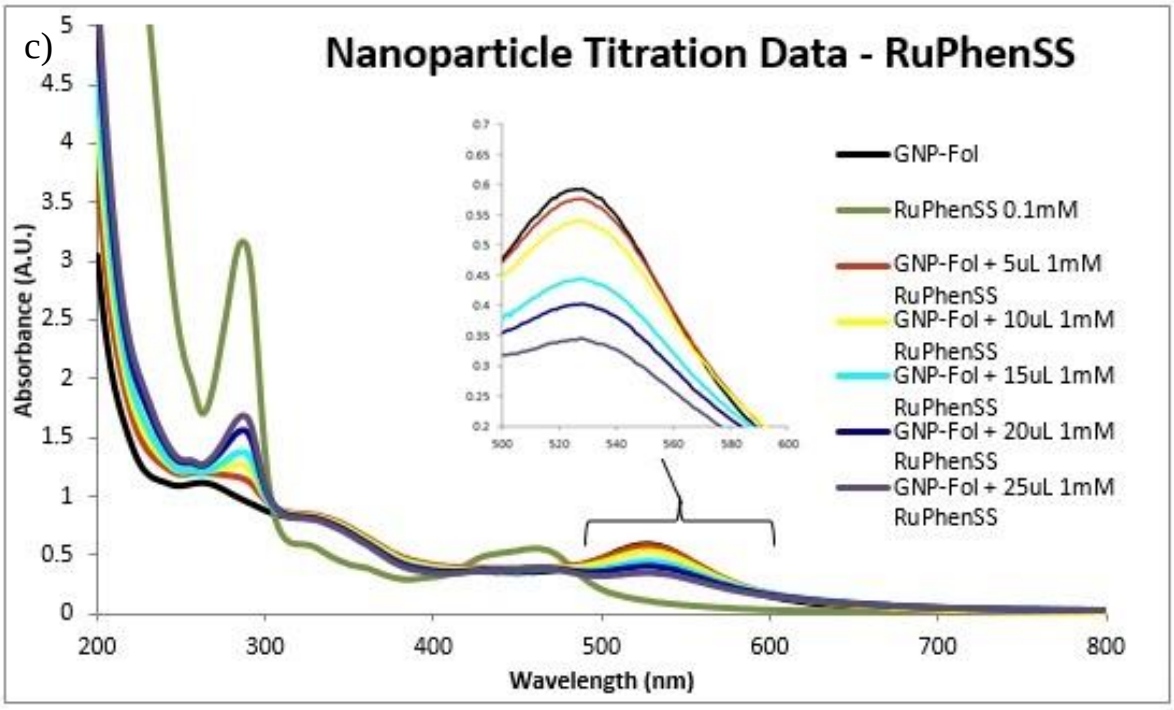

Figure 208: UV-Vis absorption spectra recorded for titrations of transition metal probes into a suspension of GNP-Fol (1mL ~1nM). a) Titration of RuBpySS (1mM), b) titration of IrBpySS (1mM) and c) titration of RuPhenSS (1mM).

	λ_{max} (nm)			Shift (nm), Intensity and wavelength		
Titration Volume (uL)	RuBpySS	IrBpySS	RuPhenSS	RuBpySS	IrBpySS	RuPhenSS
0	526	"	"	0	0	0
5	528	528	526	+0.01, +2	+0.01, +2	-0.02, 0
10	529	528	528	+0.01, +3	-0.02, +2	-0.03, +2
15	532	530	528	+0.02, +6	+0.04, +4	-0.13, +2
20	535	536	528	+0.04, +9	+0.01, +8	-0.19, +2
25	536	537	528	+0.05, +10	-0.02, +11	-0.27, +2

Table 203: Tabulated UV-Vis data in relation to shift of the SPR band in the UV-Vis absorption spectrum of GNP-Fol solutions upon titration with their respective transition metal probe. Data shows a significantly less affected λ_{max} shift for RuPhenSS titrations by comparison to the other probes, whilst a significant decrease in the absorption intensity is observed by comparison to the other probes.

It is evident from the data displayed in Figure 208 and Table 203 there are some quite important differences that can be observed in the aforementioned titration experiments. With regards to the RuBpySS and IrBpySS titrations, there is a steady incremental increase observed in the λ_{max} with incremental increases in the number of transition metal probe units available to bind to the surface of the nanoparticles. With each titration of 5µL of the respective fluorescent probe, there is a general shift of 1-4nm in the λ_{max} for the respective system. Where these systems differ however, is in the change in the intensity of the SPR band, with the band generally increasing in intensity for RuBpySS, whilst the band fluctuates and stays relatively similar in the IrBpySS system. Theoretically, it is assumed that upon successful binding of agents to the surface of nanoparticles the intensity of the SPR band should increase or decrease dependent upon the nature of the agent that is now bound.

Therefore, it might be assumed that the IrBpySS probes were not binding as successfully as the RuBpySS probes and therefore are less feasible for imaging studies. This theory is somewhat hard to prove / disprove on account of the differences in the excitation and emission profiles of the respective probes. An alternative owould be to utilise ICPMS so as analyse and quantify any present Ir within a nanoparticular system. ICPMS was not used within these loading studies as the unsuccessful loading was proved via nanosight nanoparticle fluorescence. This

equipment allows for live tracking of nanoparticles in solution via scatter or, alternatively, tracking via monitoring emissions. The latter was employed as a means to ascertain whether the imaging probe had indeed bound to the surface of the nanoparticles or whether it was merely suspended in solution. The IrBpySS solution displayed no measurable fluorescence and therefore was no longer considered for cellular imaging studies.

Upon reviewing RuPhenSS loading studies it is evident that the system displays reduced shifting of the λ_{max} of the system, displaying an overall shift of 2nm vs the 10nm and 11nm of RuBpySS and IrBpySS respectively. Moreover, the RuPhenSS system showed a quite significant decrease in the intensity of the SPR band (-0.27), which as aforementioned, is considered indicative of more efficient loading of the probe onto the surface of the nanoparticle system. Similar to the IrBpySS case, direct comparison of loading efficiency is theoretically difficult between RuBpySS and RuPhenSS on account of the fact that the two probes have different ligands and therefore, difference in loading efficiency could actually be miss-represented by emissive capabilities. Accordingly, the emissive capabilities of the two systems were compared via the use of nanosight live nanoparticle fluorescence studies, with some of the key data represented in Figure 209. Further research should look to incorporate ICPMS so as to quantify the amounts of RuBpySS and RuPhenSS that may be loaded onto the surface of the particles. This data, in combination with the emissive data reported herein, would allow for a more complete investigation of the more optimal system.

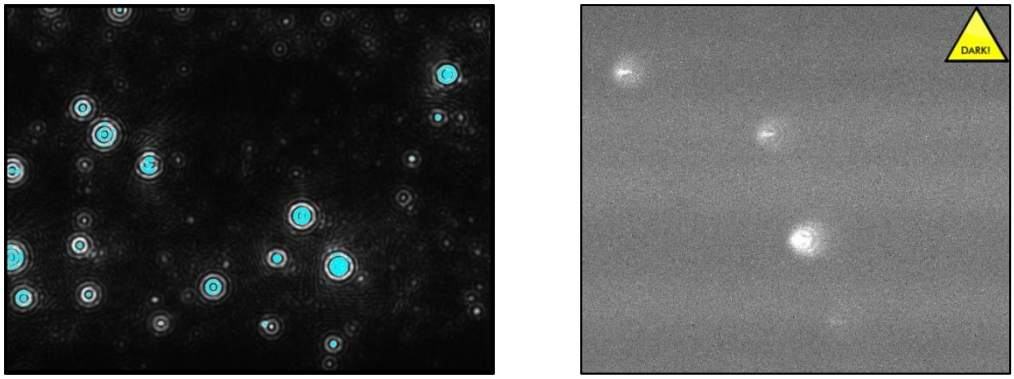

Figure 209: Screen shots from Nanosight live nanoparticle tracking system for GNP-Fol-RuBpySS system, left – scatter channel and right-fluorescence channel (using a 488nm laser for excitation and 500nm filter).

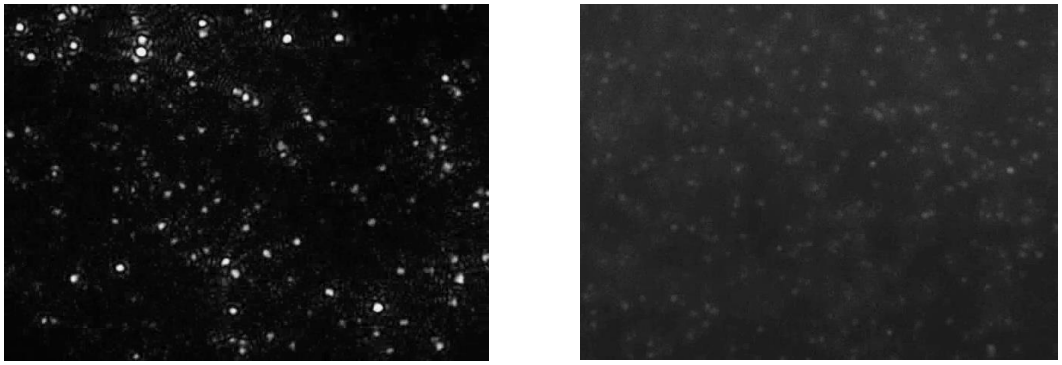

Figure 210: Screen shots from Nanosight live nanoparticle tracking system for GNP-Fol-RuPhenSS system, left – scatter channel and right-fluorescence channel (using a 488nm laser for excitation and 500nm filter).

A number of observations can be drawn from the nanosite data of Figures 209 and 210 for the RuBpySS and RuPhenSS systems respectively. The first and perhaps most notable observation is that both fluorescent probe systems afford nanoparticles that display measurable fluorescence. That is to say, the nanosite data collected has confirmed successful binding of the respective fluorescent probes to the surface of the respective nanoparticle systems and, furthermore, that the fluorescence capabilities of the probes remain intact. There appears to be

a relatively consistent degree of emission across the populations which is most likely indicative of even surface functionalisation of the particles with the probes across the respective suspensions. Any uneven loading would likely result from variations in particle size across the suspension and therefore variation in surface area available for binding. It is also noteworthy that this instrument uses a 488nm laser, which falls well outside of the primary absorbance band of 290nm. Accordingly, the systems may actually be capable of significantly stronger emission.

2.3. CONCLUSIONS

A new protocol for the direct synthesis of folate capped gold nanoparticles was developed in the present research. This protocol produces folate capped gold nanoparticles that are more batch consistent, mono disperse and are typically more stable than those reported in the literature.

The capacity of these particles to be surface functionalised with ruthenium based polypyridyl probes was investigated and compared to the capacity of citrate capped gold nanoparticles that had previously been reported by the Pikramenou group. The specific probes of use were RuPhenSS and RuBpySS. It is evident that these citrate and folate capped gold nanoparticle systems have comparable loading capacities with these probes and that the emissive properties of the probes appear unaffected. Later research by the Pikramenou group ascertained that the RuPhenSS probe displays fluorescence with improved photophysical properties when loaded onto the GNP-Cit system over the RuBpySS probe. Key parameters of improvement were emission strength and lifetime. These findings and conclusions for the RuPhenSS were therefore carried over in the present research and the RuPhenSS probe utilised for the resulting research detailed herein.

Future research into this area should look to quantitatively assess the photophysical parameters of the GNP-Fol-RuBpySS and GNP-Fol-RuPhenSS systems for potential optimisation before subsequent cellular studies are conducted.

2.4. EXPERIMENTAL

2.4.1. Materials

All materials were purchased from Sigma-Aldrich (now Merck), Fischer Scientific, ThermoFisher, VWR or MatTek. All solvents were of standard grade and were used without purification unless otherwise stated. All synthesis under N_2 employed standard Schlenk line techniques.

2.4.2. General Analytical Techniques

All characterisation techniques were conducted within either the School of Chemistry or Biosciences at the University of Birmingham. Nuclear Magnetic Resonance (NMR) spectra were recorded in CDCl3, CD_3CN, MeOD and d_6-DMSO. ^{1}H-NMR and ^{13}C-NMR spectra were recorded on either a Bruker AV(III)300 or AV(III)400 spectrometer. Electrospray mass spectrometry and Matrix Assisted Laser Desorption Ionisation Time of Flight (MALDI-TOF) spectra were collected by Dr. Chi Tsang (Analytical Facility). Spectra were recorded on a Waters LCT Time of Flight Spectrometer. UV-Visible (UV-Vis) spectra were recorded on a Varian Cary 5000 spectrometer. Dynamic Light Scattering (DLS) sizing measurements were carried out on a Malvern Zetasizer ZSP (Malvern Instruments) and nanoparticle fluorescence / scatter flow imaging was carried out on a Malvern Nanosight NS300. Transmission electron microscopy (TEM) was performed at the Centre for Electron Microscopy, University of

Birmingham by Theresa Morris, using a JEOL JEM-1200EX electron microscope. Inductively coupled plasma optical mass spectrometry (ICP-MS) measurements were performed on a 7500cx IPC-MS at the University of Warwick by Lijiang Song. Metal concentrations were determined using PlasmaCal calibration standards (QMX laboratories), with R2 > 0.999 linear calibration curves. Samples were digested in freshly prepared ultrapure aqua-regia and concentrated Nitric acid, samples were subsequently diluted accordingly.

2.4.3. Synthesis of Gold Nanoparticles

GNP-Cit (Citrate capped 13nm Gold Nanoparticles)

This method was developed by Shani Osborne[3] and based on the protocol of Vossmeyer *et al*[4]. A solution of trisodium citrate dihydrate (60 mg, 0.2 mmol), citric acid (13 mg, 0.07 mmol) and ethylenediaminetetraacetic acid (EDTA) (1.5 mg, 0.004 mmol) in deionised water (100 mL) brought to reflux for 10 minutes under aggressive stirring. A preheated (~80°C) solution of gold(III) chloride trihydrate $H[AuCl_4].3H_2O$ (8 mg, 0.02 mmol) in deionised water (25 mL) was added rapidly to the centre of the vortex and the solution refluxed for a further 15 minutes. The solution was allowed to gradually cool to room temperature within the heating mantle to form a ~1nM solution of GNP-Cit. λmax 517nm (SPR). The resulting particles were then stored in a stoppered round bottom flask wrapped in foil. Diameter / nm = 13 ± 3 (DLS number distribution), PDI = 0.2.

GNP-GSH-Fol (Citrate capped 13nm Gold Nanoparticles with Folate Moieties Tethered)

These particles were developed exactly as per the method of the published work of Zhang *et al*[5]. For the citrate capped foundation particles, a ~1nM solution of GNP-Cit was freshly prepared as per the S.Osborne protocol above.

50µl of a 0.05mol glutathione (GSH) solution was added to 10mL of ~1nM GNP-Cit, with the resulting solution stirred overnight at room temperature for surface conjugation (~12 hours). The resulting solution was dialysed in a semi permeable membrane (Spectra-Por® Float-A-Lyzer® G2, 5 mL, MWCO 8-10 kDa) in deionised water for 6 hours to remove unreacted materials. 25µL each of a 0.05mol DCC solution in DMSO and a 0.05mol NHS solution in DMSO were added and the solution further stirred for an hour. An excess of folic acid was added to the solution and stirred overnight (~12 hours) before being dialysed for a further 12 hours to remove excess and unreacted materials, yielding ~0.6nm GNP-GSH-Fol. λmax 526nm (SPR), Diameter / nm = 41.71 ± 20 (DLS number distribution), PDI = 0.52.

GNP-Fol (Zhang Method)

These particles were developed exactly as per the method of the published work of Zhang *et al*[6].

Approximately 30-40µL 1M sodium hydroxide (NaOH) was added to a suspension of folic acid (0.012g) in 10mL deionised water, generating soluble sodium folate. This sodium folate solution was added dropwise to a stirring solution of H[AuCl4].3H2O (5mL, 1mM) and a further 50µL of 1M NaOH added, with the resulting solution stirred at room temperature for a further 30 minutes. The solution was heated to 50°C for 8 hours, yielding ~0.5nm GNP-Fol. λmax 540nm (SPR), Diameter / nm = 38 ± 15 (DLS number distribution), PDI = 0.36.

GNP-Fol (Caballero Method)

This method was developed by Ana Caballero and based on the above protocol of Zhang *et al*[6]. A mixture containing 18 mL of 0.8 mM solution HAuCl4, 90 µl NaOH 1 M and 0.72 mL of sodium folate 1 mM (prepared by adding 21 uL NaOH 1M to 5 mL folic acid 1 mM solution) was stirred at room temperature for 30 min. Subsequently, the mixture was heated to 180 ºC

for 5 minutes within a single-mode microwave reactor (CEM Instruments) at 200 W and left to cool slowly until room temperature. The solution was purified via dialysis (Spectra-Por® Float-A-Lyzer® G2, 5 mL, MWCO 8-10 kDa) for two days against deionized water with NaOH (pH 10), yielding ~0.3nm GNP-Fol. λmax 530nm (SPR), Diameter / nm = 30 ± 10 (DLS number distribution), PDI = 0.18.

GNP-Fol (Young Protocol, used for the remainder of the research)

This method was developed by Richard Young in the present research and was based on the protocols of Caballero and Vossmeyer[4].

A solution of sodium folate (0.72mL, 2mM) was added to 20mL deionised water and refluxed for 10 minutes with stirring in an oil bath. 1mL of a pre-heated (~80°C) $HAuCl_4.3H_2O$ solution (5.7mg, 0.015mmol) was added rapidly by a Gilson pipette to the centre of the vortex, followed immediately by 90µL of a 1M NaOH solution. The resulting solution was refluxed for a further 20 minutes and allowed to gradually cool to room temperature within the oil bath, yielding ~1nm GNP-Fol. λmax 530nm (SPR), Diameter / nm = 15 ± 30 (DLS number distribution), PDI = 0.18.

$HAuCl_4.3H_2O$ (5.7mg, 0.015mmol) dissolved in 1mL deionised water and heated to ≈120°C in oven. HAuCl4.3H2O (6mg, 1mL) added in one go from a Gilson pipette followed immediately by NaOH (90uL, 1M). Refluxed for 20 mins and allowed to cool gradually in the oil bath for 1 hour.

2.4.4. Imaging Agent Synthesis

RuPhenSS

Compound 201: N-(Boc)-5-amino-1-pentanol

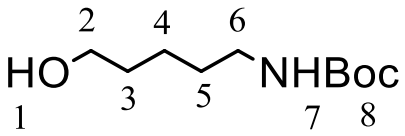

Compound 1 was synthesised as per the method developed by Sam Adams[7].

Potassium bicarbonate (14.12g, 141.1 mmol) was suspended in a solution of 5-amino-1-pentanol (4.96, 48.0 mmol) in H_2O:THF (70mL1:1). The white suspension was cooled to approximately 0°C and a solution of di-tert-butyl dicarbonate (11.11g, 50.9mmol) in H_2O:THF (80mL 1:1) was added dropwise over 15 minutes. The resulting biphasic mixture was then heated to 50°C and stirred for 24hours. The organic phase was separated and reduced under vacuum until the solution formed an opaque white microsuspension. Diethyl ether (50mL) was added and the resulting solution washed with deionised water (4 x 25mL). The organic layer was separated, the aqueous fractions washed with diethyl ether (50mL) and organic fractions combined. The organic solution was then dried over Na_2SO_4, filtered and solvent removed under vacuum, yielding the product as a clear oil (7.55g, 77%). Characterisation agrees with that of the literature. δ_H(300 MHz; $CDCl_3$); 1.32-1.63 (6 H, m, H-3,4,5), 1.42 (9 H, s, H-8), 2.05 (1 H, s, OH), 3.11 (2 H, dd, *J* = 6.3, 12.7, H-6), 3.54 (2 H, dd, *J* = 6.4, 11.6, H-2) and 4.59 (1 H, s, NH) m/z (ES); $[M+Na]^+$ 226.

Compound 202: N-(Boc)-5-amino-1-tosylpentane

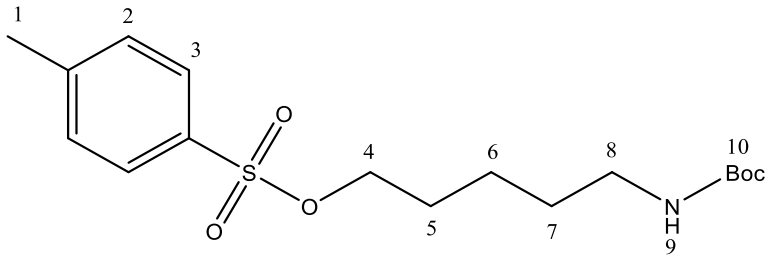

Compound 2 was synthesised as per the method developed by Sam Adams[7].

A solution of N-(Boc)-5-amino-1-pentanol (7.80g, 38.4mmol) and pra-toluene sulfonyl chloride (9.76g, 51.24mmol) in anhydrous DCM (50mL) was cooled to approximately 0°C under nitrogen. Pyridine (11mL, 149.0mmol) was added dropwise over 5 minutes and the resulting reaction mixture was allowed to come to room temperature and stirred for 24 hours. The mixture was concentrated under vacuum yielding a white suspension. The suspension was added to H_2O:Et_2O (100 mL 1:1) and separated, followed by washing the organic layer with aqueous $NaHCO_3$ (50 mL) and brine (50 mL). The solution was dried (Na_2SO_4), filtered, and the solvent was removed under vacuum to give a clear oil, which was triturated in hexane (50 mL), with the resulting solid filtered and washed with cold hexane (2 x 30 mL) to give a white solid N-Boc-5-amino-1-tosylpentane (5.8g, 44%). Characterisation agrees with that of the literature. δ_H(300 MHz, $CDCl_3$); 1.40-1.72 (6 H, m, H-5,6,7), 1.52 (9 H, s, H-10), 2.59 (3 H, s, H-1), 3.18-3.29 (2 H, m, H-8), 4.13 (2 H, t, *J* = 6.6, H-4), 4.71 (1 H, s, NH), 7.46 (2 H, d, *J* = 8.2, H-2) and 7.90 (2 H, d, *J* = 8.1, H-3) m/z (ES); $[M+Na]^+$ 380.

Compound 203: 4,4'-dihydroxy-2,2'-bipyridine

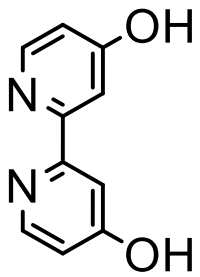

Compound 3 was synthesised as per the method developed by Sam Adams[7].

A solution of 4,4'-dimethoxy-2,2'-bipyridine (2.48g, 12 mmol) in hydrobromic acid (48 % w/v, 20 mL, 180mmol) and glacial acetic acid (150 mL) was heated under reflux for 6 hours. The mixture was cooled and the solvent was removed under vacuum, affording a white/cream solid which was dissolved in H_2O (125 mL) and neutralised with aqueous ammonia solution (31% by weight, dropwise). The resulting precipitate was filtered and washed with H_2O (50 mL) and ice cold acetone (2 x 10 mL) before being dried at 60 °C for 1 hour to give the product as a white solid (1.65g, 73%). Characterisation agrees with that of the literature. m/z (ES); $[M+H]^+$ 189.

Compound 204: 4,4'-di-(N-(Boc)-5-amino-1-pentoxy)-2,2'-bipyridine

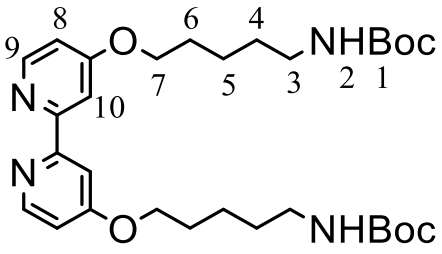

Compound 4 was synthesised as per the method developed by Sam Adams[7].

Potassium carbonate (2.22 g, 15.8 mmol) was suspended in a solution of N-(Boc)-5-amino-1-tosylpentane (6.67 g, 15.7 mmol), 4,4'-dihydroxy-2,2'-bipyridine (0.94 g, 4.9 mmol) and 18-crown-6 (catalytic) in acetone (208 mL). The mixture was heated to 60 °C and stirred for 36 hours. The reaction mixture was hot filtered to give a yellow filtrate, which afforded a

precipitate as it cooled to room temperature. The precipitate was filtered and washed with ice cold acetone (20 mL). The filtrate was concentrated under vacuum (~30 mL), affording a precipitate which was filtered at 0-5 °C and washed with ice cold acetone (20 mL). The two crops were combined to give a pale yellow solid (0.91g, 35%). Characterisation agrees with that of the literature. δ_H(300 MHz; $CDCl_3$; 1.43 (18 H, s, H-1), 1.48-1.61 (8 H, m, H-4,5), 1.87 (4 H, qu, *J* = 6.9, H-6), 3.14 (4 H, m, H-3), 4.13 (4 H, t, *J* = 6.5, H-7), 4.59 (2 H, s, N*H*), 6.80 (2 H, dd, *J* = 2.6, 5.5, H-10), 7.91 (2 H, d, *J* = 2.7, H-8) and 8.45 (2 H, d, *J* = 5.6, H-9) m/z (ES); $[M+H]^+$ 559, $[M+Na]^+$ 581.

Compound 205: 4,4'-di-(5-amino-1-pentoxy)-2,2'-bipyridine

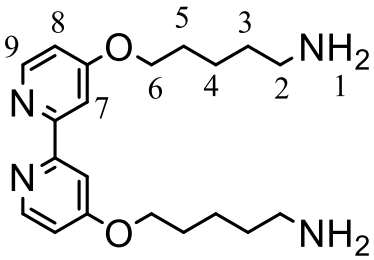

Compound 5 was synthesised as per the method developed by Sam Adams[7].

A solution of 4,4'-di-(N-(Boc)-5-amino-1-pentoxy)-2,2'-bipyridine (0.97 g, 1.7 mmol) in trifluoroacetic acid (14.9 mL) was stirred under N_2 for 1 hour, affording a white microsuspension. The solvent from the suspension was removed under vacuum, before separation (approximately NaOH (1M) to neutralise the pH/ 50 mL chloroform). The aqueous layer was extracted with chloroform (8 x 30 mL), and the combined organic extracts were dried (Na_2SO_4) and filtered. The solvent was then removed under vacuum to give a white solid (0.34g, 84%). Characterisation agrees with that of the literature. δ_H (300 MHz; $CDCl_3$); 1.19 (4 H, s, NH_2), 1.49-1.59 (8 H, m, H-4,3), 1.79-1.92 (4 H, m, H-5), 2.69-2.78 (4 H, m, H-2), 4.13 (4 H, t, *J* = 6.6, H-6), 6.81 (2 H, dd, *J* = 5.9, 2.5, H-8), 7.92 (2 H, d, *J* = 2.7, H-7) and 8.47 (2 H, d, *J* = 5.5, H-9) m/z (ES); $[M+H]^+$ 359, $[M+Na]^+$ 381.

Compound 206 (BpySS): 4,4'-di-(5-lipoamido-1-pentoxy)-2,2'-bipyridine

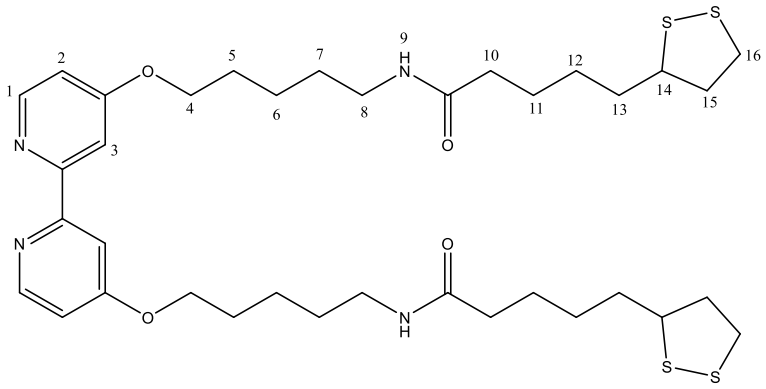

Compound 6 was synthesised as per the method developed by Sam Adams[7].

A solution of α-lipoic acid (0.48 g, 2.3 mmol) and 1-hydroxybenzotriazole hydrate (0.36 g, 2.7 mmol) in anhydrous DMF (8.8 mL) was cooled to 0-5 °C, upon which 1-Ethyl-3-(3-dimethylaminopropyl)carbodiimide (EDC) (0.41 g, 2.6 mmol) was added and stirred, maintaining this temperature until the EDC had dissolved (ca. 1 hour). The solution was allowed to warm to room temperature and stirred for a further hour. A solution of N-ethylmorpholine (N-EM) (0.27 g, 2.4 mmol), and 4,4'-di-(5-amino-1-pentoxy)-2,2'-bipyridine (0.35 g, 0.98 mmol) in anhydrous DMF (12.3 mL) was added to the reaction mixture and the resulting cream precipitate was stirred overnight, filtered and dried in air to give a cream powder. The crude product was slurried in $CHCl_3$ (50 mL) and filtered again, before washing with $CHCl_3$ (2 x 10 mL) to give a pale yellow powder bpySS (0.35g, 33%). Characterisation agrees with that of the literature. δH (300 MHz; CDCl3) 1.31-1.56 (12 H, m, H-5,6,7), 1.56-1.68 (8 H, m, H-11,12), 1.74-1.89 (6 H, m, H-13,15'), 2.11 (4 H, t, J = 7.3, H-10), 2.38 (2 H, m, H-15), 2.99-3.15 (4 H, m, H-16), 3.22 (2 H, q, J = 6.5, H-14), 3.45-3.54 (4 H, m, H-8), 4.06 (4 H, t, J = 6.3, H-4), 5.48 (2 H, s, NH), 6.75 (2 H, dd, J = 5.7, 2.6, H-3), 7.87 (2 H, d, J = 2.6, H-1) and 8.38 (2 H, d, J = 5.7, H-2). m/z (ES); [M+H]+ 735, [M+Na]+ 757.

Compound 207: cis-Ru(Bpy)$_2$(Cl)$_2$

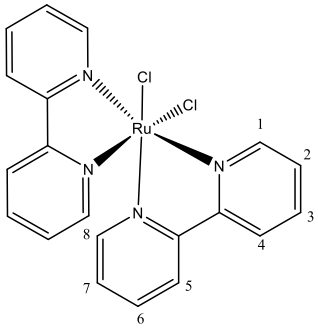

cis-Ru(Bpy)$_2$(Cl)$_2$ was prepared as per the synthetic procedure developed by Sullivan, Salmon and Meyer[8].

$RuCl_3.3H_20$ (0.7852g, 3mmol), bipyridine (0.9371g, 6mmol), and LiCl (0.84g, 0.2 mmol) were heated at reflux in dimethylformamide (10 mL) for 8 h with stirring. After the reaction mixture was cooled to room temperature, 250 mL of reagent grade acetone was added and the resulting solution cooled at 0°C overnight. Filtering yielded a red to red-violet solution and a dark green-black microcrystalline product. The solid was washed three times with 25mL portions of water followed by three 25mL portions of diethyl ether and then it was dried by suction filtration, yielding the final product (40%). Characterisation agrees with that of the literature. δ_H (300 MHz; $CDCl_3$); 7.11 (1H, m, H-1), 7.52 (1H, m, H-2), 7.69 (1H, m, H-3), 7.78 (1H, m, H-6), 8.08 (1H, m, 5-H), 8.49 (1H, m, 4-H), 8.66 (1H, m, 7-H), 9.94 (1H, m, 8-H). m/z (ES); $[M+H]^+$ 481 (one chloride ligand exchanged with a Cl ligand) $[M+Na]^+$ 503.

Compound 8: [RuBpySS](PF$_6$)$_2$

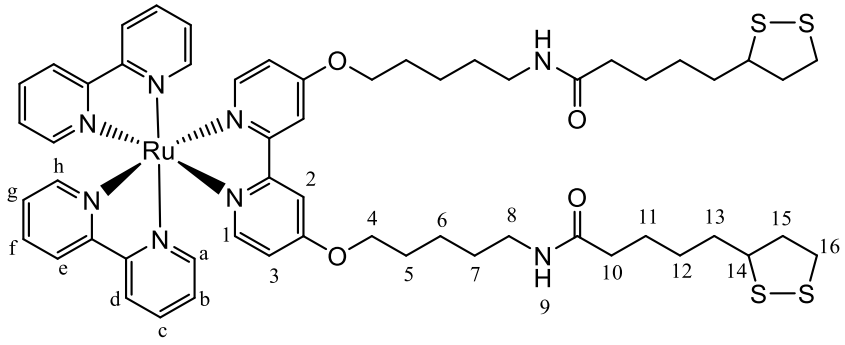

A solution of bpySS (0.12 g, 0.16 mmol) and Ru(bpy)2Cl2 (0.08 g, 0.16 mmol) in ethanol (80 mL) was heated under reflux (95°C) for 16 h. The red/orange solution was cooled to room temperature and concentrated under vacuum (~25 mL). H2O (35 mL) was added, forming a fine cream precipitate, which was filtered. A saturated methanolic solution of ammonium hexafluorophosphate (0.25 g, 1.5 mmol in 2 mL of MeOH) was added to the filtrate to give an orange precipitate. The precipitate was filtered and washed with ice cold H2O and ice cold Et2O to give the crude product as an orange/red solid. The solid was dissolved in a minimal amount of acetonitrile and the solvent removed under vacuum to give a red crystalline solid RubpySS (0.1866 g, 80%). Characterisation agrees with that of the literature. δ_H (300 MHz; $CDCl_3$); 1.32−1.75 (16 H, m, H-5,6,12,13), 1.75−1.81(4 H, m, H-11), 1.84−1.94 (6 H, m, H-7,H-15'), 2.14 (4 H, t, J= 7.0,H-10), 2.39−2.50 (2 H, m, H-15), 3.04−3.12 (4 H, m, H-16), 3.12−3.22 (4 H, m, H-8), 3.52−3.61 (2 H, tdd, J=2.8, 6.5, 6.6, H-14), 4.19 (4 H, t, J= 6.7, H-4), 6.39 (2 H, m, NH), 6.91 (2 H, m, H-3), 7.39 (2 H, m, H-1), 7.42 (4 H, m, H-b,g), 7.70 (2 H, m, H-a/h), 7.82 (2 H, m, H-a/h), 8.00−8.09 (4 H, m, H-c,f), 8.08 (2H, m, H-2), and 8.48−8.52 (4 H, m, H-d,e). m/z (ES); $[M\text{-}2(PF_6)]^{+2}$ 574.

Compound 9: cis-[IrBpy$_2$Cl]$_2$

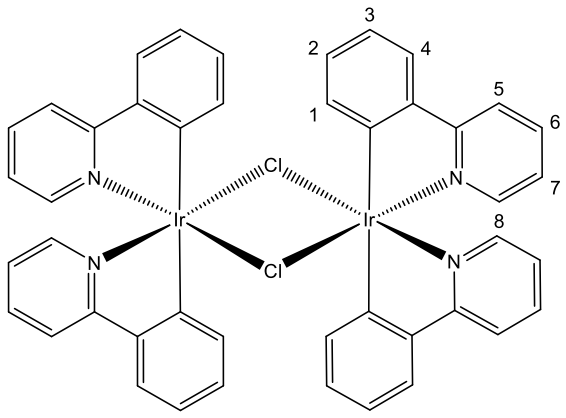

cis-[IrBpy$_2$Cl]$_2$ was prepared as per the synthetic procedure developed by Choe *et al.*[9 & 10] and as provided by Siobhan King of the Pikramenou group. Iridium trichloride hydrate (0.35g, 1mmol) was combined with 2-phenylpyridine (0.8g, 5mmol) and dissolved in a mixture of ethanol (30 mL) and deionised water (10 mL), and refluxed overnight (~24 hours). The solution was allowed to cool to room temperature and the yellow precipitate was subsequently collected via filtration. The precipitate was washed with ethanol (~60 mL) and acetone (~60 mL) and subsequently dissolved in DCM (~60mL). Toluene (25 mL) and hexane (10 mL) were added to the filtrate and the resulting mixture reduced in vacuo to approximately 30 mL. The concentrated solution was cooled to ~4°C and the crystalline product collected [Ir(ppy)$_2$Cl]$_2$ (0.479 g, 81%). Characterisation agrees with that of the literature. δ_H (300 MHz; $CDCl_3$); 5.91 (1H, d J = 7.9, H-1), 6.63 (1H, m, H-2), 6.88 (2H, m, H-3), 7.54 (1H, d, J = 78.0, H-6), 7.78 (1H, m, H-5), 7.92 (1H, d J = 7.8, H-4), 8.23 (1H, m, H-7), 9.30 (1H, d, J = 5.9, H-8); MS (ESI+) m/z: 1078 $(M)^+$.

Compound 10: [IrBpySS](PF$_6$)$_2$

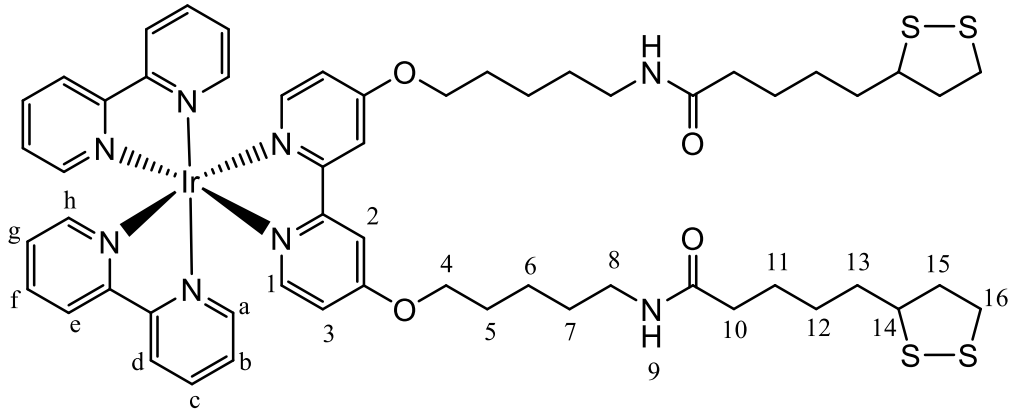

This method was developed by Sam Adams[7] and was based on the method of Slinker *et al.*[10]

[Ir(Bpy)$_2$Cl]$_2$ (66.6 mg, 0.06 mmol) and BpySS (100 mg, 0.14 mmol) were suspended in ethanol (6.5 mL) and heated to 150 °C for 19 hours. The solution was allowed to cool to room temperature, H_2O (~150 mL) was added, and the mixture re-heated to 60-70 °C. Saturated

aqueous ammonium hexafluorophosphate (1 g in 2.5 mL H2O) was added and the solution cooled to ~4°C, forming a yellow precipitate. The precipitate was filtered and washed with H_2O, before being re-suspended in minimal acetone and the solvent removed in vacuo to give IrBpySS (117.4 mg, 69%). Characterisation agrees with that of the literature. δH (300 MHz; d6-acetone) 1.15-1.66 (20 H, m, H-5,6,7,11,13), 1.60-1.83 (6 H, m, H-12,15'), 2.05 (4 H, t, J = 7.3, H-10), 2.20-2.41 (2 H, m, H-15), 2.86-3.10 (8 H, m, H-8,16), 3.30-3.57 (2 H, m, H-10), 4.23 (4 H, t, J = 6.7, H-4), 6.29 (2 H, dd, J = 1.1, 7.9, H-h), 6.84 (2 H, td, J = 1.4, 7.3, H-g), 6.94 (2 H, td, J = 1.3, 7.4, H-f), 6.94 (2 H, s, NH), 7.09-7.15 (4 H, m, H-3,c), 7.65 (2 H, d, J = 6.6, H-1), 7.70-7.88 (4 H, m, H-d,e), 7.92 (2 H, dd, J = 1.4, 7.7, H-b), 8.17 (2 H, d, J = 8.5, H-a) and 8.25 (2 H, m, H-2); m/z (ES+) 1235 ([M-PF_6]+).

Compound 11: $RuPhenCl_2$

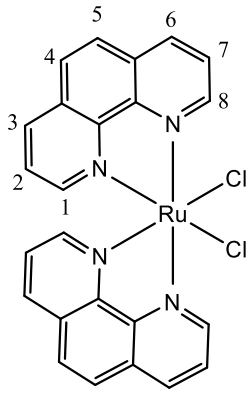

This method was developed by Shani Osborne and was based on the method of Gunlaugsson *et al.*[12]

Ruthenium trichloride (0.8g, 3mmol), 1,10 phenanthroline (1.1g, 6mmol) and lithium chloride (0.8g, 20mmol) were dissolved in 5 mL DMF and refluxed under N_2 for 6 hours. Acetone (20 mL) was added and the solution cooled to ~4°C overnight. The suspension was filtered and the precipitate washed with water (~100 mL) and diethyl ether (~50 mL) to produce a black compound (0.64g, 1.2 mmol, 40%). δH (300 MHz; DMSO): 7.30-7.40 (4H, m, H-2,7); 7.79

(2H, d, 5.4, H-4); 7.85 (2H, d, 8.3, H-5); 8.3 (4H, m, H-3,6); 10.10 (4H, m, H-1,8). m/z (TOF MS ES+) 497.0 ([M-Cl]+).

Compound 12: RuPhenSS

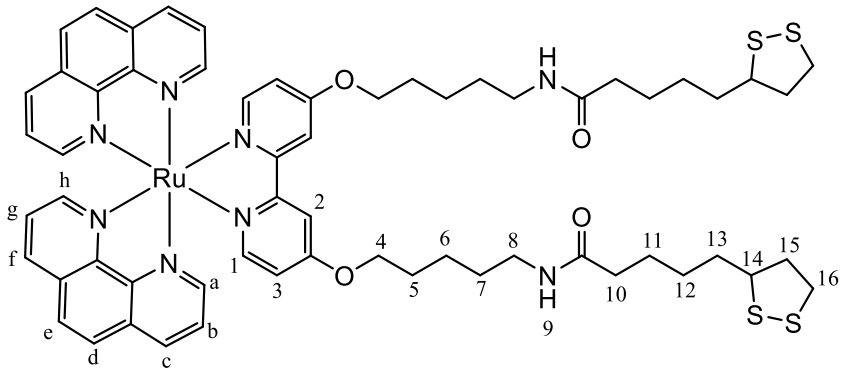

This method was originally developed by Shani Osborne based on the method of Gunlaugsson *et al*.[12] The method herein represents a minor modification in the purification step.

$RuPhen_2Cl_2$ (50mg, 0.09mmol) and 4,4-dimethyllipoamide 2,2-bipyridine (100 mg, 0.14 mmol) were suspended in ethanol (40mL) and refluxed overnight (~12 hours). The solvent was removed under vacuum and the resulting red solid was dissolved in minimal water (~8mL), cooled to ~4°C and the subsequent precipitate filtered. A saturated methanolic solution of ammonium hexafluorophosphate (0.25 g, 1.5 mmol in 2 mL of MeOH) was added to the filtrate to give a red precipitate. The precipitate was filtered and washed with ice cold H_2O and ice cold Et_2O to give the crude product as a red solid. The solid was dissolved in a minimal amount of acetonitrile and the solvent removed under vacuum to give a red solid RuPhenSS (43 mg, 0.034 mmol, 38%). Characterisation agrees with that of the literature. δH (300 MHz; MeOD): 1.27 (4H, m, H4); 1.45 (16H, m, H5,6,12,13); 1.78 (10H, m, H-7,11,15'); 2.09 (4H, m, H-10); 2.30 (2H, m, H-15); 2.94 (4H, m, H-16); 3.17 (4H, m, H-8); 3.19 (2H, m, H-14); 4.14 (4H, dt, 6.4, 1.3, H-4); 6.57 (2 H, m, NH), 6.94 (2H, m, H-3); 7.45 (2H, m, H-1); 7.56-7.84 (4H, m, H-b,g); 7.88 (2H, m, H-d); 8.25 (6H, m, H-2,e); 8.35 (2H, m, H-c); 8.57 (2H, m, H-f); 8.75 (4H, m, H-a,h). m/z (TOF MS ES+) 598.2.

2.5. REFERENCES

1 - Schulz F, Homolka T, Bastús NG, Puntes V, Weller H and Vossmeyer T. Little Adjustments Significantly Improve the Turkevich Synthesis of Gold Nanoparticles. Langmuir. 30.35 (2014), 10779–10784.

2 - Turkevich J, Stevenson PC, and Hillier J. The Formation of Colloidal Gold. The Journal of Physical Chemistry. 57.7 (1953), 670–673.

3 - Schulz F, Homolka T, Bastús NG, Puntes V, Weller H and Vossmeyer T. Little Adjustments Significantly Improve the Turkevich Synthesis of Gold Nanoparticles. Langmuir. 2014, 30, 10779-10784

4 - Osborne SAM and Pikramenou Z. Highly luminescent gold nanoparticles: effect of ruthenium distance for nanoprobes with enhanced lifetimes. Faraday Discussions. (2015) 185, 1-14.

5 - Zhang Z, Jia J, Lai Y, Ma Y, Weng J, Sun L. Conjugating folic acid to gold nanoparticles through glutathione for targeting and detecting cancer cells. Bioorganic & Medicinal Chemistry. (2010) 18, 5528–5534.

6 - Li G, Li D, Zhang L, Zhai J and Wang E. One-Step Synthesis of Folic Acid Protected Gold Nanoparticles and Their Receptor-Mediated Intracellular Uptake. Chemistry European Journal (2009). 15, 9868–9873.

7 - Adams SJ, Lewis DJ, Preece JA, and Pikramenou Z. Luminescent Gold Surfaces for Sensing and Imaging: Patterning of Transition Metal Probes. ACS Applied Matter Interfaces. (2014) 6, 11598−11608.

8 - Sullivan, B. P, Salmon, D. J and Meyer, T. J. Mixed Phosphine 2,2′- Bipyridine Complexes of Ruthenium. Inorganic Chemistry. (1978), 17, 3334− 3341.

9 - Lo, K. K.-W, Choi, A. W.-T and Law, W. H.-T. Applications of Luminescent Inorganic and Organometallic Transition Metal Complexes as Biomolecular and Cellular Probes. Dalton Trans. (2012), 41, 6021−6047.

10 - Park S, Sunesh CD, Kim H, Chae H, Lee J and Choe Y. Preparations of iridium complexes containing phenanthroline ancillary ligands and electrical properties of cationic iridium-based lightemitting electrochemical cells. Surface Interface Analytics. (2012) 44, 1479–1482.

11 - Slinker, J. D, Gorodetsky, A. A., Lowry, M. S, Wang, J., Parker, S, Rohl, R., Bernhard, S, Malliaras, G. G. Efficient Yellow Electrochemiluminescence from a Single Layer of a Cyclometalated Iridium Complex. Journal of American Chemical Society. (2004), 126, 2763−2767.

12 - Martínez-Calvo M, Orange KN, Elmes RBP, Poulsen BLC, Williams DC and Gunnlaugsson T. Ru(II)-polypyridyl surface functionalised gold nanoparticles as DNA targeting supramolecular structures and luminescent cellular imaging agents. Nanoscale, (2016) 8, 563–574.

Chapter 3 - Cellular Uptake Studies

3.1. Principle Uptake

Following the loading studies of ruthenium probes (RuBpySS and RuPhenSS) onto GNP-Fol and GNP-Cit nanoparticular systems (see Section 2.2.2), cellular uptake was investigated using confocal microscopy, TEM and Flow Cytometry (Fluorescence-Activated Cell Sorting (FACS)). Cellular uptake of GNP-Cit is well established in the literature and has also been investigated thoroughly by the Pikramenou group, the latter research utilising the Ruthenium based probes of the present research, as well as Iridium based alternatives[1]. By contrast however, and as previously discussed (see introduction section 1.2), the cellular localisation of folate coated gold nanoparticles is relatively unexplored within the literature. Accordingly, initial cellular uptake studies of the present research sought to establish the feasibility of cellular uptake for the ruthenium loaded GNP-Fol system. The system was investigated utilising folate receptor positive cell lines (HeLa and A549) and folate receptor negative cell lines (MSC), seeking to establish any relationship between degree of uptake and presence of folate receptors.

Cellular studies were conducted with GNP-Fol that was freshly synthesised and dialysed no more than one week prior to the experiments employed, with the nanoparticles being sonicated for 30 minutes before being loaded with RuPhenSS. Cells were seeded at a density of 0.8×10^6 cells per MatTek culture dish (as per the advised cellular confluency for a $35cm^2$ culture well[2]), cultured at standard incubation conditions for 24 hours to allow the cells to adhere, before dosing each MatTek dish with GNP-Fol-RuPhenSS (1mL of ~1nM GNP-Fol, loaded with 12µL of 1mM RuPhenSS) and incubating for 24 hours. The cells were then washed three times with PBS before being re-suspended in live cell imaging solution and analysed immediately via confocal microscopy in a live cell chamber.

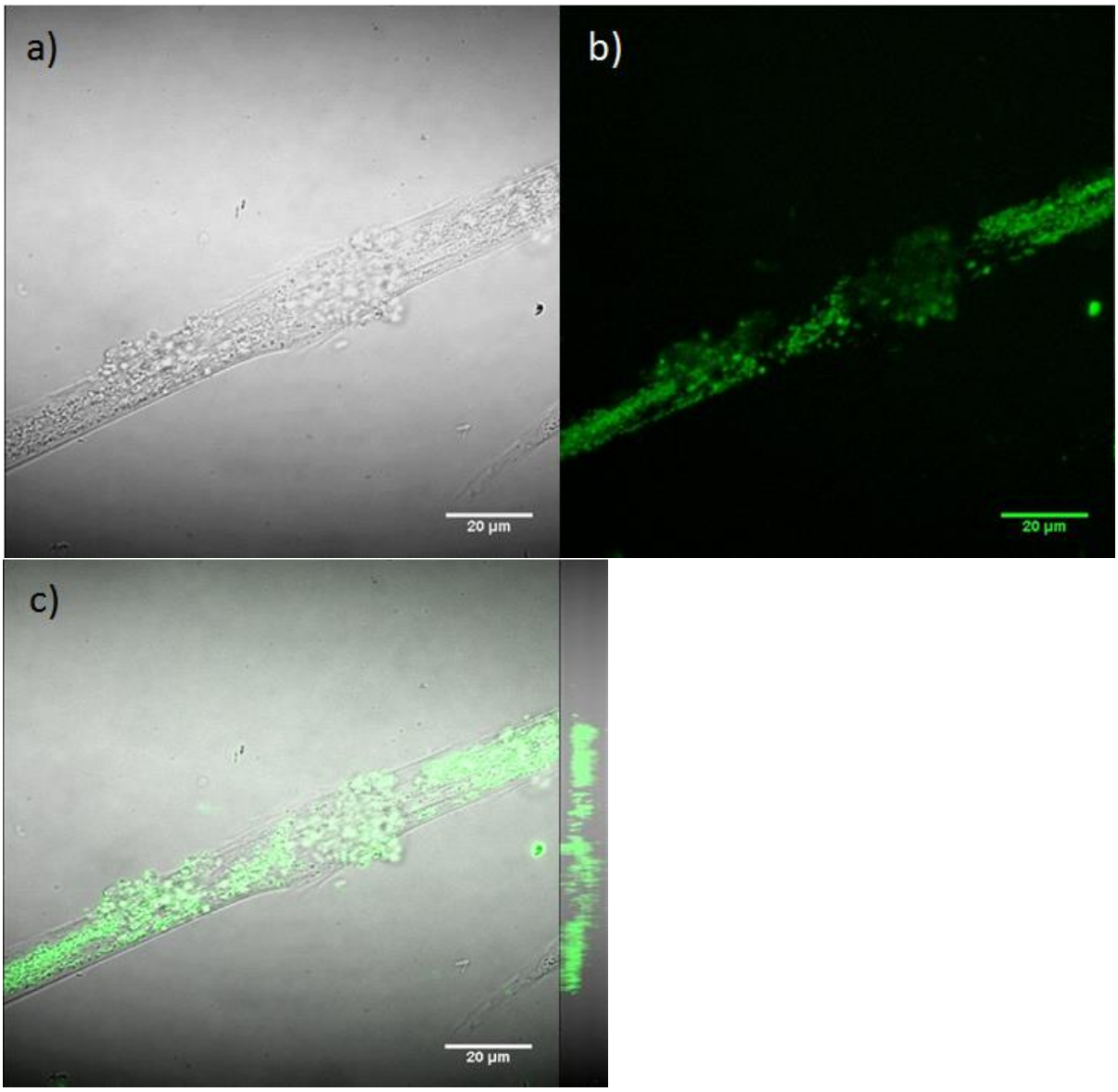

Figure 301: Confocal images collected for cellular dosing with GNP-Fol (900uL of ~1nM GNP) loaded with RuPhenSS (12uL of 1mM solution) suspended in 2mL of media for 24hours. Culture dishes were washed three times with PBS, immersed in 2mL of imaging media and immediately imaged under live cell chamber conditions. a) – c) represent MSCs at 100x magnification, where a) is brightfield, b) is the RuPhenSS fluorescence signal (λ_{ex} 488nm, λ_{em} 580-680nm) collected from a z stack profile and averaged, c) is an overlay of a) and b) with the corresponding z stack profile rotated 90° anti-clockwise, aligned side on to represent probe penetration through the sample. No auto-fluorescence was observed under the excitation/collection conditions utilised as proven with an untreated cellular sample.

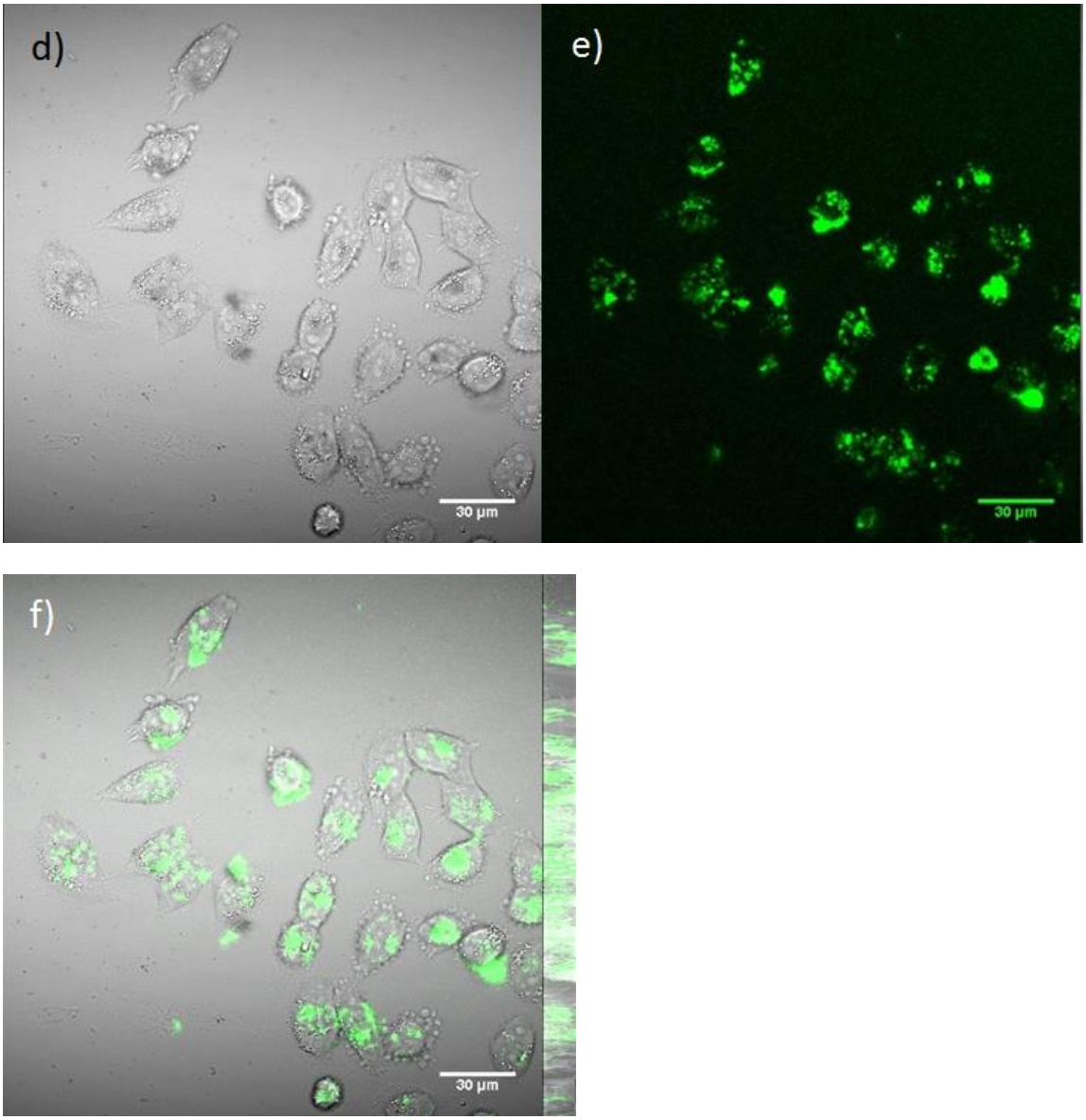

Figure 302: Confocal images collected for cellular dosing with GNP-Fol (900uL of ~1nM GNP) loaded with RuPhenSS (12µL of 1mM solution) suspended in 2mL of media for 24 hours. Culture dishes were washed three times with PBS, immersed in 2mL of imaging media and immediately imaged under live cell chamber conditions. d) – f) represent HeLa cells at 60x magnification, where d) is brightfield, e) is the RuPhenSS fluorescence signal (λ_{ex} 488nm, λ_{em} 580-680nm) collected from a z stack profile and averaged, f) is an overlay of d) and e) with the corresponding z stack profile rotated 90° anti-clockwise, aligned side on to represent probe penetration through the sample. No auto-fluorescence was observed under the excitation/collection conditions utilised.

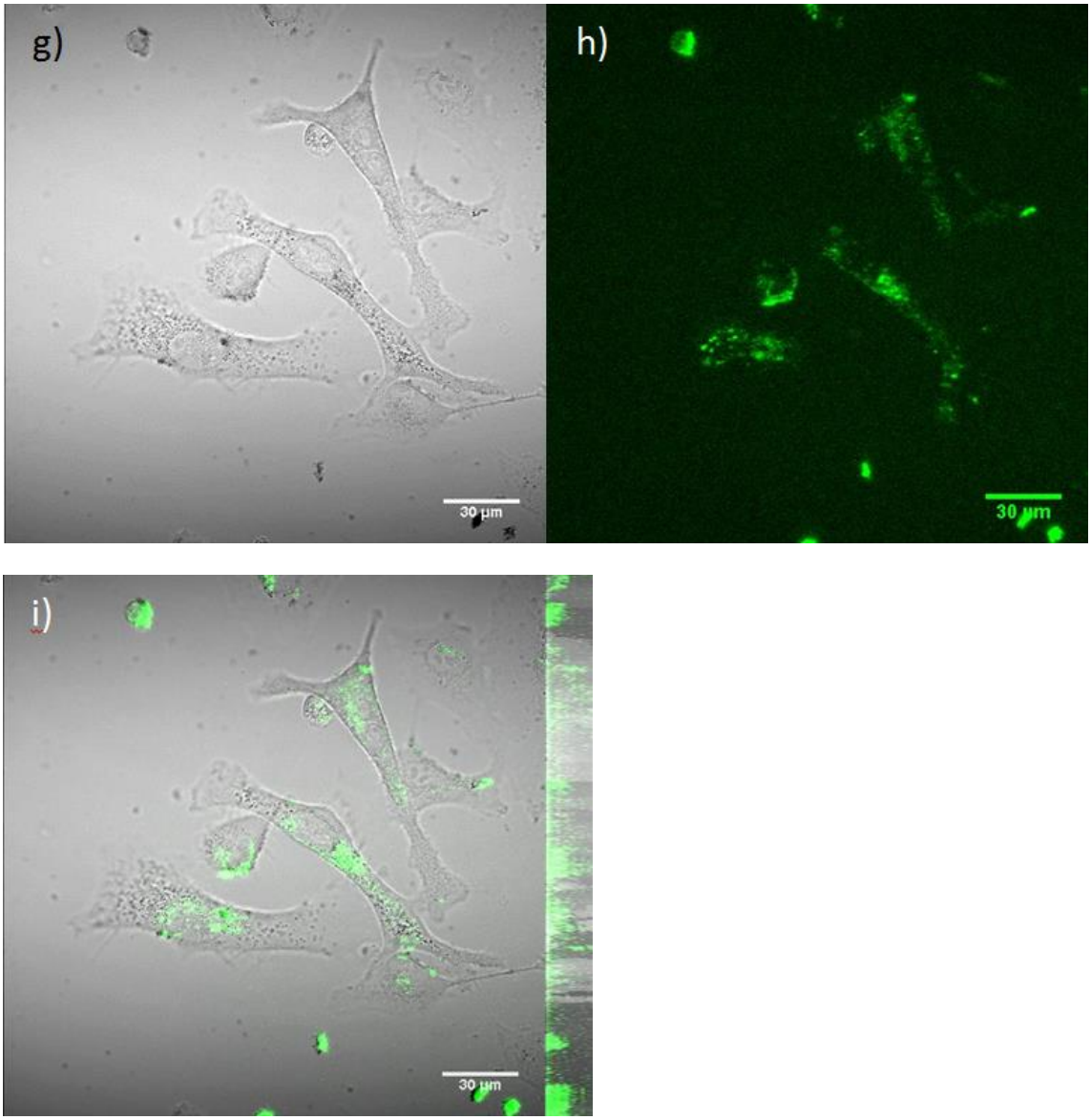

Figure 303: Confocal images collected for cellular dosing with GNP-Fol (900uL of ~1nM GNP) loaded with RuPhenSS (12µL of 1mM solution) suspended in 2mL of media for 24 hours. Culture dishes were washed three times with PBS, immersed in 2mL of imaging media and immediately imaged under live cell chamber conditions. g) – i) represent A549 cells at 60x magnification, where g) is brightfield, h) is the RuPhenSS fluorescence (λ_{ex} 488nm, λ_{em} 580-680nm) signal collected from a z stack profile and averaged, i) is an overlay of g) and h) with the corresponding z stack profile rotated 90° anti-clockwise, aligned side on to represent probe penetration through the sample. No auto-fluorescence was observed under the excitation/collection conditions utilised.

The images of Figures 301-303 demonstrate that folate capped GNPs loaded with RuPhenSS are able to penetrate into and throughout cells that are both folate receptor positive (HeLa and A549s, Figures 302 and 303 respectively) and negative (MSCs, Figure 301) within a 24 hour window at the concentrations and conditions employed (see experiment section 3.8.1 for full details). It is noteworthy that there is no visible probe signal emitted from the nucleus of the cells, which may be indirect evidence that the probes are still bound to the surface of the nanoparticles: one would assume that within a 24 hour window there would be some degree of diffusion of the free probe into the nucleus. The nanoparticles are likely to be too large to pass through the nuclear pores and therefore present no measurable signal. Samples were also incubated with the same concentration of imaging probe alone (6uL 1mM RuPhenSS) as a control to investigate whether there would be measurable fluorescence (and therefore uptake) of the probes if they were not bound to the nanoparticles. These samples showed no fluorescence signal at the same microscope settings, which might be indicative that the free complex does not accumulate in sufficient concentrations to be visible, or indeed that the free complex may not be taken up by the cells. The laser power was increased in an attempt to capture very weak signals; however, instrumental noise was prolific and weak auto-fluorescence was observed in the control. Thus, no measurable probe signal was achieved without nanoparticular loading / uptake within the cellular systems.

3.2. Dose-Time Optimisation

Following on from these 24 hour uptake studies the minimum treatment time required to record a sufficiently visible signal from GNP-FOL-RuPhenSS was investigated. This is important given that both the nanoparticular systems being investigated (folate or citrate capped) have been proven to show significant uptake within folate receptor positive and negative cell lines within a 24 hour dose period. Therefore, in order to prove selectivity, or at

least preferential or rapid uptake of folate capped nanoparticles over citrate, in a folate receptor positive cell line, the treatment times must be sufficient to allow for measurable uptake, whilst being short enough to limit passive uptake of nanoparticles. Non folate receptor mediated uptake (be it passive diffusion or any other viable uptake methodology) would essentially nullify or at least reduce the clarity and perceived impact of the efficacy of the folate receptor mediated pathway and hence must be limited as much as possible.

Initial uptake studies ascertained that measurable uptake was achieved after as little as 4 hours, however, it was also found that comparable levels of uptake of the citrate capped nanoparticular system were evident even in the folate receptor positive cell lines. It was hypothesised that the levels of folate receptor expressed by the cell lines employed as well as their metabolic rates would most likely vary quite significantly from one another. As such, it is desirable to conduct all competitive uptake studies within one cell line and to ideally modulate that cell lines ability to express the folate receptors. The ideal scenario therefore would be a cell line that inherently expresses high levels of folate receptor which is capable of being manipulated in a manner that the genes coding for folate receptor generation are knocked down. This would therefore generate two sub-types of the cell line that are otherwise identical except for the presence or lack thereof of folate receptors.

While gene knockdown studies are commonplace in the literature for various cell lines[3, 4], to the best of our knowledge, there has not been any published work on the knockdown of all three folate receptor genes (FOLR1 (α), FOLR2 (β), FOLR3 (γ)). Whilst it is possible to purchase CRISPR (Clustered Regularly Interspaced Short Palendromic Repeats) products which may allow for the eventual knockdown of folate expressing genes, this approach would be time consuming to establish. An alternative therefore, was to adopt the methodology of

Mornet *et al* and manipulate the levels of folate receptor α in a given cell line[5]. This research showed that by culturing different folate receptor positive cell lines in high and low folic acid containing culture medias, it is possible to lower and raise (respectively) the levels of folate receptor α expression. Examples of this manipulation can be seen in Figure 304 below, taken from Mornet's study.

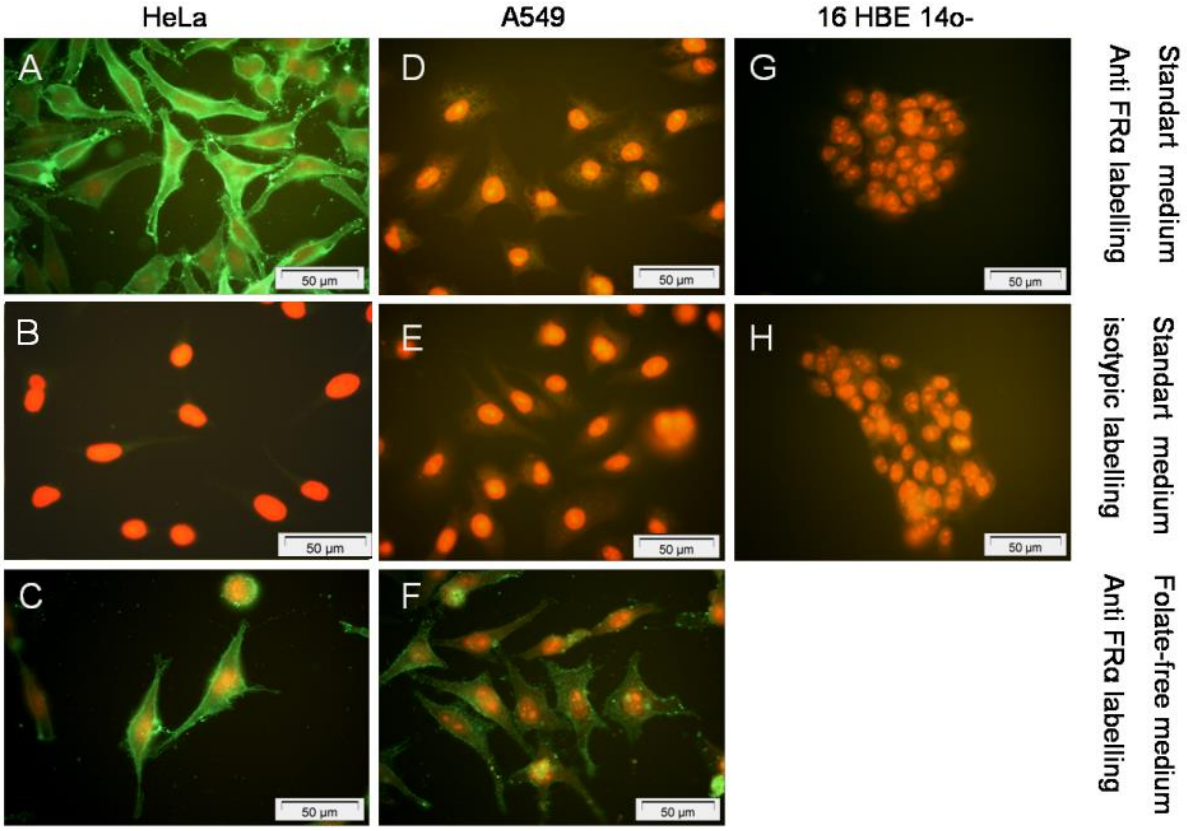

Figure 304: Image and figure description were accessed and utilised on 19/02/2017 from Mornet et al's paper in the International Journal of Molecular Sciences[5].

FR-α receptor expression on the membrane surface of HeLa, A549 and 16HBE14o(-) cells after indirect immunocytochemistry staining, showing the impact of folate content within the cell culture media on folate receptor α expression. Propidium iodide was used as nuclear counterstaining.

Folate receptors α and β are believed to be responsible for the vast majority of folic acid based compound uptake, whereas γ is primarily an efflux protein (see introduction section 1.1.1). It is believed that β receptor levels are typically significantly fewer than those of α receptors. Accordingly, it was hypothesised that manipulating the levels of α receptor expression within a given cell line would have a significant impact on folic acid based compound uptake, perhaps even to a comparable level associated with complete folate receptor gene knockdown.

Building upon the research conducted by Mornet et al, three cell lines were explored, HeLa, A549 and A2780s, employing the high and low folate media manipulation technique of the literature[5]. This research looked to ascertain whether any of these cell lines would show a significant shift in folate receptor α expression. Moreover, establishment of whether these cell lines might exhibit lesser levels of β and γ receptors, or indeed, no expression at all was favourable. In this regard, it was hoped that a cell line would be discovered that would exhibit high levels of folate receptor α, whilst exhibiting minimal or no expression of folate receptors β and γ, so that manipulation of folate receptor α levels would theoretically yield a folate receptor negative variant of an otherwise folate receptor positive cell line, without the need for gene knockout experiments.

3.3. Polymerase Chain Reaction (PCR) Studies

To investigate the extent of folate receptor expression within these cell lines, PCR experiments were employed. The principle of PCR is that it allows for the amplification (and for qPCR, quantification) of levels of specific gene expression within a given cell culture. Therefore, by investigating the expression of the genes which code for folate receptors α, β and γ via PCR, it is possible to establish which receptors are present, and, the potential extent of their expression[6]. PCR itself is the final stage of a number of precursor experiments, the first

of which is the purification and isolation of RNA from a cultured cell line using an RNA isolation kit (see Experimental section 3.8.2 for further details). Subsequently, the isolated RNA is converted to complementary DNA (cDNA) via the use of a cDNA synthesis kit, which utilises various solutions which include oligomers, dNTPs (Nuclear Triphosphates), buffers, an RNAse inhibitor and a reverse transcriptase enzyme. Finally, PCR is conducted, utilising the cDNA, gene specific primers (forward and reverse), buffers, dNTPs, and a Taq Polymerase solution (DNA polymerase enzyme). In short, the PCR stage allows for significant replication of specific genes by repeated cycles of separation of cDNA strands and pairing with complementary primers. Flow diagrams are depicted in Figures 305 and 306 to represent a broad overview of each of these processes.

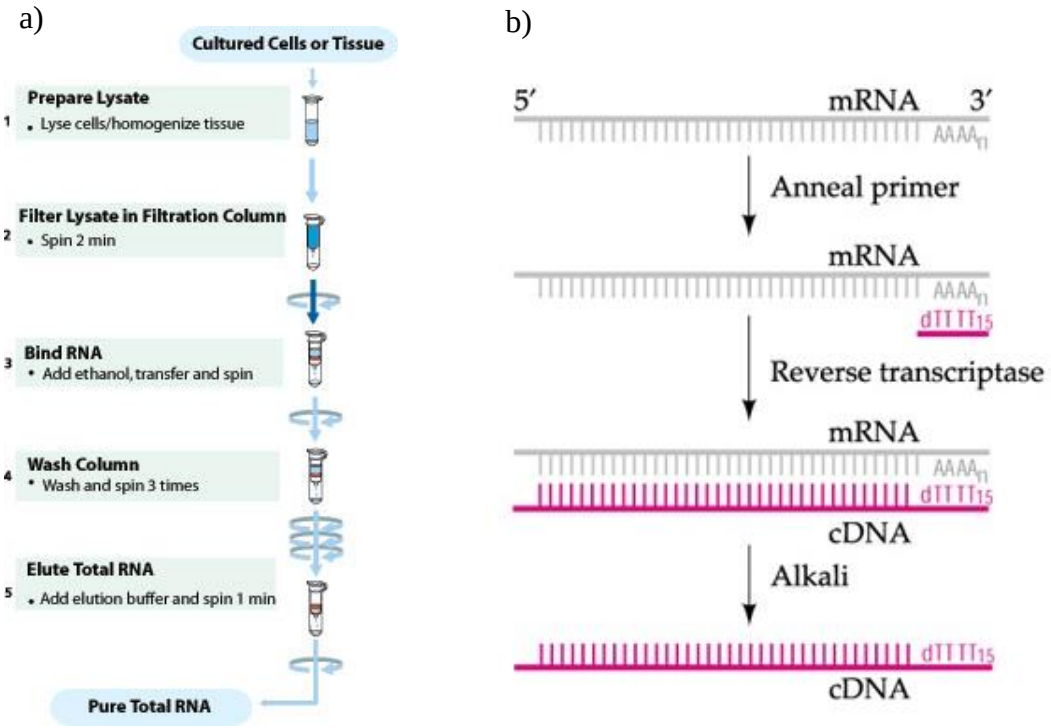

Figure 305: a) Diagrammatical representation of the various steps associated with the employment of a typical RNA isolation kit. Cells are lysed and homogenised (1) before being loaded onto the spin column (2 + 3). The column is then washed with various solutions (4) before eluting the purified RNA for analysis (5). Diagram sourced from Sigma Aldrich's

website on the 22/02/2017 at 12:30[7]. b) Depiction of the steps associated with cDNA synthesis, showing the annealing of the Oligo dT_{18} (primer) followed by the reverse transcription to produce the cDNA. In this example the cDNA is dissociated from the RNA via raising the pH with an alkali solution as opposed to raising the temperature to merely terminate the transcription. Diagram sourced from DevBio website on the 22/02/2017 at 15:30[8].

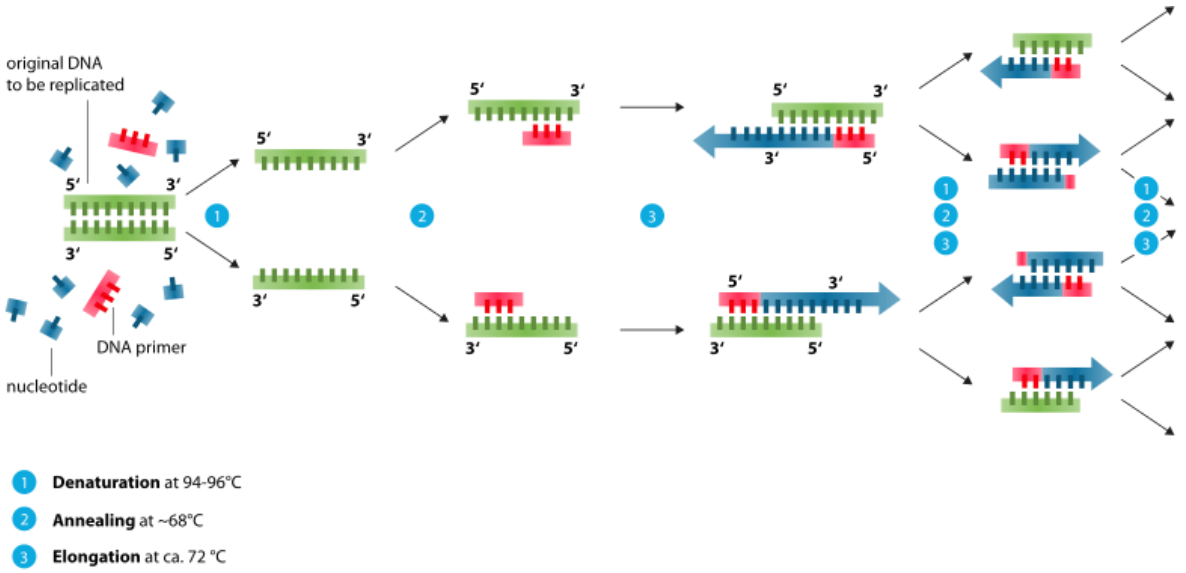

Figure 306: Representation of the sequence of events associated to PCR, depicting the separation of DNA (denaturation, 1), the binding of gene specific primers (annealing, 2), the construction of complementary DNA strands (elongation, 3) and finally, the repetition of termination and denaturation for X cycles until appropriate gene amplification is achieved. Diagram sourced from WikiMedia website on 14/03/2017 at 11:00[9].

Whilst the cell lines used for the initial loading studies were assumed to be folate receptor positive or negative based on the literature, these cell lines could have changed quite significantly from their originating parent cell line. Therefore, these cells may not exhibit the same genetic traits of the respective parent cell lines[10]. Accordingly, PCR was employed to crudely indicate the levels of gene expression for folate receptors α, β and γ in A549, HeLa and A2780 cancer cell lines. Forward and reverse sequence primers were ordered freshly and as

per the specification of Matsushita et al, whilst the PCR protocol was adapted from that of Shen et al (protocol and primer selection are discussed in experimental section 3.8.2)[11, 12].

Whilst PCR studies were conducted for these various cell lines, a number of issues arose, with blurring of PCR product bands within the gels and in some instances, no measurable PCR gene amplification products at all (including the control band for β Actin, a gene which is omnipresent). From the experiments conducted, A549s showed the most promising response to PCR and the clearest representation via agarose gel electrophoresis. Therefore, whilst the literature indicated A549s are folate receptor positive for all sub-categories, it was important to explicitly ascertain expression within the A549 cell culture utilised in the present research. Moreover, whilst Mornet et al indicated that A549s were susceptible to folate receptor α manipulation, the present research looked to establish the level of gene expression manipulation that might be achievable. Accordingly, PCR was employed to crudely indicate the levels of gene expression for folate receptors α, β and γ in the A549 cell line cultured in high folate media as well as low folate media. Agarose gel electrophoresis images of said PCR experimentation is represented in Figure 307.

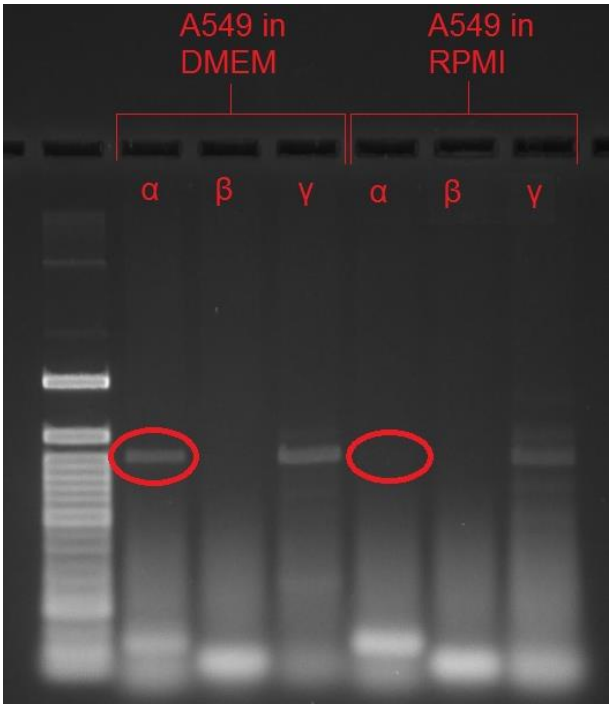

Figure 307: Agarose gel image of PCR products for A549 cells cultured in high and low folic acid containing medium (DMEM and RPMI respectively). Cells were cultured in T25 flasks for 4 weeks and were split every 3-4 days at around 90% confluency. RNA isolation, cDNA synthesis and PCR were conducted as per section 3.8.2. Red circles indicate the apparent suppression of the folate receptor alpha gene in the low folate cultured A549s (RPMI media) vs the high folate cultured A549s (DMEM).

As aforementioned, the principle of this technique resides in the amplification of the gene / genes of interest via the PCR. More specifically, due to a lack of sensitivity, only the genes that are amplified are typically observed as a strong band within the agarose gel. Figure 307 shows a total of 6 channels, three per A549 cell culture (DMEM vs RPMI), with successive channels representing attempted amplification of folate receptors α, β or γ respectively.

With regards to the α channel (lane 1 – DMEM cultured A549s and lane 4 – RPMI cultured A549s), there is clear presence of a band centred at 787bp for the DMEM culture (lane 1),

whilst there is no observable band at 787bp for the RPMI culture (lane 4). It is therefore evident from Figure 308, in contrast to the works of the literature (Mornet et al), the high folic acid media cultured A549s displayed a high level of folate receptor α gene expression, whilst the low folic acid media cultured A549s displayed an effective folate receptor α gene suppression[5]. That is to say, the present research contradicts the literature, which displayed that culturing A549s in low folate medium significantly increased surface folate receptor expression.

It is noteworthy however, that in line with the literature, no folate receptor β gene expression, nor amplification, was observable regardless of the media manipulation of the A549 cultures. Moreover, there is a measurable presence of folate receptor γ in both samples (332bp), with arguably a slightly stronger band represented in the high folate cultured A549s than that of the low folate cultured cells (lanes 3 and 6 respectively). To the best of our knowledge, this has not been discussed within the literature to any great extent. However, the persistent expression of folate receptor γ, regardless of α and β expression, is perhaps to be expected, on account of its primary function as a folate efflux protein. That being said, whilst a slight decrease is observed in the expression of γ protein for the low folate cultured A549s, on account of the apparent lack thereof of any folate receptor uptake proteins, one might expect that the efflux protein gene should also be equally suppressed. The effective maintenance of the efflux protein γ may therefore indicate that whilst the cells have effectively turned off the expression of α and β genes (in the zero folate culture), the cells may still comprise the corresponding receptor proteins on their surface and therefore, maintain a need for said efflux protein expression. Moreover, it is established within the literature that folate uptake is not exclusive to the active uptake via the aforementioned receptors, therefore, the cells may still take up folate via passive mechanisms, potentially further maintaining the need for folate efflux proteins.

The experiment was repeated in triplicate, with all agarose gels displaying the same down regulation of α in low folate media, zero expression of β in both and a maintained expression of γ in both. It is noteworthy that these experiments were conducted using two different types of media as opposed to using zero folate RPMI & a supplemented RPMI. Accordingly, the expressions observed cannot be directly compared. Later efforts for cellular utilisation used such zero and supplemented media and is discussed in greater depth later. Accordingly, to verify the PCR results, a commercial antibody system was used to visualise folate receptor alpha in the A549s that were cultured in the two different media via immunocytochemistry, in both confocal microscopy and FACS.

3.4. Immunocytochemistry Studies

Immunocytochemistry is the process of staining for a specific protein or antigen of interest via the employment of antibodies. The folate receptor primary antibody employed in the present research was raised in rabbits, was polyclonal, and displayed activity in human cell lines for folate receptor α (see experimental section 3.8.3). The secondary antibody of the present research was appropriately paired with the primary and comprised an Alexa Fluor dye, emissive within the green channel. Immunocytochemistry can be carried out on live or fixed cells dependent on the localisation of the target protein. In the present study, folate receptor α is a surface localised protein and therefore live cell studies were conducted as the antibody is not required to penetrate the cell. In the case of an internal target, live cell studies are not possible as the cells need to be permeabilised in order for the antibodies to reach their intended target.

Live cell immunocytochemistry gives the added advantage that the cells do not require a permeabilisation stage in order for the utilised antibody to reach its intended target.

Subsequently, this live cell technique obviates substantial chemical alteration of the cells permeability and thus represents a more biologically unaltered experiment. A Hodges group routine protocol was implemented, with adjustments being made to incubation times and antibody concentrations in line with manufacturer instructions (see experimental section 3.8.3).

In brief, A549s from low and high folate cultures were seeded into separate MatTek dishes and allowed to adhere overnight (typically 12 hours). The cells were then washed with PBS and incubated with primary antibody (Folate Receptor Alpha Polyclonal Antibody, 2µg/mL in 2mL media (DMEM or RPMI dependent on which culture the cells were from)) for 45 minutes. Cells were then washed three times with PBS and incubated with secondary antibody (Goat anti-rabbit Secondary Antibody, Alexa Fluor 488, 2µg/mL in 2mL media) for 30 minutes. The cells were then washed three times with PBS and immersed in 1mL imaging media before being imaged via live confocal microscopy within a pseudo incubation chamber. Images collected for these studies are represented in Figures 308 and 309.

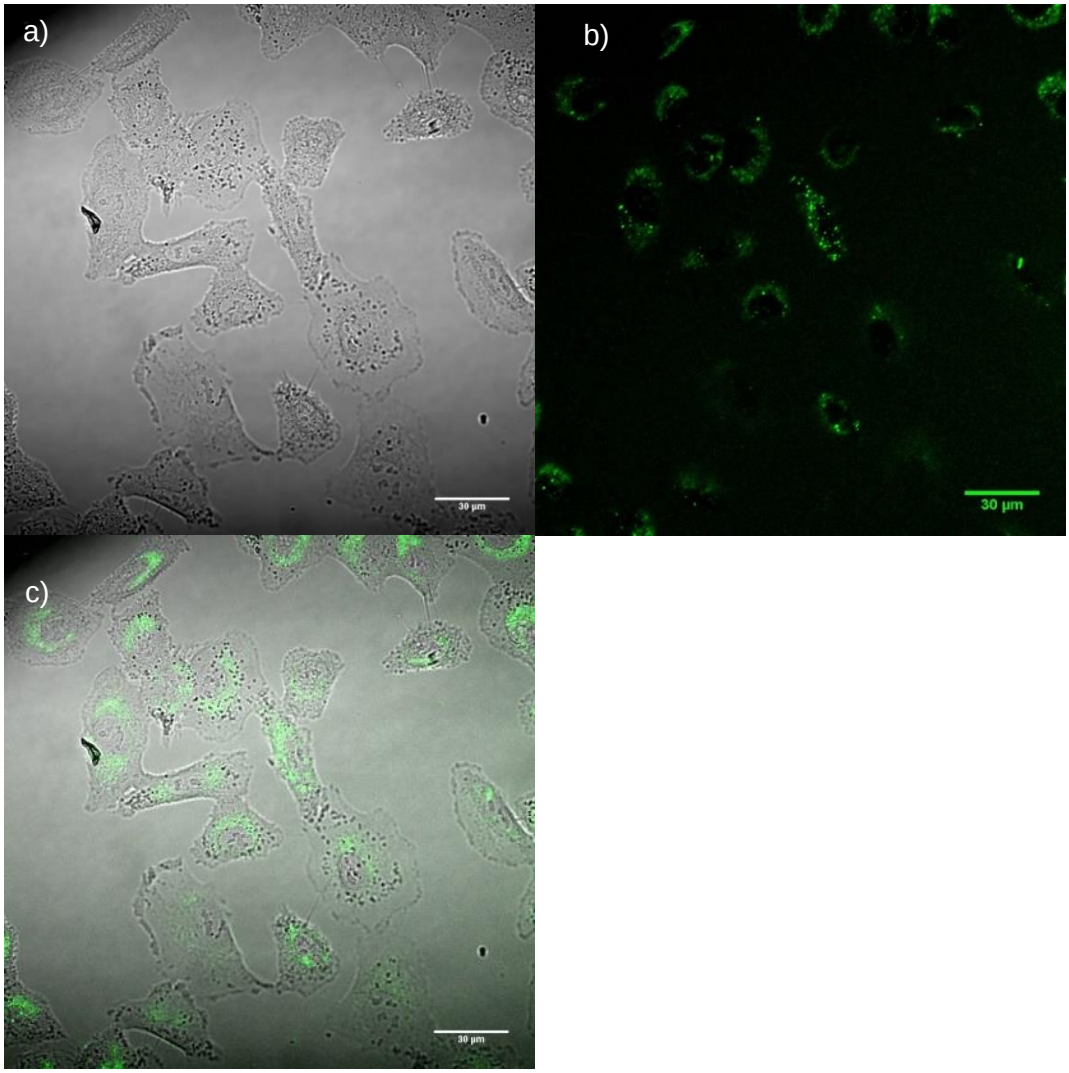

Figure 308: Blank A549s taken from supplemented folate RPMI media culture. Cells were seeded overnight onto MatTek dishes and subsequently treated with folate receptor alpha polyclonal antibody (2µg/mL in 2mL supplemented RPMI) for 45 minutes. Cultures were washed, immersed in imaging media and immediately transferred to a live cell imaging chamber for confocal microscopy studies. A) in focus brightfield plane of the collected z stack profile, B) averaged fluorescence signal over the z stack and C) overlay of the average antibody fluorescence signal over the respective in focus brightfield image. High folate cultured A549s show a relatively low emission intensity and distribution in comparison to the low folate cultured A549s of Figure 309.

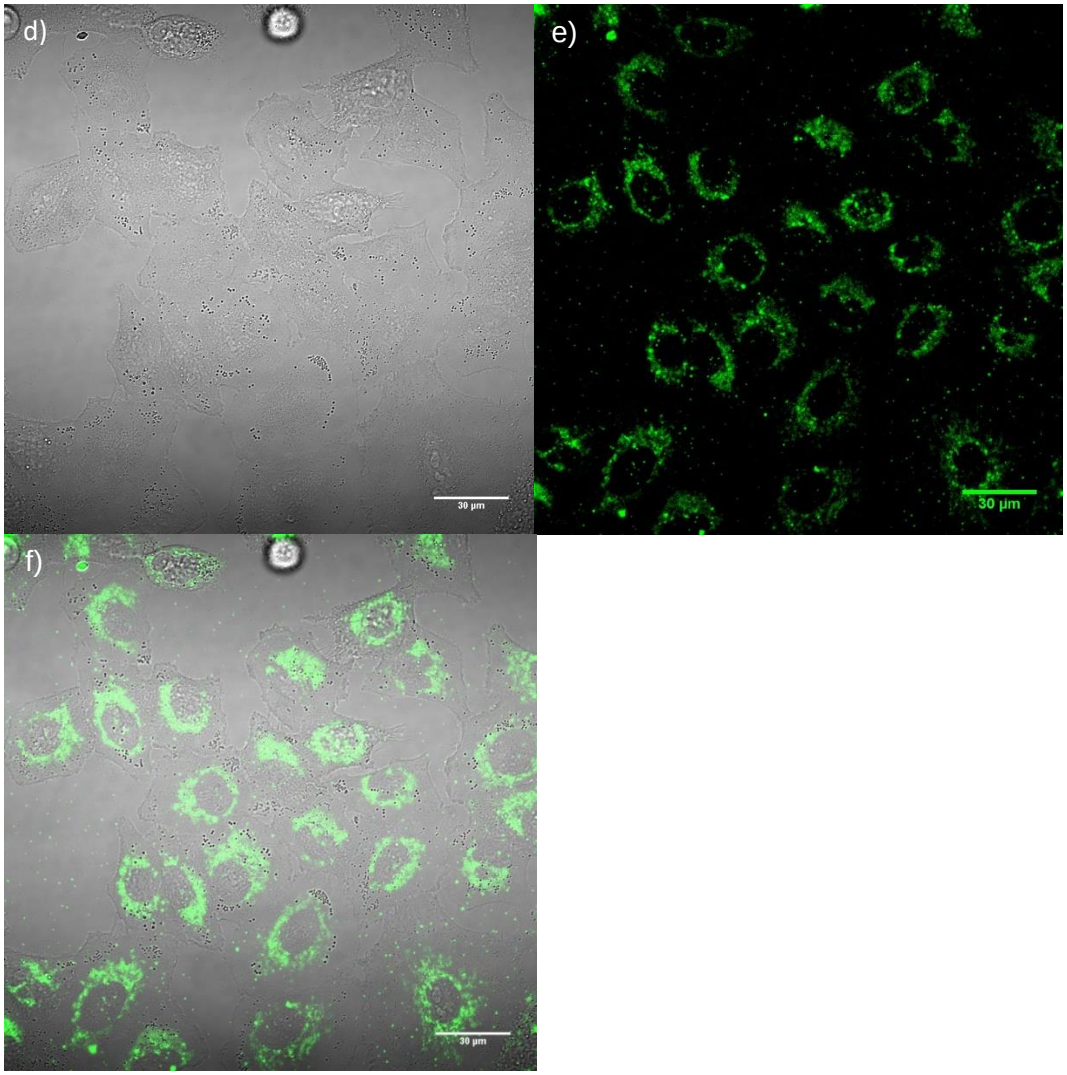

Figure 309: Blank A549s taken from zero folate RPMI media culture. Cells were seeded overnight onto MatTek dishes and subsequently treated with folate receptor alpha polyclonal antibody (2µg/mL in 2mL supplemented RPMI) for 45 minutes. Cultures were washed, immersed in imaging media and immediately transferred to a live cell imaging chamber for confocal microscopy studies. D) in focus brightfield plane of the collected z stack profile, E) averaged fluorescence signal over the z stack and F) overlay of the average antibody fluorescence signal over the respective in focus brightfield image. Low folate cultured A549s show a relatively high emission intensity and distribution in comparison to the high folate cultured A549s of Figure 308.

The confocal images of Figures 308 and 309 evidence that, in line with the literature, when A549s are cultured in low folate media there is a marked increase in the expression of folate receptor α on the surface of the cells. That is to say, upon review of the compressed z stack fluorescence images b) and e) of Figures 308 and 309 respectively, it is evident that there is significantly more measurable fluorescence in the low folate media cultured A549's (e) than in the high folate media cultured A549's (b). As aforementioned, immunocytochemistry is receptor dependent cellular staining. Therefore, greater emission is indicative of greater primary and secondary antibody binding, which is in turn indicative of greater surface protein expression. It is noteworthy that some degree of internalisation of the fluorophore was recorded, most likely due to internalisation of what were originally surface receptors which had bound the fluorescently tagged antibody during staining, thus some strong fluorescence signal was observed within the cells (observable via numerous z-stack slices). This signal was ruled out as auto-fluorescence on account of no such signal observable within the blank samples (no antibody loading) under the same microscope conditions. Such internalisation is to be expected on account of routine cellular folate receptor internalisation and recycling cycles[13]. Further research could look to confirm this hypothesis by conducting the staining using a fixed cell sample and no permeabilisation.

Moreover, given the substantially convex longitudinal cross section of the cell surface, each slice of the z stack image is representative of the signal measured at a portion of the cell. Therefore, whilst the overlay images of c) and f) are somewhat indicative of surface localised fluorescence, it does not exclusively represent the progression of fluorescence from the lowest point of the cell to the top, which would signify the fluorescence progressing from the periphery of the cell to the centre. Instead, some of the signal of internalised fluorescence is averaged into the final data observable in images b) and e). It would be excessive to represent each slice

of the corresponding z-stacks within Figures 308 and 309, however, the general progression of this fluorescence may be observed for the low folate cultured z stack in Appendix Section 7.1, so as to evidence the surface localisation over internalisation.

Summary of Findings

It is therefore evident from the above, and in agreement with the literature, that low folate cultured A549s do indeed exhibit upregulated surface expression of folate receptor α. This would therefore appear to contradict the earlier PCR data, which showed that culturing A549s in low folate media significantly reduced expression of the folate receptor α gene, which would subsequently imply a reduction in folate receptor α protein expression.

The significant difference between the antibody signal observed in the confocal z stack data for the high and low folate cultured A549s served as sufficient evidence of an imposed modulation of folate receptor α expression, and therefore, high and low folate cultured A549s were carried forward for future cellular experimentations. All future high and low folate manipulations were conducted using zero folate RPMI and a supplemented high folate RPMI (using a separate flask of zero folate RPMI with the addition of 20mg folic acid). Through supplementation of RPMI with folic acid it is ensured that the only difference in media formulation is that of the folate content, thus, any imparted differences in the A549 cultures would be purely as a result of the folic acid available to the cells.

3.5. Comparative Uptake Studies

Proof of Concept

Subsequent research sought to ascertain whether the presence of folate moieties on the surface of GNP-Fol does indeed lead to enhanced nanoparticular cellular uptake when compared to the citrate coated surface of GNP-Cit. Accordingly, initial research comprised confocal microscopy, qualitatively assessing ruthenium probe fluorescence in high and low folate media cultured A549s dosed with RuPhenSS loaded GNP-Fol and GNP-Cit separately. The results of these studies are represented in Figures 311 to 314. The principle being that for the high folate receptor expressing cells, more prominent FITC and RuPhen signals should be observable, on account of higher antibody staining and GNP-Fol-RuPhen uptake. In contrast, the low folate receptor A549s should display the opposite. This hypothesis is displayed grammatically in Figure 310 below.

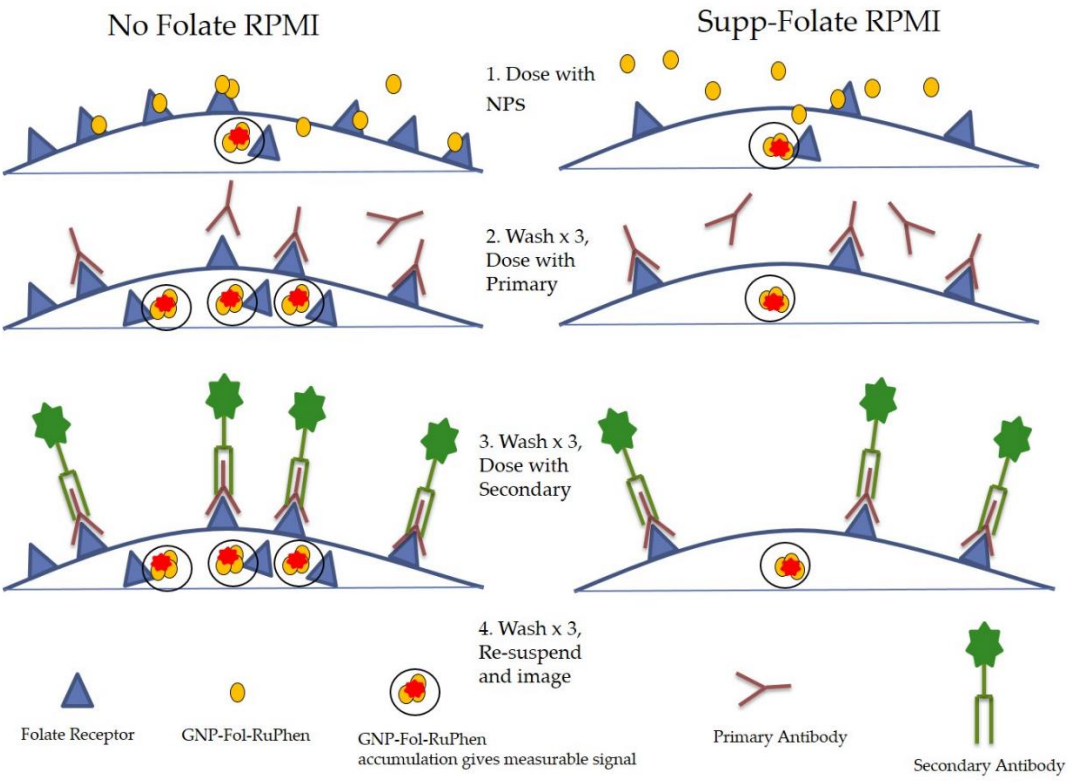

Figure 310: Diagrammatic representation of high and low folate receptor expressing A549 cells with corresponding antibody / RuPhen dosing levels.

As noted, comparable size of the two nanoparticular systems is important so as to theoretically afford systems with comparable surface loading of RuPhenSS and featuring largely similar physical limitations in relation to cellular uptake. Accordingly, the GNP-Fol and GNP-Cit nanoparticular systems were made to be within ±5nm of each other, with the typical size of GNP-Fol being ~15nm and GNP-Cit ~13nm, so as to give theoretically equivalent surface loading potential and geometric uptake limitations. The cell samples were loaded with identical concentrations and volumes of GNP-Fol-RuPhenSS or GNP-Cit-RuPhenSS (10µL of 1mM solution per 1mL of ~1nM GNP), with identical dosing times (3 hours) and cell seeding densities (800,000) employed (see Experimental section 3.8.4).

Sephadex filtration is the means typically employed within the literature for removal of non-nanoparticular bound molecules within GNP-Cit solutions. However, sephadex purification was unsuitable for GNP-Fol as the resulting filtered system would become unstable and aggregate (typically within one hour). On review of the literature, no protocol was found for the filtration of GNP-Fol by sephadex. It is hypothesised herein that the instability of the GNP-Fol system post sephadex filtration stems from the removal of excess folate from the system. Therefore, through sephadex filtration, it is hypothesised that the pH of the system is dramatically altered through removal of unreacted sodium folate, as well as potential removal of loosely associated folate moieties to the surface of the nanoparticles. As an alternative, GNP-Fol-RuPhenSS and GNP-Cit-RuPhenSS systems were subjected to 24 hour dialysis in deionised water to remove the majority of unbound RuPhenSS whilst preserving an appropriate amount of excess folate for maintenance of system stability (see experimental section 3.8.4).

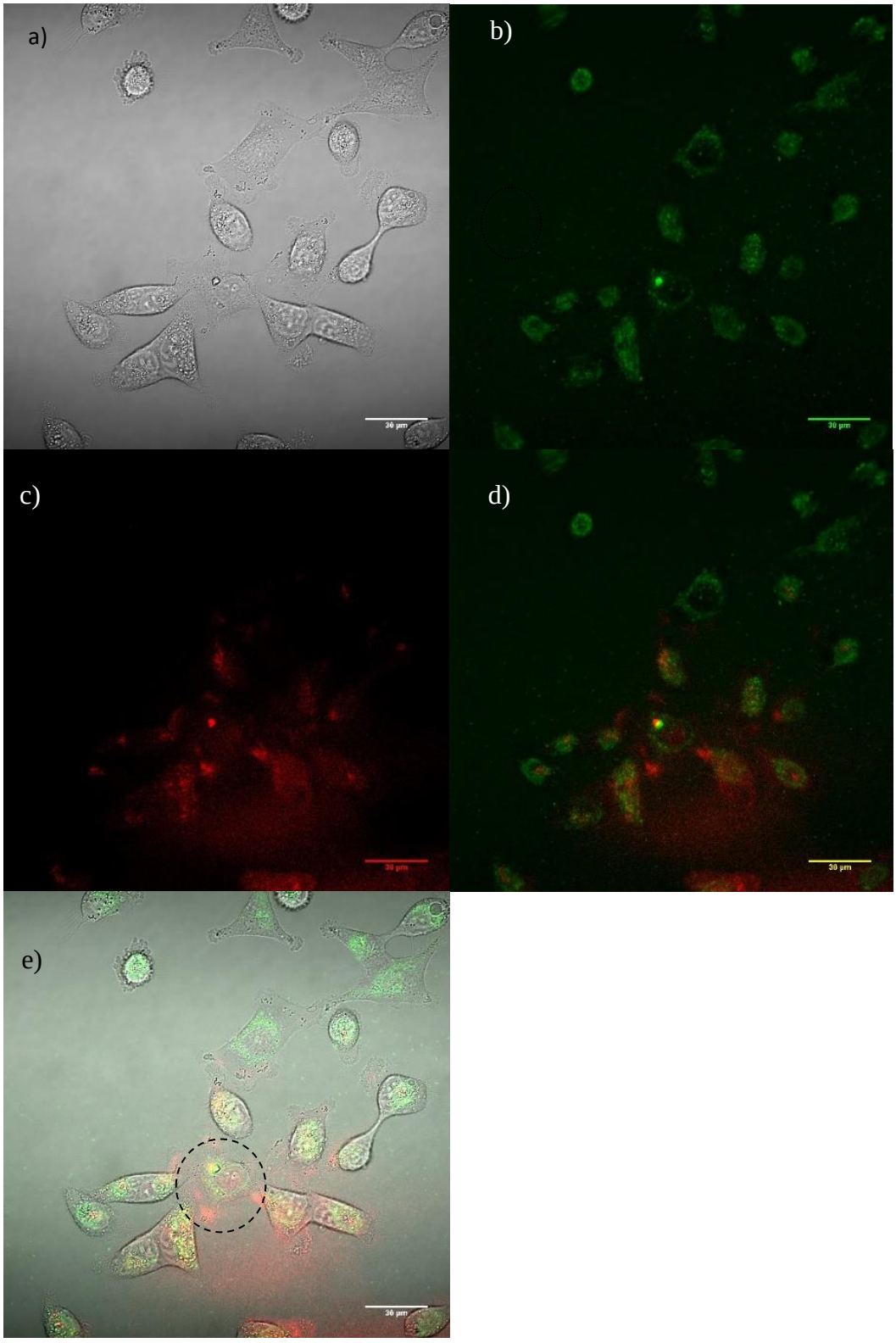
a)
b)
c)
d)
e)

f) g)

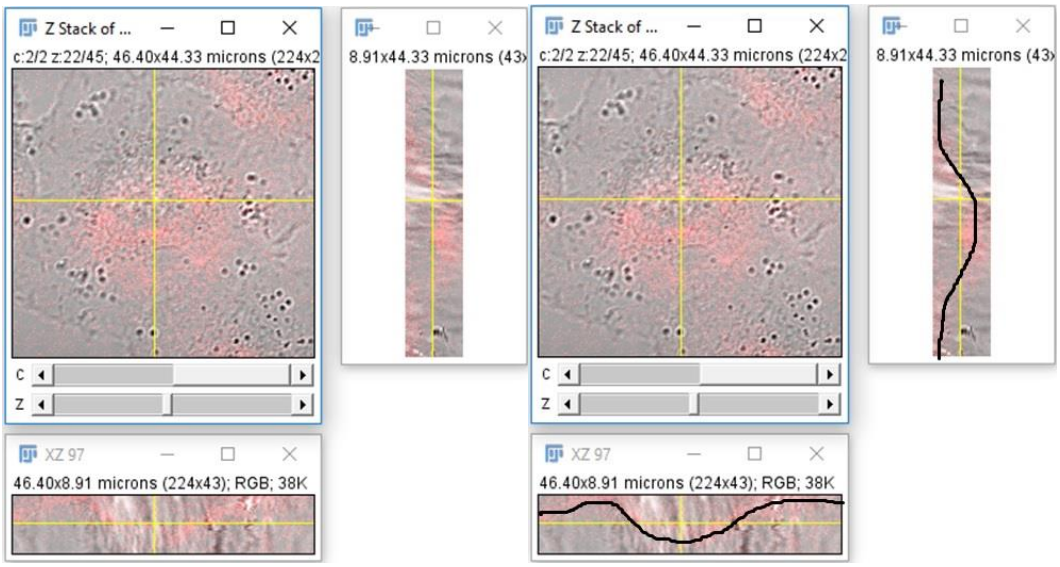

Figure 311: Live cell confocal microscopy images of A549s that have been cultured in high folate RPMI (lower folate receptor α expression) and subsequently dosed with antibodies and GNP-Fol-RuPhen. Cells were dosed with 1mL of ~1nM GNP-Fol loaded with 12µL RuPhen (1mM) for 3 hours. a) in focus plane of the brightfield z stack; b) average antibody fluorescence signal across the z stack; c) average RuPhen fluorescence signal across the z stack; d) overlay of the average antibody and RuPhen signals, e) overlay of all channels, f) and g) are orthogonal representations of the RuPhen fluorescence signal collected across the z stack profile for the single cell represented with a dotted outline in image e).

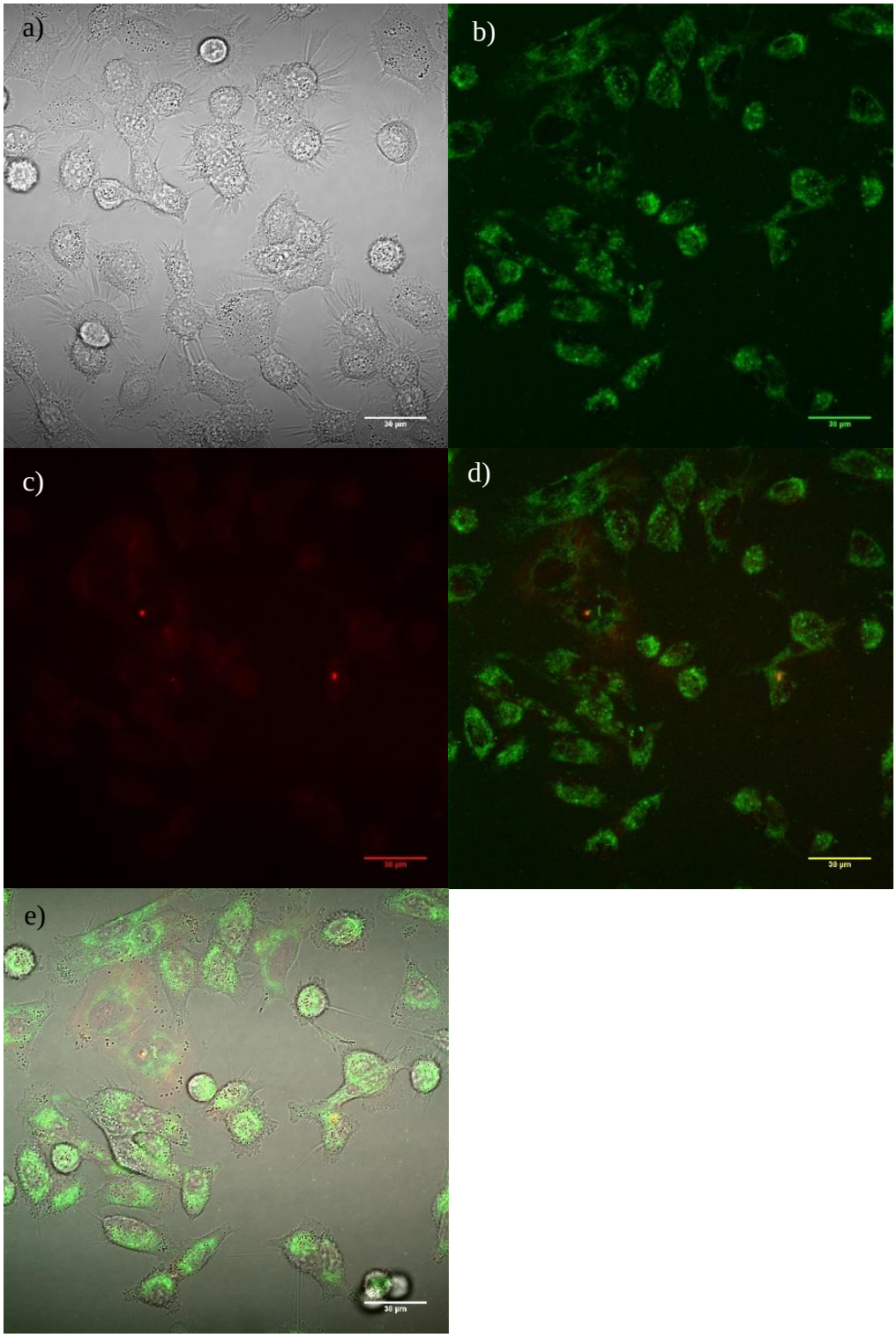

Figure 312: Live cell confocal microscopy images of A549s that have been cultured in high folate RPMI (lower folate receptor α expression) and subsequently dosed with antibodies and GNP-Cit-RuPhen. Cells were dosed with 1mL of ~1nM GNP-Cit loaded with 12µL RuPhen (1mM) for 3 hours. a) in focus plane of the brightfield z stack; b) average antibody fluorescence signal across the z stack; c) average RuPhen fluorescence signal across the z stack; d) overlay of the average antibody and RuPhen signals and e) overlay of all channels.

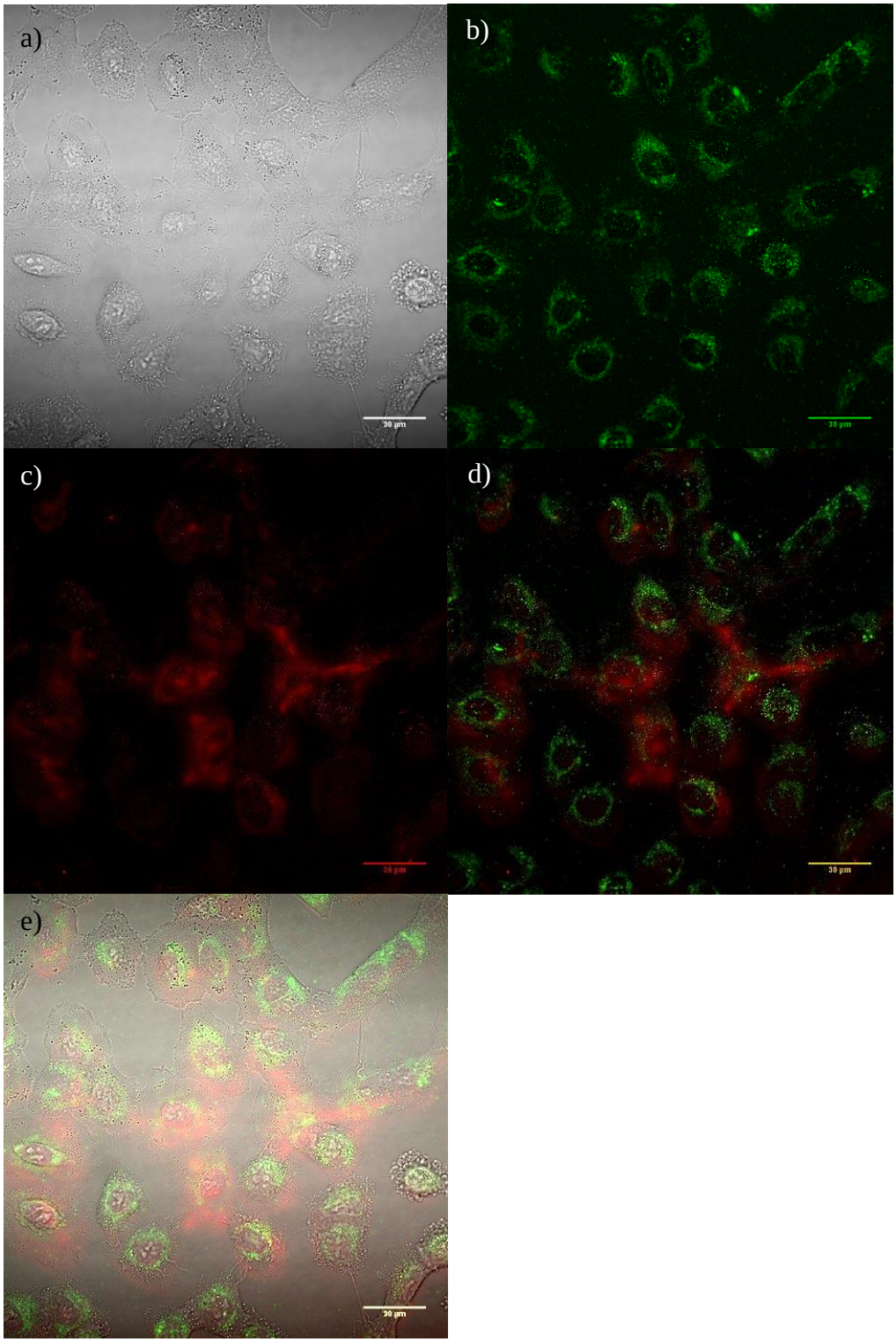

Figure 313: Live cell confocal microscopy images of A549s that have been cultured in low folate RPMI (higher folate receptor α expression) and subsequently dosed with antibodies and GNP-Fol-RuPhen. Cells were dosed with 1mL of ~1nM GNP-Fol loaded with 12µL RuPhen (1mM) for 3 hours. a) in focus plane of the brightfield z stack; b) average antibody fluorescence signal across the z stack; c) average RuPhen fluorescence signal across the z stack; d) overlay of the average antibody and RuPhen signals and e) overlay of all channels.

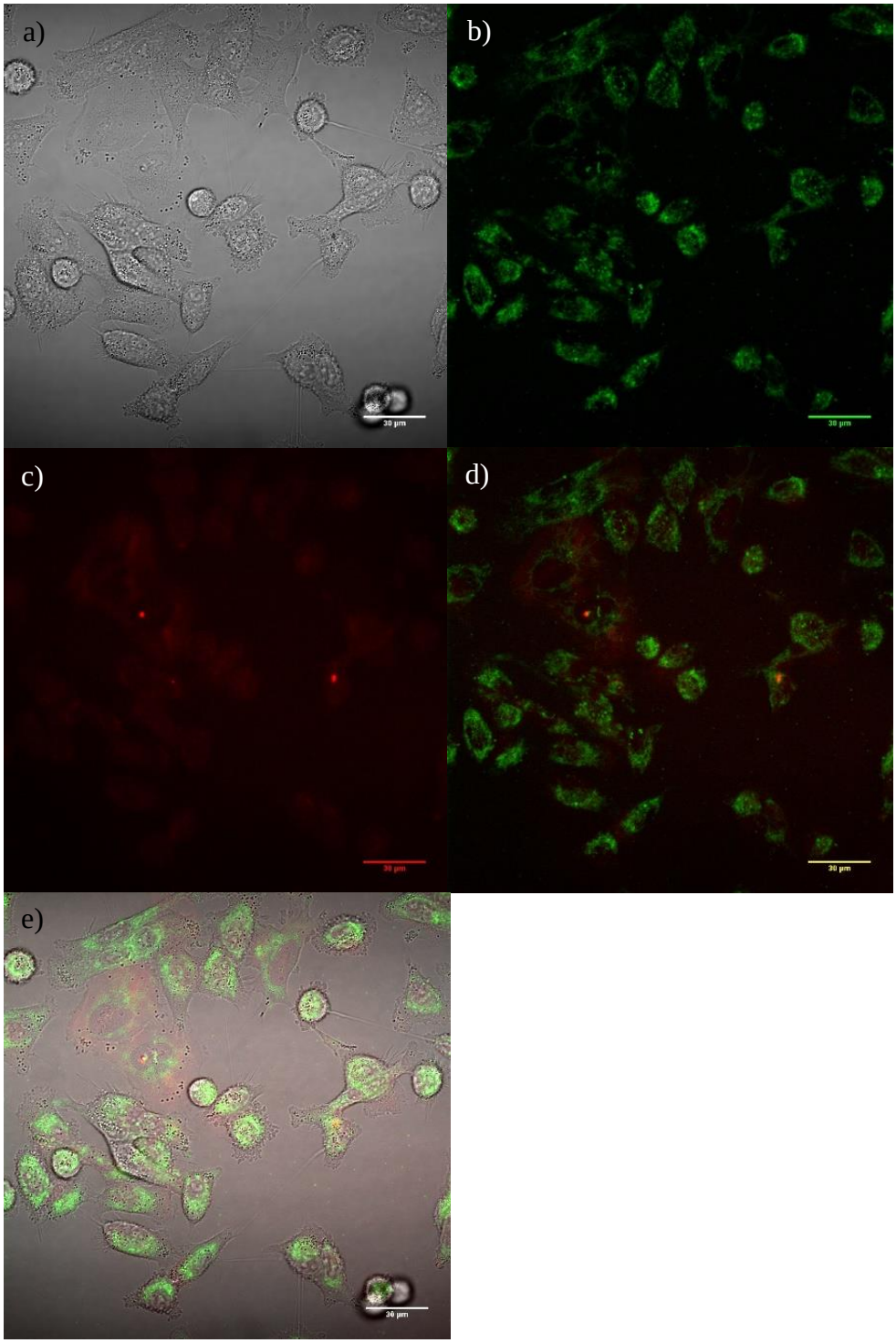

Figure 314: Live cell confocal microscopy images of A549s that have been cultured in low folate RPMI (higher folate receptor α expression) and subsequently dosed with antibodies and GNP-Cit-RuPhen. Cells were dosed with 1mL of ~1nM GNP-Cit loaded with 12µL RuPhen (1mM) for 3 hours. a) in focus plane of the brightfield z stack; b) average antibody fluorescence signal across the z stack; c) average RuPhen fluorescence signal across the z stack; d) overlay of the average antibody and RuPhen signals and e) overlay of all channels.

From the above confocal studies it is evident that there is significantly greater ruthenium probe fluorescence intensity and signal prevalence in the high folate receptor expressing A549s dosed with GNP-Fol-RuPhenSS (Figure 311) by comparison to GNP-Cit-RuPhenSS (Figure 312). In contrast however, in the low folate receptor expressing A549s, a largely comparable level of fluorescence is observed for the two nanoparticular systems (Figures 313 and 314). The RuPhenSS signal (red) can be seen permeating throughout the cells, with varying intensities and localisations within individual cells. Furthermore, there are small, intense, localised spots or clusters of signal, which may be as a result of vesicles or endosomes carrying bulk materials. It is noteworthy that no signal was observed in the nucleus of the cells, which may serve as proof that the fluorescent probe remains attached to the surface of the nanoparticles and / or free fluorophore is not released from the endosomes. Some signal is observable within the nuclear region of the cells as an artefact stemming from surface signal which has been collapsed into a single plane from the z stack. To evidence this, images f) & g) of Figure 311 represent orthogonal signal profiles of a single cell, showing fluorescence intensity throughout a cell from bottom to top. Image f) represents the orthogonal profile unedited whilst image g) shows the same profile with the additional of manual fluorescent periphery marking. The markings in image h) are to help represent the convex nature of the cell and localisation of the RuPhen fluorescence signal across the cell.

As a final note, there was a marked difference in uptake between GNP-Fol-RuPhen and GNP-Cit-RuPhen in the high folate receptor expressing A549s and a marginal difference in uptake in the low folate receptor expressing A549s. This is of particular significance, given the continuity of all other experimental and environmental conditions, as it evidences the considerable impact that the surface functionalisation of the nanoparticular systems plays in the mediated uptake of said system.

3.6. Competitive Uptake Studies

3.6.1. Combined Cell Cultures

Moving on from comparison of uptake in isolated systems, it is important to fundamentally evidence that the increased cellular uptake of GNP-Fol is not just merely because of a more rapid uptake system or a more prevalent one. Instead, it must be evidenced that this is as a result of a targeted system that has a preference for the folate receptor mediated uptake over other pathways. In order to address this, a co-culture of the two A549 cell systems was established, comprising the high folate receptor expressing and low folate receptor expressing A549s. For tracking purposes, the low folate receptor expressing A549s had their nuclei stained with Hoechst and washed five (5) times prior to tripsination, mixing with a suspension of non-stained high folate receptor expressing A549s and seeding onto 6 well plates. Once this co-culture cell system had then adhered to the culture dish (~4 hours) they were treated with GNP-Fol-RuPhenSS and their uptake compared qualitatively by confocal microscopy. Dosing procedures and loading times mimicked that of the previous experiments. Captured confocal images are represented in Figure 315.

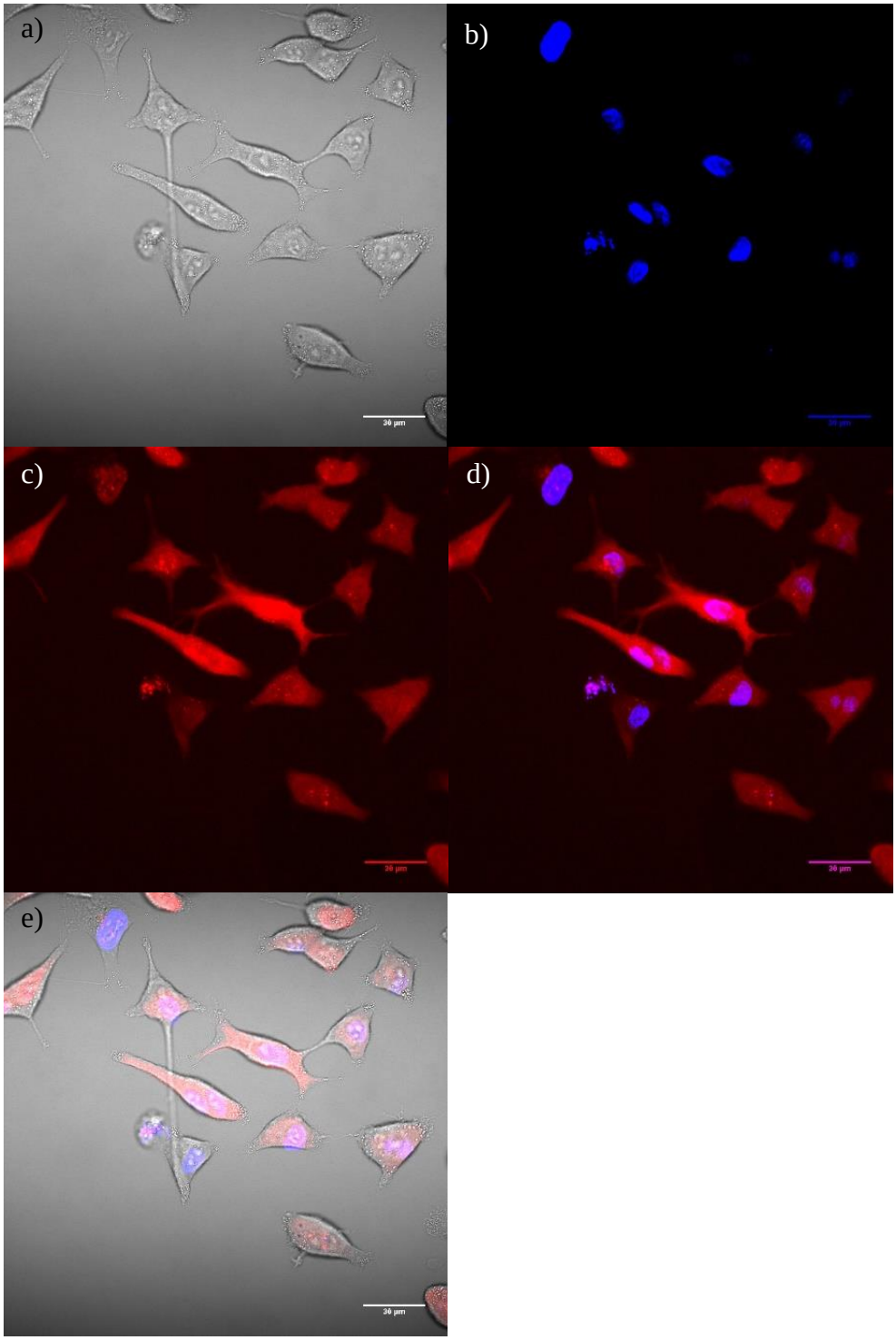

Figure 315: Live cell confocal microscopy images of a co-culture high and low receptor expressing A549 cultures. High folate receptor α expressing A549s had their nuclei stained and were washed prior to being mixed with low folate receptor α expressing A549s. After 4 hours, the co-culture was dosed with 1mL of ~1nM GNP-Fol loaded with 6µL RuPhen for 3 hours: a) in focus brightfield plane of the z stack; b) average Hoechst fluorescence across the z stack; c) average RuPhen fluorescence across the z stack; d) overlay b and c; and e) an overlay of all channels.

A number of issues were apparent from these confocal studies. Firstly, it is evident from the images of Figure 315, that there was a degree of Hoechst bleed through from the high folate receptor expressing A549s into the low folate receptor expressing A549s. More specifically, images b) - d) show a number of cells with a strong blue channel signal for the nuclei and a weak red channel signal for the RuPhen probe. However, the same images also show a number of cells with a weak blue channel signal for the nuclei with a strong red channel signal for the RuPhen probe. One possibility in this regard is that there is a mixture of high and low folate receptor expressing A549s within the low folate receptor cell culture, and that there was inconsistent nuclei staining within the preparation. Alternatively, and in line with the prior imaging studies, there is a consistent degree of folate receptor expression in both cultures, albeit at alternative extremities, and the inconsistency arises through bleed-through of Hoechst dye within the co-culture. This bleed-through may be as a result of insufficient washes prior to lysing and mixing of the two cell cultures, or perhaps, during the plating procedure, some of the Hoechst dyed cells die or rupture, releasing Hoechst dye which subsequently stains cells from the other originating culture (low folate receptor expressing). This issue prevents any degree of certainty in the qualitative analysis of the difference in nanoparticular uptake, and effectively nullifies the possibility of quantitative analysis / comparison. Accordingly, co-culture studies were not further investigated.

Subsequently, it was hypothesised that the lack of differential uptake within the cell co-culture may be as a result of the nanoparticles settling within the culture dish. Moreover, it was hypothesised that the settled nanoparticles were merely being taken up by any viable uptake mechanism, of any particular cell they may happen to fall within the vicinity of. It was further apparent that were the present nanoparticular system to be employed in any later in vivo studies, said system would be required to exhibit a preferential uptake whilst being constantly subjected

to flow. Therefore, in order to crudely model this need for selective uptake whilst being subjected to flow, ruthenium probe based loading studies were repeated with the samples being dosed and incubated on a plate rocker.

3.6.2. Subjected Flow Uptake Studies

Theoretically, incubating the cells on a plate rocker would prevent the nanoparticles within the media from settling onto the MatTek dish. Instead, the nanoparticles would hypothetically gently pass over the cell surface, thus presenting an opportunity for the folate moieties on the surface of the GNP-Fol system to bind to the receptors of the cells. In contrast, the GNP-Cit system should pass over the cell surfaces, exhibiting some uptake (be it passive or active), but theoretically exhibiting significantly less folate receptor mediated uptake. Therefore, there should be less uptake within the high folate receptor expressing A549s of GNP-Cit-RuPhen vs GNP-Fol-RuPhen; no apparent difference in uptake of GNP-Cit-RuPhen across high and low folate receptor expressing A549s; and, significant difference in uptake of GNP-Fol-RuPhen in going from high to low folate receptor expressing A549 cultures. Confocal images for said studies are represented in Figures 316 to 319 and full experimental details are available in section 3.8.5.

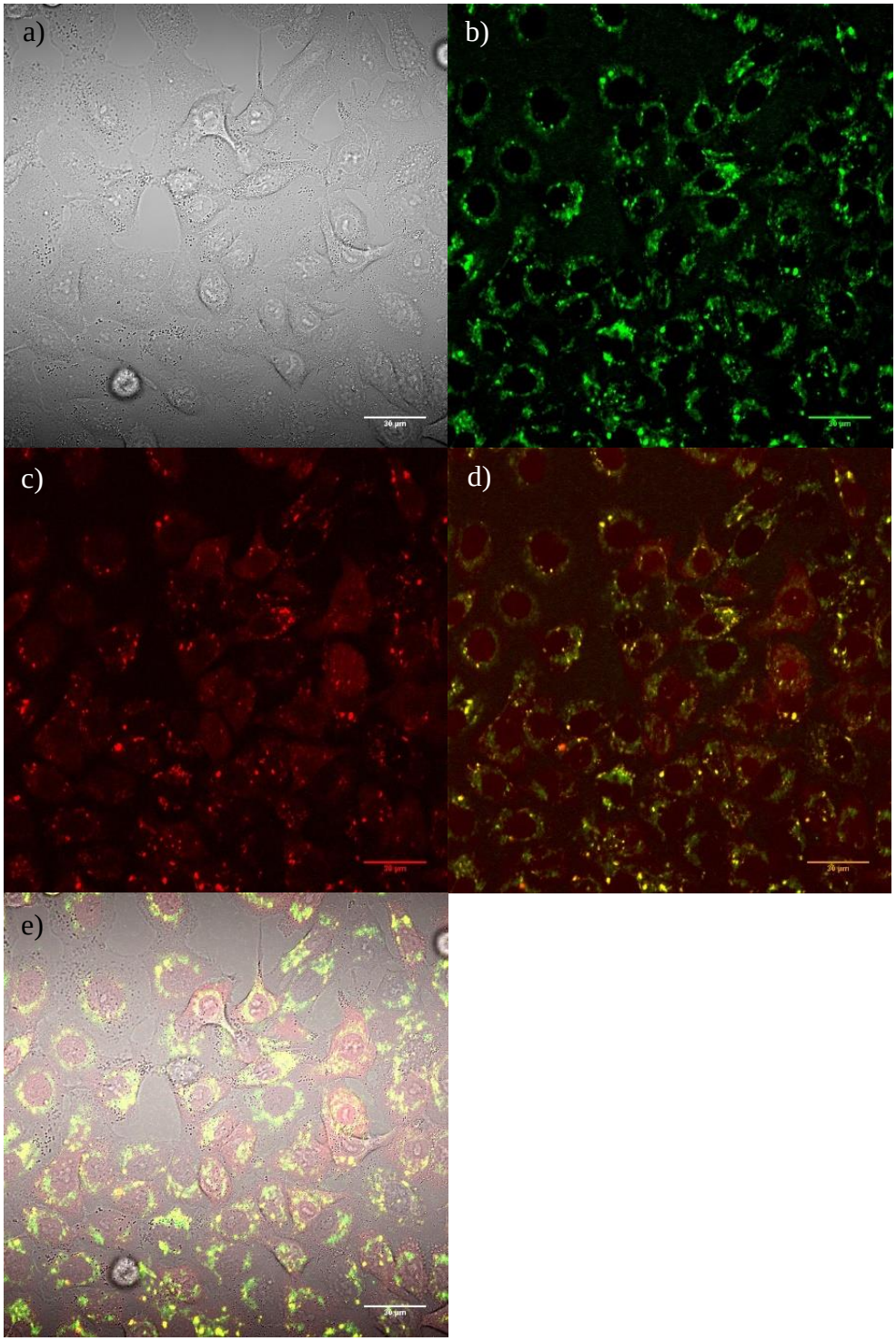

Figure 316: Confocal microscopy images of high folate receptor α expressing A549s dosed for 24 hours on a plate rocker with GNP-Fol-RuPhen (1mL of ~1nM GNP-Fol loaded with 12µL 1mM RuPhen). Folate receptors were subsequently stained with Folate Receptor Alpha Polyclonal Antibody (2µg/mL in 2mL media), washed three times with PBS and incubated with secondary antibody (Goat anti-rabbit, Alexa Fluor 488, 2.5µg/mL in 2mL media). a) in focus brightfield plane of z stack; b) average antibody fluorescence across z stack; c) average RuPhen fluorescence across z stack; d) overlay of b and c and e) overlay of all channels.

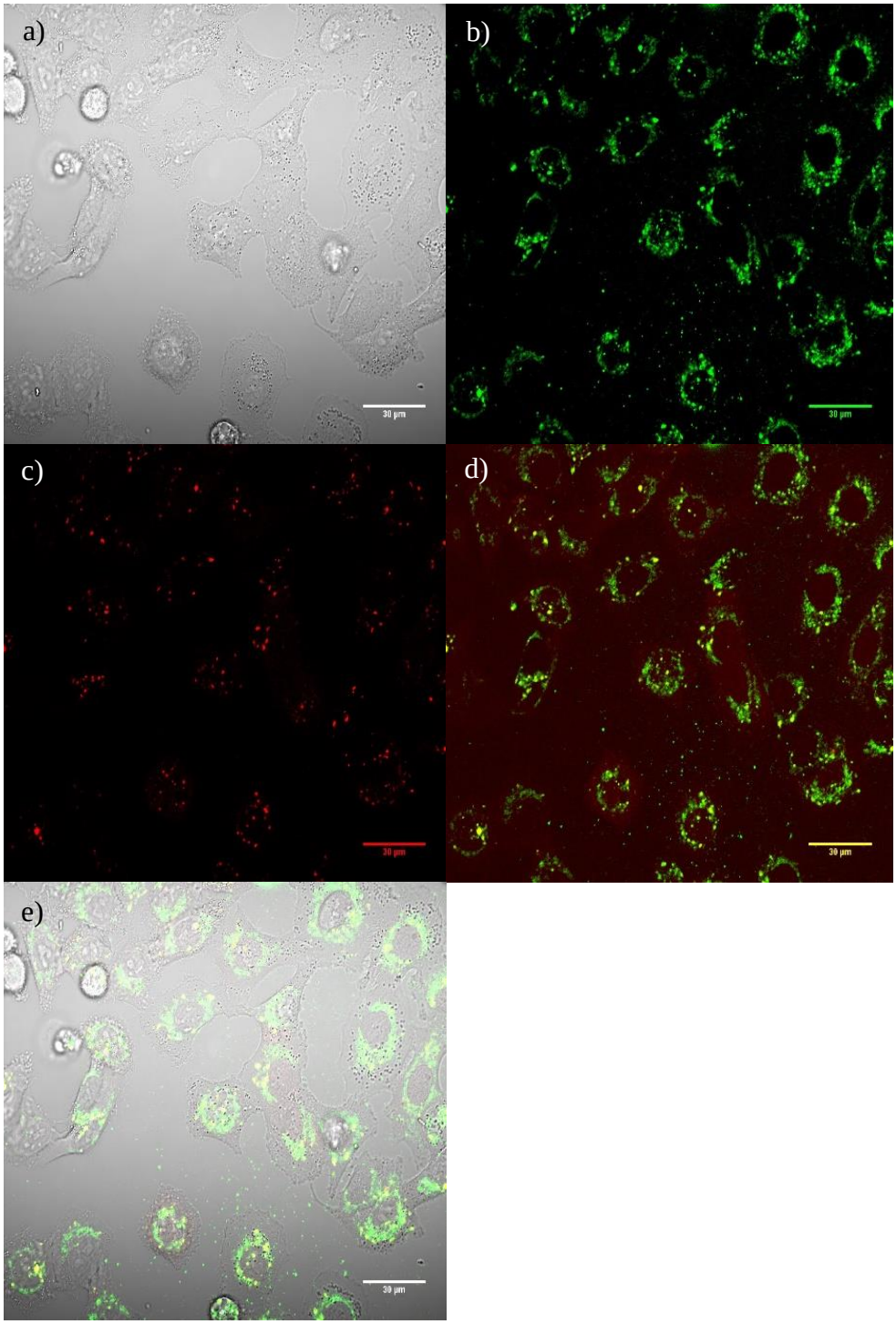

Figure 317: Confocal microscopy images of high folate receptor α expressing A549s dosed for 24 hours on a plate rocker with GNP-Cit-RuPhen (1mL of ~1nM GNP-Cit loaded with 12µL 1mM RuPhen). Folate receptors were subsequently stained with Folate Receptor Alpha Polyclonal Antibody (2µg/mL in 2mL media), washed three times with PBS and incubated with secondary antibody (Goat anti-rabbit, Alexa Fluor 488, 2.5µg/mL in 2mL media). a) in focus brightfield plane of z stack; b) antibody fluorescence across z stack; c) RuPhen fluorescence across z stack; d) overlay of b and c; and e) overlay of all channels.

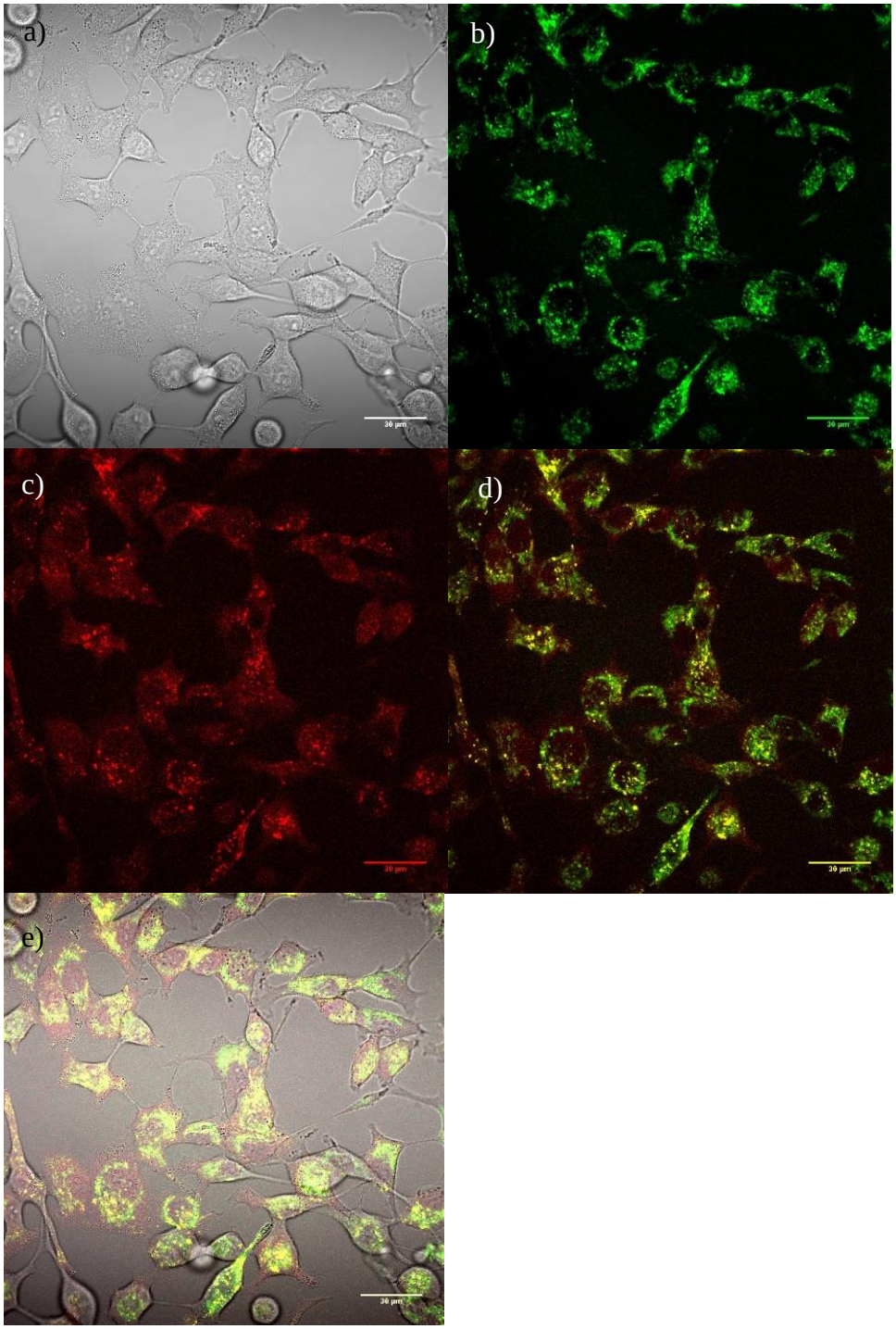

Figure 318: Confocal microscopy images of low folate receptor α expressing A549s dosed for 24 hours on a plate rocker with GNP-Fol-RuPhen (1mL of ~1nM GNP-Fol loaded with 12µL 1mM RuPhen). Folate receptors were subsequently stained with Folate Receptor Alpha Polyclonal Antibody (2µg/mL in 2mL media), washed three times with PBS and incubated with secondary antibody (Goat anti-rabbit, Alexa Fluor 488, 2.5µg/mL in 2mL media). a) in focus brightfield plane of z stack; b) antibody fluorescence across z stack; c) RuPhen fluorescence across z stack; d) overlay of b and c; and e) overlay of all channels.

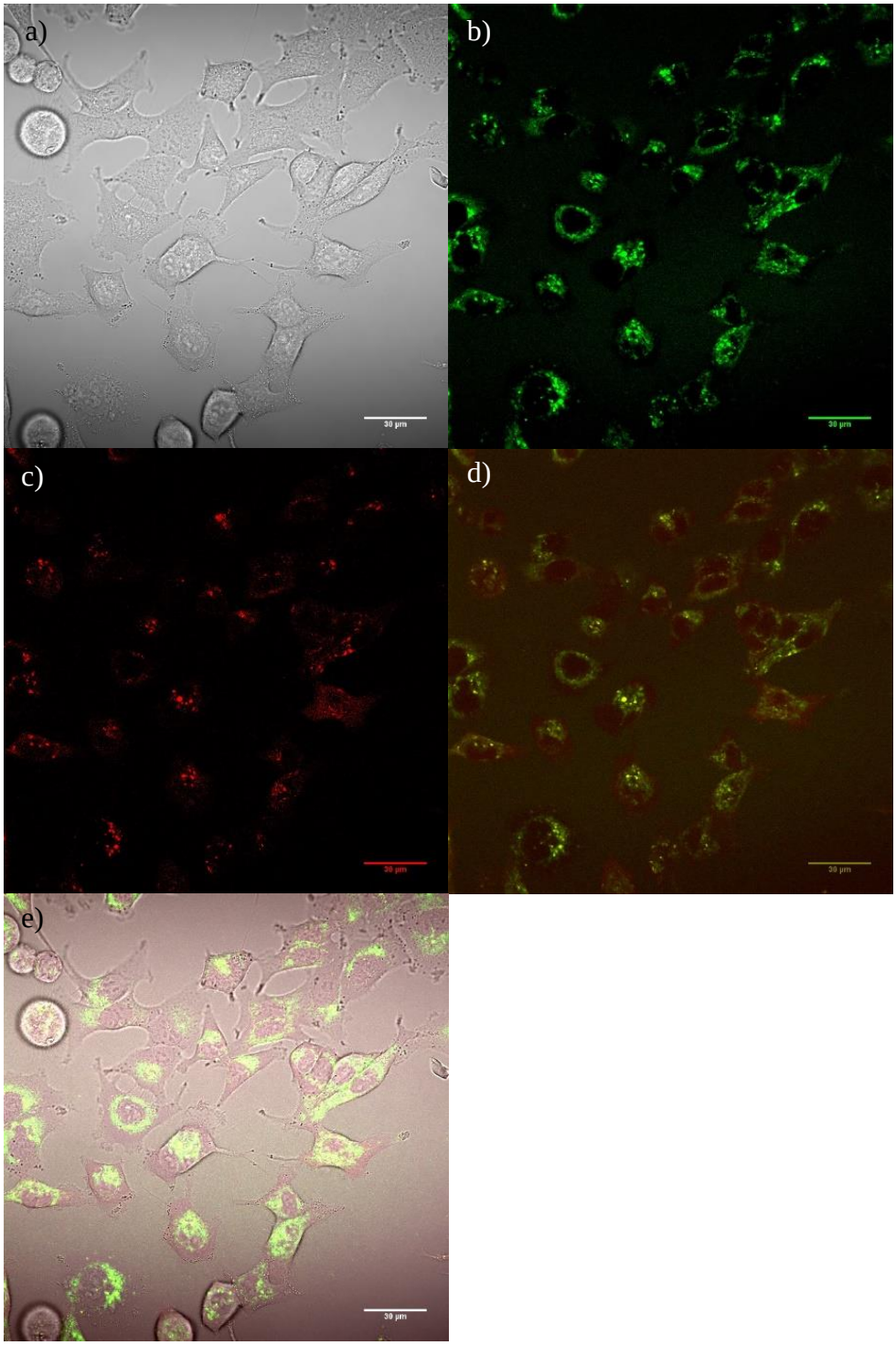

Figure 319: Confocal microscopy images of low folate receptor α expressing A549s dosed for 24 hours on a plate rocker with GNP-Cit-RuPhen (1mL of ~1nM GNP-Cit loaded with 12µL 1mM RuPhen). Folate receptors were subsequently stained with Folate Receptor Alpha Polyclonal Antibody (2µg/mL in 2mL media), washed three times with PBS and incubated with secondary antibody (Goat anti-rabbit, Alexa Fluor 488, 2.5µg/mL in 2mL media). a) in focus brightfield plane of z stack; b) antibody fluorescence across z stack; c) RuPhen fluorescence across z stack; d) overlay of b and c; and e) overlay of all channels.

From the images of Figures 316 to 319 it is evident that there is a difference in the level of GNP-Fol-RuPhen and GNP-Cit-RuPhen uptake within A549 cells irrespective of the number of folate receptors present. Specifically, it is evident that in both the high folate receptor α expressing (Figure 316, 317) and low folate receptor α expressing (Figure 318, 319) A549 cultures there was a greater level of RuPhen signal present for the GNP-Fol system (Figures 316 and 318) vs the GNP-Cit system (Figures 317 and 319). This is in support of the theory that the GNP-Fol system should present a greater level of uptake than GNP-Cit in the presence of flow due to surface folate receptor binding.

However, it is not readily discernible from the confocal data whether there is indeed any difference in levels of uptake of GNP-Fol-RuPhen between the high receptor (Figure 316) and low receptor samples (Figure 318). A number of potential conclusions could be drawn, which include: there is a negligible level of difference in uptake between the samples, irrespective of level of receptors available; there is not a significant difference in the level of receptors between the samples; or, there is a significant difference in receptor levels, but there are alternative means of uptake available to the GNP-Fol system that are not present for the GNP-Cit system. It is also evident that there was little observable difference between the level of uptake displayed across the high and low folate receptor expressing A549s for the GNP-Cit system (Figures 317 and 319). However, given the lack of difference in the GNP-Fol system samples, this result could merely be coincidental for the GNP-Cit system.

In order to further polarise the different levels of folate receptors available for nanoparticular uptake, receptor blocking studies were conducted via utilisation of primary antibody. Additionally, differences in uptake were quantitatively assessed through utilisation of Fluorescence Activated Cell Sorting (FACS) microscopy.

3.7. Folate Receptor Blocking Studies

Subsequent research focussed on the more readily comparable difference in uptake stemming solely from the availability of folate receptor mediated uptake (levels of receptors available). To achieve this, folate receptor blocking was utilised, with folate receptors actively blocked through dosing high folate receptor α expressing A549 cultures with the folate receptor α primary antibody before subsequently dosing the cells with the appropriate nanoparticular solutions.

In brief, the high folate receptor α expressing A549s were plated onto MatTek dishes and half the samples had had their α folate receptors blocked via incubation with α primary antibody (2μg / mL in 2mL media) for 1 hour. Subsequently, samples were incubated with either GNP-Fol-RuPhen or GNP-Cit-RuPhen on a plate rocker for 24 hours. The premise of this experiment being that if the majority of cellular uptake of the GNP-Fol system originates from folate receptor α mediated endocytosis, any blocking of the receptors should have a marked effect on the extent of uptake. Furthermore, the extent of the effect of blocking should be more evident in the high folate receptor α A549 culture by comparison to the low receptor α A549 culture given that there are more receptors available for blocking. Inversely, there should be little to no effect observed in the cellular uptake of the GNP-Cit based system as it is hypothesised that these nanoparticles should not be targeting the folate receptor uptake system and instead are being taken up via other means.

Cellular uptake of the two systems (GNP-Fol-RuPhen and GNP-Cit-RuPhen) was investigated in the high folate receptor bearing A549s via confocal microscopy (Figures 320 to 323) and FACS analysis (Figures 324 to 328). See experimental section 3.8.6 for full details. The samples of the present confocal and FACS studies are represented in Table 301.

HIGH FOLATE RECEPTOR α EXPRESSING A549S DOSED WITH:	
No Blocking	**With Receptor α Blocking**
Sample a) Blank	-
Sample b) GNP-Fol-RuPhen	Sample d) GNP-Fol-RuPhen
Sample c) GNP-Cit-RuPhen	Sample e) GNP-Cit-RuPhen

Table 301: Overview of confocal microscopy and flow cytometry samples.

3.7.1. Confocal Microscopy Studies

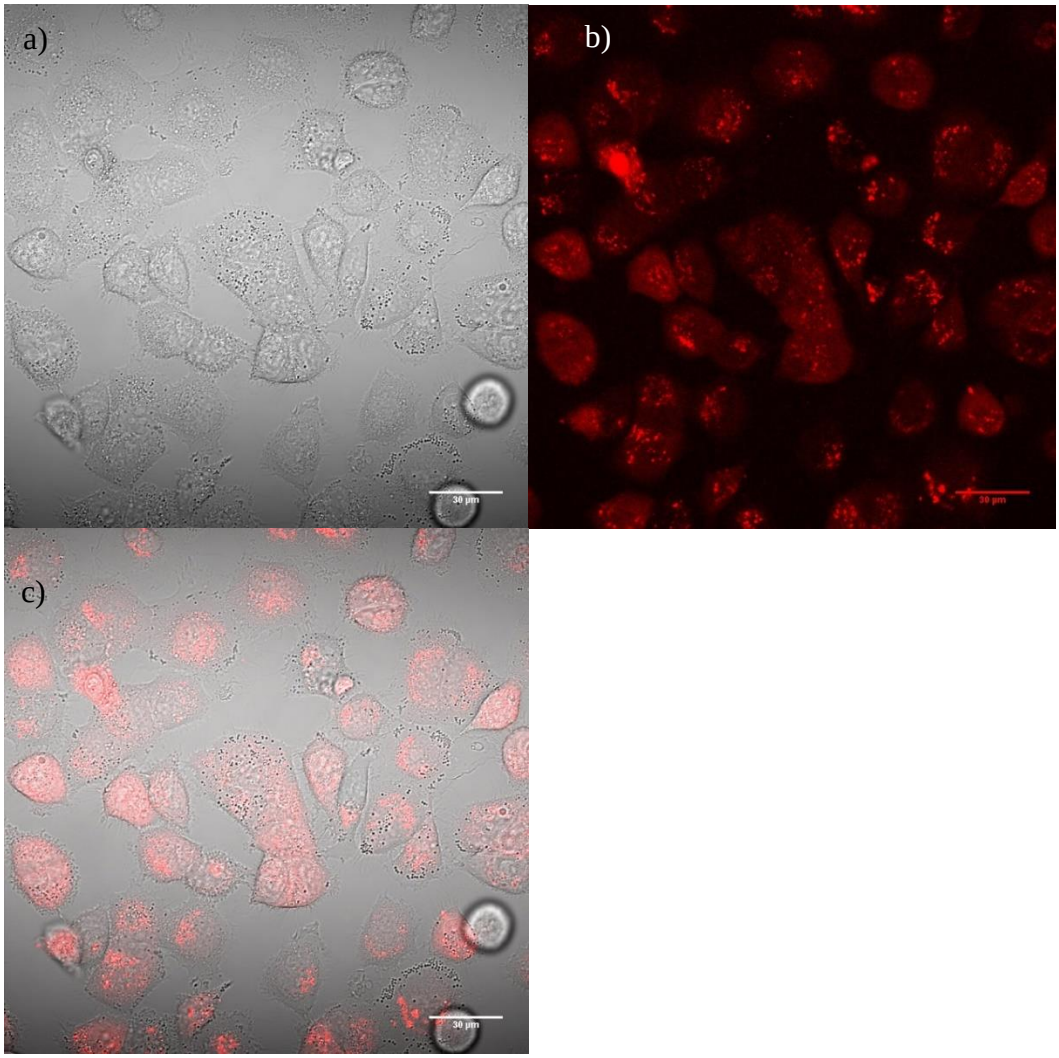

Figure 320: Confocal microscopy images collected for high folate receptor α expressing A549s that have been dosed for 24 hours on a plate rocker with GNP-Fol-RuPhen (1mL of ~1nM GNP-Fol loaded with 12µL 1mM RuPhen). NO RECEPTOR BLOCKING.

a) brightfield in focus plane of the z stack; b) average RuPhen fluorescence signal across z stack and c) overlay of channels.

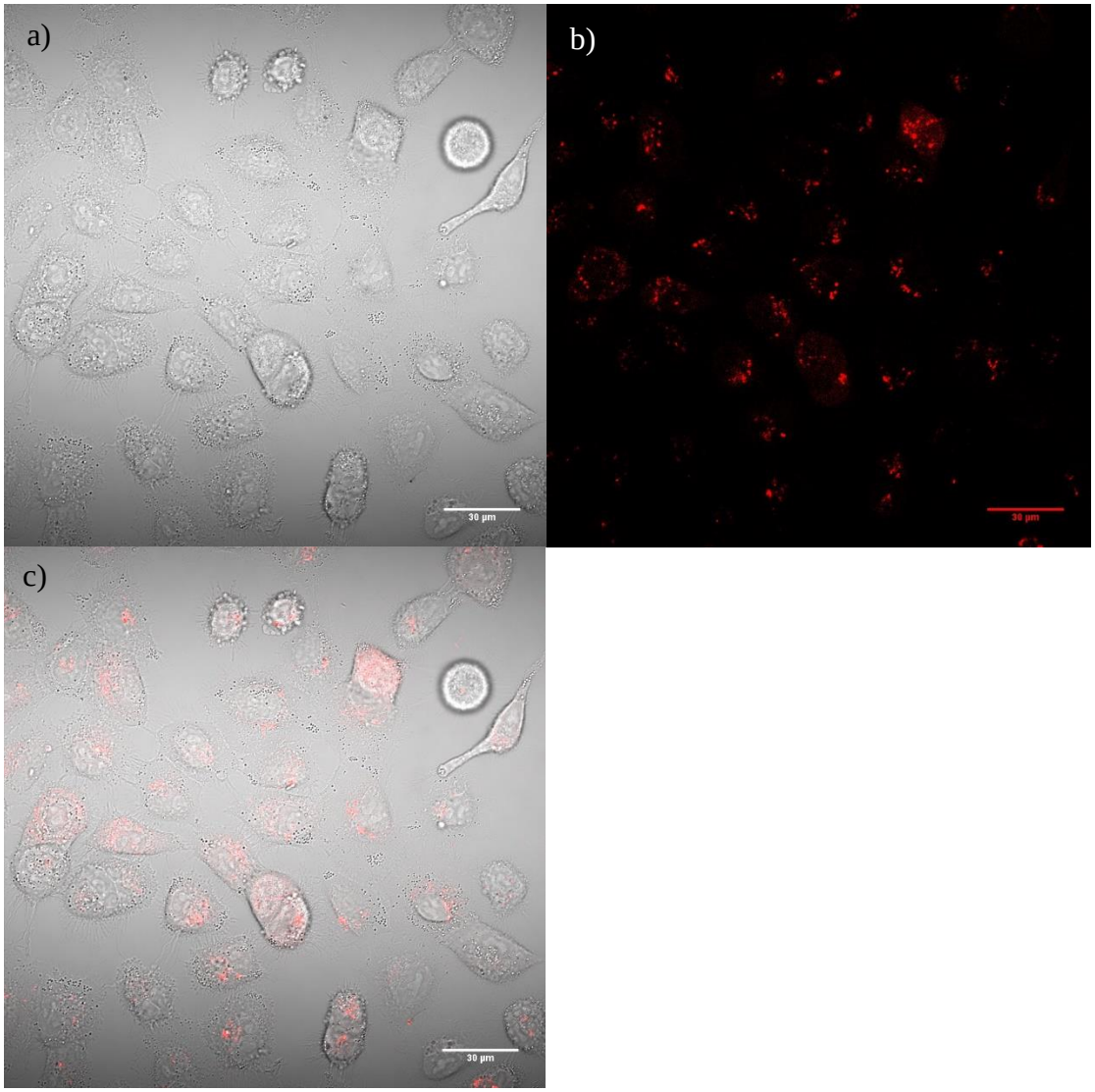

Figure 321: Confocal microscopy images collected for high folate receptor α expressing A549s that have been dosed for 24 hours on a plate rocker with GNP-Cit-RuPhen (1mL of ~1nM GNP-Fol loaded with 12µL 1mM RuPhen). NO RECEPTOR BLOCKING.

a) brightfield in focus plane of the z stack; b) average RuPhen fluorescence signal across z stack and c) overlay of channels.

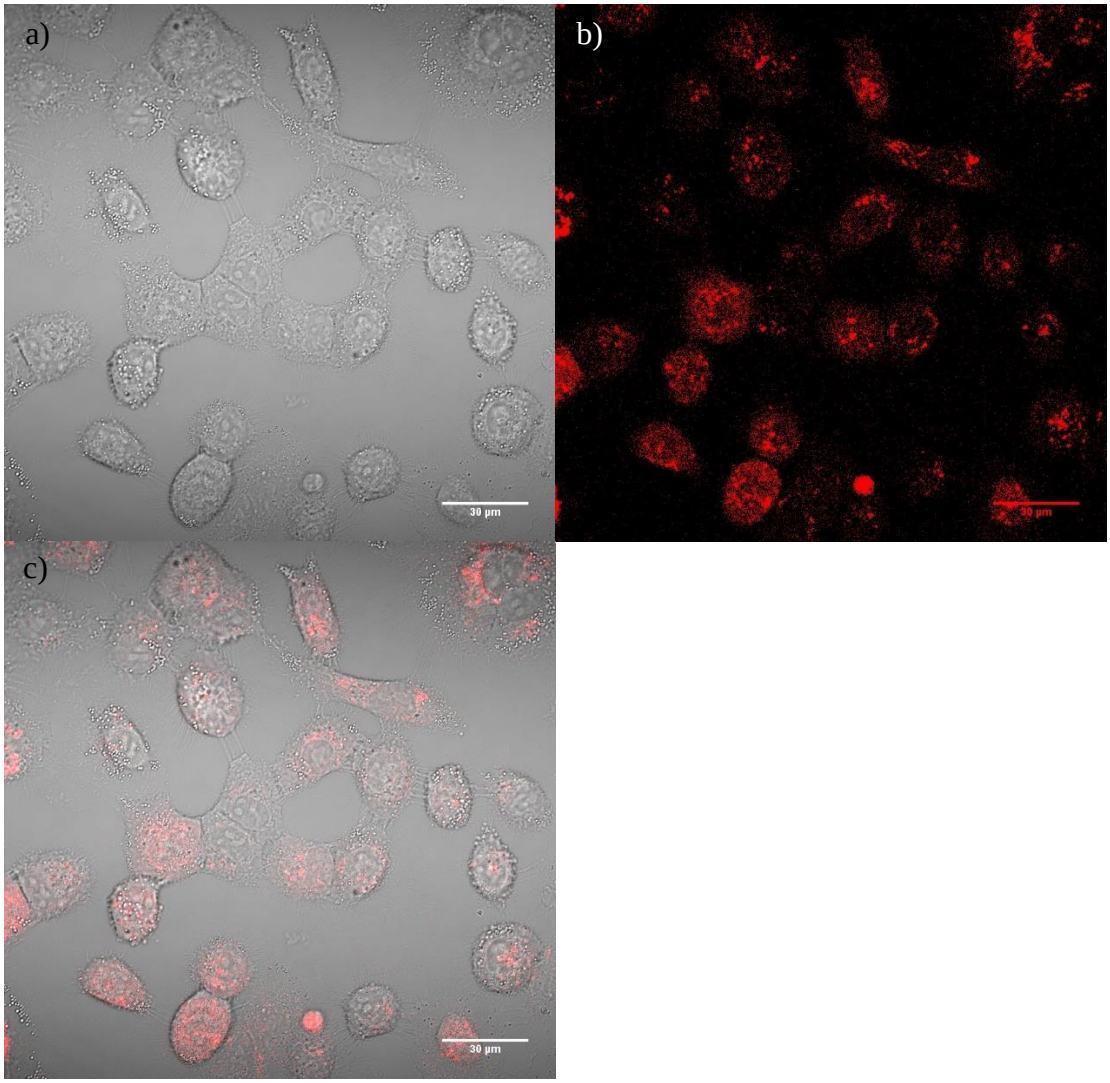

Figure 322: Folate Receptors Pre-Blocked - Confocal microscopy images collected for high folate receptor α expressing A549s that have been pre-dosed with Folate Receptor Alpha Polyclonal Antibody (2µg/mL in 2mL media) for one hour before being co-dosed for 24 hours on a plate rocker with GNP-Fol-RuPhen (1mL of ~1nM GNP-Fol loaded with 12µL 1mM RuPhen). a) brightfield in focus plane of the z stack; b) average RuPhen fluorescence signal across z stack and c) overlay of channels.

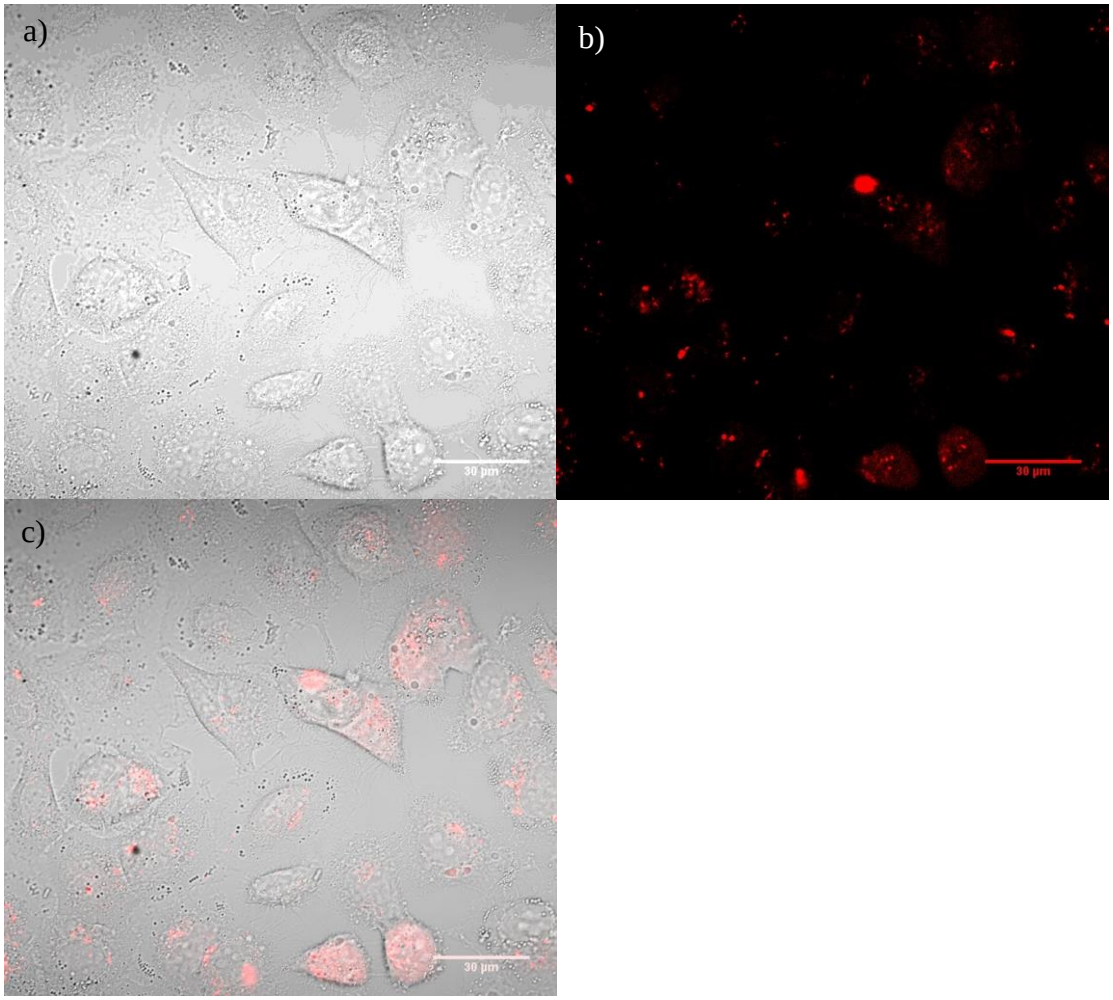

Figure 323: Folate Receptors Pre-Blocked - Confocal microscopy images collected for high folate receptor α expressing A549s that have been pre-dosed with Folate Receptor Alpha Polyclonal Antibody (2µg/mL in 2mL media) for one hour before being co-dosed for 24 hours on a plate rocker with GNP-Cit-RuPhen (1mL of ~1nM GNP-Cit loaded with 12µL 1mM RuPhen). a) brightfield in focus plane of the z stack; b) average RuPhen fluorescence signal across z stack and c) overlay of channels.

Discussion

The results indicate that upon blocking folate receptor α with primary antibody there is a significant decrease in RuPhen probe signal for the GNP-Fol-RuPhen samples (see Figures 320 & 322). Through qualitative comparison of images b) and c) of Figure 320 (unblocked A549s with GNP-Fol-RuPhen) and Figure 322 (blocked A549s with GNP-Fol-RuPhen), there appears

to be less distribution of signal, although the signal intensity seems comparable across the samples. This would therefore indicate that less nanoparticles are taken up by the blocked system as a whole, leading to less distribution, but when the particles are in, they display a comparable intensity as they are evenly loaded with the RuPhen probe. This therefore potentially indicates that folate receptor α plays a key role in the uptake of GNP-Fol-RuPhen into the high folate receptor α expressing A549 cells.

It also appears that folate receptor α blocking does not lead to any significant change in RuPhen signal intensity or distribution when A549 cells are dosed with GNP-Cit-RuPhen (Figures 321 and 323). This is evident through qualitative comparison of images b) and c) of Figure 321 (unblocked A549s with GNP-Cit-RuPhen) and Figure 323 (blocked A549s with GNP-Cit-RuPhen). This would therefore indicate that there is no significant difference in the amount of GNP-Cit-RuPhen taken up by the high folate receptor α expressing A549 cells irrespective of receptor blocking, which is in turn potentially indicative of the utilisation of alternative receptors for the uptake of GNP-Cit into the cells.

Lastly, through comparison of the GNP-Fol sample images (Figures 320 and 322) and the GNP-Cit sample images (Figures 321 and 323) that both the blocked and unblocked GNP-Fol-RuPhen samples presented greater levels of RuPhen emission than the GNP-Cit-RuPhen samples. This is to be expected and is in alignment with the above findings, as it is evident that the GNP-Fol system displays a high dependency on the levels of folate receptor α for cellular uptake. Accordingly, in a cell line displaying high levels of folate receptor α, the GNP-Fol based system will inherently have an advantage in cellular uptake with respect to the GNP-Cit system.

3.7.2. Flow Cytometry Studies

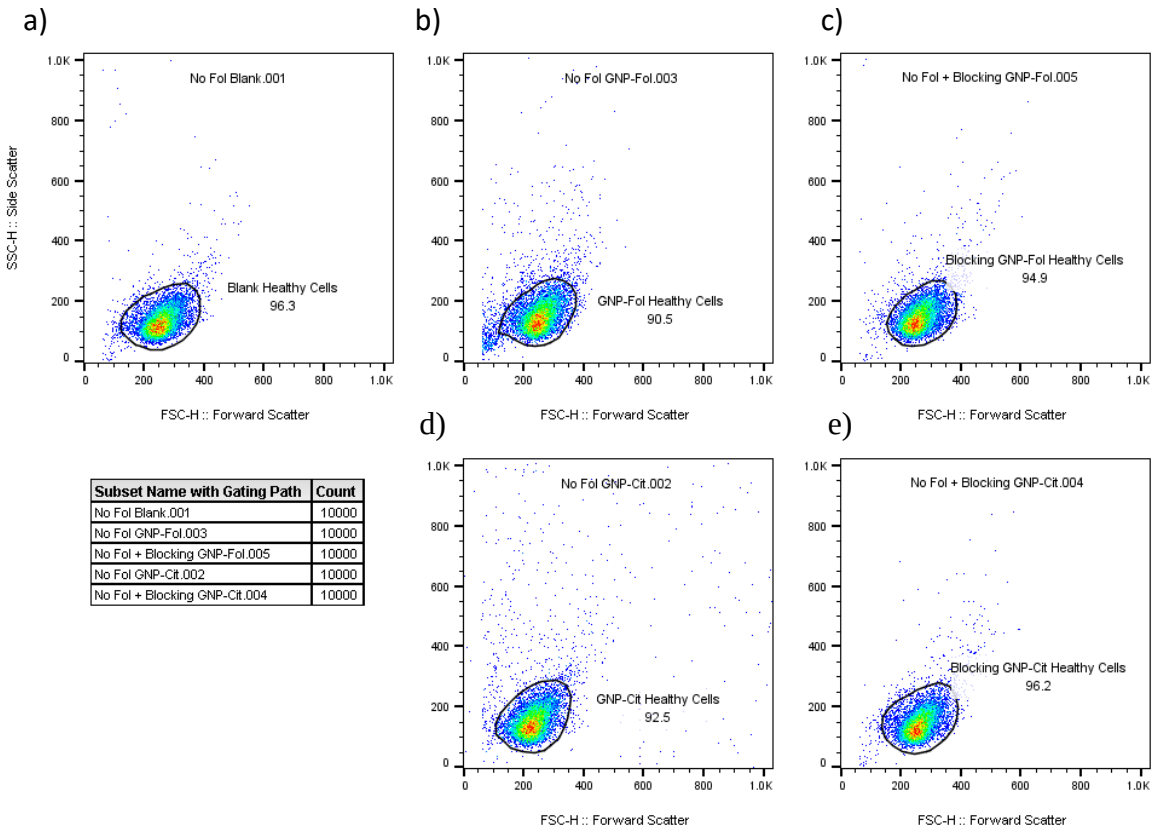

Subset Name with Gating Path	Count
No Fol Blank.001	10000
No Fol GNP-Fol.003	10000
No Fol + Blocking GNP-Fol.005	10000
No Fol GNP-Cit.002	10000
No Fol + Blocking GNP-Cit.004	10000

Figure 324: FACS dot-plot data of forward scatter (particle size) vs side scatter (particle granularity) for the samples of Table 301 in high folate receptor α expressing A549 cells. a) Blank untreated cells, b) GNP-Fol-RuPhen, c) GNP-Fol-RuPhen + receptor blocking, d) GNP-Cit-RuPhen and e) GNP-Cit-RuPhen + receptor blocking. The circled population represents gating of fragments, with the cited number representing the percentage of the population corresponding to healthy cells.

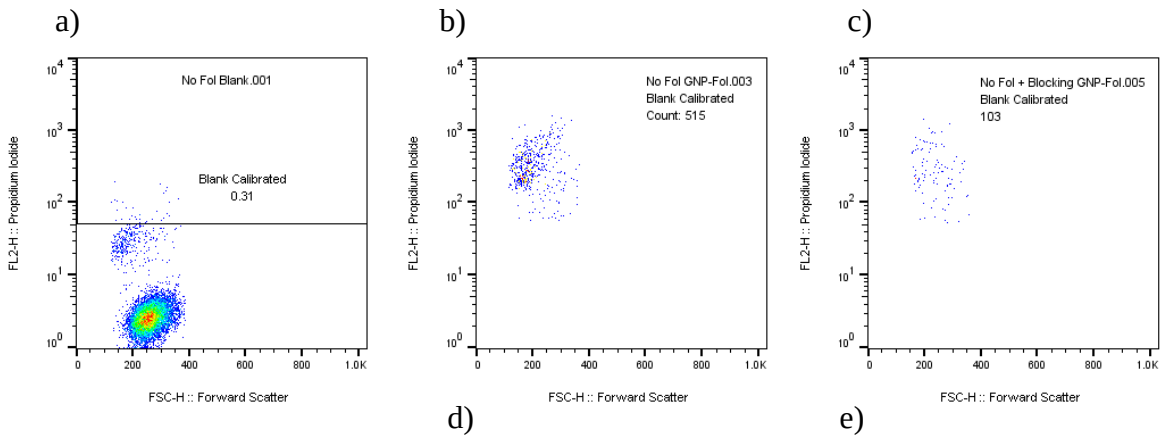

Subset Name with Gating Path	Count	Mean : FL2-H	Median : FL2-H
No Fol Blank.001/Blank Healthy Cells/Blank Calibrated	30.0	88.9	69.0
No Fol GNP-Fol.003/GNP-Fol Healthy Cells/Blank Calibrated	515	359	290
No Fol + Blocking GNP-Fol.005/Blocking GNP-Fol Healthy Cells/Blank Calibrated	103	346	259
No Fol GNP-Cit.002/GNP-Cit Healthy Cells/Blank Calibrated	356	296	231
No Fol + Blocking GNP-Cit.004/Blocking GNP-Cit Healthy Cells/Blank Calibrated	316	212	192

Figure 325: FACS dot-plot data of forward scatter (particle size) vs Propidium Iodide channel signal intensity (red channel, RuPhen emission intensity) for the samples of Table 301 in high folate receptor α expressing A549 cells. a) Blank untreated cells, b) GNP-Fol-RuPhen, c) GNP-Fol-RuPhen + receptor blocking, d) GNP-Cit-RuPhen and e) GNP-Cit-RuPhen + receptor blocking. “Blank Calibrated” represents cells with RuPhen channel fluorescence equal to or greater than the strongest emission of the blank sample (upper limit of auto-fluorescence). Any signal therefore should represent RuPhen fluorescence signal.

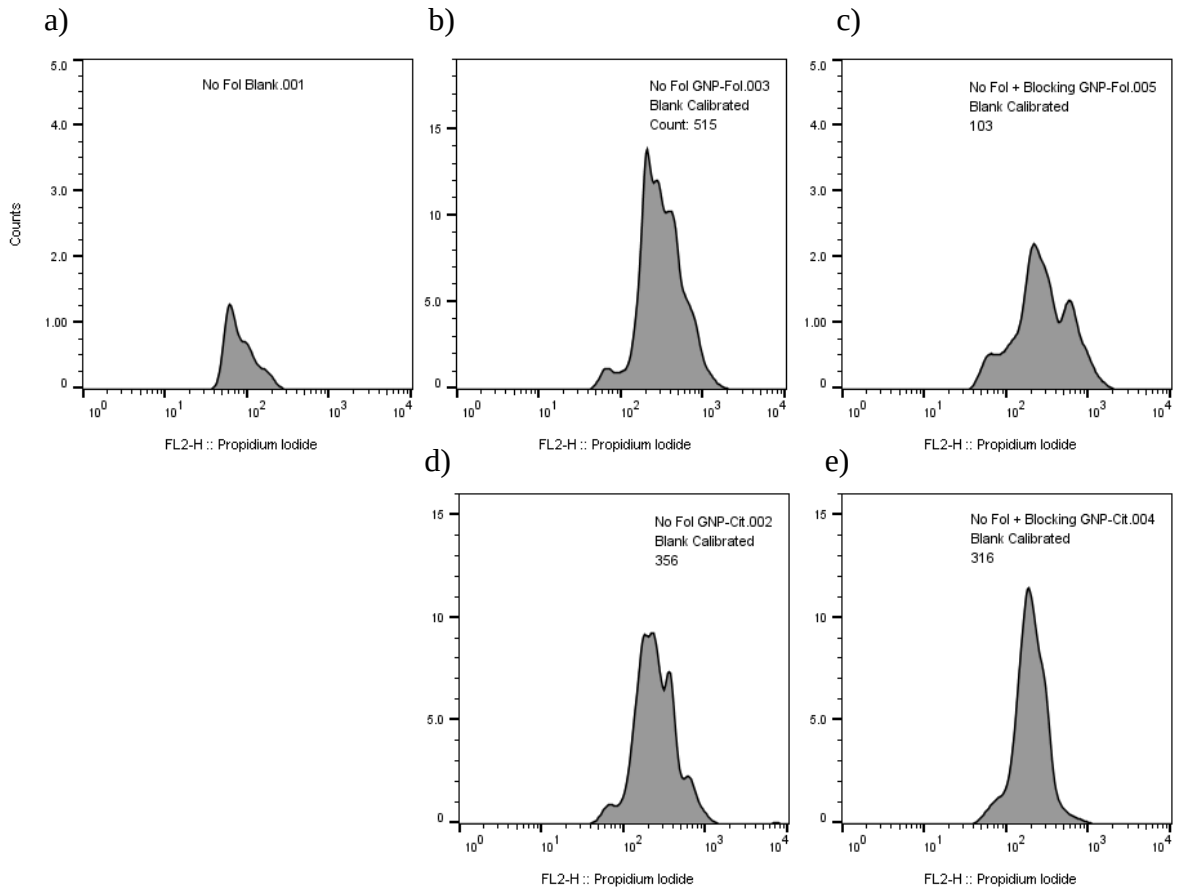

Subset Name with Gating Path	Count	Mean : FL2-H	Median : FL2-H
No Fol Blank.001/Blank Healthy Cells/Blank Calibrated	30.0	88.9	69.0
No Fol GNP-Fol.003/GNP-Fol Healthy Cells/Blank Calibrated	515	359	290
No Fol + Blocking GNP-Fol.005/Blocking GNP-Fol Healthy Cells/Blank Calibrated	103	346	259
No Fol GNP-Cit.002/GNP-Cit Healthy Cells/Blank Calibrated	356	296	231
No Fol + Blocking GNP-Cit.004/Blocking GNP-Cit Healthy Cells/Blank Calibrated	316	212	192

Figure 326: FACS Histogram data of RuPhen channel signal for the Blank calibrated sub-population of the samples of Table 301 in high folate receptor α expressing A549 cells. a) Blank untreated cells, b) GNP-Fol-RuPhen, c) GNP-Fol-RuPhen + receptor blocking, d) GNP-Cit-RuPhen and e) GNP-Cit-RuPhen + receptor blocking. The associated table provides the statistics of each said sample for comparison.

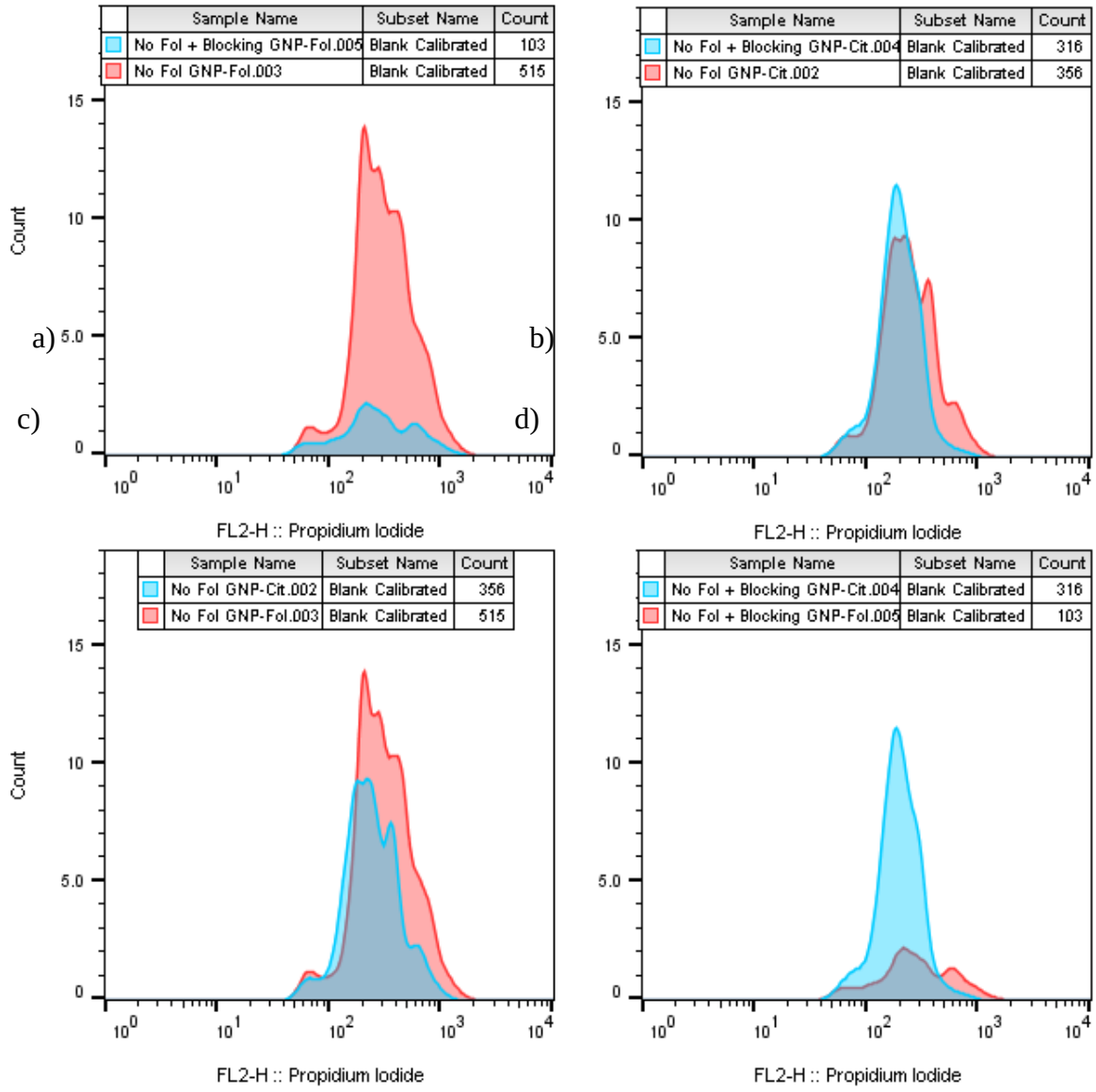

Figure 327: FACS Overlay histogram data of RuPhen channel signal for the Blank calibrated sub-population of the samples of Table 301 in high folate receptor α expressing A549 cells. a) Overlay of GNP-Fol-RuPhen and GNP-Fol-RuPhen + Blocking; b) overlay of GNP-Cit-RuPhen and GNP-Cit-RuPhen + Blocking; c) overlay of GNP-Fol-RuPhen and GNP-Cit-RuPhen; and d) overlay of GNP-Fol-RuPhen + Blocking and GNP-Cit-RuPhen + Blocking.

	RuPhen Signal (RuPhen Loaded Cells Sub-Culture)		
Samples	**Events**	**Mean**	**Median**
Blank	30	88.9	69
GNP-Fol-RuPhen	515	359	290
GNP-Fol-RuPhen + Block	103	346	259
GNP-Cit-RuPhen	356	296	231
GNP-Cit-RuPhen + Block	316	212	192

Table 302: Statistical data from the FACS histogram plots of samples b)-e) of Table 301 and Figure 326, corresponding to the red channel measurements (RuPhen Signal) from the Blank calibrated sub culture.

Discussion

Encouragingly, the FACS data supports the findings of the confocal studies in that the use of folate receptor α blocking has aneffect on the uptake on GNP-Fol-RuPhen in the high folate receptor bearing A549s and a negligible effect on the uptake of GNP-Cit-RuPhen.

In particular, it is evident that there is a considerable decrease in the number of events above the RuPhen signal threshold upon blocking the receptors in the GNP-Fol-RuPhen samples (Table 302, 80% reduction in events), with a modest reduction in fluorescence intensity (5% reduction in mean intensity). By comparison, there is a reasonable reduction in events for the GNP-Cit system (Table 302, 11% reduction in events) and a larger shift in fluorescence intensity (29% reduction in intensity). As per the findings of the confocal microscopy studies,

the GNP-Fol-RuPhen system displayed greater events and fluorescence intensity over the GNP-Cit-RuPhen system (31% more events and 18% greater mean fluorescence).

From the above confocal and FACS microscopy studies it is hypothesised that folate receptor α blocking has a reasonably strong impact on the cellular uptake of GNP-Fol-RuPhen, especially when combined with the plate-rocker dosing protocol. Accordingly, this formed the primary protocol for cellular uptake comparison studies for all subsequent experiments, allowing for meaningful comparison of the folate receptor targeted GNP-Fol system over the GNP-Cit system for delivery of theranostic agents to folate receptor positive cancer cell lines.

3.8. Conclusions

The folate receptor targeting capabilities of folate capped gold nanoparticles was investigated in the present research. The ruthenium probe functionalised folate and citrate capped gold nanoparticle systems of chapter 2 were utilised in a variety of cells in order to observe differences in the rate and specificity of their cellular uptake in folate receptor positive and negative cell lines. It was not possible to draw accurate comparisons between the uptake of the two systems when utilising different cell lines for receptor positive and negative studies on account of different cellular properties.

Various methods were investigated for control of the levels of folate receptors observed within A549 cells. These cells were chosen as they only presented with folate receptor α, and the levels of this expression can be modulated with use of folate deficient / supplemented medias. Through manipulation of the levels of receptor, combined with receptor blocking utilising a folate receptor α polyclonal antibody and simulating flow within the samples, significant differences in cellular uptake of the folate and citrate capped gold nanoparticle systems were

observed. In particular, it was found via confocal microscopy and flow cytometry that the folate capped gold nanoparticle system displayed greater uptake and emission than the citrate capped system, which is most likely indicative of targeted delivery by way of folate receptor mediated endocytosis.

3.9. Experimental

3.9.1. General Cell Culture

Media Preparation

Human carcinoma cells were routinely cultured in either Dulbecco's Modified Eagles Medium (DMEM) or Gibco 1640 Roswell Park Memorial Institute (RPMI) medium, supplemented with 10% foetal calf serum, 100 units/mL penicillin and 0.1 mg/mL streptomycin, within an incubator (37°C, 95% relative humidity and 5 % CO_2). Cells were cultured in T75 flasks unless otherwise stated and split every 3-4 days when they had reached 80-100% confluency.

Cellular Passage

Cells were passaged approximately twice weekly. Appropriate media, phosphate buffered saline (PBS) and trypsin were warmed to 37 °C in a water bath. Media was removed from the culture flask and the cells washed with PBS (10 mL) to remove dead cells and old media. Trypsin (5 mL) was added and the flak incubated at 37 °C for 5 minutes. Flasks were gently tapped and visualised under light microscope to confirm detachment. Fresh media (10 mL) was then added to prevent further cellular digestion by the trypsin and the solution pipetted oer the bottom of the flask to ensure full cellular detachment. The cellular suspension was transferred to a 15 mL falcon tube and centrifuged (Rotofix 32, Hettich Zentrifugen) at 1500 rpm for 5 minutes at room temperature. The supernatant was discarded and the cell pellet re-suspended

in 5 mL appropriate media ready for counting and seeding into new culture flasks, or to be used for experiments accordingly.

Cell Counting

Cells were counted using a Neubauer haemocytometer. 10 µL of the 5mL cellular suspension was pipetted underneath each side of the coverslip of the haemocytometer. The grid was viewed under a microscope (10× objective lens) and cells present in two of the grids were counted and averaged ('N'x10^4 cells/mL). Then, ($1x10^5$/'N'x10^4) x volume wanted = volume needed to be added in order to give 'x' mL at $1x10^5$ cells/mL concentration. Cells were carried forward as appropriate.

3.9.2. Principle Uptake Confocal Microscopy Studies

T75 flasks of Mesenchymal Stem Cells (MSCs), HeLa cells and A549 cells were each maintained via the general cellular practice as outlined in section 3.8.1. These cells were split and plated onto 35mm MatTek imaging dishes with a density of 0.3 x 10^6 cells per well for A549s and HeLa cells and 0.2 x 10^6 cells per well for MSCs. The cells were suspended in 2mL of DMEM and cultured for 24 hours in an incubation chamber to allow them to adhere and stabilise. Old media was removed via pipetting and the cells washed with PBS solution three times to remove dead cells and residual media. The remaining cells were immersed with a solution of GNP-Fol (900uL of ~1nM GNP) loaded with RuPhenSS (12uL of 1mM solution) suspended in 2mL of DMEM and returned to the incubator for a further 24hours. Old media was removed via pipetting and the samples washed with PBS three times to remove dead cells, unbound particles and old media. The cells were re-suspended in imaging media (ThermoFisher, Invitrogen, Live Cell Imaging Solution, A14291DJ) and immediately analysed in a live cell chamber of a confocal microscope. The samples were excited using a 488nm laser

and emission was collected across a 580-680nm range. The laser strength and signal gain of the microscope were calibrated using untreated MSCs as these cells displayed the most prominent auto-fluorescence within the collection range.

3.9.3. PCR Studies

RNA Isolation

T25 culture flasks of the appropriate cell lines were cultured until confluent in appropriate media (RPMI, supplemented RPMI or DMEM). Cells were subsequently washed, lysed and pelted as per the general methods section 3.8.1. RNA was extracted from the cell pellets via utilisation of Qaigen RNA isolation kit (Qaigen RNeasy Mini Kit) according to the manufacturer's instructions.

First, the cell pellet is suspended in 350µL Buffer RLT and vortexed for 10 seconds. 350µL of ethanol (~70%) was added to the lysate and the resulting mixture mixed via pipetting. The sample was then transferred to an RNEasy spin column, the column placed within a 2mL eppendorf and then subsequently centrifuged for 15 seconds at 8000RCF. Through-flow was discarded and the column returned to the eppendorf. 700µL of buffer RW1 was added to the column and the column centrifuged for a further 15 seconds at 8000RCF. Through-flow was discarded, column returned to the eppendorf. 500µL buffer RPE was added to the column and the column centrifuged for a further 15 seconds at 8000RCF. Through-flow was discarded, column returned to the eppendorf. This step was repeated. The spin column was then transferred to a new eppendorf and centrifuged at the maximum speed for one minute to dry the membrane. The spin column was then inserted in a fresh 1.5mL eppendorf, was loaded with 50µL RNAse free water and centrifuged for one minute at 8000RCF to elute RNA. Purity and concentration were ascertained via analysis of 260/280nm ratio of UV-Vis spectrum.

cDNA Synthesis from total RNA

First strand cDNA synthesis was performed using BioLine Tetro cDNA Synthesis Kit (BioLine Reagents Ltd, UK) according to the manufacturer's instructions.

Total RNA (4µg) in RNAse free water was added to sterile RNAse free micro-centrifuge tubes containing a mixture of 1µL Oligo $(dT)_{18}$ Primer Mix, 1µL of 10mM dNTP mix, 4µL 5xRT Buffer, 1µL RiboSafe RNAse Inhibitor, 1µL Tetro-Reverse-Transcriptase (200µg/µL) and 20µL DEPC-treated water. This solution forms a priming pre-mix, which was alliquated into the micro-centrifuge tubes in ice. The solutions were mixed gently by pipetting before being incubated at 45°C for 30 minutes within a pcr chamber. The reaction was terminated by incubation at 85°C for 5 minutes before being chilled on ice. Solutions were either carried forward immediately for PCR or stored at -20°C.

PCR

PCR studies were carried out utilising a protocol adapted from that of Shen *et al*[12]. Forward and reverse primers were freshly ordered and matched the sequences set forth by Matsushita *et al*[11].

10pM / µL stock solutions of the folate receptor α, β and γ forward and reverse primers were prepared separately in DEPC treated water, as well as β Actin control primers. PCR mixtures were prepared in micro-centrifuge tubes, comprising 10x NH_4 Reaction Buffer (5µL), $MgCl_2$ (4µL of a 50mM solution), dNTP Mix (1µL of a 100mM solution), BioTaq Polymerase (1µL), cDNA, appropriate Primer (1µL of 10pM/µL stock soltion) and DEPC water (up to 50µL total volume). The micro-centrifuge tubes were placed in a PCR incubation chamber and subjected to the following amended PCR cycle: 5 minutes at 94°C, 35 cycles of (45 seconds at 94°C, 60 seconds at 59°C and 90 seconds at 72°C) befoe terminating the reaction at 72°C for 10 minutes.

PCR products then purified with a Qaigen PCR Purification Kit and had their concentrations analysed via UV-Vis.

PCR Purification

PCR products were purified via utilisation of Qaigen PCR Purification Kit according to the manufacturer's instructions.

5 volumes of Buffer PB were added to 1 volume PCR Mix and 10µL of a 3M sodium acetate solution added. The resulting solution was transferred to a spin column within a centrifuge tube and centrifuged at 13000rpm form 60 seconds, with any flow-through discarded. 750µL Buffer PE was added to the spin column and the column centrifuged for a further 60 seconds at 13000rpm, flow-through was discarded. The membrane was dried by a further round of centrifugation as above, and the dried column placed in a fresh centrifuge tube. 30µL Buffer EB was added and the purified PCR product eluted by centrifugation at 13000rpm for 60 seconds. Purified PCR products were either carried directly forward for agarose gel electrophoresis or stored at -80°C.

Agarose Gel Electrophoresis

Agarose gel electrophoresis was conducted as per the protocol of fellow Hannon group doctoral researcher Peter Cail.

100mL of a 3% agarose gel was freshly prepared via heating 2.7g agarose stock in 97mL of TEA buffer. Fresh agarose gel solution was poured into a gel column and had lane inserts were placed at the top of the gel column. The solution was allowed to cool to room temperature and set for one hour. Once set, the lane inserts were removed and the gel column transferred to an electrophoresis tank and submerged in fresh TEA solution. 50bp ladder stock was placed within the first lane (1µL of a 1µg/10µL fresh stock solution) followed by the appropriate PCR

products, which had been diluted to give a unified concentration with the weakest PCR product solution and (10µL of appropriate PCR stock, mixed with 2µL Loading Dye). A current was applied across the agarose gel and the solutions allowed to migrate across the gel for two hours to give appropriate separation. The gel was removed, TEA solution drained and el replaced back in the chamber. The gel was then submerged in a fresh TEA solution containing a DNA stain stock. The gel was covered with foil and allowed to stain for 40 minutes. Stain solution was removed and the gel immediately analysed within a photo-illuminator.

3.9.4. Immunocytochemistry Studies

Cell Plating

A549 cells were cultured as two separate cultures for 2 months, the first in zero folate RPMI medium (ThermoFisher, Gibco RPMI) and the second in supplemented folate RPMI medium (zero folate RPMI media supplemented with 20mg folic acid). Cells were maintained as per the general cellular practice as outlined in section 3.8.1, with mere supplementation of appropriate media. Cells were then washed, lysed, pelleted, re-suspended and counted. 0.8x106 cells were then seeded onto MatTek dishes in appropriate medium and allowed to adhere overnight (~12 hours).

Antibody Staining

Old media was removed from the MatTek dishes and each dish washed with PBS (2mL x 3) via pipetting. The cells were then incubated with primary antibody (Folate Receptor Alpha Polyclonal Antibody, 2µg/mL in 2mL media (zero folate RPMI or supplemented RPMI dependent on cell culture used)) for 45 minutes. Cells were then washed with PBS (2mL x 3) and incubated with secondary antibody (Goat anti-rabbit Secondary Antibody, Alexa Fluor 488, 2µg/mL in 2mL media) for 30 minutes. The cells were then washed with PBS (2mL x 3),

immersed in 1mL imaging media and immediately imaged via live confocal microscopy within a pseudo incubation chamber.

Confocal Microscope Settings

Green Channel: Excitation, 514nm Emission, 490-570nm

3.9.5. Comparative Uptake Studies

Nanoparticle Purification

GNP-Fol and GNP-Cit were freshly prepared as per section 2.3.2. Each system was dialysed overnight in a semi permeable membrane (Spectra-Por® Float-A-Lyzer® G2, 5 mL, MWCO 8-10 kDa) in deionised water to remove unreacted reagents and excess folate. The systems then had their concentrations roughly calculated via UV-Vis and the stronger system diluted to the same concentration as the weaker system (~1nM). 24µL of a 1mM RuPhen stock was then titrated into 2mL of GNP-Fol in increments of 6µL under magnetic stirring to afford GNP-Fol-RuPhen. The same was carried out for GNP-Cit to afford GNP-Cit-RuPhen. The systems were stirred at room temperature for ~30 minutes and were subsequently dialysed in a semi permeable membrane overnight (~12 hours) to remove unbound RuPhen and excess folate / remaining reagents. The resulting systems were carried forward for immediate cellular studies.

Dosing Protocol

Cells were cultured and plated onto MatTek dishes as per section 3.8.3. The following samples were prepared as separate MatTek dish cultures:

A549s (zero folate culture)	**A549s (supplemented folate culture)**
1. Blank	2. Blank
3. Secondary Antibody Only	4. Secondary Antibody Only
5. Pri + Sec Antibodies (AB)	6. Pri + Sec Antibodies (AB)
7. GNP-Fol-RuPhen + AB	8. GNP-Fol-RuPhen + AB
9. GNP-Cit-RuPhen + AB	10. GNP-Cit-RuPhen + AB

After overnight culture in MatTek dishes, old media was removed from samples 1-10 and the dishes washed with PBS (2mL). 2mL of fresh media (zero folate samples 1, 3 and 5; supplemented folate samples 2, 4 and 6) was added to samples 1-6 and the samples returned to the incubation chamber. 1mL of GNP-Fol-RuPhen was mixed gently by pipetting into 1mL of zero folate RPMI and 1mL of GNP-Fol-RuPhen was mixed with 1mL of supplemented RPMI. The same was repeated for GNP-Cit-RuPhen. These nanoparticular-media suspensions were then pipetted into the appropriate MatTek dishes (7-10) and the dishes returned to the incubator. Samples were incubated for 3 hours, then old media was removed from samples 5-10 and the samples washed with PBS (3 x 2mL). 2mL of a 2µg/mL solution of folate receptor alpha polyclonal antibody (ThermoFisher, 548908) in RPMI was added to each sample and the samples incubated for a further 45 minutes. Old media was removed from samples 3-10 and the cells washed with PBS (3 x 2mL). 2mL of a 2.5µg/mL solution of secondary antibody (Goat anti-Rabbit IgG (H+L) Secondary Antibody, Alexa Fluor 488) in RPMI was added to each sample and the samples incubated for a further 30 minutes. Old media was removed from all

samples and each sample washed with PBS (3 x 2mL). Imaging media (2mL) was added to each sample and the samples immediately imaged via confocal microscopy.

Confocal Microscope Settings

Green Channel: Excitation, 514nm Emission, 490-570nm

Red Channel: Excitation, 488nm Emission, 580-680nm

3.9.6. Subjected Flow Uptake Studies

Cell Culture

High and low folate receptor α expressing A549s were cultured and maintained as per section 3.8.4.

Nanoparticle Preparation

Fresh batches of GNP-Fol and GNP-Cit were synthesised as per section 2.3.2 and were subsequently loaded with RuPhen (1mM) and purified ready for cell culture experiments as per section 3.8.4.

Dosing Protocol

Samples and antibodies were prepared as per section 3.8.4, dosing times and protocols are equally identical. The only modification to this dosing protocol was the utilisation of a plate rocker. Said plate rocker weas pseudo sterilised through extensive washes with 70% ethanol. Cells were only subjected to plate rocking on its lowest setting within an incubator at the point of nanoparticular dosing (12 hours post plating onto MatTek dishes). All samples were subjected to plate rocking, not just those being dosed with nanoparticles. The plate rocker was

removed and samples stained with appropriate antibodies statically within the incubation chamber.

3.9.7. Folate Receptor Blocking Studies

Cell Culture

High folate receptor α expressing A549s were cultured and maintained as per section 3.8.5.

Nanoparticle Preparation

Fresh batches of GNP-Fol and GNP-Cit were synthesised as per section 2.3.2 and were subsequently loaded with RuPhen (1mM) and purified ready for cell culture experiments as per section 3.8.5.

Dosing Protocol

Cells were cultured and plated onto MatTek dishes as per section 3.8.5. The following samples were prepared as separate MatTek dish cultures (for confocal studies) and 6 well plates (for FACS studies):

A549s - No Blocking	**A549s – With Folate α Blocking**
1. Blank	-
2. GNP-Fol-RuPhen	3. GNP-Fol-RuPhen
4. GNP-Cit-RuPhen	5. GNP-Cit-RuPhen

Samples and antibodies were prepared as per section 3.8.5, dosing times and protocols are equally identical. The only modification to this dosing protocol was the pre-dosing of samples 3 and 5 with folate receptor alpha primary antibody prior to nanoparticular dosing (as per section 3.8.5). Accordingly, prior to nanoparticular dosing the media was removed from

samples 3 and 5 and the samples washed with PBS (3 x 2mL). The samples were stained with appropriate antibodies statically within the incubation chamber. 1mL of a 4µg/mL solution of folate receptor alpha polyclonal antibody (ThermoFisher, 548908) in RPMI was added to each sample and the samples incubated for 30 minutes on a plate rocker. Subsequently, 1mL of either GNP-Fol-RuPhen or GNP-Cit-RuPhen was added to samples 3 and 5 respectively. Samples 1, 2 and 4 had their old media removed, were washed with PBS (3 x 2mL) and supplemented with fresh RPMI (2mL per sample). All samples were returned to the incubator and were incubated / worked up as per the remainder of the protocol for section 3.8.5 for confocal microscopy samples.

Confocal Microscope Settings

Green Channel: Excitation, 514nm Emission, 490-570nm
Red Channel: Excitation, 488nm Emission, 580-680nm

FACS

High folate receptor α expressing A549 cells were seeded onto 6 well plates (300,000 cells per well) and supplemented with 2mL supplemented RPMI. The cells were incubated for 24 hours before treatment with appropriate solutions to allow cell adhesion to the well base. Old media was removed from the plates and each well washed with PBS (2mL) to remove residual media and dead cells. Each well was subsequently dosed with the same protocol as above for confocal studies, one well for each sample condition, no replicates. The cells were washed with 2 mL PBS before being lysed, pelleted and re-suspsended as per section 3.8.1. Samples were subsequently analysed by flow cytometry.

3.10. References

1 - King SM, Claire S, Teixeira RI, Dosumu AN, Carrod AJ, Dehghani H, Hannon MJ, Ward AD, Bicknell R, Botchway SW, Hodges NJ, and Pikramenou Z. Iridium Nanoparticles for Multichannel Luminescence Lifetime Imaging, Mapping Localization in Live Cancer Cells. Journal of American Chemical Society. (2018), 140, 10242−10249.

2 – "Useful Numbers for Cell Culture", ThermoFisher Scientific, Cell Culture Protocols, accessed 01st February 2016, https://www.thermofisher.com/uk/en/home/references/gibco-cell-culture-basics/cell-culture-protocols/cell-culture-useful-numbers.html

3 - Lu H, Zhu H. Effect of siRNA-mediated gene silencing of transketolase on A549 lung cancer cells. Oncology Letters. (2017), 14(5), 5906-5912.

4 - Kim HS, Lee K, Bae S, Park J, Lee CK, Kim M, Kim E, Kim M, Kim S, Kim C, and Kim JS. CRISPR/Cas9-mediated gene knockout screens and target identification via whole-genome sequencing uncover host genes required for picornavirus infection. Journal of Biological Chemistry. (2017), 292(25), 10664 –10671.

5 –Mornet E, Carmoy N, Lainé C, Lemiègre L, Gall TL, Laurent I, Marianowski R, Férec C, Lehn P, Benvegnu T and Montier T. Folate-Equipped Nanolipoplexes Mediated Efficient Gene Transfer into Human Epithelial Cells. International Journal of Molecular Sciences. (2013), 14, 1477-1501.

6 - Necela BM, Crozier JA, Andorfer CA, Lewis-Tuffin L, Kachergus KM, Geiger XJ, Kalari KR, Serie DJ, Sun Z, Aspita AM, O'Shannessy DJ, Maltzman JD, McCullough AE, Pockaj BA, Cunliffe HE, Ballman KV, Thompson EB and Perez EA. Folate Receptor-α (FOLR1) Expression and Function in Triple Negative Tumors. Plos One. (2015), 1-19.

7 – "Total RNA Bacteria Purification Kit", Sigma-Aldrich, DNA & RNA purification, Accessed on 22nd February 2017 at 12:30, http://www.sigmaaldrich.com/life-science/molecular-biology/dna-and-rna-purification/total-rna-bacteria.html.

8 – "Techniques of Molecular Biology", DevBio, The Embryological Origins of the Gene Theory, accessed on 22nd February 2017 at 15:30, http://11e.devbio.com/wt031001.html.

9 – "Polymerase chain reaction", WikiMedia, accessed on 14th March 2017 at 11:00, https://www.google.co.uk/search?rlz=1C1CHBD_en-gbGB708GB709&espv=2&biw=1280&bih=918&tbm=isch&q=pcr+amplification&sa=X&ved=0ahUKEwjb753O6dXSAhXJAsAKHfr3DPkQhyYIIQ#imgrc=jySMDOFzPOnfsM.

10 - Fillmore CM and Kuperwasser C. Human breast cancer cell lines contain stem-like cells that self-renew, give rise to phenotypically diverse progeny and survive chemotherapy. Breast Cancer Research. (2008), Vol 10, 1-13.

11 - Nakashima-Matsushita N, Homma T, Yu S, Matsuda T, Sunahara N, Nakamura T, Tsukano M, Ratnam M, Matsuyama T. Selective expression of folate receptor beta and its possible role in methotrexate transport in synovial macrophages from patients with rheumatoid arthritis. Arthritis Rheumatology. (1999), 42(8), 1609-1616.

12 - Shen F, Ross JF, Wang X, and Ratnam M. Identification of a novel folate receptor, a truncated receptor, and receptor type .beta. in hematopoietic cells: cDNA cloning, expression, immunoreactivity, and tissue specificity. Biochemistry. (1994), 33 (5), 1209–1215.

13 –Elnakat H and Ratnam M Distribution, functionality and gene regulation of folate receptor isoforms: implications in targeted therapy. Advanced Drug Delivery Reviews. (2004), 54, 1067–1084.

Chapter 4 – Platinum(IV) Anticancer Agents and Cellular Uptake

4.1. Platinum(IV) Pro Drug Design and Synthesis

In tandem with the research of chapter 3 into the development and utilisation of nanoparticle bound ruthenium imaging agents, and as previously discussed, it was a further objective of the present research to design, develop and utilise a platinum(IV) pro drug. In this regard, a number of platinum(IV) compounds with potential pro-drug capabilities were investigated in the present research, with early efforts utilising compounds of the literature and latter efforts focussing on a number of novel compounds being conceptualised and synthesised. Two compounds of the literature (Pelosi *et al*[1]. and Lippard *et al.*[2]) as well as two novel platinum(IV) species (Trial Compounds 1 and 2) were investigated in early efforts of the present research and are outlined in Figure 401. However, the primary novel platinum(IV) species conceptualised and utilised throughout the research and reported herein is represented in Figure 402, along with its synthetic protocol (hereafter "Pt(IV)LipA").

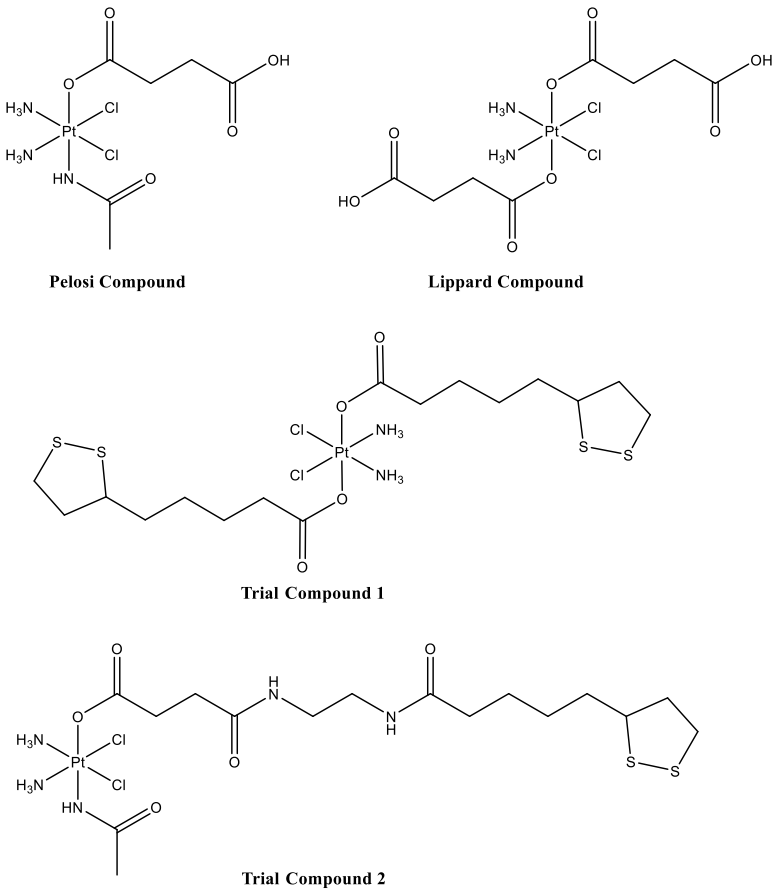

Figure 401: Pt(IV) compounds investigated during preliminary nanoparticle loading, stability and cytotoxicity studies. Pelosi and Lippard compounds have been reported to exhibit antiproliferative and cytotoxic properties respectively, whilst novel Trial Compounds 1 and 2 were based on those compounds but with added thiol anchoring groups in the pursuit of enhanced gold nanoparticle loading and subsequent cytotoxicity.

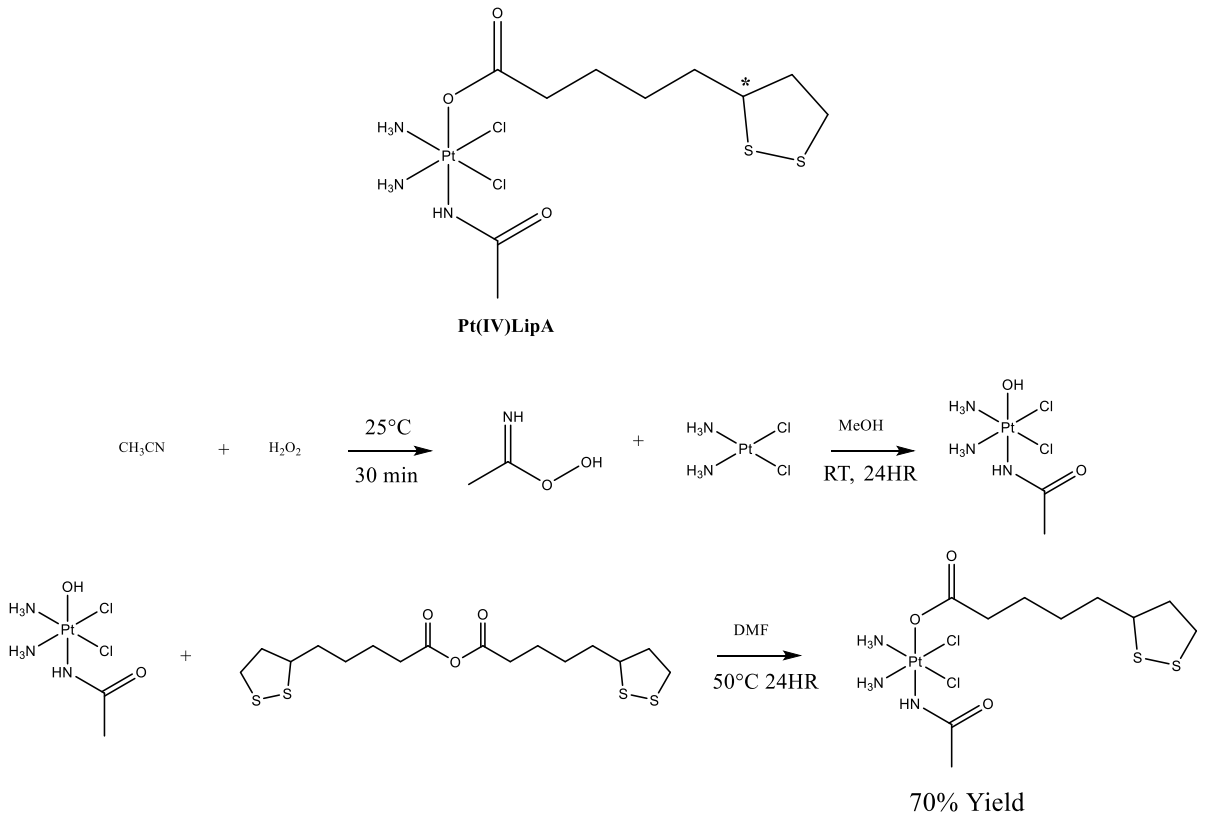

Figure 402: The novel Pt(IV) compound (Pt(IV)LipA) conceptualised and utilised throughout the presently reported research along with its corresponding synthetic protocol.

The lack of specificity of traditional platinum based chemotherapeutic agents such as cisplatin, and the ability of cancer cells to build resistance to such agents are key aspects for consideration when designing new chemotherapeutic agents[3, 4]. In this regard, platinum(IV) agents afford the opportunity to incorporate additional moieties to the platinum centre through the addition of two axial binding sites (the compounds are octahedral, bearing 6 ligands – an improvement over the four of square planar or tetrahedral platinum(II) compounds)[5].

In this vein, the Pelosi and Lippard Pt(IV) compounds were developed so as to provide chemotherapeutic Pt based agents which present increased solubility whilst theoretically maintaining a level of cytotoxicity that would be therapeutically beneficial, or indeed, enhancing said cytotoxicity[1]. The present research employed these two compounds for initial

nanoparticle loading studies so as to establish key concepts such as the ability to load gold nanoparticles (both GNP-Fol and GNP-Cit systems) with Pt(IV) agents bearing an axially bound carboxylic acid motif and subsequently, explore what affect this has on the system's ability to deliver said agents and induce DNA-cisplatin adduct formation.

Nanoparticle loading studies were conducted using the same protocol as the Ruthenium based loading studies in section 2.2.2, loading 1mL of ~1nM GNP-Fol or GNP-Cit (as separate systems) with a stock solution (1mg/mL) of either the Pelosi or Lippard Pt(IV) agents (as separate systems). However, these nanoparticle loading studies were unsuccessful, with both GNP-Fol and GNP-Cit systems seemingly unable to support even 1µg of either of the Pelosi or Lippard compounds. Specifically, the nanoparticle systems either showed no shift in the SPR band in the subsequent UV-Vis spectrum post titrations (which would have been indicative of surface binding of reagents) or the SPR band broadened significantly and the solution became polydisperse and purple (indicative of agglomeration/aggregation).

It was therefore hypothesised that the unsuccessful nanoparticle loading of these compounds was likely the result of instability in the resulting solution post titration (circa 99% water) or because of unfavourable surface coordination conditions between the nanoparticles and the carboxylic acid motifs (the former being associate with the Lippard compound and the latter with the Pelosi compound). Accordingly, subsequent efforts sought to design and synthesise a novel Pt(IV) agent that demonstrated improved solubility over Lippard and loading capabilities over Pelosi.

In order to address nanoparticle loading, the incorporation of lipoic acid was investigated. As reported herein, transition metal probes of varying nature have been synthesised within the

Pikramenou group, the majority of which feature at least one lipoic acid unit. These probes present quite significant loading capabilities within the nanoparticle systems employed (as per chapter 2 of the present research) and this is believed to be partly as a result of the di-sulphur containing 5 membered ring of lipoic acid. Of course, many other factors contribute to the stability of a system and the capability of a compound to be successfully loaded onto a nanoparticle surface, however, the utilisation of lipoic acid was a logical succession for the present drug design studies.

Trial compound 1 was a first attempt at a novel Pt(IV) agent, based on the synthetic protocol of the Lippard compound[2], but replacing the use of succinic anhydride with lipoic acid anhydride. This Pt(IV) complex incorporates axially coordinated lipoic acid ligands via the oxygen atoms of the terminal hydroxyl group. This design was the most simplistic of those considered as it resembled a straight adaptation of the common Pt(IV) pro drug intermediate *c,c,t*-$[Pt(NH_3)_2(Cl)_2(OH)_2]$ (compound 401, see experimental section 4.6.1). This complex was more soluble than the Lippard complex, yet it was found to still lack sufficient solubility for application in subsequent nanoparticle studies. Moreover, the reaction was not clean, with a number of unidentifiable and inseparable by-product peaks observable within the mass and NMR spectra.

Trial compound 2 was based on the aforementioned Pelosi compound and sought to incorporate lipoic acid by way of an amine linker to the axially coordinated carboxylic acid motif. Trial compound 2 was also associated with a number of impurities and it was again not possible to separate out the target compound to a sufficiently pure solution. It was hypothesised that this crude reaction mixture was as a result of non-uniform mono-protection of the di-amine. More particularly, despite stoichiometric control of the amine and protecting groups, there would

inherently be irregularities in the protective step, with a mixture of mono-protection, di-protection and no protection. The result would in turn give a mixture of lipoic-amine intermediates. Poor purification at this stage would lead to impurities being carried over and inherently lead to further irregularities. Accordingly, due to the expense of platinum reagents and difficulties in post-reaction purification, amine linkages were subsequently abandoned as a route to future lipoic acid incorporation.

Subsequent research efforts sought to simply amend the Pelosi complex through replacement of the axial succinic anhydride ligand with a lipoic acid ligand, leading to the formation of the Pt(IV)LipA complex (Figure 402).

4.2. Pt(IV)LipA Complex Synthesis and Characterisation

The principal concept behind the design of the Pt(IV)LipA complex was the incorporation of a lipoic acid ligand to facilitate nanoparticle loading, whilst preserving the acetylamido ligand of the Pelosi complex, which is thought to be responsible for the increased solubility of the Pelosi complex[1]. The Pt(IV)LipA complex was synthesised through amending the second stage of the Pelosi synthesis (see Experimental section 4.6.1) replacing succinic anhydride with lipoic acid anhydride. A 10 times molar excess of a lipoic acid anhydride solution was utilised so as to help increase product yield, with no effect on the purification stage of the synthesis due to polar differences in solubility of reactants and the target complex. The Pt(IV)LipA complex was easily separated by trituration with diethyl ether. The complex was subsequently washed several times with diethyl ether and dried under high vacuum overnight. No further purification was required and the overall yield of the complex was 70% (for full details, see Experimental Section 4.6.1). The characterisation of the Pt(IV)LipA complex is represented in Figure 403 and discussed below.

a)

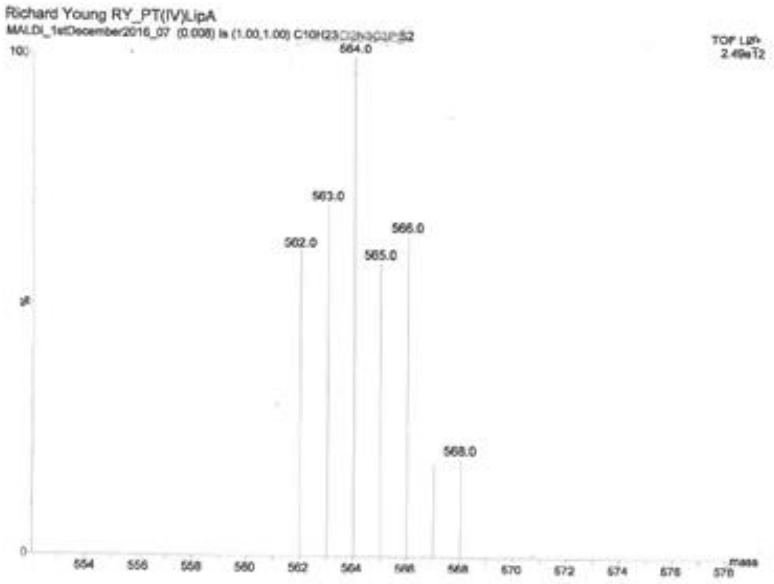
Richard Young RY_PT(IV)LipA
564.0
563.0
566.0
562.0
565.0
568.0

b)

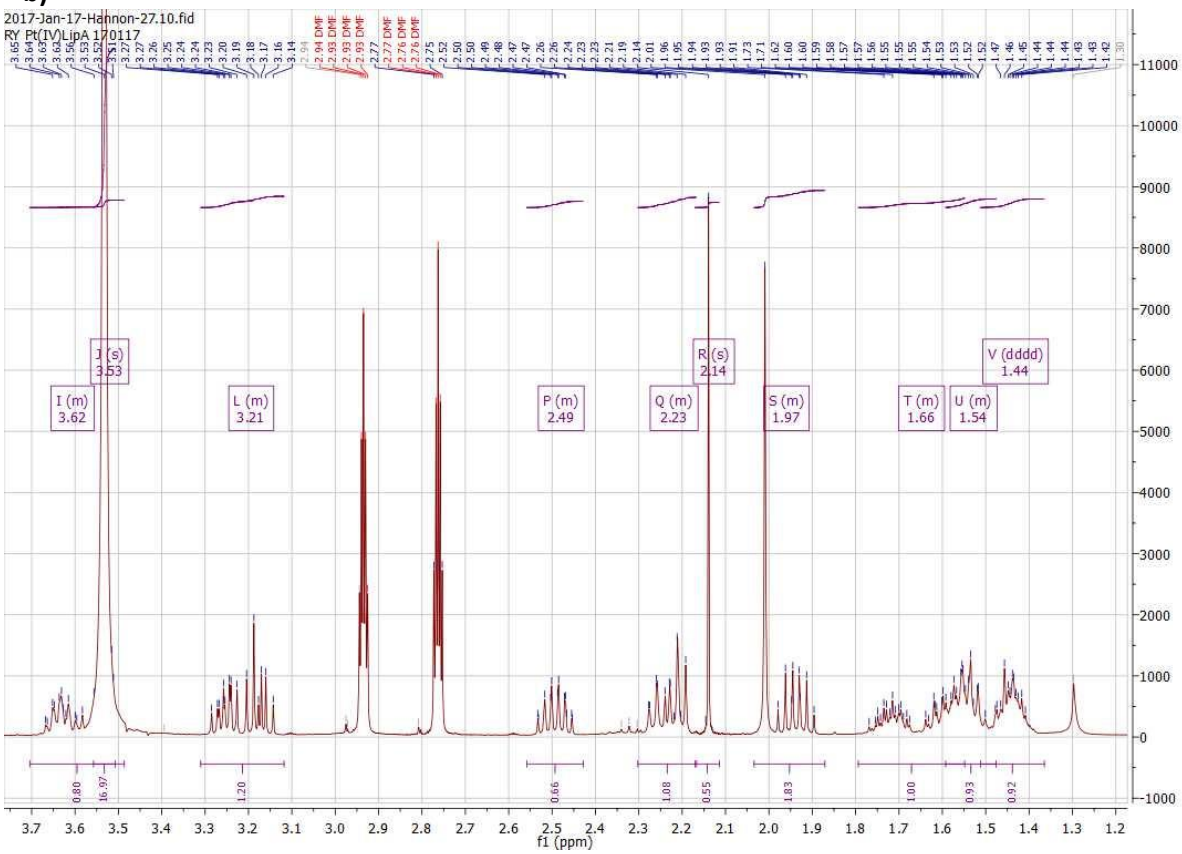
2017-Jan-17-Hannon-27.10.fid
RY Pt(IV)LipA 170117
I (s)
3.53
I (m)
3.62
L (m)
3.21
P (m)
2.49
Q (m)
2.23
R (s)
2.14
S (m)
1.97
T (m)
1.66
U (m)
1.54
V (dddd)
1.44
f1 (ppm)

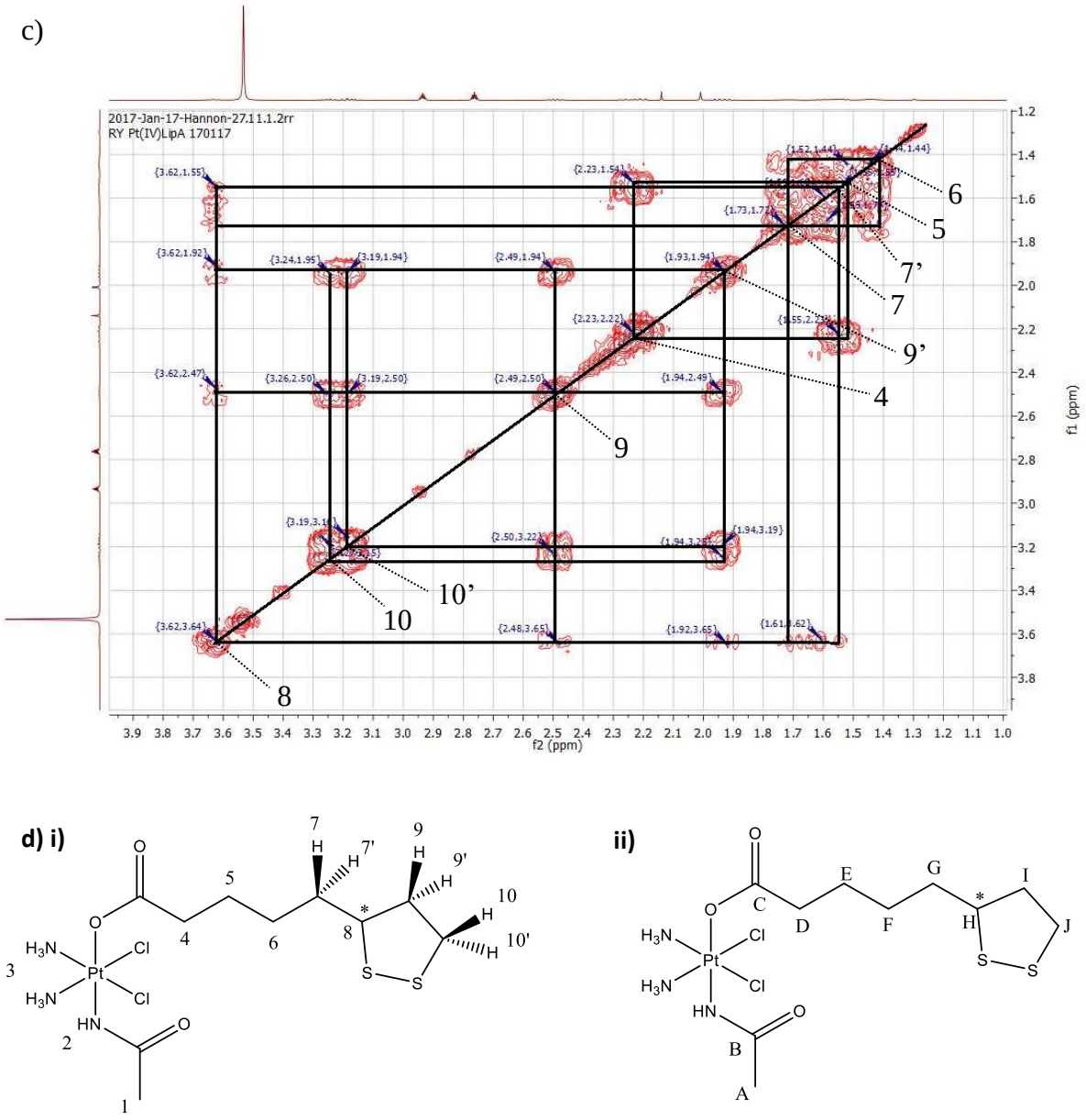

Figure 403: MS and NMR studies of the Pt(IV)LipA complex and associated characterisation. **a)** MALDI-TOF showing product $[M+H]^+$ peak at 564.0g/mol along with corresponding isotope peaks; **b)** 1H NMR spectrum; **c)** COSY spectrum with signals ranging ≈1.4-3.7ppm, showing close range couplings of different proton environments, facilitating allocation of 7, 7', 9, 9', 10 and 10'; **d)** Chemical structure and numerical allocations for Pt(IV)LipA, **i)** Proton environments (1-10') and **ii)** Carbon environments (A-J). Full corresponding analytical data is available in Appendix section 7.2.

Proton peaks 1-5 and carbon peaks A-E were readily assigned by comparison with the Pelosi and Lippard complex assignments in the literature, with only small shifts in relative peaks of circa 0.1-0.3ppm. Proton peak 6 and carbon peaks F-J were again somewhat readily assigned through comparison to the literature of lipoic acid NMR data, which in turn helped to appropriately assign proton peaks 7-10' within the COSY and HSQC spectra.

The Pt(IV)LipA complex incorporates the solubility prospects of the Pelosi complex (through the acetylamido ligand) with the loading potential of lipoic acid by way of the two axial positions. It was hypothesised that upon reduction, either by reductive species within endosomes of target tumour cells or within the hypoxic environment of the tumour / cells, these axial ligands would dissociate, leaving the active Pt(II) complex cisplatin[6]. Accordingly, it was envisaged that the Pt(IV)LipA complex would present a viable Pt(IV) pro-drug candidate with enhanced solubility over typical complexes of such nature and with the ability to coordinate to the surface of gold nanoparticles. Attractively, Pt(IV)LipA is readily synthesised via a two-stage one-pot protocol with a high overall yield (≈70%).

4.3. Testing Reduction Capabilities

Prior to nanoparticle loading studies, the potential for the Pt(IV)LipA complex to be reduced to the active anticancer agent cisplatin was investigated. Whilst there is a wealth of research into the cellular application and reduction of Pt(IV) pro-drugs, there is still some debate surrounding the proposed mechanism of reduction of the Pt(IV) centre to Pt(II) at the target location. At present, it is largely believed that it is as a result of either the hypoxic environment of a tumour and/or the presence of reductive agents within endosomes that may reduce the pro drug[7].

As a crude test of reductive capabilities and subsequently induced cytotoxicity (prior to implementation in more representative cellular studies) Circular Dichroism (CD) Spectroscopy was employed. The CD spectrum of Calf Thymus (ct) DNA possesses a characteristic signal in the region of 300-200nm, displaying a peak at 275nm, a trough at 245nm and another peak at 220nm[8]. This region is essentially the fingerprint of the calf thymus DNA, highlighting its varying absorption of left and right circularly polarized light. It has been shown in the literature that when Pt agents bind to CT DNA its fingerprint region is altered, giving shifts in the characteristic peaks and troughs, thus forming a means of detection of DNA binding[9]. Accordingly, titration experiments were conducted utilising CT DNA and the Pt(IV)LipA complex, with results represented in Figure 404 (see experimental section 4.6.2).

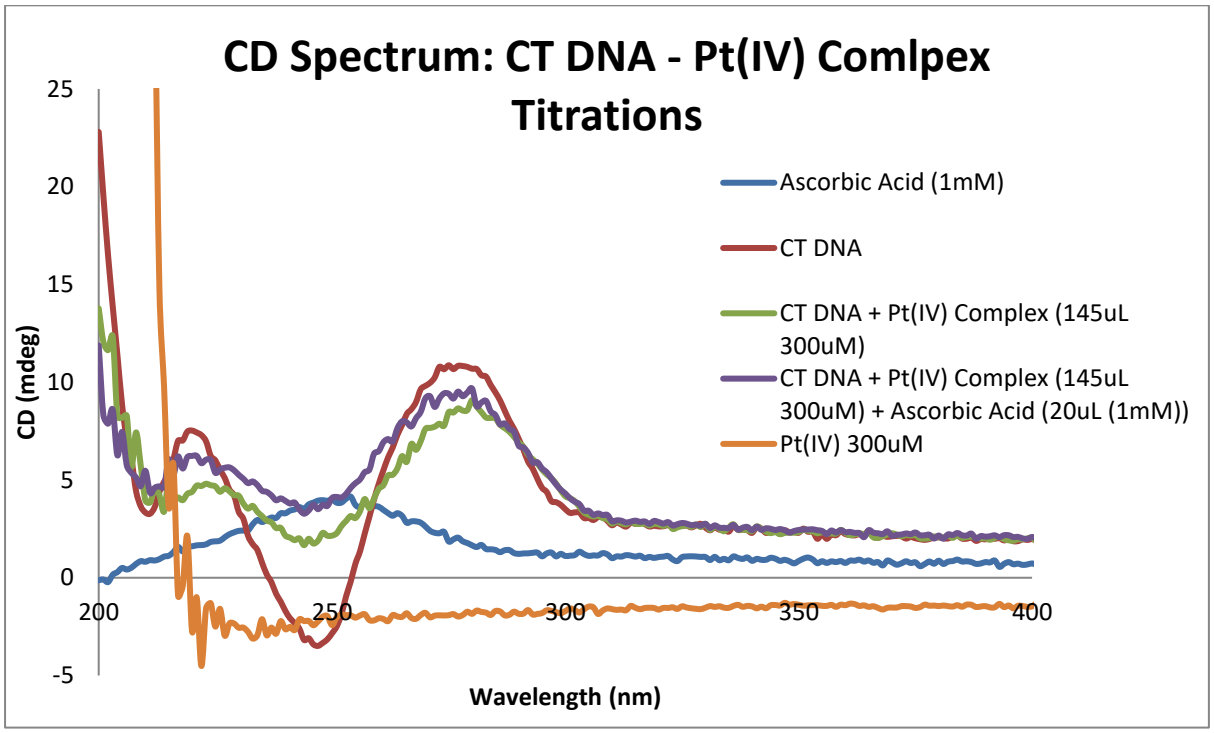

Figure 404: Circular Dichroism Spectrum data for titrations of Pt(IV)LipA complex (145µL, 300µM) and a reductive agent (20µL, 1mM ascorbic acid) into a CT DNA stock solution (comprising 98µM of CT DNA in NaCl, Na cacodylate and Milli Q water). The solution was stirred at room temperature for 5 minutes after each titration and its CD spectrum recorded promptly.

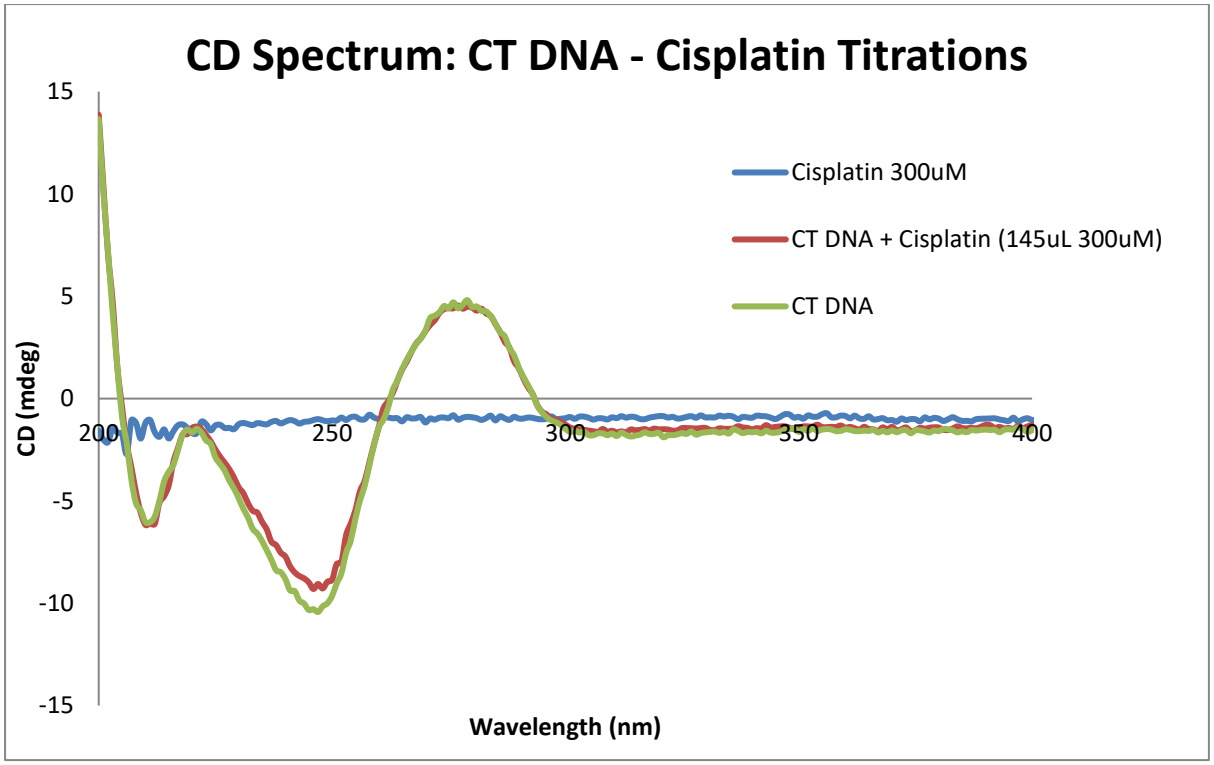

Figure 405: Circular Dichroism Spectrum data for titrations of cisplatin (145µL, 300µM) into a CT DNA stock solution (comprising 98µM of CT DNA in NaCl, Na cacodylate and Milli Q water).

It was hypothesised that upon titration of a solution of Pt(IV)LipA alone into a CT DNA stock solution there would be minimal change to the spectrum as a result of the compound being theoretically unable to interact with the DNA in the same way as cisplatin. That is to say, the Pt(IV)LipA complex should not display the ability to form intra-strand covalent bonds to adjacent Guanine residues of the DNA helix, therefore no "kink" should be formed and subsequently, there should be a relatively insignificant shift in the spectrum, unless the complex presents another method of binding[10]. Whilst Pt(IV)LipA has a chiral centre (indicated with * in Figure 402) and displays absorption within the 200-220nm region of the CD spectrum, only minor shifts in the signal are to be expected as a result of its own chiral activity.

It was further anticipated that upon titration of the reducing agent into the solution (ascorbic acid), the Pt(IV) centre would be reduced to Pt(II), thus facilitating binding with the CT DNA and in turn altering the fingerprint region of the spectrum[11]. Unfortunately, ascorbic acid displays an absorption within the fingerprint region of CT DNA (220-280nm). However, due to its weak absorption at its severely diluted titration state, along with its use within the literature for reduction tests of Pt(IV)[11], its use was maintained. A 1mM solution of ascorbic acid was utilised so as to give a greater probability that the Pt(IV) complex would be reduced and thus give the potential for binding.

Upon titration of the Pt(IV)LipA complex into the CT DNA solution (in the absence of a reducing agent) shifts can be observed in the fingerprint region of the spectrum (Figure 404), with a reduction in the peaks at 275nm and 220nm (circa 16% and 20% reduction respectively) and an increase in the trough signal at 245nm (circa 200% increase). Whilst the Pt(IV) complex is optically active, it is unlikely that its activity and individual CD signal alone would induce such a significant shift in the fingerprint region of the spectrum. It was therefore subsequently hypothesised that either; the complex was reduced in the solution upon titration, perhaps as a result of the other agents present, generating cisplatin and thus inducing cisplatin-DNA adduct formation; the axial ligands dissociated in solution due to poor stability / solubility, or: the Pt(IV)LipA complex has another mechanism of interaction with the DNA helix, aside from the intended cisplatin mimicking methodology. Accordingly, further research in this area should look at the specifics of the Pt structure pre and post titration, perhaps utilising NMR studies to ascertain any structural differences, as well as monitoring the stability of the complex in solution with the other reagents.

Rather unexpectedly, upon titration of the ascorbic acid solution into the CT DNA / Pt(IV) solution an increase was observed across each of the peaks / troughs of the fingerprint region (220nm – 34%, 245nm – 65% and 275nm – 4%). This may be as a result of reduction of the Pt(IV) complex as expected and thus induced cisplatin activity. Subsequent cellular studies were employed to investigate the potential of Pt(IV)LipA to act as an anticancer agent as well as its specific mode of action.

For completeness, the mirror titration experiment utilising cisplatin was conducted and is represented in Figure 405 (see experimental section 4.6.2). As reported in the literature, there is a shift in the trough of the CT DNA fingerprint spectrum at 275nm, most likely as a result of the binding and subsequent DNA alteration imparted by cisplatin. Interestingly, this shift is relatively small by comparison to that demonstrated by the Pt(IV)LipA complex and only the single trough of the spectrum was affected, as opposed to the entire fingerprint region.

4.4. Nanoparticle Loading Studies

Having confirmed the structure of the Pt(IV)LipA complex and crudely ascertained its ability to bind to ct DNA, subsequent efforts were made into the nanoparticle loading of the complex onto the GNP-Fol and GNP-Cit systems. The same loading protocol was employed for the Pt(IV) complex titrations into GNP solutions as utilised for the ruthenium probe loading studies (see section 2.2.2), with constant stirring and subsequent sonication of samples prior to running UV-Vis and DLS scans to confirm binding and ascertain solution stability (see experimental section 4.6.3). The collated data from these loading studies are represented in Figures 406 and 407.

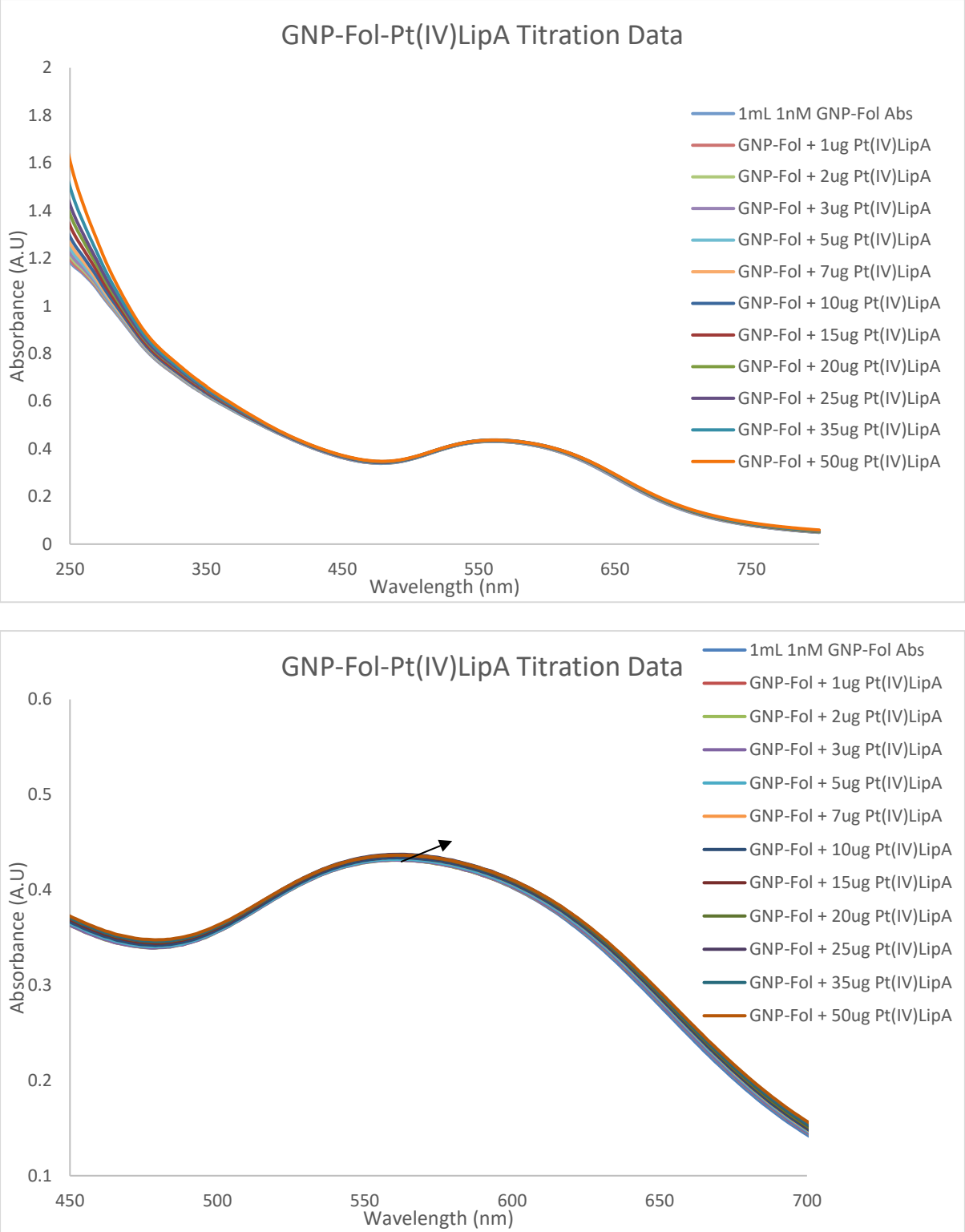

Figure 406: UV-Vis absorption spectrum data for titration of a 1mg/mL Pt(IV)LipA stock solution into 1mL of 1nM GNP-Fol. Titration volumes of Pt(IV)LipA were varied to give incrementally increases in µg Pt(IV) added as opposed to traditional mmol added. Only minor SPR band shifts were observed, with the SPR band λ_{max} shifting by 2nm from 562nm to 564

nm and the SPR band broadening from 478-630nm to 478-634nm. Shift and broadening of the SPR band are indicative of surface binding in the nanoparticle system.

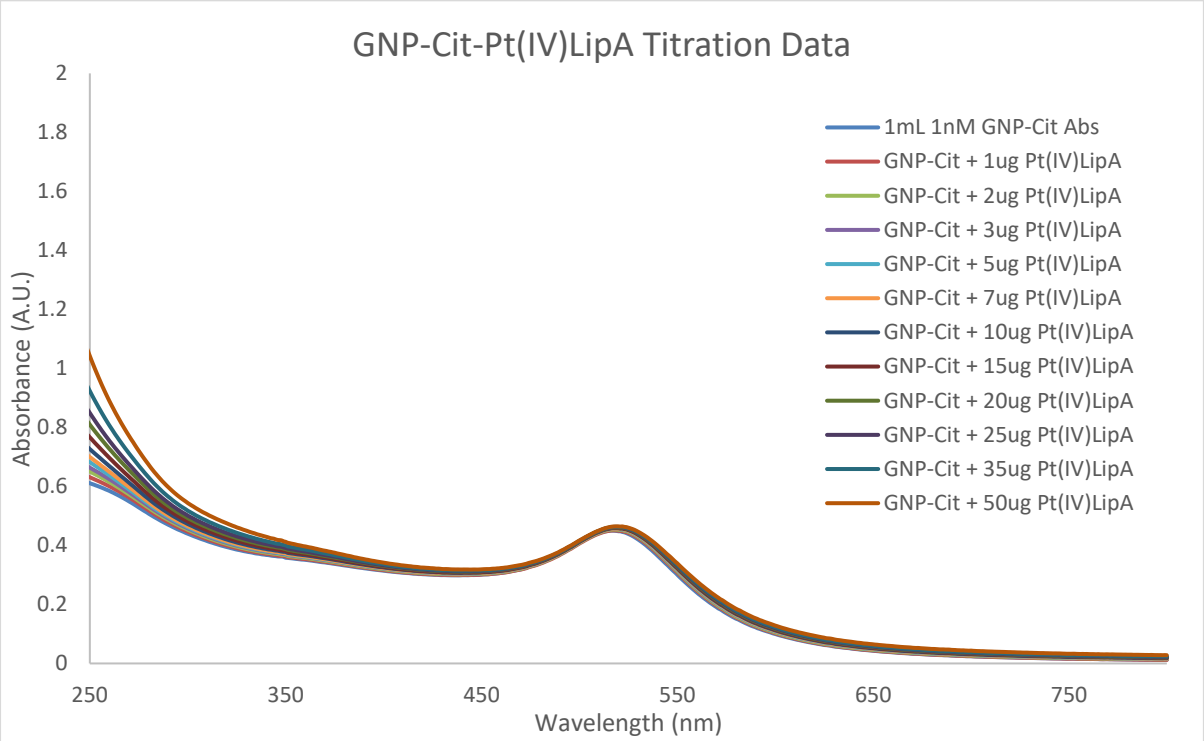

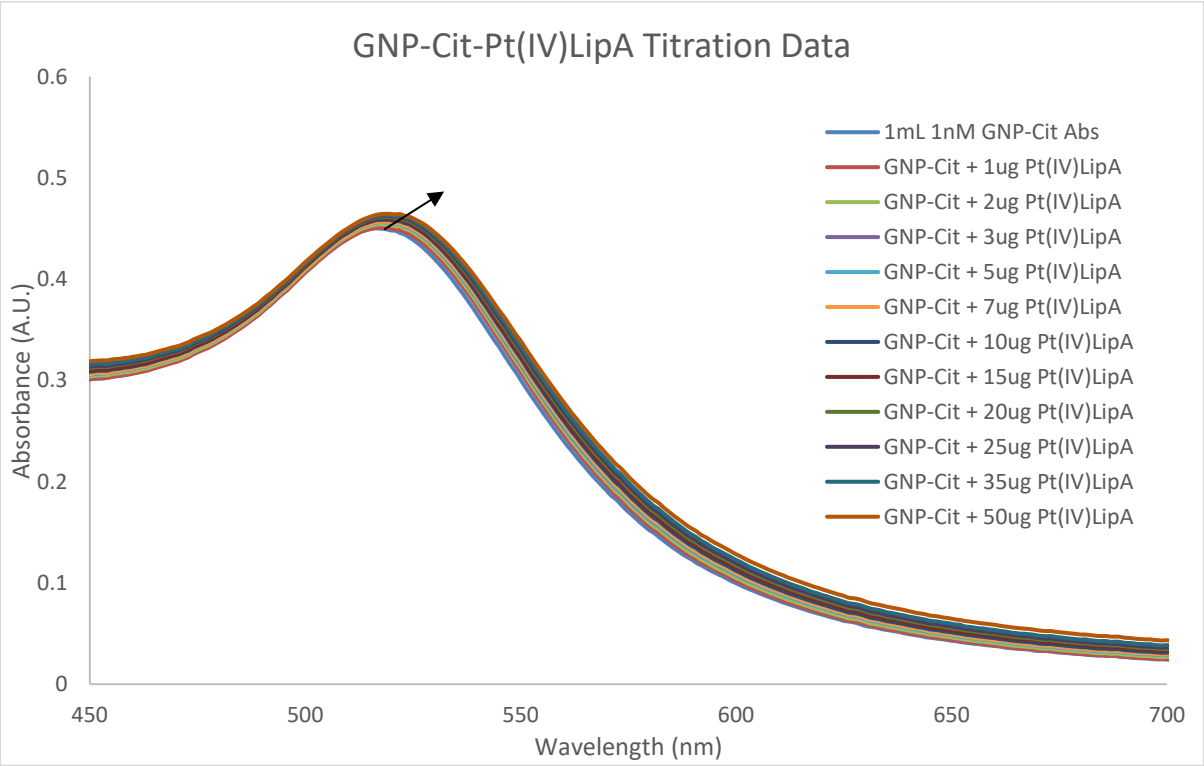

Figure 407: UV-Vis absorption spectrum data for titration of a 1mg/mL Pt(IV)LipA stock solution into 1mL of 1nM GNP-Cit. Titration volumes of Pt(IV)LipA were varied to give

incrementally increases in µg Pt(IV) added as opposed to traditional mmol added. The SPR band λ_{max} shifted by 2nm from 516nm to 518 nm and the SPR band also shifted and narrowed from 436-551nm to 443-556nm. Shift and narrowing of the SPR band are also indicative of surface binding in the nanoparticle system.

The UV-Vis titration data (Figures 406 and 407) for the GNP-Fol and GNP-Cit systems showed some minor differences in the effect of Pt(IV) loading. In the case of the GNP-Fol system, the SPR band λ_{max} shifted by 2nm and the band broadened, which is a typical response expected in nanoparticle loading experimental data. However, for the GNP-Cit system, the SPR band λ_{max} also shifted, but the SPR band actually narrowed by 2nm and the entire band shifted by 5nm with respect to its minima at 551nm v 556nm. It is not understood why one system would show broadening of the SPR band and the other narrowing, however, it is understood in the literature that any such alteration to the SPR band is indicative of surface binding[12]. More particularly, it is believed that whilst alteration of the SPR band is indicative of nanoparticle binding, the specific change that is imparted is more dependent on the polarity and degree of interaction of the respective titrated compound with the SPR of the nanoparticle system itself.

Much the same as the ruthenium probe loading studies, the nanoparticle systems were not able to be filtered by sephadex on account of loss of stability of the system (most likely through removal of too much environmentally stabilising folate / citrate in solution). Accordingly, the systems were dialysed for 24 hours in appropriately pH balanced deionised water (circa pH 9 for GNP-Fol and pH 7 for GNP-Cit) within microporous dialysis tubing to remove the majority of any unbound Pt(IV) agent (see experimental section 4.6.3). The solutions were subsequently sonicated for 10 minutes and filtered through a rudimental cotton plug to remove any precipitated material. Solutions were monitored via DLS at 24 hour intervals to ascertain

stability and it was found that the systems remained disperse and non-agglomerated for up to 96 hours, irrespective of sonification.

4.5. Cellular Activity Studies

Subsequent research efforts sought to ascertain the cytotoxic capabilities of the Pt(IV)LipA complex within cancer cell systems. For continuity, high folate receptor α expressing A549 cells were utilised for these cytotoxicity experiments going forwards. Particular objectives of this research were to ascertain the degree of cytotoxic activity of Pt(IV)LipA, provide an indication of the method of action of the cytotoxic agent and the cellular localisation of said agent.

4.5.1. MTT Assays

To investigate the cytotoxic activity of the Pt(IV)LipA agent, MTT assays were conducted for high folate receptor α expressing A549s dosed with the agent. MTT assays are a form of colorimetric measurement of cellular metabolic activity[13 & 14]. More particularly, it is a means of measuring a cell culture's ability to reduce MTT (a tetrazolium dye, 3-[4,5-dimethylthiazole-2-yl]-2,5-diphenyltetrazolium bromide) to the insoluble MTT-Formazan by-product. This process of reduction of MTT is governed by the activity of oxido-reductase enzymes which in-turn is governed by cellular viability. Accordingly, the more surviving cells within a cell culture, the better the collective ability to process the MTT dye to MTT-Formazan. This MTT-Formazan is subsequently solubilised and gives a strong purple solution with absorption within the UV-Vis spectrum. Therefore, the UV-Vis spectrum of the sample in relation to appropriate controls can give an indication of relative cytotoxicity.

MTT assays were utilised to ascertain the cytotoxicity of Pt(IV)LipA on its own as well as when loaded onto GNP-Fol (GNP-Fol-Pt(IV)) and GNP-Cit (GNP-Cit-Pt(IV)) systems in comparison to cisplatin. The results of these studies are graphically represented in Figure 408. See experimental section 4.6.4 for full details.

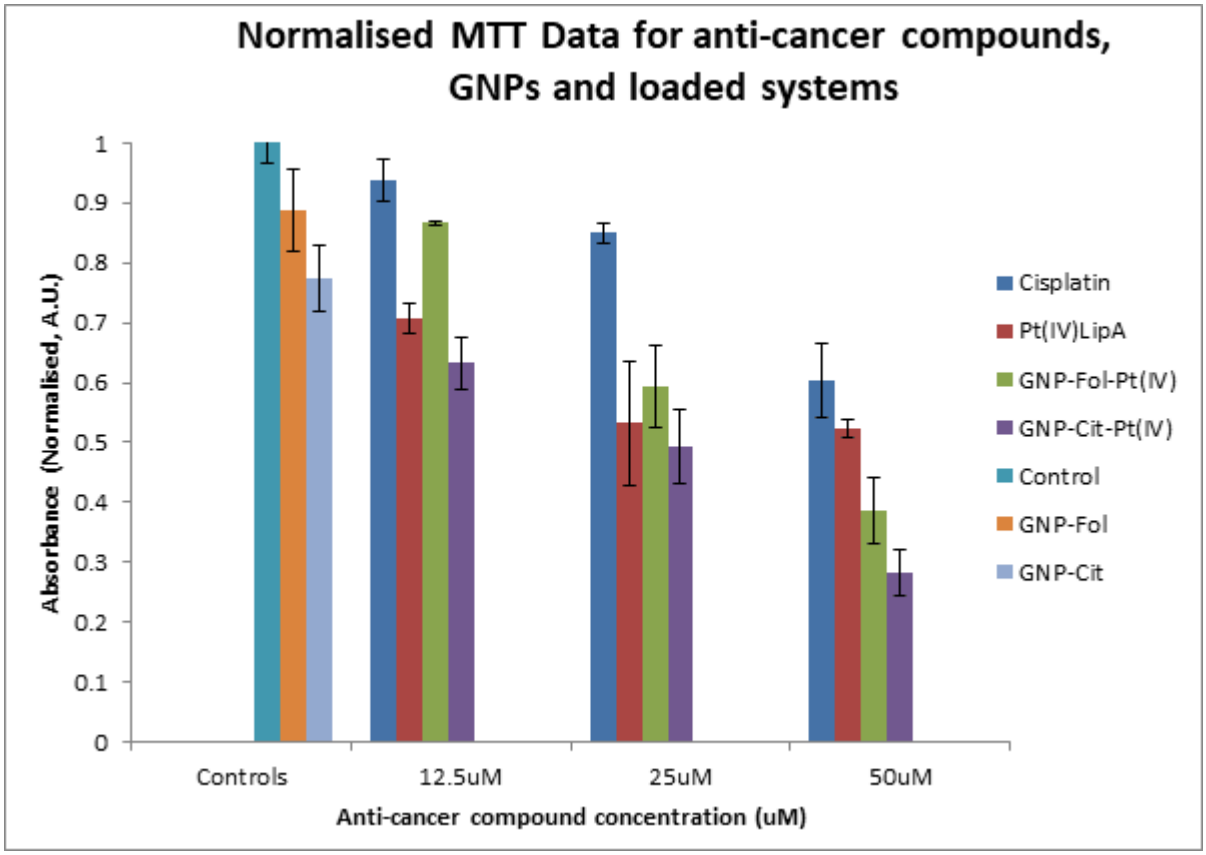

Figure 408: Normalised MTT data recorded for A549 cell cultures dosed with anti-cancer compounds in varying doses. Normalised absorbance reflects % cell viability, with the control data resembling 100% viability. 12.5µM, 25µM and 50µM solutions of cisplatin and Pt(IV)LipA were investigated, along with the Pt(IV)LipA compound when loaded onto GNP-Fol and Cit nanoparticle systems.

The MTT data of Figure 408 shows that at low to medium concentrations the Pt(IV)LipA complex displays significantly greater cytotoxicity than cisplatin in A549 cells, with 70% vs

93% cell viability respectively at 12.5µM and 53% vs 85% cell viability respectively at 25µM. However, in contrast to the trend, the Pt(IV)LipA complex displays no significant increase in cytotoxicity in going from medium to high dose (53% to 51% viability going from 25µM to 50µM respectively) whereas cisplatin displays a considerable increase in toxicity across this range (85% to 60% viability respectively). It is believed that the small difference in cytotoxic affect in going from 25µM to 50µM of Pt(IV)LipA is likely due to limited solubility of the complex at high concentrations. In this regard, it was noted that some degree of precipitation was observed during the loading studies at high concentrations. A similar hypothesis is put forwards for cisplatin, albeit with a reduced impact on the resulting incremental increase in cytotoxicity.

Higher concentrations were not investigated within these studies on account of the limitations on nanoparticle loading and the solubility of the complexes, which would artificially skew the effective IC_{50} values for the complexes. It should also be noted that, as per introduction section 1.3.1, cisplatin resistant A549 cells are available to purchase, displaying typically much higher levels of resistance to cisplatin than the parent cell line. As previously discussed, this formed an additional incentive for the utilisation of A549s over other folate receptor positive cell lines, as it might afford the opportunity to subsequently investigate and compare the efficacy of the Pt(IV) agents ability to deliver cisplatin in alternative forms to resistant cells in later research.

The MTT results also show that the impact of Pt(IV)LipA is typically enhanced when loaded onto nanoparticle systems. For the GNP-Fol-Pt(IV) system, the lowest concentration of Pt(IV) gave significantly less cytotoxicity than the Pt(IV) agent alone, with 86% vs 70% respectively. However, at 25µM there was comparable cytotoxicity (59% vs 53% viability respectively) and at 50µM GNP-Fol-Pt(IV) displayed a significant increase in cytotoxicity over Pt(IV) alone

(38% vs 52% respectively). It is hypothesised that the reduced efficacy at lower concentrations within the GNP-Fol-Pt(IV) system may be as a result of the effective amount of free Pt(IV) agent delivered. That is to say, it is assumed that there will be an effective percentage range of the Pt(IV) complexes present that actually dissociate from the nanoparticle surface, thus, forming an effective concentration of Pt(IV) agent that may actually be delivered relative to the overall concentration present. Accordingly, at lower concentrations, more Pt(IV) complex may reach the cells as part of the GNP-Fol-Pt(IV) system over the free Pt(IV) system, but less dissociated Pt(IV) is available vs the free Pt(IV) system. Carrying this effect over, the greater the number of Pt(IV) complexes there are relative to nanoparticle carriers, the greater the number of complexes that are likely to dissociate, skewing the effective percentage and improving efficacy.

Unlike the GNP-Fol-Pt(IV) system, the GNP-Cit-Pt(IV) system displayed increased cytotoxicity over the free Pt(IV) agent at all concentrations. However, it is noteworthy that the nanoparticles themselves displayed a high level of toxicity to the cells which may be associated with the surface surfactant zonyl. In order to obviate the toxic effect of zonyl as much as possible, the nanoparticles were subjected to extra rounds of sonification and centrifugation prior to being loaded with the Pt(IV)LipA complex. Despite these efforts however, the nanoparticle system itself displayed a cell viability of 77%, which therefore means that the nanoparticles alone are more cytotoxic than cisplatin at 25µM.

Whilst GNP-Cit-Pt(IV) displays significantly higher cytotoxicity at each concentration increment than all of the other systems (63%, 49% and 28% for 12.5µM, 25µM and 50µM respectively), these effects are likely also as a result of the toxicity of the particles themselves. Accordingly, these statistics are likely not indicative of the number of Pt(IV) complexes

delivered to the cells or even the number of nanoparticles taken up by cells, given that free zonyl may diffuse through the culture and damage cells which have not taken up any GNP-Cit-Pt(IV).

The GNP-Fol system also displayed some small level of cellular toxicity (viability of 89%) and this may result from the basic pH of the system. Whilst the present studies utilised 1mL of ~1nM GNP-Fol and GNP-Cit for continuity from earlier studies, future studies could look to vary the concentration or volume of nanoparticles with concentration of Pt(IV)LipA loading, to give optimal dose delivery vs system toxicity.

The MTT studies therefore indicate that the GNP-Fol system likely delivers more Pt(IV) complex than the free Pt(IV) agent alone and that the Pt(IV) agent is more cytotoxic to cisplatin resistant A549 cells than cisplatin. No conclusion can be drawn from the MTT studies as to the implied level of nanoparticle uptake or imparted platinum based cytotoxicity of the GNP-Fol-Pt(IV) and GNP-Cit-Pt(IV) systems on account of GNP-Cit cellular toxicity. In order to ascertain levels of nanoparticle uptake and effective Pt(IV) agent delivery, immunonocytochemical and ICPMS studies were conducted.

4.5.2. Confocal Microscopy Studies

4.5.2.1. Cisplatin-DNA Adduct Imaging Principle

Whilst the MTT data of section 4.5.1 provided a cellular means of ascertaining the extent of cytotoxicity of the Pt(IV)LipA agent with respect to cisplatin, this does not give an indication of its specific method of action. In particular, these studies do not help to prove nor disprove whether cisplatin-DNA adducts are indeed formed. Moreover, whilst these studies support the theory that GNP-Fol-Pt(IV) is more cytotoxic than Pt(IV) alone, it does not indicate

that this increase in cytotoxicity is purely from increased levels of uptake of the GNP-Fol system and subsequently, nanoparticle bound Pt(IV)LipA. These raised levels of cytotoxicity could merely be due to the highly basic nature of the GNP-Fol system and similarly, in the case of the GNP-Cit system, on account of the surface surfactant Zonyl FSA.

Accordingly, it was an object of subsequent studies to investigate the formation of cisplatin-DNA adducts when the Pt(IV)LipA complex is administered to A549s. It was a further object of the research to ascertain the levels of any such cisplatin-DNA adduct formation in an attempt to give an indication of the level of successful Pt(IV) drug delivery in the different systems.

Through the use of immunocytochemistry, these cisplatin-DNA adducts were investigated both qualitatively (confocal microscopy) and quantitatively (FACS analysis). In this regard, a commercial antibody was purchased (Anti-Cisplatin modified DNA antibody [CP9/19], see experimental section 4.6.5). This primary antibody displays selective binding to kinks in DNA formed by cisplatin-DNA adducts. A secondary antibody was selected with an Alexa Fluor 488 dye, displaying fluorescence in the green channel. Alexa Fluor 488 dye was selected as it presented an emissions profile which fell outside of both the ruthenium based molecular probe employed in nanoparticle tracking studies as well as the blue channel emission of the nuclear stain Hoechst. Accordingly, through utilisation of the CP9/19 antibody system, the DNA-damage antibody signal was measured in combination with nuclear staining with minimal signal bleed-through, utilising confocal microscopy and FACS analysis. The present studies did not include the use of the ruthenium probe, these results are discussed in Chapter 5 as the complete theranostic nanoparticle system studies.

The dosing protocol of the present Pt(IV) immunocytochemistry confocal cellular studies was adapted from the protocol employed in the folate receptor α immunocytochemistry confocal studies (see Experimental section 4.6.5). As before, high folate receptor α expressing A549s were used to present a more polar difference in nanoparticle uptake in the GNP-Fol system upon cellular blocking with folate receptor α primary antibody (as previously discussed in Chapter 3). In principle, upon blocking the A549 cells with a folate receptor α primary antibody prior to and during cellular dosing with GNP-Fol-Pt(IV), a large shift should be observed in cisplatin based adduct formation, which should in turn lead to significant reduction in FITC based fluorescence (green channel fluorescence). Such significant spectral shifts should not be observed within the GNP-Cit-Pt(IV) samples.

High folate receptor α expressing A549 cells were seeded onto coverslips within 6 well plates and cultured for 24 hours; samples were then either incubated with appropriate solutions for 24 hours or had their media changed and incubated for a further 24 hours (as represented in Table 401) on a plate rocker; samples were subsequently washed, fixed and permeabilised, prior to staining with appropriate CP9/19 antibodies and Hoechst stains. With regard to cell staining, unlike the previous folate receptor immunocytochemistry studies, the target of interest was within the cell membrane. Due to the size of the antibodies employed in such studies it was therefore not possible to conduct live cell studies targeting the cisplatin-DNA adducts. Accordingly, and as briefly noted above, the present immunocytochemistry studies were conducted on fixed cells that had been subsequently permeabilised to allow influx of the appropriate antibody (see experimental section 4.6.5 for full details on fixed cell immunocytochemistry studies).

4.5.2.2. Fixed Cell Confocal Immunocytochemistry Images

The fixed cell confocal microscopy images for the samples of Table 401 are represented in Figures 409-416. All confocal images were collected within a single scan as a z-stack profile, utilising the brightfield, blue and green channels simultaneously, ensuring complete signal overlap and homogeneity. So as to ensure localisation of green channel signal with respect to blue (Cisplatin-DNA adduct signal vs Hoechst nuclei signal) the blue channel signal was used to set the bottom and top of the z stack profile range to be collected. Therefore, the z stack profiles collected across Figures 409 – 416 represent the range across the samples corresponding from the bottom of the nuclei to the top of the nuclei. It shall be appreciated that the entire range from bottom of the cell to the top of the cell was also collected for each sample so as to evidence the entirety of the localisation of the antibody signal. These results are omitted here as no such signal was observable after the microscope had been calibrated to account for and obviate recording false-positive signal and non-selective biding signal (discussed further in section 4.4.2.3).

HIGH FOLATE RECEPTOR α EXPRESSING A549S DOSED WITH:	
No Blocking	**With Receptor α Blocking**
Blank (not shown)	-
Figure 409 - Secondary Antibody Only	-
Figure 410 – Pri + Sec Antibodies (AB)	-
Figure 411 - Cisplatin + AB	-
Figure 412 - Pt(IV)LipA + AB	-
Figure 413 - GNP-Fol-Pt(IV) + AB	**Figure 415** - GNP-Fol-Pt(IV) + AB
Figure 414 - GNP-Cit-Pt(IV) + AB	**Figure 416** - GNP-Cit-Pt(IV) + AB

Table 401: Overview of fixed cell confocal immunocytochemistry samples.

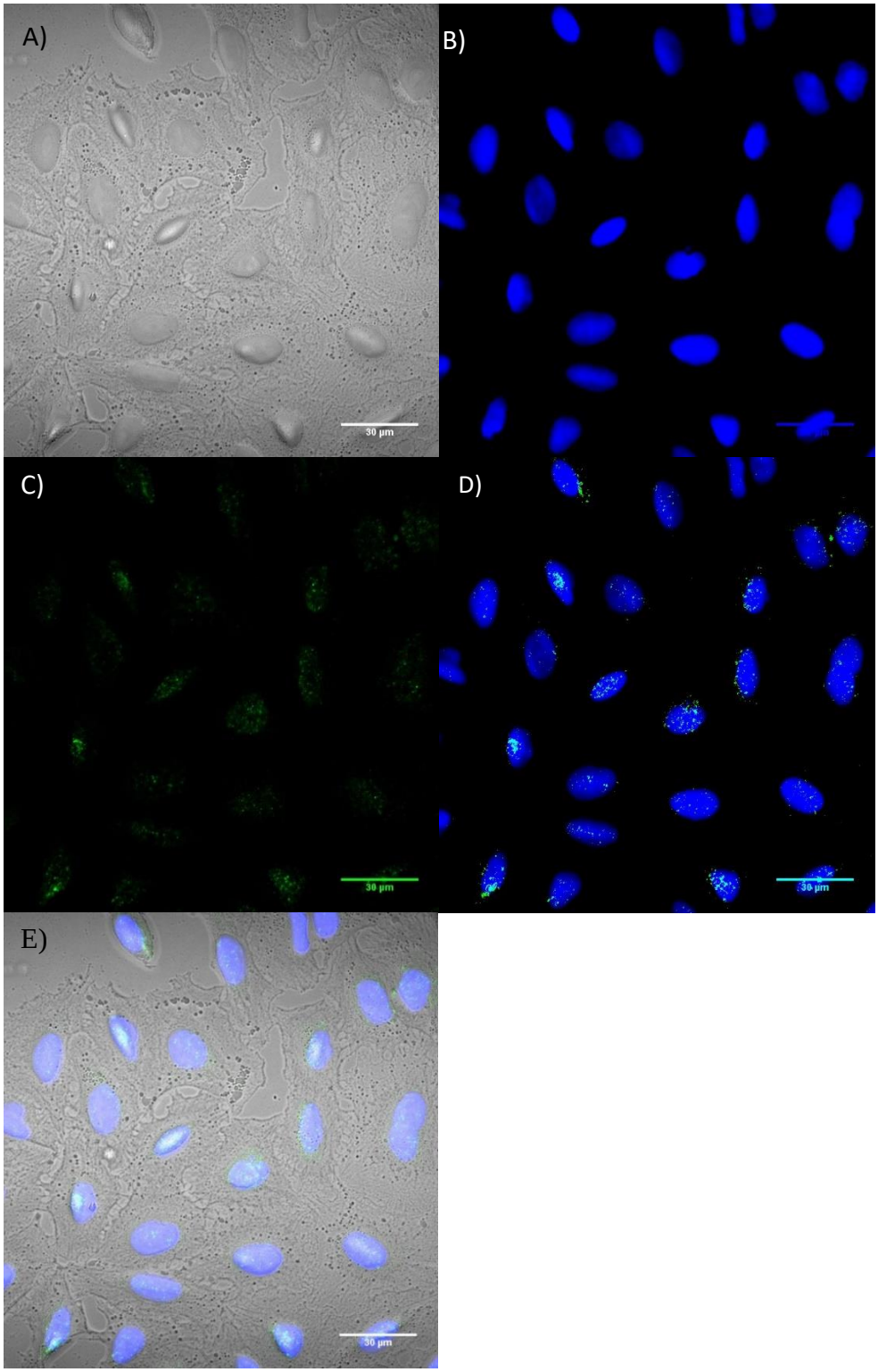

Figure 409: Fixed cell immunocytochemistry confocal studies of high folate receptor α expressing A549 cells stained with secondary antibody bearing Alexa-Fluor 488, illustrating non-selective binding of antibody or artificial signal. A) in focus plane of brightfield channel; B) Hoechst signal across Z stack; C) Antibody fluorescence across Z stack; D) Overlay of B and C; and E) Overlay of all channels.

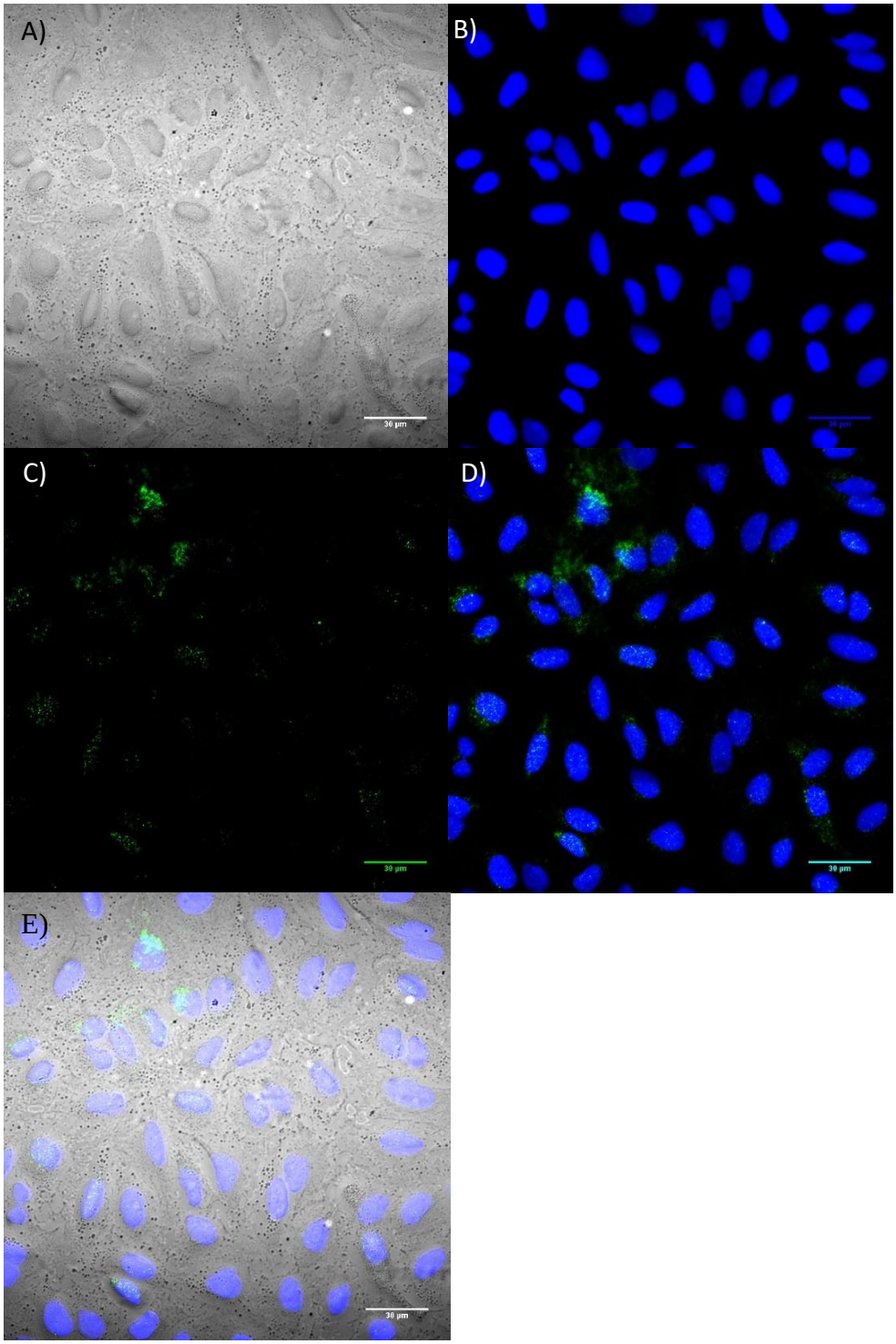

Figure 410: Fixed cell immunocytochemistry confocal studies of high folate receptor α expressing A549 cells stained with primary antibody CP9/19 and secondary antibody bearing Alexa-Flour 488, illustrating non-selective binding of antibody pair. A) in focus plane of brightfield channel; B) Hoechst signal across Z stack; C) Antibody fluorescence across Z stack; D) Overlay of B and C; and E) Overlay of all channels.

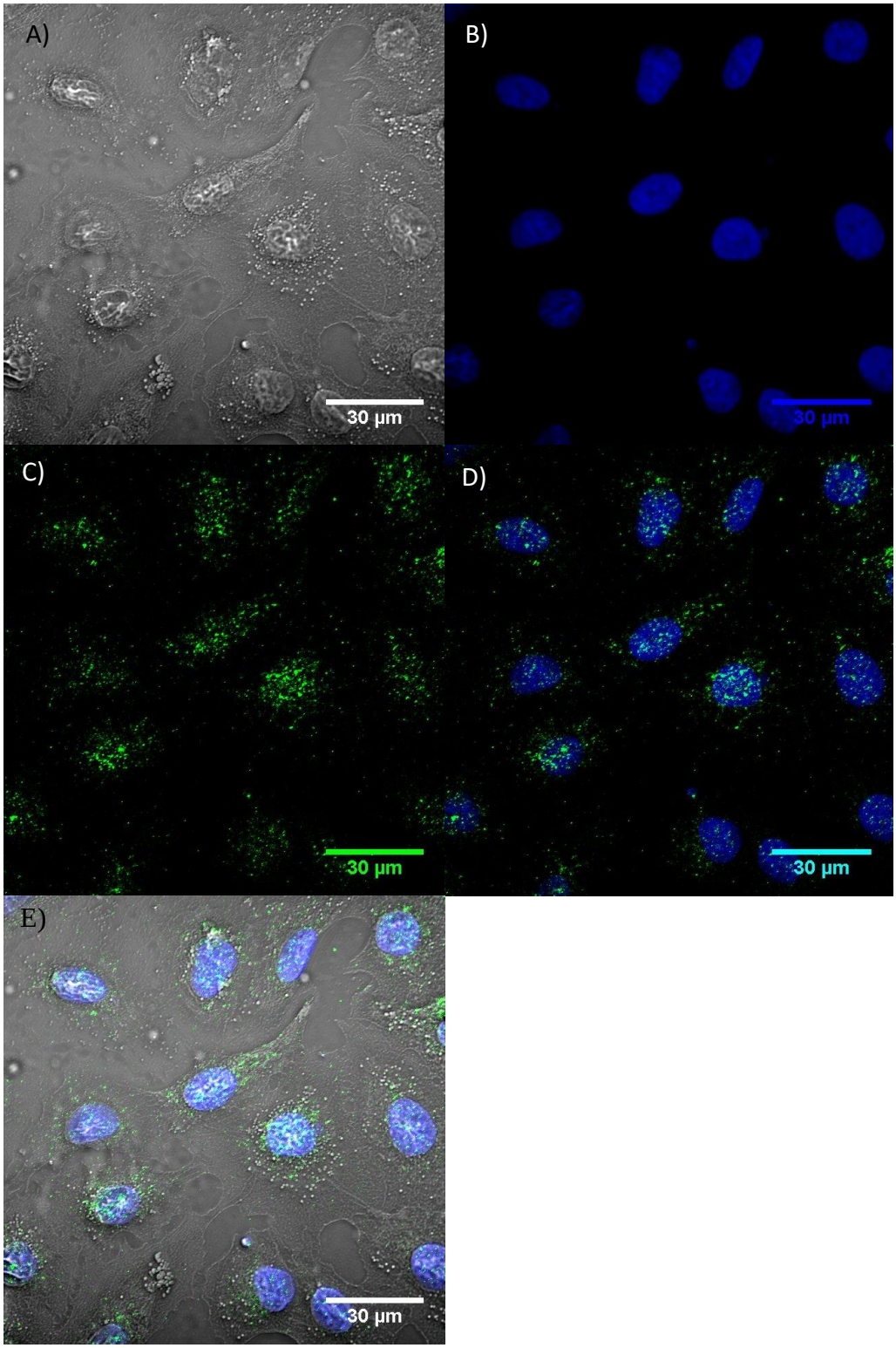

Figure 411: Fixed cell immunocytochemistry confocal studies of high folate receptor α expressing A549 cells dosed with 25µM cisplatin for 24 hours before being fixed, permeabilised and stained with CP9/19 and secondary antibody. A) in focus plane of brightfield channel; B) Hoechst signal across Z stack; C) Antibody fluorescence across Z stack; D) Overlay of B and C; and E) Overlay of all channels.

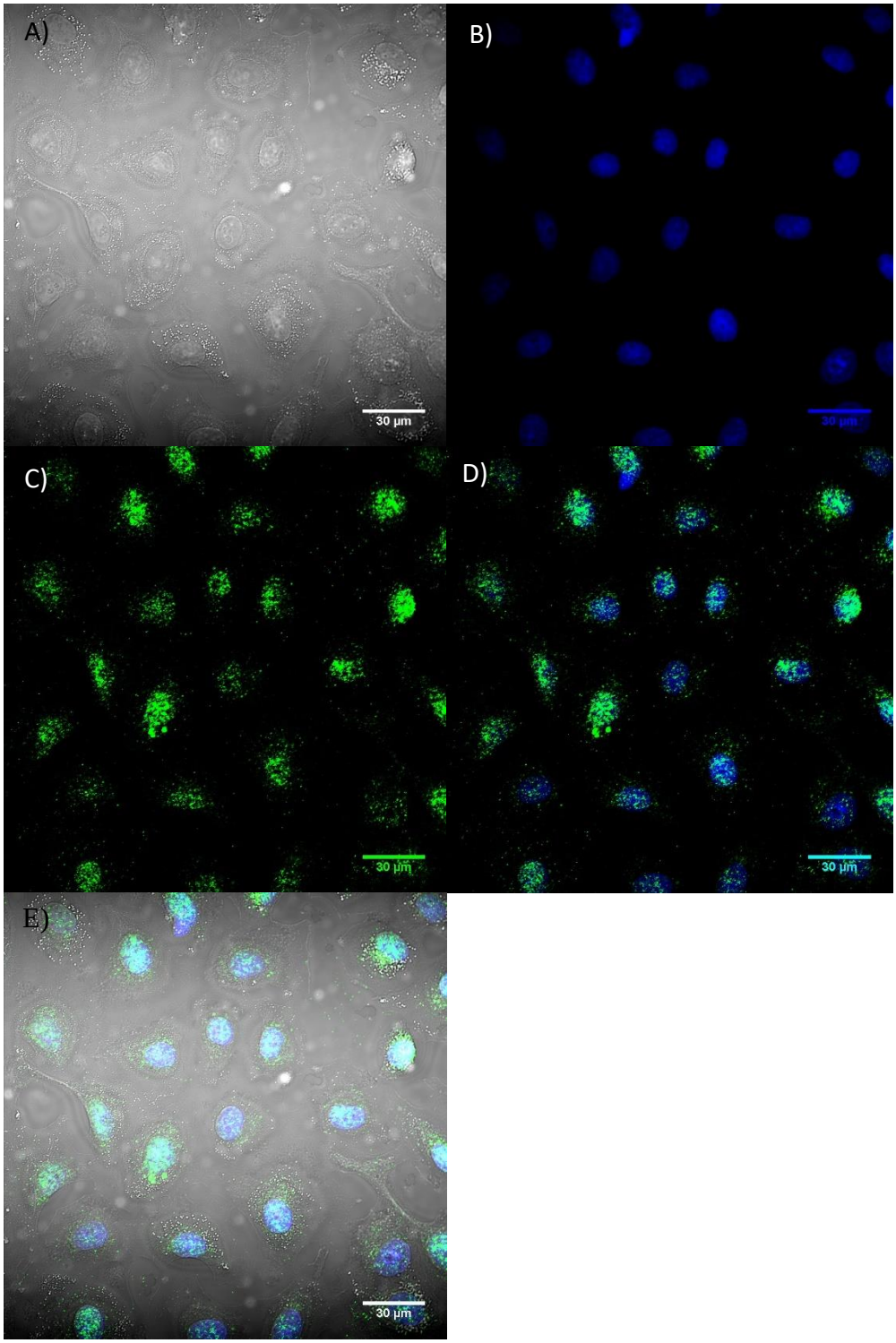

Figure 412: Fixed cell immunocytochemistry confocal studies of high folate receptor α expressing A549 cells dosed with 25µM Pt(IV)LipA for 24 hours before being fixed, permeabilised and stained with CP9/19 and secondary antibody. A) in focus plane of brightfield channel; B) Hoechst signal across Z stack; C) Antibody fluorescence across Z stack; D) Overlay of B and C; and E) Overlay of all channels.

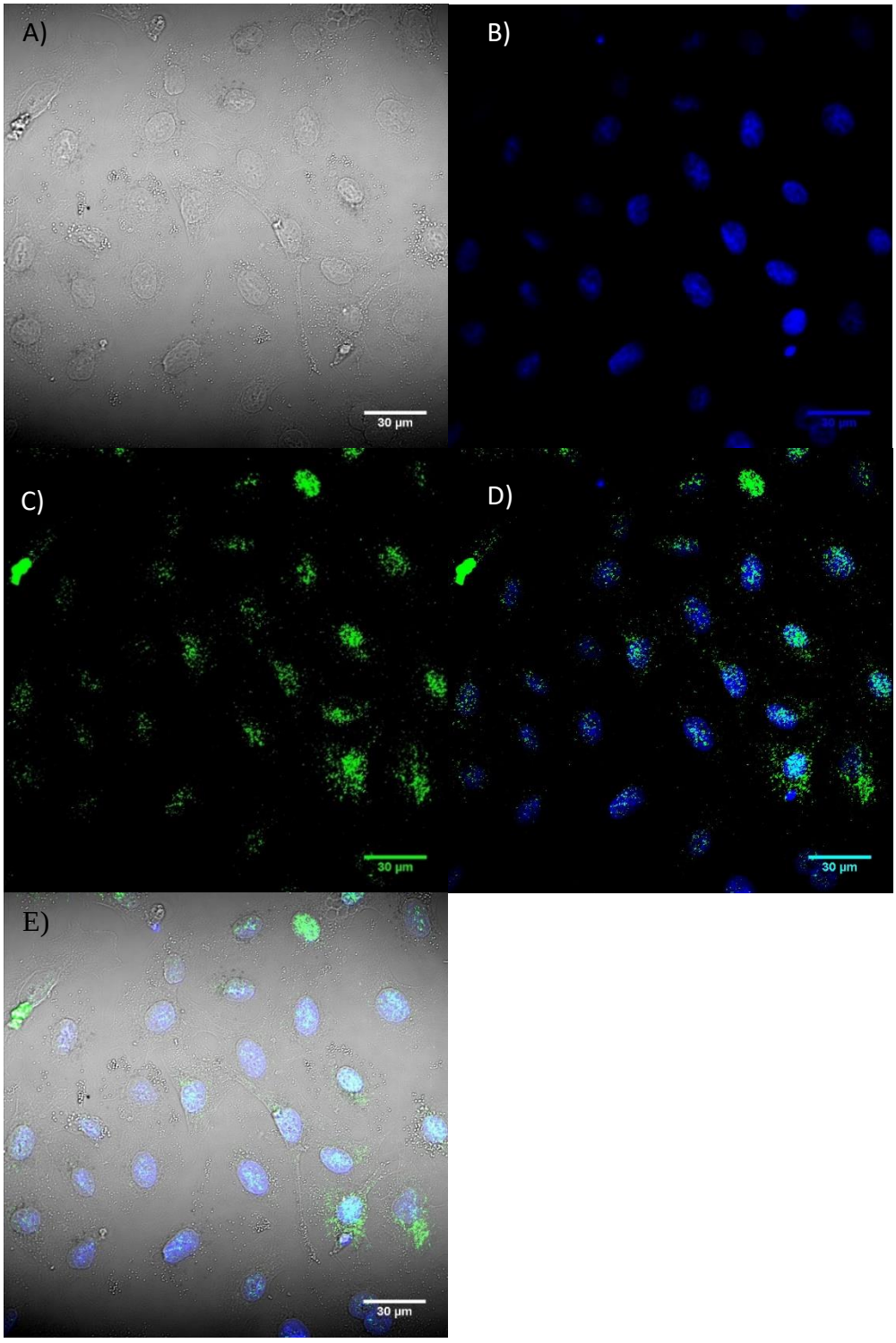

Figure 413: Fixed cell immunocytochemistry confocal studies of high folate receptor α expressing A549 cells dosed GNP-Fol-Pt(IV) (1ml 1nM GNP-Fol 25µM + Pt(IV)LipA) for 24 hours before being fixed, permeabilised and stained with CP9/19 and secondary antibody. A) in focus plane of brightfield channel; B) Hoechst signal across Z stack; C) Antibody fluorescence across Z stack; D) Overlay of B and C; and E) Overlay of all channels.

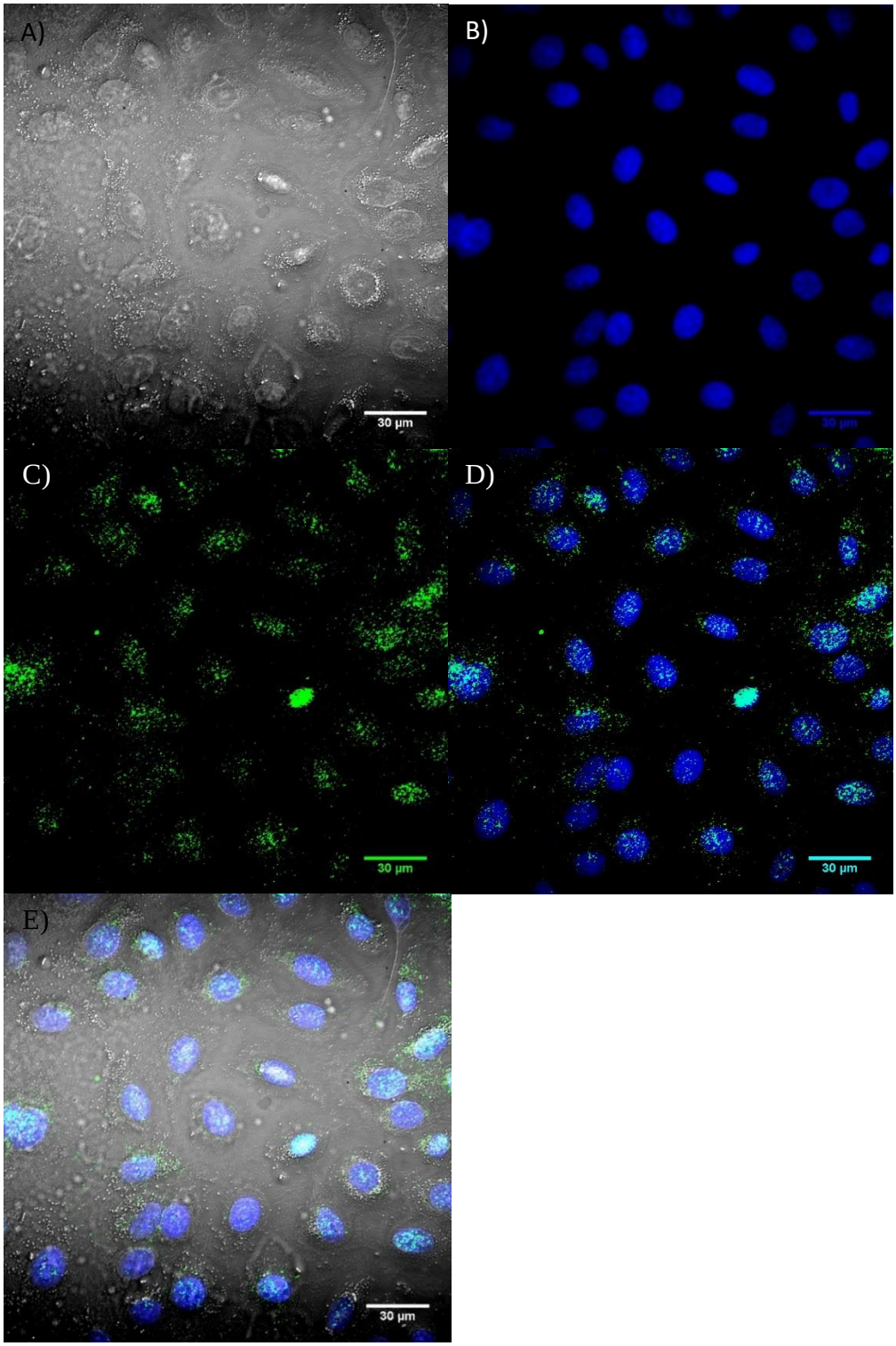

Figure 414: Fixed cell immunocytochemistry confocal studies of high folate receptor α expressing A549 cells dosed GNP-Cit-Pt(IV) (1ml 1nM GNP-Cit + 25µM Pt(IV)LipA) for 24 hours before being fixed, permeabilised and stained with CP9/19 and secondary antibody. A) in focus plane of brightfield channel; B) Hoechst signal across Z stack; C) Antibody fluorescence across Z stack; D) Overlay of B and C; and E) Overlay of all channels.

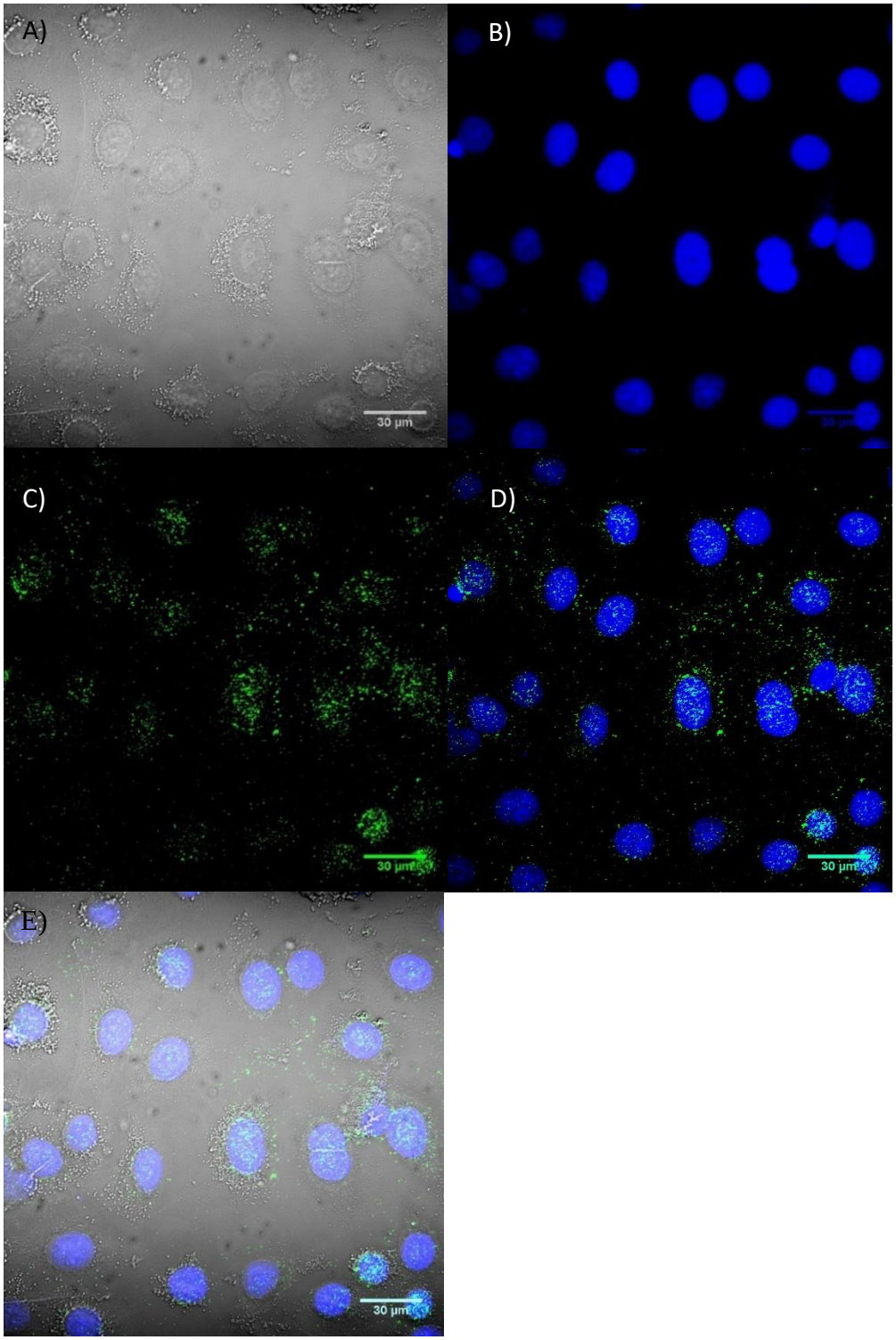

Figure 415: Fixed cell immunocytochemistry confocal studies of high folate receptor α expressing A549 cells dosed with GNP-Fol-Pt(IV) (1ml 1nM GNP-Fol + 25µM Pt(IV)LipA) in the presence of folate receptor α blocking for 24 hours before being fixed, permeabilised and stained with CP9/19 and secondary antibody. A) in focus plane of brightfield channel; B) Hoechst signal across Z stack; C) Antibody fluorescence across Z stack; D) Overlay of B and C; and E) Overlay of all channels.

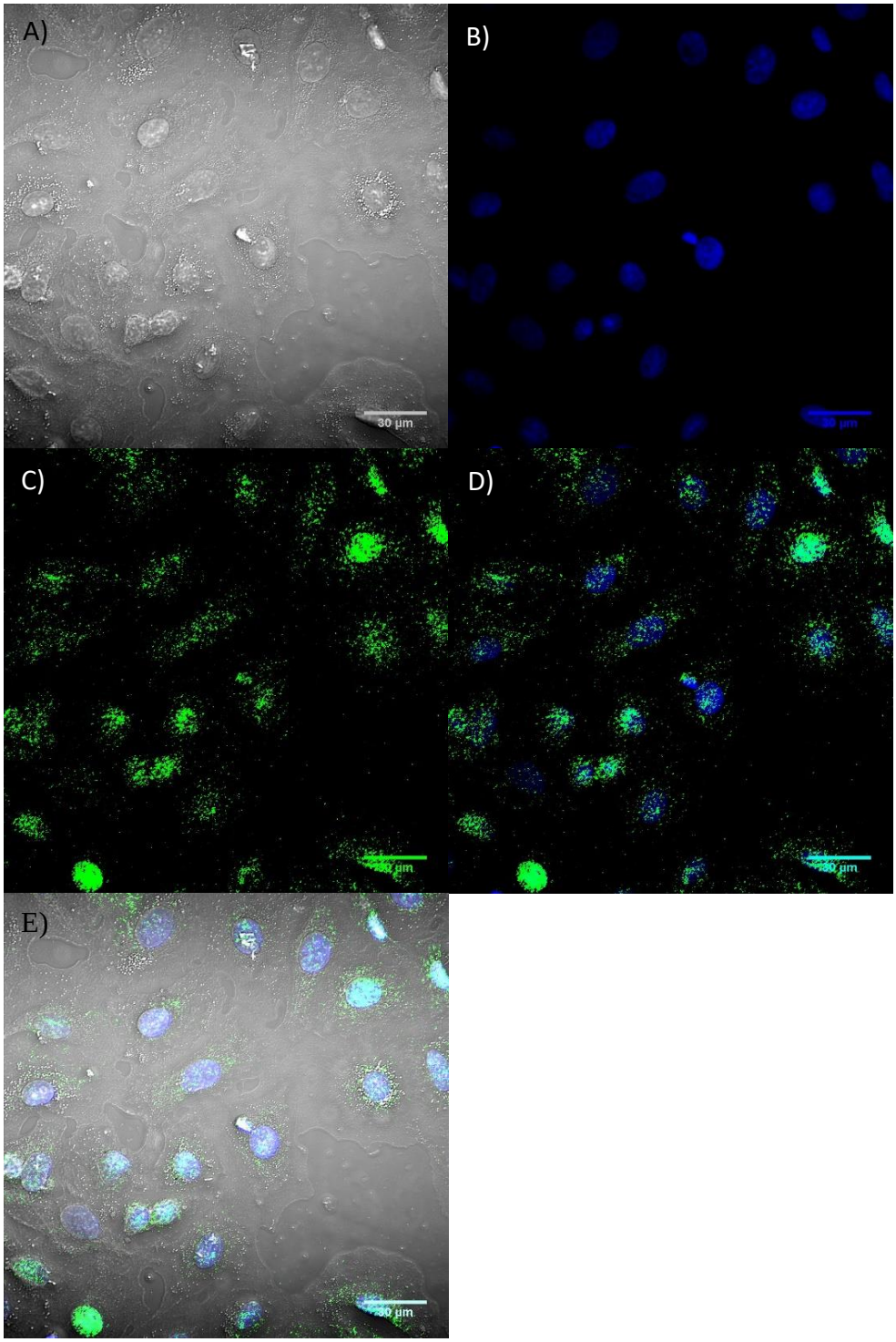

Figure 416: Fixed cell immunocytochemistry confocal studies of high folate receptor α expressing A549 cells dosed with GNP-Cit-Pt(IV) (1ml 1nM GNP-Cit + 25µM Pt(IV)LipA) in the presence of folate receptor α blocking for 24 hours before being fixed, permeabilised and stained with CP9/19 and secondary antibody. A) in focus plane of brightfield channel; B) Hoechst signal across Z stack; C) Antibody fluorescence across Z stack; D) Overlay of B and C; and E) Overlay of all channels.

4.5.2.3. Fixed Cell Confocal Immunocytochemistry Results Discussion

A number of control samples were analysed via confocal microscopy in order to appropriately threshold the lasers and respective channels of the microscope prior to collecting images of the samples that were treated with appropriate solutions (see Table 401 and corresponding Figure 409 – 416). Firstly, a blank sample of clean, untreated A549s that had merely been stained with nuclear dye (Hoechst) were imaged. These blank cells were imaged to threshold the blue channel laser so as to ensure there was no Hoechst fluorescence signal noise observable within the green channel. Secondly, blank A549s were fixed and subsequently treated with the secondary antibody and Hoechst only (Figure 409). This provided a means of ascertaining non-selective binding of the secondary antibody within the cells / the degree of signal remaining post washing. In this regard, there will inevitably be some secondary antibody remaining within the cells, either non-selectively bound or completely unbound, post washing. Accordingly, the green channel signal was calibrated through lowering laser power and signal gain to nullify any such signal. Lastly, blank A549s were fixed and subsequently treated with primary and secondary antibodies as well as Hoechst (Figure 410). The signal within the green channel in this sample therefore represents false positives, where the primary antibody is likely inadvertently binding to healthy or slightly defective DNA as opposed to DNA kinks caused by cisplatin adducts. Again, the green channel signal was calibrated to nullify any such signal.

All images collected across the samples (Figures 409-416) were obtained through use of a 60x magnification oil lens. However, the sample images of Figure 411 have been artificially magnified through image processing software, showing a smaller section of the sample that was imaged. This is so as to obviate presentation of artefacts produced by non-homogeneous coating of the fixative across the focal plane of the sample. All other samples (Figures 409, 410

and 412-416) were homogeneously coated in fixative and accordingly, the entirety of their respective images are shown.

Upon review of the cisplatin studies (Figure 411) and Pt(IV)LipA studies (Figures 412) it appears that the majority of the antibody fluorescence signal appears to be localised to the nuclei of the cells, with said signal overlapping with that of the Hoechst nuclei stain. This is particularly clear from review of Image D of Figures 411 and 412, which shows overlap of the average antibody and Hoechst signals from across the collated z stacks for the respective samples. It is hypothesised that the green antibody signal situated outside the nuclear regions of the samples is likely as a result of damage to mitochondrial DNA.

It is also evident from a comparison of Images B-E of Figures 411 and 412 that there is a difference in the prominence of antibody signal between the samples. More particularly, that the Pt(IV)LipA complex gives greater antibody signal than cisplatin, which is potentially indicative of greater platinum induced DNA damage to the nuclei of the cells. Whilst this would imply that the Pt(IV)LipA complex on its own imparts greater cisplatin-DNA adducts than cisplatin alone, likely through obviating the cisplatin resistance pathways of the cells (see introduction section 1.3.1), further investigations into the exclusivity of the antibody binding shall be required. In this regard, further investigations shall be required into whether platinum based anti-cancer agents that are known to be effective in the field but possessing substantially different methods of effect than cisplatin must be tested with the CP9/19 antibody to establish whether the antibody still binds / represents adducts. Comparison of Figures 411 and 412 makes a promising case for the efficacy of the Pt(IV)LipA agent over cisplatin, which also aligns with the MTT data collected at the respective concentrations and as reported in section 4.4.1.

Subsequent samples (Figures 413 – 416) sought to compare the imparted DNA damage of GNP-Fol-Pt(IV) and GNP-Cit-Pt(IV) systems on the cells both with folate receptor α blocking (Figures 415 and 416 respectively) and without folate receptor α blocking (Figures 413 and 414 respectively). The principle being that the GNP-Fol-Pt(IV) system should demonstrate greater platinum induced DNA adducts than the GNP-Cit-Pt(IV) system and that upon blocking the α folate receptors, the imparted damage of the GNP-Fol-Pt(IV) system should be significantly reduced and the imparted GNP-Cit-Pt(IV) system damage should be largely unaffected.

Comparison of the images collected for the GNP-Fol-Pt(IV) and GNP-Cit-Pt(IV) samples (images A-E, Figures 413 and 414) show a substantially similar localisation and prevalence of antibody induced signal. Therefore, there appears to be minimal qualitative difference in DNA damage antibody signal across the systems. In comparison to the free Pt agent studies of Figures 411 and 412, there appears to be a more diffuse localisation of the antibody signal with respect to the nuclei of the cells, which is potentially indicative of more non-target delivery of therapeutic agents in the nanoparticlely delivered systems. Accordingly, it is possible that there is a greater amount of mitochondrial DNA damage rather than nuclear DNA damage for the nanoparticle systems.

Encouragingly, and in line with the hypothesis, through blocking of the α folate receptors there appears to be a substantial decrease in the antibody signal of the GNP-Fol-Pt(IV) sample (Figure 415, Images A-E). By contrast, the antibody signal of the GNP-Cit-Pt(IV) sample with blocking appears largely unaffected (Figure 416, A-E). In this regard, qualitative comparison of Figures 413 and 415 shows a significant decrease in antibody signal (thus indicative of less platinum induced DNA-adducts / damage) for the GNP-Fol-Pt(IV) system, whereas

comparison of Figures 414 and 416 show largely unchanged antibody signal for the GNP-Cit-Pt(IV) system. Lastly, the localisation of the induced antibody signal across Figures 413 – 416 appears largely unchanged, which implies that the blocking merely affects uptake of the GNP-Fol-Pt(IV) system and thus the quantity of Pt(IV)LipA agent that is delivered to the cell. It would appear that the localisation of the Pt(IV)LipA agent is unchanged, implying that the method of uptake is independent on the subsequent production of active agents and induced cytotoxicity.

4.5.3. Flow Cytometry (Fluorescence Assisted Cell Sorting)

Subsequent research sought to quantitatively assess the induced antibody signal of the GNP-Fol-Pt(IV) and GNP-Cit-Pt(IV) systems so as to accurately assess the impact of the systems across the cellular population, as opposed to qualitative assessment of isolated quadrants. Accordingly, FACS studies were conducted. For continuity, the same sample conditions employed for the confocal microscopy studies of section 4.5.2 were carried over. The samples of the present FACS studies are represented in Table 402.

HIGH FOLATE RECEPTOR α EXPRESSING A549S DOSED WITH:	
No Blocking	**With Receptor α Blocking**
Blank (not shown)	-
Pri + Sec Antibodies (AB)	-
Cisplatin + AB	-
Pt(IV)LipA + AB	-
GNP-Fol-Pt(IV) + AB	GNP-Fol-Pt(IV) + AB
GNP-Cit-Pt(IV) + AB	GNP-Cit-Pt(IV) + AB

Table 402: Overview of fixed cell Fluorescence-Activated Cell Sorting (FACS) samples.

The cell samples were identical to those of the previous confocal studies, with high folate receptor α expressing A549s seeded within 6 well plates and allowed to adhere overnight before being subjected to the appropriate conditions of table 402. The cells were subsequently washed with PBS before being tripsinised and fixed in suspension ready for permeabilisation and immunocytochemical staining (see experimental section 4.6.5 for full details). In order to preserve as much data as possible, the PBS washes of each sample were retained, pelleted and also subjected to immunocytochemical analysis, so as to allow for an analysis of the most severely damaged A549 cells and give an overall indication of population damage. Post sample-staining, the samples were washed and re-suspended multiple times to remove free reagents and subsequently analysed by FACS microscopy.

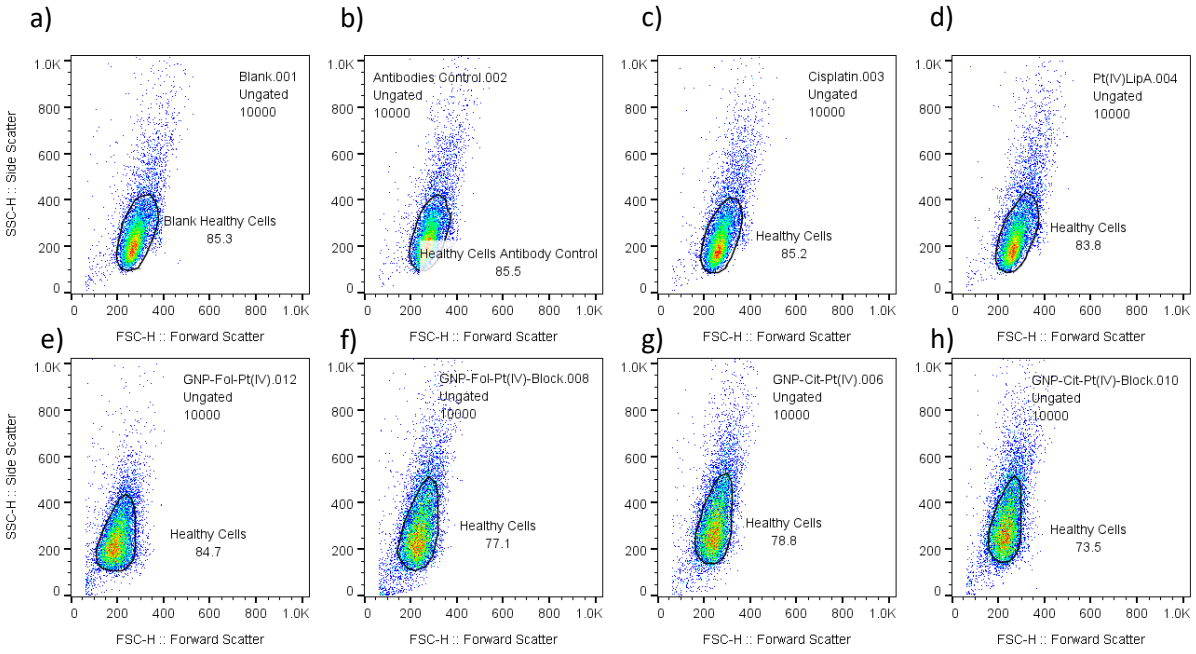

Figure 417: FACS dot-plot data of forward scatter (particle size) vs side scatter (particle granularity) for the samples of Table 402 in high folate receptor α expressing A549 cells. A) Blank sample, b) Antibody control, c) Cisplatin, d) Pt(IV)LipA, e) GNP-Fol-Pt(IV), f) GNP-Fol-PtIV)-Block, g) GNP-Cit-Pt(IV) and h) GNP-Cit-Pt(IV)-Block. The circled population represents gating of fragments, with the cited number representing the percentage of the population corresponding to healthy cells.

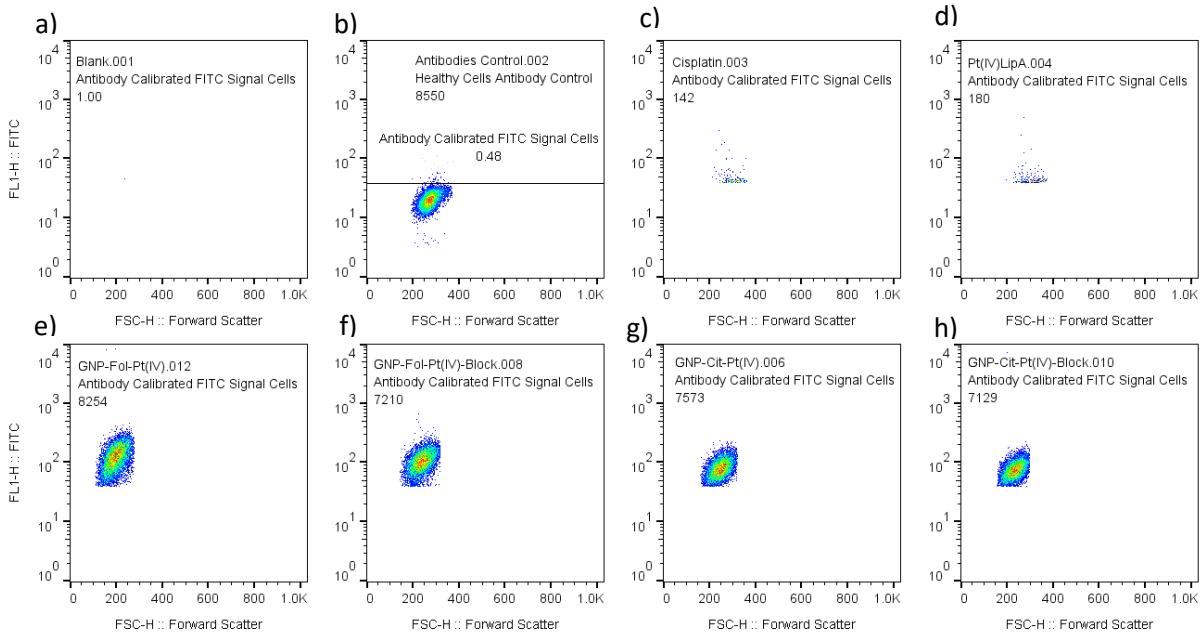

Subset Name with Gating Path	Count	Freq. of Total	Mean : FL1-H	Median : FL1-H
Blank.001/Blank Healthy Cells/Blank Calibrated/Antibody Calibrated FITC Signal Cells	1.00	0.0100	45.6	45.6
Antibodies Control.002/Healthy Cells Antibody Control/Antibody Calibrated FITC Signal Cells	41.0	0.41	55.0	46.9
Cisplatin.003/Healthy Cells/Antibody Calibrated FITC Signal Cells	142	1.42	51.2	42.5
Pt(IV)LipA.004/Healthy Cells/Antibody Calibrated FITC Signal Cells	180	1.80	49.6	42.6
GNP-Fol-Pt(IV).012/Healthy Cells/Antibody Calibrated FITC Signal Cells	8254	82.5	129	119
GNP-Fol-Pt(IV)-Block.008/Healthy Cells/Antibody Calibrated FITC Signal Cells	7210	72.1	107	102
GNP-Cit-Pt(IV).006/Healthy Cells/Antibody Calibrated FITC Signal Cells	7573	75.7	81.8	77.2
GNP-Cit-Pt(IV)-Block.010/Healthy Cells/Antibody Calibrated FITC Signal Cells	7129	71.3	77.8	73.3

Figure 418: FACS dot-plot data of forward scatter (particle size) vs FITC channel signal intensity (antibody emission intensity) for the samples of Table 402 in high folate receptor α expressing A549 cells. A) Blank sample, b) Antibody control, c) Cisplatin, d) Pt(IV)LipA, e) GNP-Fol-Pt(IV), f) GNP-Fol-PtIV)-Block, g) GNP-Cit-Pt(IV) and h) GNP-Cit-Pt(IV)-Block. "Antibody Calibrated" represents cells with FITC channel fluorescence equal to or greater than the strongest emission of the antibody control sample (upper limit of non selective binding). Any signal therefore should represent cisplatin-DNA conjugate FITC fluorescence signal. Associated statistics are tabulated beneath within the FACS analysis software and are represented again later in Table 403.

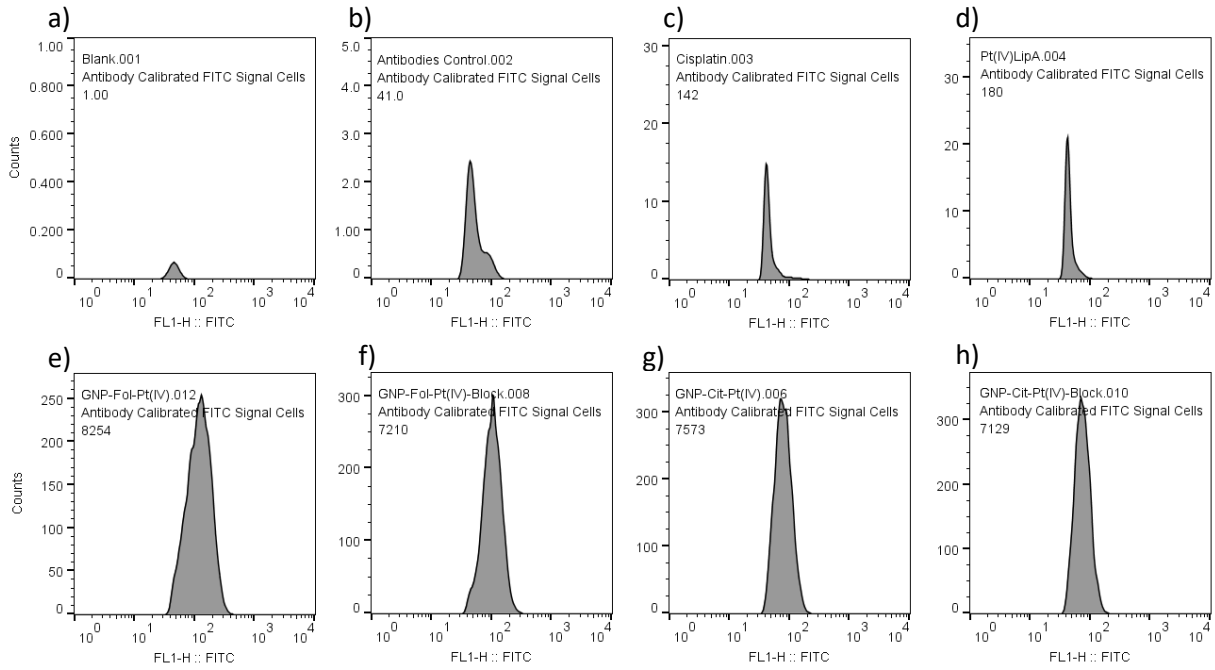

Figure 419: FACS Histogram data of FITC channel signal for the "Antibody Calibrated" sub-population of the samples of Table 402 in high folate receptor α expressing A549 cells. A) Blank sample, b) Antibody control, c) Cisplatin, d) Pt(IV)LipA, e) GNP-Fol-Pt(IV), f) GNP-Fol-PtIV)-Block, g) GNP-Cit-Pt(IV) and h) GNP-Cit-Pt(IV)-Block.

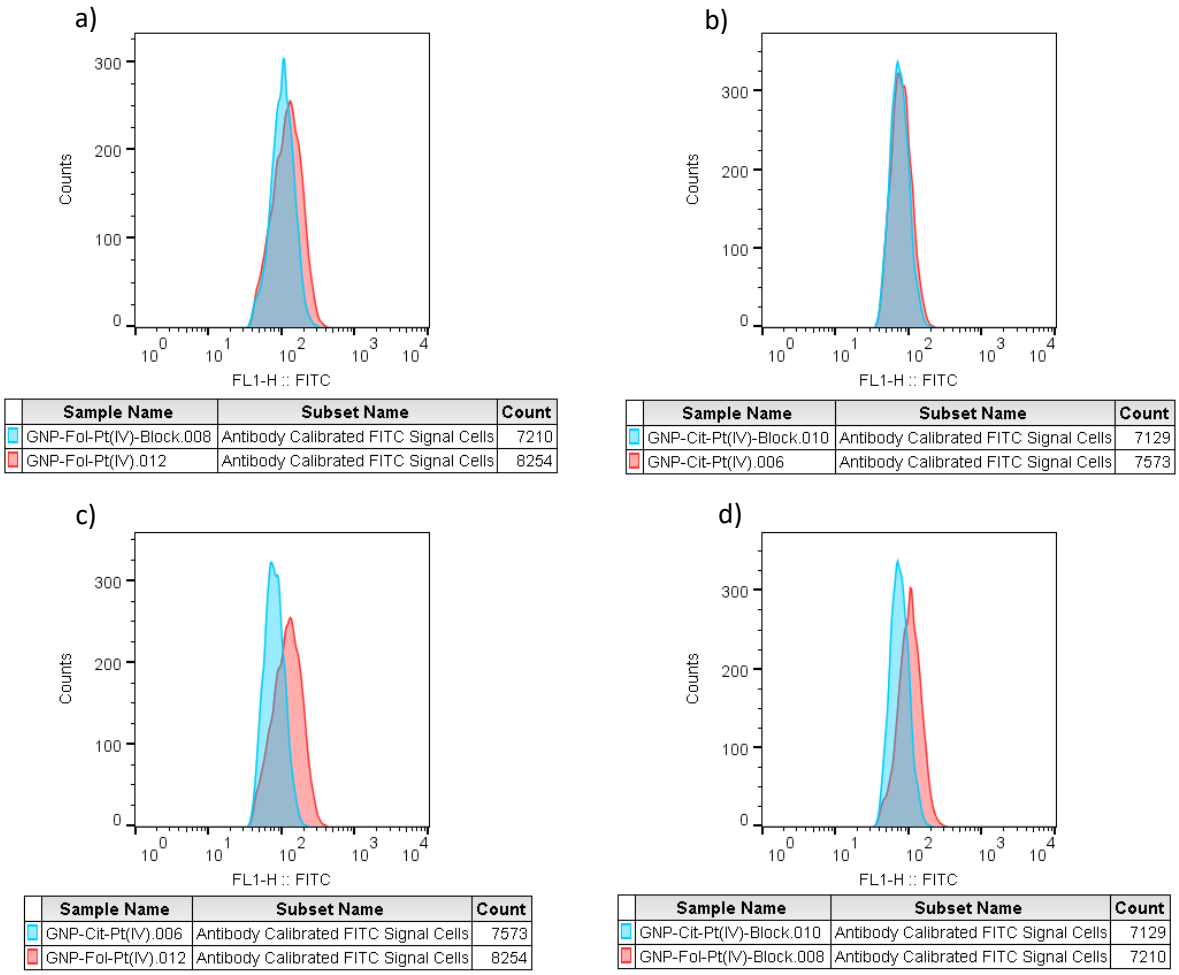

Sample Name	Subset Name	Count
GNP-Fol-Pt(IV)-Block.008	Antibody Calibrated FITC Signal Cells	7210
GNP-Fol-Pt(IV).012	Antibody Calibrated FITC Signal Cells	8254

Sample Name	Subset Name	Count
GNP-Cit-Pt(IV)-Block.010	Antibody Calibrated FITC Signal Cells	7129
GNP-Cit-Pt(IV).006	Antibody Calibrated FITC Signal Cells	7573

Sample Name	Subset Name	Count
GNP-Cit-Pt(IV).006	Antibody Calibrated FITC Signal Cells	7573
GNP-Fol-Pt(IV).012	Antibody Calibrated FITC Signal Cells	8254

Sample Name	Subset Name	Count
GNP-Cit-Pt(IV)-Block.010	Antibody Calibrated FITC Signal Cells	7129
GNP-Fol-Pt(IV)-Block.008	Antibody Calibrated FITC Signal Cells	7210

Figure 420: FACS Overlay histogram data of FITC channel signal for the "Antibody calibrated" sub-population of the samples of Table 402 in high folate receptor α expressing A549 cells. A) Overlay of GNP-Fol-Pt(IV) and GNP-Fol-Pt(IV)-Block; b) Overlay of GNP-Cit-Pt(IV) and GNP-Cit-Pt(IV)-Block; c) Overlay of GNP-Fol-Pt(IV) and GNP-Cit-Pt(IV); and d) Overlay of GNP-Fol-Pt(IV)-Block and GNP-Cit-Pt(IV)-Block.

SAMPLES	EVENTS	% OF SAMPLE	MEAN	MEDIAN
Blank	1	0.01	45.6	45.6
Antibodies Control	41	0.41	55.0	46.9
Cisplatin	142	1.42	51.2	42.5
Pt(IV)LipA	180	1.8	49.6	42.6
GNP-Fol-Pt(IV)	8254	82.5	129.0	119.1
GNP-Fol-Pt(IV)-Block	7210	72.1	107.0	102.1
GNP-Cit-Pt(IV)	7573	75.7	81.8	77.2
GNP-Cit-Pt(IV)-Block	7129	71.3	77.8	73.3

Table 403: Statistical data drawn from FACS histogram plots of samples a)-h) of Figure 419.

A number of potential observations can be drawn from the FACS data collected for the above A549 immunocytochemical studies. Upon review of Figures 417 and 418 there appears to be an increase in DNA damage induced FITC signal within the nanoparticle samples (e – h) over cisplatin (c) and Pt(IV)LipA alone (d). More particularly, Figure 418 represents dot-plot data for the samples of Table 402, plotting FITC channel signal (antibody fluorescence intensity) against forward scatter (cell size), having already been gated to remove fragments (as represented in Figure 417). The "Antibody Calibrated" sub-population of the dot-plots represents the threshold for false positive fluorescence signal and therefore identifies the minimal fluorescence required for data points to be considered representative of DNA-Cisplatin adduct induced antibody fluorescence signal. Accordingly, any particles displaying a FITC intensity above this threshold fall within the "Antibody Calibrated" sub-culture. Therefore, simple visual comparison of the plots shows that cisplatin (c) and Pt(IV)LipA (d) show significantly less particles beyond the DNA damage antibody signal threshold vs all of the nanoparticle samples (e – h, ~70-80% total sample difference). As noted, Figure 417

represents dot-plot data of forward scatter (particle size) vs side scatter (particle granularity) and therefore shows the standard distribution of the data cloud for samples a)-h).

Figure 419 represents histogram plots of the data collected for samples a) – h), showing the distribution of particles displaying FITC channel fluorescence which exceeds the Antibody Calibrated threshold. This data, in combination with the histogram-overlay data of Figure 420 and statistics of Table 403, better represents the relationship of the DNA damage with respect to the different samples. In this regard, from overlay-histogram A) (overlap of plots e) and f) of Figure 418) it appears that there is a decrease in the overall population displaying FITC fluorescence above the threshold for samples treated with GNP-Fol-Pt(IV) vs GNP-Fol-Pt(IV)-Block. More particularly, when A549 cells are treated with GNP-Fol-Pt(IV) in the presence of folate receptor blocking there is a 13% decrease in the number of events (8254 vs 7210), a 17 % reduction in the mean fluorescence intensity (129.0 vs 107.0) and a 14% reduction in the median fluorescence intensity (119.0 vs 102.0). This data therefore appears to agree with the hypothesis (and prior research detailed herein) that blocking the folate receptors leads to a reduction in the uptake of GNP-Fol within high folate receptor α expressing A549s, which in turn, leads to a reduction in cytotoxic events.

Upon review of overlay-histogram B) (overlap of plots g) and h) of Figure 418) it also appears that there is no clear relationship between nanoparticle loading with the GNP-Cit-Pt(IV) system in the presence of folate receptor α blocking in A549s. More particularly, when A549 cells are treated with GNP-Cit-Pt(IV) in the presence of folate receptor blocking there is a 4% decrease in the number of events (7573 vs 7129), a 3% reduction in the mean fluorescence intensity (81.8 vs 77.8) and a 5% reduction in the median fluorescence intensity (77.2 vs 73.3). This data therefore appears to agree with the hypothesis (and prior research detailed herein) that blocking

the folate receptors leads to no significant change in the uptake of GNP-Cit within high folate receptor α expressing A549s.

Overlay histogram C) compares the particle distribution for GNP-Fol-Pt(IV) vs GNP-Cit-Pt(IV) within the FITC channel beyond the threshold (plots e) and g) of Figure 418). From this overlay histogram and the accompanying statistics it is shown that the GNP-Fol-Pt(IV) system displays 10% more events (8254 events vs 7573 respectively), 37% higher mean fluorescence intensity (129.0 vs 81.8 respectively) and 35% higher median fluorescence intensity (119.0 vs 77.2 respectively) over the GNP-Cit-Pt(IV) system within the high folate receptor α expressing A549 cells. The same trend (albeit with different statistics) is observable for the blocked GNP-Fol-Pt(IV) system over the blocked GNP-Cit-Pt(IV) system.

Accordingly, from the above FACS studies it is further hypothesised that the GNP-Fol-Pt(IV) system displays increased cisplatin-DNA adduct formation over cisplatin, Pt(IV)LipA alone and the GNP-Cit-Pt(IV) system in high folate receptor α expressing A549 cells. Through comparing the above data, as well as the confocal data or earlier studies, it appears that folate receptor blocking has an affect on GNP-Fol system uptake, thus indicating that folate receptor mediated uptake plays a key role in uptake of the system. The GNP-Cit system appears to either operate independently of folate receptor α or with a lesser dependence on said receptor mediated uptake.

4.5.4. ICPMS

Following the immunocytochemical confocal and FACS microscopy studies detailed herein, subsequent research sought to identify and quantitatively assess the cellular localisation of the sample components within A549 cells. In particular, it was an objective of the research

to quantify the localisation of gold salt and platinum species within the whole cell, cytosol and nucleus. Accordingly, Inductively Coupled Plasma Mass Spectrometry (ICPMS) was utilised, assessing the localisation of such components with high folate receptor α expressing A549 cells that have been dosed with the samples as per Table 404. For continuity, the same concentrations and dosing protocols were employed as per the previous studies (see experimental section 4.6.6 for full details). ICPMS data for these samples is represented in Figures 421 to 424 below.

HIGH FOLATE RECEPTOR α EXPRESSING A549S DOSED WITH:			
No Blocking		**With Receptor α Blocking**	
a)	Blank		-
b)	Cisplatin		-
c)	Pt(IV)LipA		-
d)	GNP-Fol-Pt(IV)	f)	GNP-Fol-Pt(IV)
e)	GNP-Cit-Pt(IV)	g)	GNP-Cit-Pt(IV)

Table 404: Overview of samples submitted for ICPMS. A549s were seeded onto 6 well plates and allowed to adhere overnight. Samples were then dosed with 25μM anti-cancer agent either alone (Cisplatin (b) and Pt(IV)LipA (c)) or as part of a nanoparticle system, loaded onto either 0.5mL ~1nM GNP-Fol (samples d) and f)) or 0.5mL ~1nM GNP-Cit (samples d) and f)).

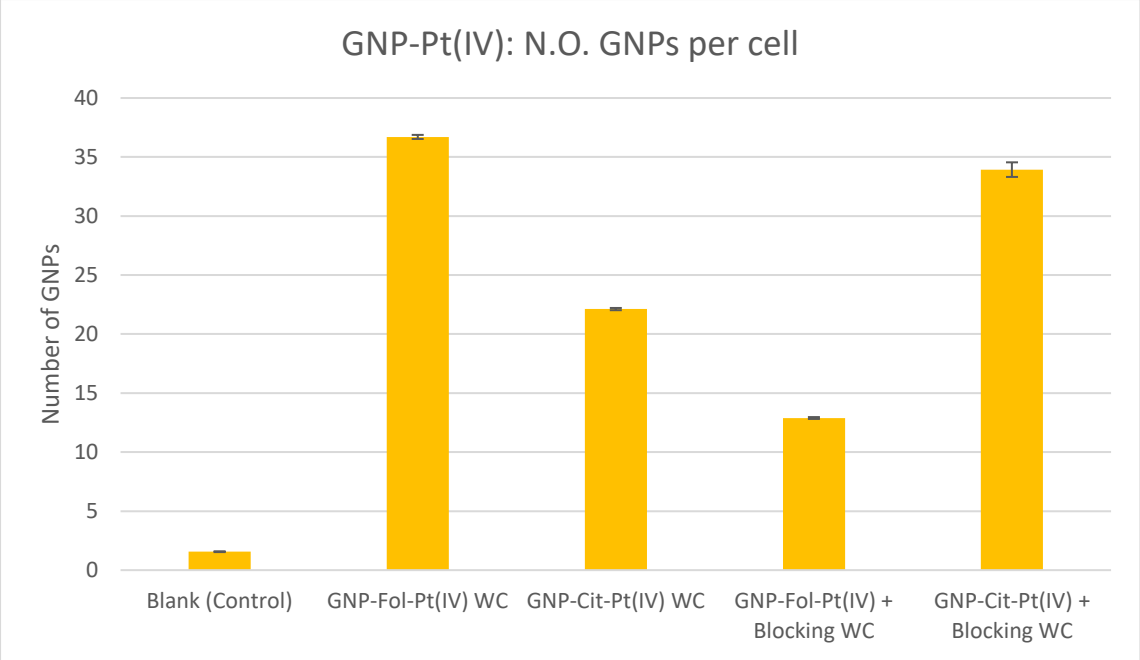

Figure 421: Graphical representation of the total number of gold nanoparticles on average per whole cell of samples d) to g) of Table 404. Expectedly, significantly fewer GNP-Fol centres are present upon blocking the folate receptors (36 vs 12). Unexpectedly, more GNP-Cit cores were found on average in the presence of folate receptor blocking.

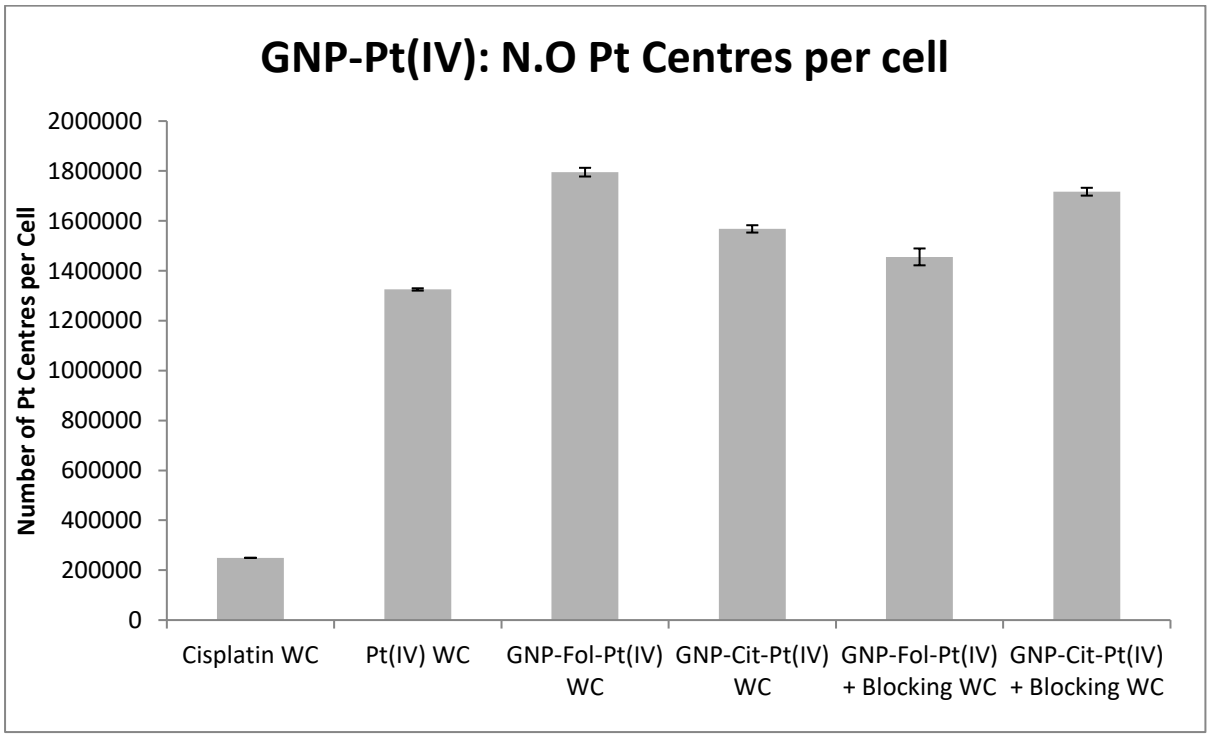

Figure 422: Graphical representation of the total number of platinum centres on average per whole cell of samples b) to g) of Table 404.

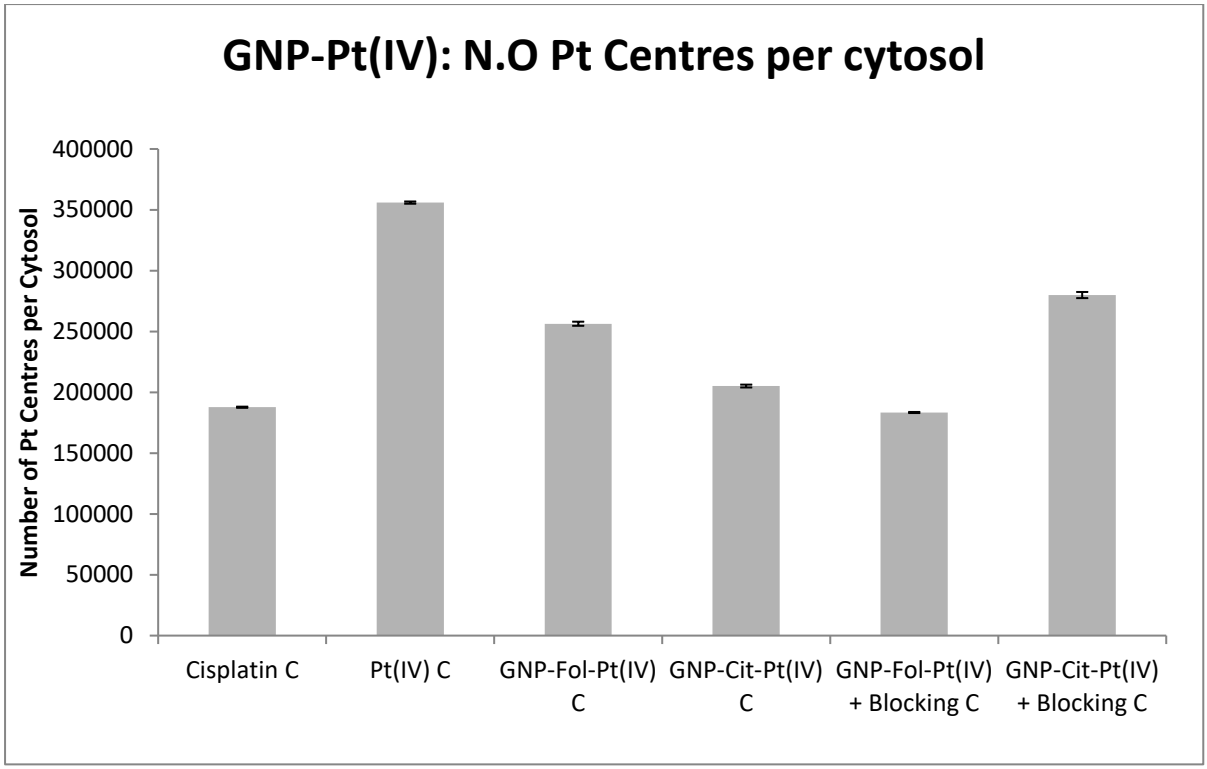

Figure 423: Graphical representation of the total number of platinum centres on average per cytosol of A549 cells dosed as per samples b) to g) of Table 404.

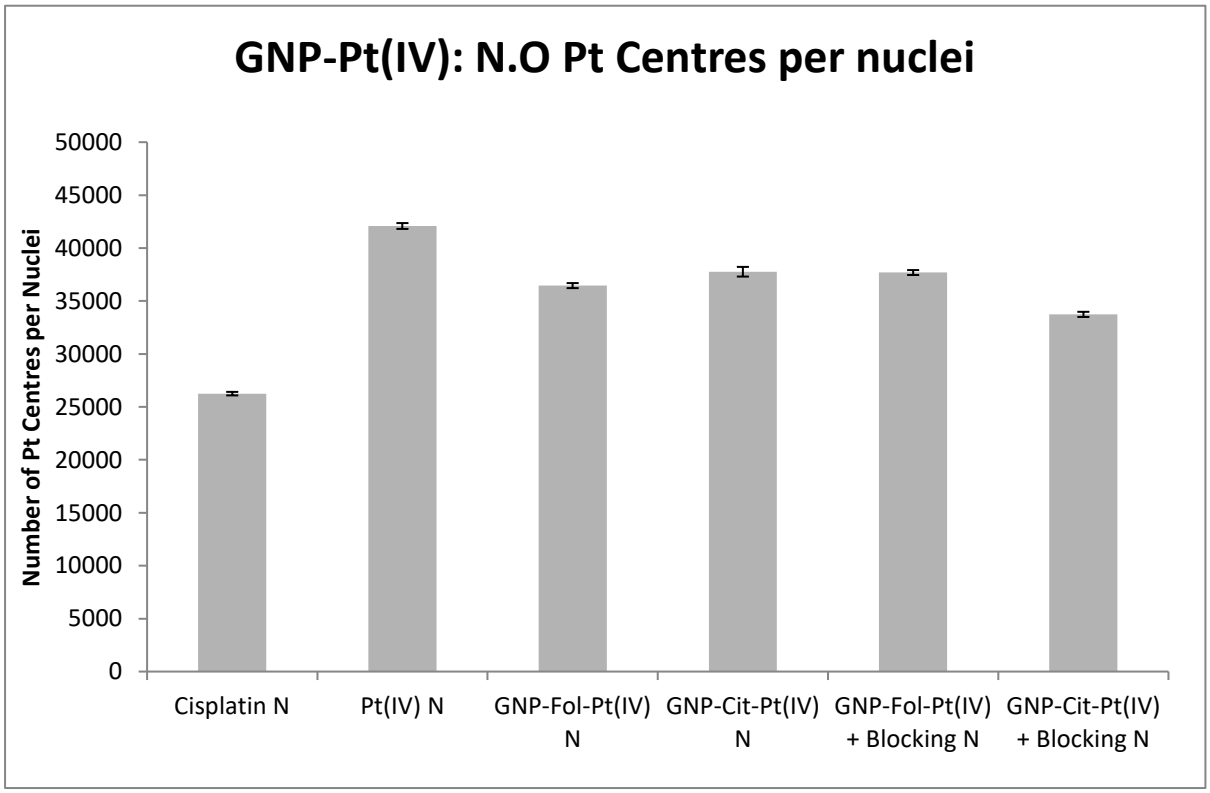

Figure 424: Graphical representation of the total number of platinum centres on average per nuclei of A549 cells dosed as per samples b) to g) of Table 404.

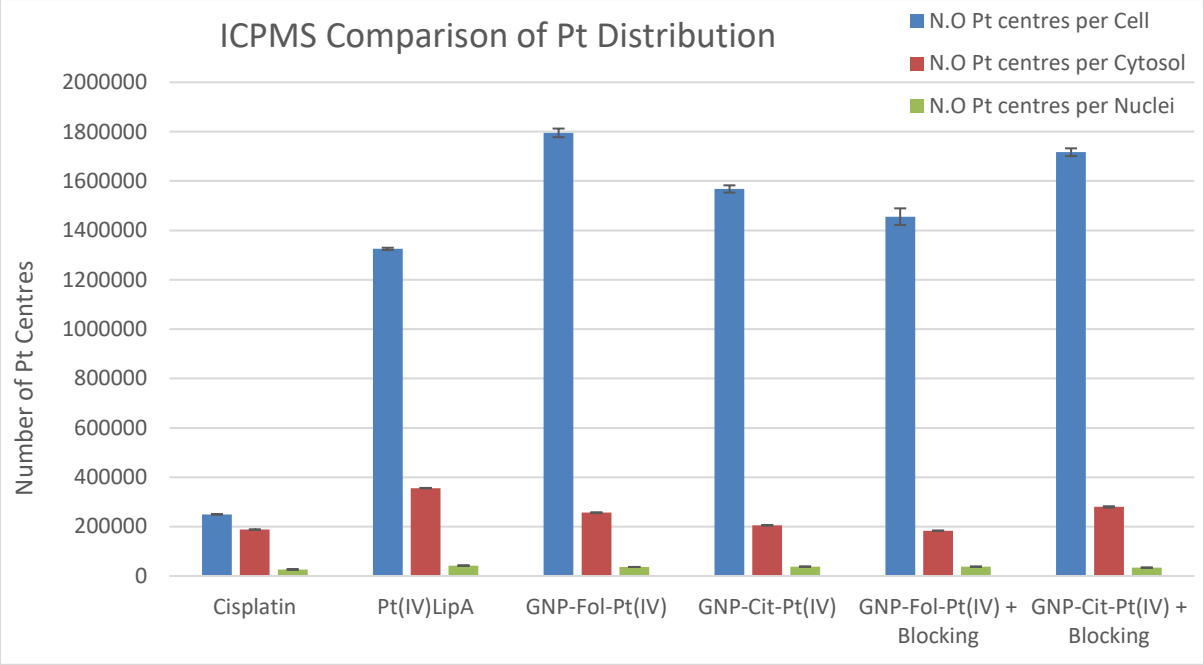

Figure 425: Graph comparing the Pt uptake statistics represented across Figures 422-424.

Upon review of the above ICPMS studies, the data of Figure 421 suggests that, in line with prior data and present hypotheses, blocking of folate receptor α with primary antibody leads to reduced levels of GNP-Fol uptake. Statistically, 64% less GNP-Fol particles were delivered to each cell upon receptor blocking (36 GNPs per cell without blocking vs 13 GNPs with blocking). However, in contrast to prior studies, the ICPMS data of Figure 421 shows an increased level of cellular uptake of GNP-Cit upon blocking of folate receptor α. Prior studies implied comparable levels of uptake, with comparable fluorescent probe emission and cytotoxic effects. It is hypothesised that this may be as a result of folate receptor blocking, forcing an alternative mechanism of uptake to be exaggerated for GNP-Cit particles. Alternatively, this may be a mere anomaly and may not be apparent upon experimental repeats. Further studies shall therefore be required in order to ascertain the appropriate conclusion in this matter.

Figure 422 represents the Pt centre data recorded by ICPMS for the average whole cell for samples b) to g) of Table 404. In line with prior cytotoxicity and immunocytochemical studies, there is less Pt present for the cisplatin sample (b) vs the Pt(IV)LipA sample (c) in the whole A549s, displaying 81% less Pt respectively (250,000 vs 1,300,000 centres). The level of Pt delivered to the cell is higher for each of the GNP-Fol and GNP-Cit systems over the Pt(IV)LipA system, with the unblocked GNP-Fol-Pt(IV) system displaying the most Pt (1,800,000) and the blocked GNP-Fol-Pt(IV) system forming the minimum (1,450,000). Accordingly, the blocked A549 cell sample dosed with GNP-Fol-Pt(IV) shows 19% less Pt present within the whole cell than the unblocked sample. In line with prior studies, levels of Pt present for the blocked and unblocked GNP-Cit samples are comparable, ranging by 9% (1,700,000 and 1,500,000 respectively).

The data of Figure 423 represents some unexpected results in relation to the levels of Pt in the cytosol of the A549 cells corresponding to samples b) to g) of Table 404. As expected, the level of Pt present in cells dosed with Pt(IV)LipA is higher than that for cisplatin, displaying 48% more Pt centres (350,000 centres vs 190,000 centres respectively). Another aspect which is as expected is the higher level of Pt present for the unblocked GNP-Fol-Pt(IV) system vs blocked, displaying 29% more Pt centres (250,000 centres vs 180,000 centres respectively). However, unexpectedly, the free Pt(IV)LipA system displayed higher levels of Pt within the cytosol of the cells than all of the Nanoparticle based systems, with 21% more Pt than the closest NP system (GNP-Cit-Pt(IV)-Blocked, 280,000 centres). It is hypothesised that the figure for Pt present in the cytosol of the sample for the nanoparticle samples is inherently low due to the method of fractioning the cellular samples prior to ICPMS analysis. In this regard, a cellular fractioning kit was used to extract the appropriate components of the cell for analysis (see experimental section 4.6.6 for full details). In brief, the sample undergoes a centrifugation step

with an appropriate lysing agent to separate out the cytosol from the nucleus, which is subsequently re-suspended and decanted for digestion. However, it was noted at this point during the fractionation that the cellular pellet did re-suspend, but the nanoparticle pellet did not. Accordingly, it is highly likely that the Pt centre measurements for the nanoparticle samples of the cytosol are only representative of free Pt and not nanoparticlely bound Pt, which may have been removed with a proportion of the nanoparticles. Thus, a large proportion of the Pt present is not recorded. This theory is also supported by the inconsistency between the combination of nuclear and cytosolic quantities not correlating approximately to whole cell quantities.

The data of Figure 424 displays a similar trend to the cytosolic data, with GNP-Fol-Pt(IV) displaying more nuclear Pt centres than the GNP-Cit-Pt(IV) system, but free Pt(IV)LipA displaying increased Pt than all other samples. The nanoparticle anomaly of the cytosolic Pt does not apply for this metric, as it would only ever be free Pt that is found within the nucleus. This statistic is therefore in contradiction to the quantitative antibody studies as per the FACS data herein, which suggests that free Pt(IV)LipA leads to less DNA damage than nanoparticle bound Pt(IV)LipA. It is therefore hypothesised that whilst the free Pt(IV)LipA system delivers more Pt to the nuclei of the cells, the nanoparticle systems still present with greater DNA damage as a result of their method of delivery. More particularly, it is assumed that the free Pt(IV)LipA complex is modified and digested by the cell, altering its structure and reducing its toxicity or method of interaction with the DNA. In comparison, the nanoparticle systems obviate these modifications and deliver the intended structure of the Pt(IV)LipA complex. Therefore, less Pt centres are delivered, but more Pt is delivered as the Pt(IV)LipA complex, thus leading to increased levels of DNA damage. This theory of course needs significant

experimental follow up in order to ascertain the structures that reach the nuclei of the cells, as well as repeats of the studies reported herein so as to enable statistical analysis of the data.

4.6. Conclusions

A novel Pt(IV) complex was synthesised and it's potential as an anti-cancer agent investigated. The Pt(IV)LipA complex comprises a lipoic acid ligand and therefore features the ability to surface functionalise gold nanoparticle systems. Accordingly, the cytotoxicity of the novel Pt(IV) agent was investigated as free agent and when loaded onto folate capped and citrate capped gold nanoparticle systems. The levels of cisplatin-DNA adducts formed for the Pt(IV) agent (both as a free agent and as part of nanoparticle systems) were also compared to those formed for cisplatin in a dosing routine for cisplatin resistant A549 cells.

MTT assays have identified that the Pt(IV)LipA complex presents with a greater cytotoxicity than cisplatin, both as a free agent and when loaded onto nanoparticles. The most potent form is when the agent is loaded onto folate capped gold nanoparticles, likely as a result of high levels of folate receptor mediated endocytosis. This latter point was proven through folate receptor positive and negative studies, via media manipulation and utilisation of folate receptor α blocking. DNA adduct formation was measured via immunocytochemistry, using a commercial antibody labelled with an alexa fluor 488 dye. The GNP-Fol-Pt(IV)LipA system displayed greater levels of uptake (ICPMS data) and levels of DNA-adduct formation (fluorescence in confocal microscopy and flow cytometry studies) over the GNP-Cit-Pt(IV)LipA system and cisplatin free agent. Greatest levels of damage and uptake were afforded to the GNP-Fol-Pt(IV)LipA system in the unblocked folate receptor positive A549 cells, which is likely indicative ofelevated levels of uptake by way of folate receptor mediated endocytosis.

4.7. Experimental

4.7.1. Synthesis

Compound 401: cis,cis,trans[$PtCl_2(NH_3)_2(OH)_2(CH_3CONH)$]

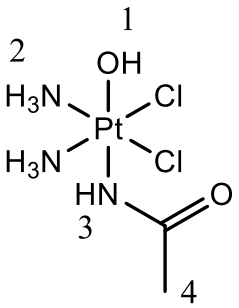

Compound 401 was prepared as per the synthetic procedure of Pelosi *et al.*[1].

A mixture of acetonitrile (10 mL) and of 30% hydrogen peroxide (1.666 mL) was stirred for 30 min at 25°C. Cisplatin (0.33 mmol, 100 mg) was added to this mixture and the resulting suspension was stirred for 5 min. Methanol (5 mL) was then added and the reaction mixture was stirred at room temperature for 24 h. The resulting pale yellow precipitate was separated by centrifugation (6000rpm, 30 minutes) and was washed with diethyl ether. Yield: 85% (106 mg). Characterisation agrees with that of the literature. δ_H (300 MHz; $CDCl_3$); 1.89 (1H, s, H-4), 5.02 (2H, m, H-3,1), 3.81-6.25 (6H, m, N*H*$_3$). m/z (ES); $[M\text{-}H_2O]^+$ 358, $[M+2Na\text{-}3H]^+$ 418.

Compound 402: cis,cis,trans[$PtCl_2(NH_3)_2(HOOC(CH_2)_2COO)(CH_3CONH)$]

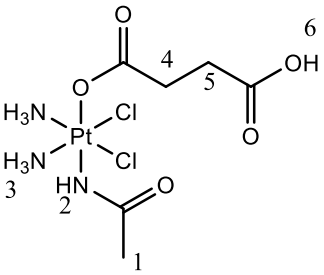

Compound 402 was prepared as per the synthetic procedure of Pelosi *et al.*[1].

cis,cis,trans[$PtCl_2(NH_3)_2(OH)_2(CH_3CONH)$] (0.11 mmol, 40 mg) was suspended in DMF (4mL) at 50°C. After 5 min succinic anhydride (1.07 mmol, 107 mg) was added. The reaction

mixture was stirred at 50°C until complete dissolution of the suspended solid (about 3 h). The solution was then allowed to cool, the solvent removed under reduced pressure and the residue triturated with diethyl ether. Yield: 38mg, (73%). Characterisation agrees with that of the literature. δ_H (300 MHz; $CDCl_3$); 1.96 (3H, s, H-1), 2.38-2.48 (2H, m, H-5), 2.49-2.58 (2H, m, H-4), 5.15 (1H, s, N*H*), 6.30-6.62 (6H, m, NH_3). m/z (ES); $[M-H]^-$ 473,474,476 (Isotope splitting pattern).

Compound 403: ***c,c,t*-[$Pt(NH_3)_2(Cl)_2(OH)_2$]**

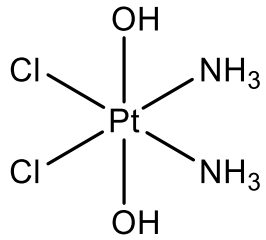

Various methods were attempted for the synthesis of compound 403, however the most successful was that of Huan Liu *et al.*[15] with modifications.

cis-$Pt(NH_3)_2Cl_2$ (40 mg, 0.13 mmol) and H_2O_2 (30% wt/vol, 1.5 mL, 50.0 mmol) were dissolved in H_2O (2 mL) and heated at 70°C, under nitrogen, with vigorous stirring for 5 h in the dark. After allowing the solution to cool to room temperature gradually, the solution was left in the fridge overnight to precipitate the insoluble product, c,c,t-$Pt(NH_3)_2Cl_2(OH)_2$ (40mg, 92%) which was obtained from filtration. Characterisation agrees with that of the literature. δ_H (300 MHz; $CDCl_3$); Solubility prevents clear characterisation (also noted in literature). m/z (ES); $[M+H]^+$ 335.

Compound 404: Lipoic Anhydride

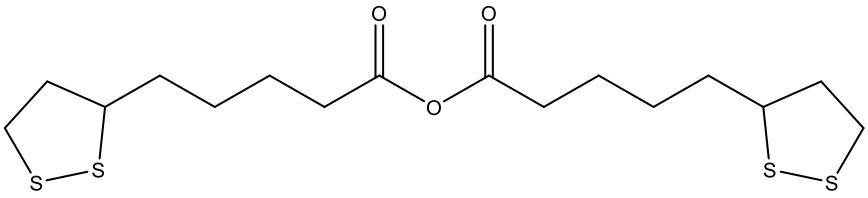

Lipoic anhydride was prepared as per the synthetic procedure of Andrzej Sadownik, James Stefely and Steven L. Regen[16]. Characterisation agrees with that of the literature.

A solution of α-lipoic acid (0.1g, 0.5mmol) and dicyclohexylcarbodiimide (0.065g, 0.3mmol) was stirred in 2 mL of dry DCM for 24 hours at room temperature under a nitrogen atmosphere. The product mixture was filtered in order to remove the urea which had formed. No yield determined as the product is an anhydride and should not be isolated. IR; 1735, 1805 (Anhydride) and lack of 1701 (Acid). m/z (ES); $[M+Na]^+$ 417.

Compound 405: *c,c,t*-$[Pt(NH_3)_2(Cl)_2(O_2C(CH_2)_4C_3H_5S_2)_2]$

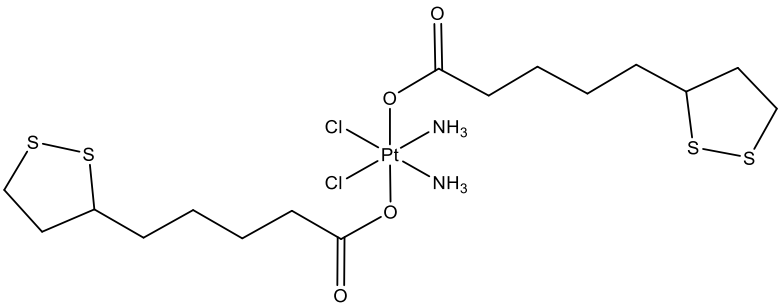

Compound 405 was prepared via a modification to a method outlined by Dhar *et al.*[2].

c,c,t-$[Pt(NH_3)_2Cl_2(OH)_2]$ (5mg, $1.5x10^{-5}$mol) in DMSO (2 mL) was heated to 50°C for 10 minutes until all suspended material was in solution. Lipoic Anhydride (135µL of a 0.0525gmL^{-1} solution, $1.8x10^{-5}$mol) was then added and the reaction mixture was stirred at 50°C under N_2 for 24 hours. Upon cooling to room temperature, the reaction mixture was centrifuged at 6000rpm for 30 minutes to pellet the insoluble product. The product was collected by suction filtration and washed with acetonitrile.

c,c,t-[$Pt(NH_3)_2(Cl)_2(O_2C(CH_2)_4C_3H_5S_2)_2$] was yielded as a pale yellow crystalline powder (0.5mg, 5%). δ_H (300 MHz; $CDCl_3$); No data available (solubility issues). m/z (ES); $[M+Na]^+$ 733.

Compound 406: cis,cis,trans[$PtCl_2(NH_3)_2(HOOC(CH_2)_4C_3H_5S_2)(CH_3CONH)$]

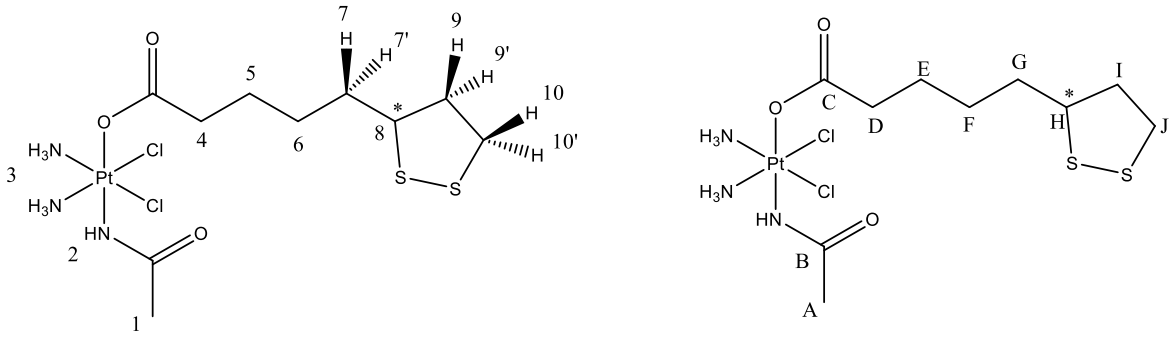

Pt(IV)LipA was prepared via a modification to a method outlined by Pelosi *et al.*[1].

cis,cis,trans[$PtCl_2(NH_3)_2(OH)_2(CH_3CONH)$] (0.12mmol, 45 mg) was suspended in DMF (1.5mL) at 50°C. After 5 min Lipoic anhydride (~4 mmol) was added. The reaction mixture was stirred at 50°C for 72 hours. The solution was then allowed to cool, the solvent removed under reduced pressure and the residue triturated with diethyl ether. Yield: 46mg, (70%).

δ_H (400 MHz; $CDCl_3$); 1.43 (2H, m, H-6), 1.55 (2H, m, H-5), 1.59 (1H, m, H-7'), 1.70 (1H, m, H-7), 1.92 (1H, m, H-9'), 1.99 (3H, s, H-1), 2.23 (2H, m, H-4), 2.48 (1H, m, H-9), 3.16 (1H, m, H-10'), 3.19 (1H, m, H10), 3.61 (1H, m, H-8), 5.32 (1H, s, N*H*), 6.33-6.80 (6H, m, NH_3). δ_c (100 MHz; $CDCl_3$); 24.5 (a), 25.7 (e), 28.8 (f), 34.7 (g), 36.7 (d), 38.3 (j), 40.2 (i), 56.7 (h), 176.4 (b) and 181.6 (c). m/z (ES); $[M-H]^+$ 563,564,566 (Isotope splitting pattern).

4.7.2. Reduction Capabilities – CD Spectroscopy

CD Spectroscopy was utilised to ascertain the DNA binding capabilities of Pt(IV)LipA, employing a protocol adapted from Dr Lois Bright (former PhD member of the Hannon group).

Calf-thymus DNA (ct-DNA) was purchased from Sigma Aldrich. DNA stock solutions were made up in ultrapure water (18.2 MΩ). CD spectra were obtained for the solutions utilising a quartz cuvette with a 1 cm path-length. A 98μM solution of CT DNA in NaCl (20mM), Na cacodylate and Milli Q water (to 1mL) was employed. 145μL of a 300μM solution of either Pt(IV)LipA or cisplatin was added and the solution gently agitated for 10 minutes. The CD spectrum was subsequently recorded. Following this addition, Ascorbic Acid (20μL, 1mM) was added to the Pt(IV)LipA sample and the solution gently agitated for a further 10 minutes. Alterations to the fingerprint region of CT DNA are indicative of DNA binding.

4.7.3. Nanoparticle Loading Studies

The loading potential of Pt(IV)LipA onto the GNP-Fol and GNP-Cit systems was conducted as per the ruthenium probe titration experiments of section 2.3.2.

Fresh solutions of GNP-Fol and GNP-Cit were prepared as per section 2.3.2 and UV-Vis absorption spectra were collected for titration of a 1mg/mL Pt(IV)LipA stock solution into 1mL of either 1nM GNP-Fol or 1mL of 1nM GNP-Cit. Titration volumes of Pt(IV)LipA were varied to give incremental increases in μg Pt(IV) added as opposed to traditional mmol added. Each system was dialysed overnight in a semi permeable membrane (Spectra-Por® Float-A-Lyzer® G2, 5 mL, MWCO 8-10 kDa) in deionised water to remove unreacted reagents. The systems then had their concentrations roughly calculated via UV-Vis and the stronger system diluted to the same concentration as the weaker system (~1nM) before being carried forward for cellular studies.

4.7.4. MTT Assays

MTT assays were conducted utilising an adapted protocol from Dr Lucia Cardo and Dr Lois Bright.

High folate receptor α expressing A549 cells were seeded into 96 well plates (8000 cells per well in 200µL supplemented RPMI media) and allowed to adhere overnight. 12 sample wells were allocated to each condition. Fresh 1mg/mL stock solutions of Pt(IV)LipA (in 90:10 ethanol and DMSO) and cisplatin (in water) were prepared, along with fresh solutions of GNP-Fol, GNP-Cit and GNP-Fol-Pt(IV) and GNP-Cit-Pt(IV). Pt loaded nanoparticle systems were prepared as 12.5, 25 and 50µM Pt solutions in 100µL of ~1nM GNPs. Old media was removed from the 96 well plates using a multi-channel pipette and each well was washed with PBS (100µL) to remove dead cells and residual media. The wells were subsequently treated as per the below figures for 24 hours, with solution made up to 200µL in fresh RPMI media.

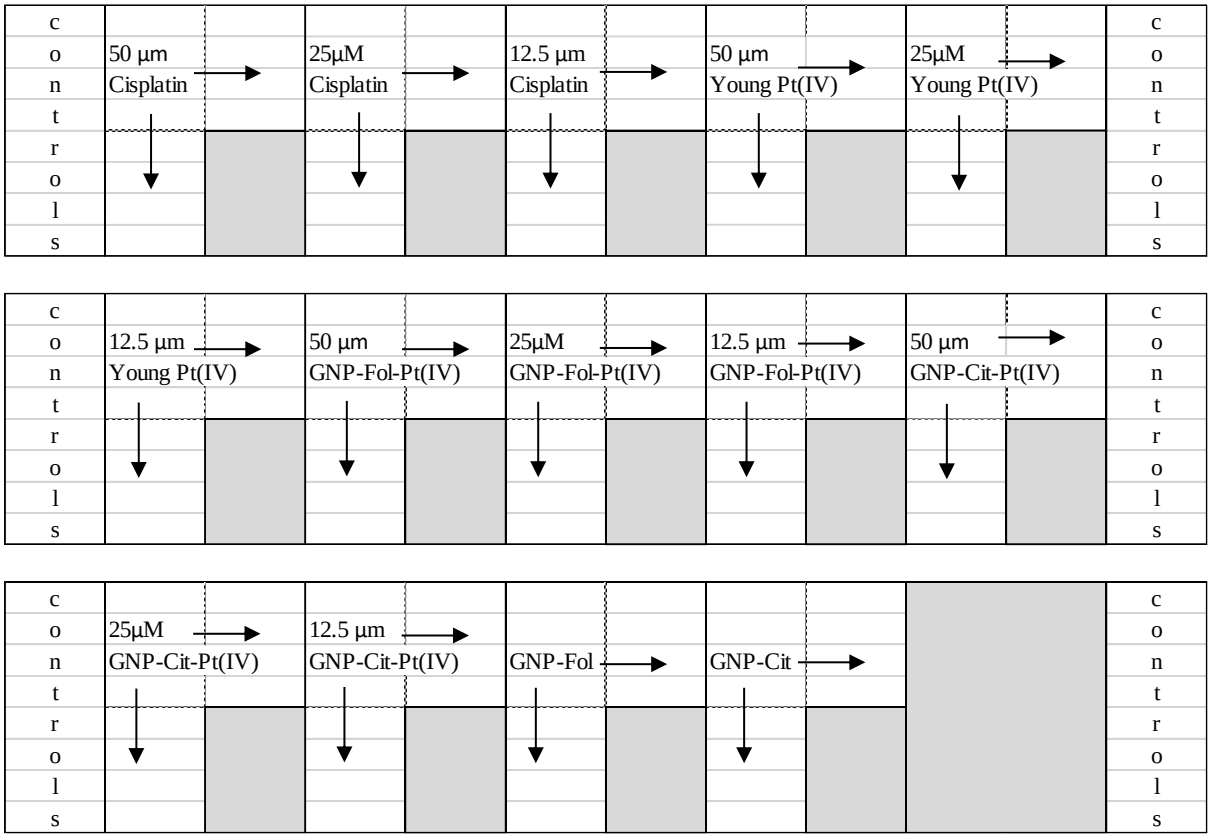

20µL of a 5 mg/mL MTT solution in PBS was added to each well, excluding one set of control wells, and incubated for two hours. The medium was carefully removed by aspiration from all wells and 200µL DMSO was subsequently added per well to dissolve the purple formazan. The

plates were incubated for a further 20 minutes before the absorbance was measured at 590 nm using a microplate reader (BioRad).

4.7.5. Fixed Cell Immunocytochemistry

Cell Culture

High folate receptor α expressing A549s were cultured and maintained as per section 3.8.5.

Nanoparticle Preparation

Fresh batches of GNP-Fol and GNP-Cit were synthesised as per section 2.3.2 and were subsequently loaded with 25μM YoungPt(IV) (14μL of a 1mg/mL stock solution) and purified ready for cell culture experiments as per section 4.6.3.

Dosing Protocol

Cover slips were washed in 70% ethanol and rinsed with PBS before being stuck to the bottom of each well of 12 well plates. These dishes were allowed to dry for 1 hour before being seeded with high folate receptor α expressing A549s (400,000 cells per well) and incubated overnight to adhere. These coverslip samples were utilised for confocal microscopy studies, plain 6 well plates were utilised for flow cytometry studies.

The following samples were prepared:

HIGH FOLATE RECEPTOR α EXPRESSING A549S DOSED WITH:	
No Blocking	**With Receptor α Blocking**
Blank	-

Secondary Antibody Only	-
Pri + Sec Antibodies (AB)	-
Cisplatin + AB	-
Pt(IV)LipA + AB	-
GNP-Fol-Pt(IV) + AB	GNP-Fol-Pt(IV) + AB
GNP-Cit-Pt(IV) + AB	GNP-Cit-Pt(IV) + AB

Fixed Cell Confocal Immunocytochemical Studies

The fixation and mounting of samples was conducted via an adapted protocol provided by Dr Lucia Cardo on 29th March 2017.

The 12 well plates were removed from the incubator and the old media aspirated from the wells. The wells were washed with PBS (1mL) to remove dead cells and residual media. Each well was then treated with either 500µL of ~1nM GNP-Fol / Cit loaded with 25µM Pt(IV)LipA, 25µM Pt(IV)LipA alone or 25µM cisplatin alone, each of which made up to 1mL in fresh supplemented RPMI media. The folate receptor blocking samples were previously blocked for one hour with folate receptor α primary antibody as per section 3.8.7. The samples were subsequently returned to the incubator and incubated on a plate rocker for 18 hours. The plates were then removed, old media gently removed and the cells gently washed with PBS (2 x 1mL) to remove unbound reagents and free nanoparticles. The cells were subsequently fixed in formalin (500µL, 10% solution) for 10 minutes at room temperature. Formalin was removed and the cells washed with PBS (3 x 1mL), before being permeabilised with 0.1% Triton X-100 (0.5mL) for 10 minutes at room temperature. Triton was removed and the cells washed with PBS (3 x 1mL), before being blocked with 10% normal goat serum (0.5mL) at room temperature for 1 hour. Goat serum was removed and the cells were dosed with anti-cispltin

modified antibody (CP9/19) at room temperature for two hours (500µL of a 2µg/mL solution in 10% normal goat serum). The primary antibody was removed and the coverslips washed with 1% goat serum (5 x 1mL). Cells were then dosed with secondary antibody (500µL of a 2µg/mL solution in 10% goat serum) for 1 hour at room temperature in the dark. Cells were rinsed with 1% goat serum (5 x 1mL) and the nuclei stained with Hoechst (500µL of a 5µg/mL solution in 1% goat serum) for 10 minutes at room temperature. The coverslips were washed with 1% goat serum (1mL x 5), then dipped in PBS before being mounted onto microscope slides with a drop of mounting medium.

Fixed Cell Flow Cytometry Studies

The utilised fixed cell FACS protocol was adapted from the published protocol of Cell Signaling Technology[17].

Cells were dosed with the appropriate samples as per the above confocal studies. The 6 well plates were then removed from the incubator, old media removed and the cells washed with PBS (1mL). The cells were then tripsinised (1mL tripsin 1X for 5 mins in an incubator) and collected with fresh RPMI media (1mL), cells were collected into 2mL Eppendorf's. The cells were pelleted at 1500rpm for 5 mins and the supernatant discarded. The cells were then re-suspended in 1mL 10% formalin, vortexed and fixed at 37°C for 10 minutes. The samples were chilled on ice for 1 minute, then centrifuged at 1500rpm for 5 minutes to remove formalin. The pellets were re-suspended in 1mL of 90% ice cold methanol and kept on ice for 30 minutes to permeabilise them. 1mL incubation buffer (0.5g Bovine Serum Albumin (BSA) in 100mL PBS) was added and the cells centrifuged. The supernatant was removed and the cells re-suspended in 1mL incubation buffer. This step was repeated three times. The cells were re-suspended in primary antibody (500µL of a 2µg/mL solution in incubation buffer) and dosed for one hour at room temperature. The cells were centrifuged, the supernatant removed and the

pellets re-suspended in incubation buffer (1mL). This step was repeated three times. The cells were re-suspended in secondary antibody (500µL of a 2µg/mL solution in incubation buffer) for 30 minutes at room temperature in the dark. The cells were centrifuged, supernatant removed and re-suspended in incubation buffer (1mL). This step was repeated three times. The cells were then centrifuged, supernatant removed and re-suspended in 1mL PBS. The samples were then analysed by flow cytometry.

Confocal Microscope Settings

Blue Channel:	Excitation, 402nm	Emission, 450-490
Green Channel:	Excitation, 514nm	Emission, 500-570nm
Red Channel:	Excitation, 488nm	Emission, 580-680nm

4.7.6. ICPMS Studies

The digestion stage of the below ICPMS protocol was adapted from protocols provided by Dr Lucia Cardo (Hannon research group, University of Birmingham) and Ms Siobhan King (Pikramenou research group, University of Birmingham), along with the recommended cell culture stage. No replicates were investigated in the present studies.

Cell Culture

High folate receptor alpha expressing A549 cells were seeded into seven T75 flasks (one flask per condition as per the below table) and cultured to 80% confluency as per section 3.8.5.

Dosing

The T75 flasks were dosed using the same protocol of 4.6.5, but with appropriately scaled reagents (approximately 7 x more cells present, therefore 7 x more nanoparticles / platinum agents used, maintaining 25μM final concentration) and alternative sample work up.

HIGH FOLATE RECEPTOR α EXPRESSING A549S DOSED WITH:			
No Blocking		**With Receptor α Blocking**	
a)	Blank		-
b)	Cisplatin		-
c)	Pt(IV)LipA		-
d)	GNP-Fol-Pt(IV)	f)	GNP-Fol-Pt(IV)
e)	GNP-Cit-Pt(IV)	g)	GNP-Cit-Pt(IV)

Sample Work Up

Old media / media containing the reagents of the above table was removed from the T75 flasks and the cells gently washed with PBS (5mL x 3) to remove unbound reagents / particles and residual media. The cells were tripsinised and pelleted as per section 3.8.5. The cells were then re-suspended in 2mL of PBS and counted using a haemocytometer. 1mL of each sample was pipetted into fresh 2mL falcon tubes, pelleted at 1500rpm for 5 minutes and supernatant removed. The whole cell pellet samples were immediately stored at -80°C ready for whole cell ICPMS analysis.

Subsequent nuclear and cytosolic fractionation was conducted as per the protocol supplied with the BioVision Nuclear/Cytosol Fractionation Kit utilised.

The remaining 1mL of suspended cells were chilled on ice for 1 minute and subsequently centrifuged at 4°C for 5 minutes at 600G. The PBS was removed and 0.2mL of Cytosol

Extraction Buffer A was added. The solutions were vortexed on the highest setting for 15 seconds and were incubated on ice for 10 minutes. 11µL of ice cold Cytosol Extraction Buffer B was added and the solution vortexed for 5 seconds. The solutions were then centrifuged at 4°C for 5 minutes at 16000G. The supernatant (cytoplasm fraction) was removed and immediately stored at -80°C ready for cytosolic ICPMS analysis.

The remaining pellet was re-suspended in 100µL ice cold Nuclear Extraction Buffer mix and vortexed on the maximum setting for 15 seconds. The samples were stored on ice for 10 minutes and this process was repeated four times. The samples were centrifuged at 16,000G, 4°C for 10 minutes. The supernatant (nuclear fraction) was transferred to a fresh Eppendorf and immediately stored at -80°C, ready for ICPMS analysis.

The resulting sample fractions (whole cell, nuclear and cytoplasm) were digested in a mixture of concentrated nitric acid (69%, 100µL) and freshly prepared aqua regia (3:1, HCl (32%) and HNO_3 (69%) 100 µL). Samples were transferred to screw cap vials and incubated overnight at 80 ºC in an oven to fully digest the metal particles and cells. Subsequently, the samples were diluted with milli-Q-water to a final acid concentration of ~2%. Samples were transferred to 15mL falcon tubes on ice and transported to the University of Warwick for sample analysis.

4.7. References

1 - Ravera M, Gabano E, Zanellato I, Fregonese F, Pelosi G, Platts JA and Osella D. Antiproliferative activity of a series of cisplatinbased Pt(IV)-acetylamido/carboxylato prodrugs. Dalton Transactions (2016), 45, 5300–5309.

2 - Dhar S, Gub FX, Langerb R, Farokhzadc OC and Lippard SJ. Targeted delivery of cisplatin to prostate cancer cells by aptamer functionalized Pt(IV) prodrug-PLGA–PEG nanoparticles. Proceedings of the National Academy of Sciences of the USA (2008), 105, 17356–17361.

3 - Johnson BW, Murray V and Temple MD. Characterisation of the DNA sequence specificity, cellular toxicity and cross-linking properties of novel bispyridine-based dinuclear platinum complexes. BMC Cancer (2016), 16:333, 1-17.

4 - Sarin N, Engel F, Kalayda GV, Mannewitz M, Cinatl Jr. J, Rothweiler F, Michaelis M, Saafan H, Ritter CA, Jaehde U, Frötschl R. Cisplatin resistance in non-small cell lung cancer cells is associated with an abrogation of cisplatin-induced G2/M cell cycle arrest. PLOS ONE (2017), 1-26.

5 - Wilson, JJ and Lippard SJ. Synthetic Methods for the Preparation of Platinum Anticancer Complexes. Chemical Reviews (2014), 114, 4470−4495.

6 - Hosios AM and Vander-Heiden MG. The Redox Requirements of Proliferating Mammalian Cells. The Journal of Biological Chemistry (2018), 293, 7490-7498.

7 - Wilson, W and Hay, M. Targeting hypoxia in cancer therapy. Nature Reviews Cancer (2011), 11, 393-410.

8 - Ranjbar B and Gill P. Circular Dichroism Techniques: Biomolecular and Nanostructural Analyses- A Review. Chemical Biology & Drug Design (2009); 74: 101–120.

9 - Chang YM, Chen CKM and Hou MH. Conformational Changes in DNA upon Ligand Binding Monitored by Circular Dichroism. International Journal of Molecular Sciences (2012), 13, 3394-3413.

10 - Kelland L. The resurgence of platinum based cancer chemotherapy. Nature Reviews (2007), 7, 573-583.

11 –Shi Y, Liu SA, Kerwood DJ, Goodisman J and Dabrowiak JC. Pt(IV) complexes as prodrugs for cisplatin. Journal of Inorganic Biochemistry (2012), 107, 6–14.

12 - Chatterjee S, Moriarty G and Gersten B. Surface Plasmon Spectral Shifts of Functionalized Gold Nanoparticles for the Use in Biosensors. Nano Science & Technology Institute-Nanotech (2006), 2, 436-439.

13 - Berridge MV, Herst PM, and Tan AS. Tetrazolium dyes as tools in cell biology: new insights into their cellular reduction. Biotechnology Annual Review (2005), 11, 127-152.

14 –Chacon E, Acosta D and Le Masters JJ. Primary Cultures of Cardiac Myocytes as In Vitro Models for Pharmacological and Toxicological Assessments. In Vitro Methods in Pharmaceutical Research (1997), 209-223.

15 - Liu H, Li Y, Lyu Z, Chen H, Chen H and Li X. Enzyme-triggered supramolecular self-assemblies of Pt prodrug for site-specific drug accumulation and Enhanced antitumor efficacy. Journal of Materials Chemistry (2014), 2, 47, 8303 – 8309.

16 - Sadownik A, Stefely J and Regen SL. Polymerized Liposomes Formed under Extremely Mild Conditions. Journal of the American Chemical Society (1986), 108, 7789-7791.

17 – “Flow Cytomoetry Protocol (flow)”, Cell Signaling Technology Ltd, accessed on 11th April 2017, https://www.cellsignal.co.uk/contents/resources-protocols/flow-cytometry-protocol-(flow)/flow.

Chapter 5 – Theranostic GNPs and Cellular Uptake

5.1. Theranostic GNPs

5.1.1. Theranostic GNP Concept

It was a final objective of the present research to prepare and investigate the use of theranostic gold nanoparticle systems within high folate receptor α expressing cell lines. Two theranostic systems were conceptualised, synthesised and utilised, comprising; GNP-Fol, RuPhen imaging probe and Pt(IV)LipA (hereafter GNP-Fol-Theranos); and GNP-Cit, RuPhen imaging probe and Pt(IV)LipA (hereafter GNP-Cit-Theranos). The "thera"-peutic aspect of these two systems stems from the incorporation of the Pt(IV)LipA complex whilst the diag-"nostic" aspect is fulfilled by incorporation of the ruthenium based RuPhen imaging probe. The general structure for these two theranostic systems is represented in Figure 501.

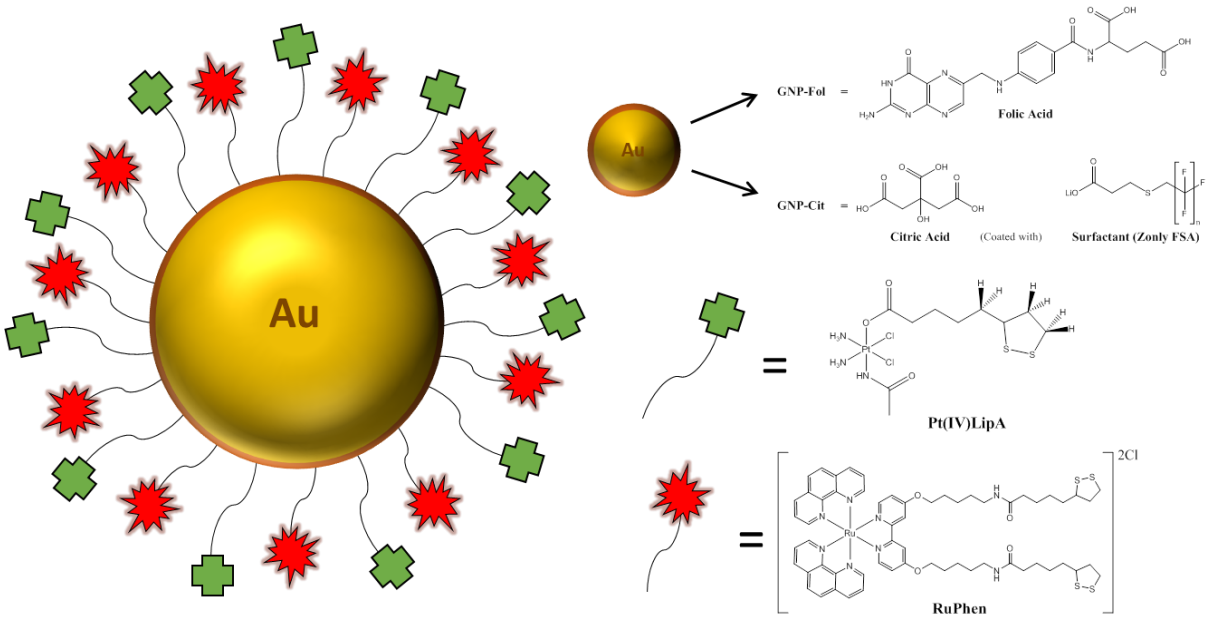

Figure 501: Representation of the general structure of the two theranostic GNP systems of the present research; GNP-Fol-Theranos and GNP-Cit-Theranos.

In principle, these particles should represent a class of cellular probes with active and passive targeting systems which facilitate fluorescence based cellular localisation studies in tandem

with cytotoxic activity studies. It was a continued objective of the present research to investigate the difference in cellular uptake of the folate capped GNP-Fol system in comparison to the citrate capped GNP-Cit system in high folate receptor α expressing A549s.

5.1.2. Theranostic GNP Loading Studies

Loading studies for the theranostic systems were conducted utilising the same protocol and reagent concentrations as employed in the prior RuPhen and Pt(IV)LipA loading studies (see experimental sections 2.2.2 and 4.4 respectively). In brief, 1mL each of ~1nM GNP-Fol and GNP-Cit were separately loaded with RuPhen (12µL of 1mM solution in titration increments of 4µL) and subsequently Pt(IV)LipA (28µL of a 1mg/mL solution in titration increments of 4µL) under constant stirring and with rounds of sonification post titration (5 minutes each titration). The collective UV-Vis data for these loading studies is represented across Figures 502 to 505. See experimental section 5.5.1 for full details.

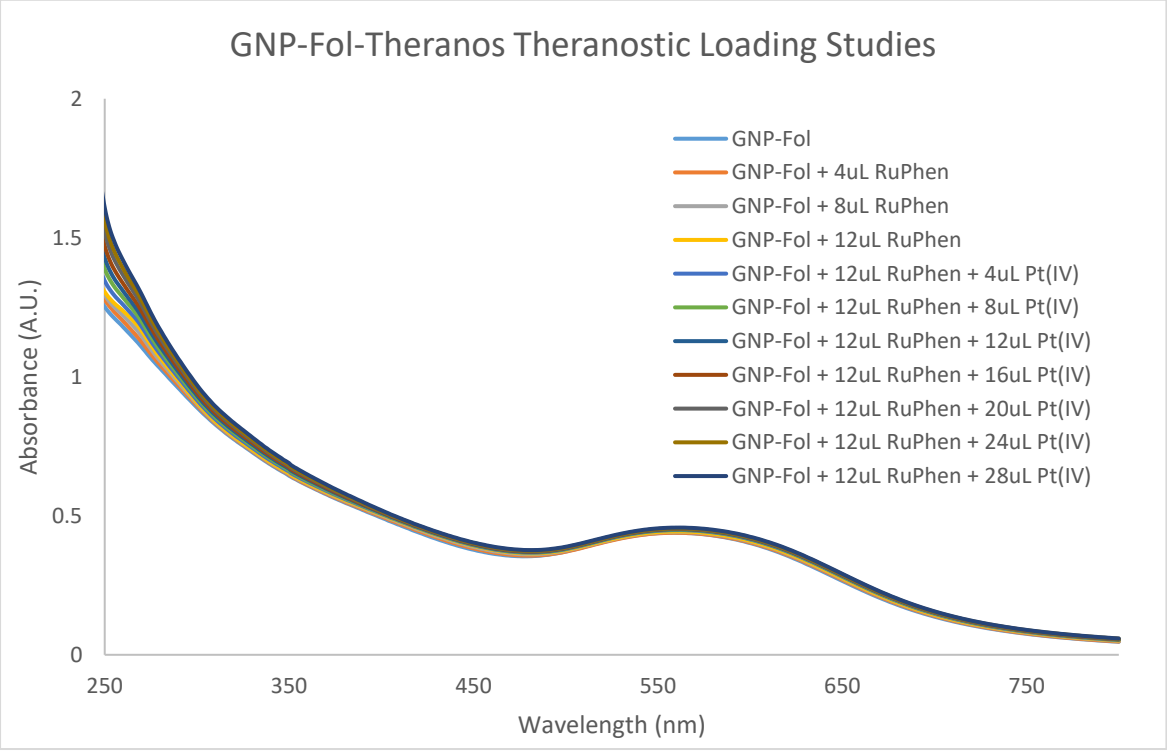

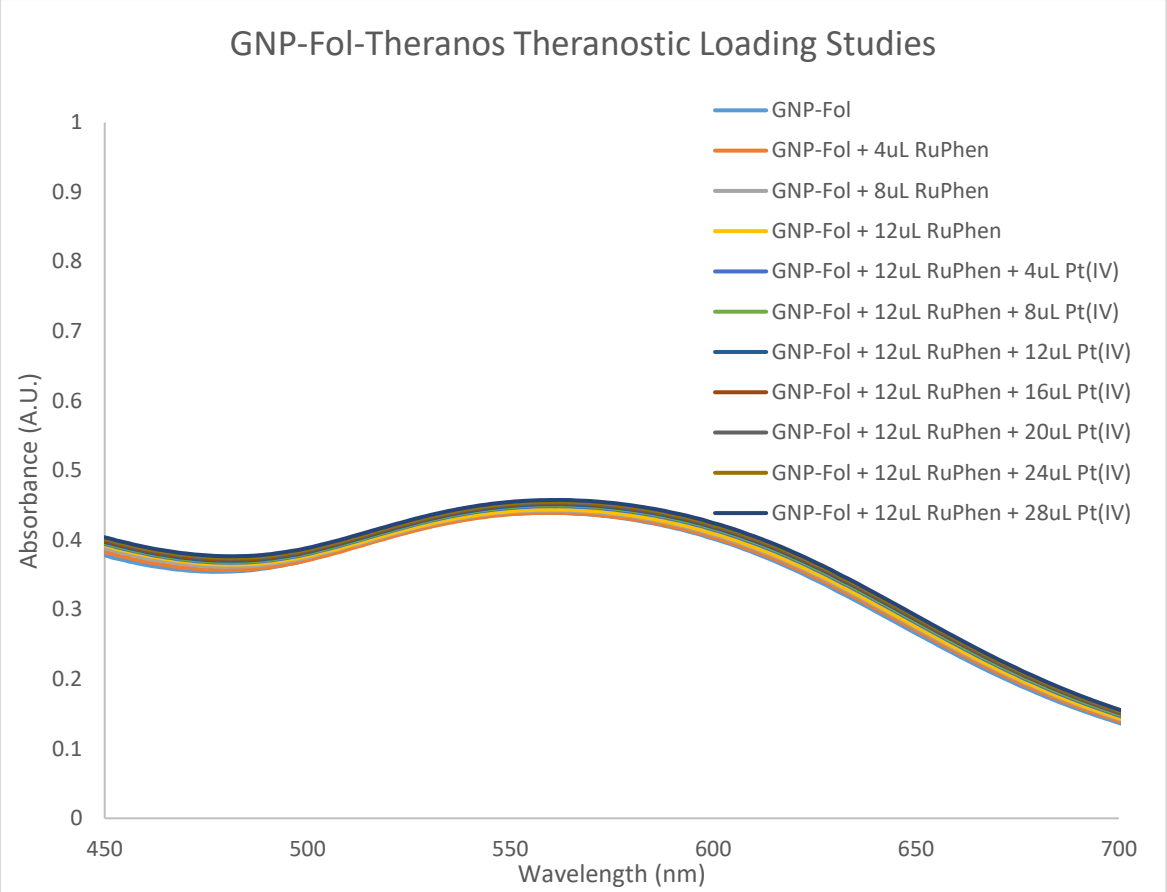

Figure 502: UV-Vis absorption spectrum data for titration of a 1mM RuPhen stock solution and a 1mg/mL Pt(IV)LipA stock solution into 1mL of 1nM GNP-Fol, affording GNP-Fol-Theranos. The RuPhen solution was titrated into the nanoparticle suspension prior to the Pt(IV)LipA solution. The SPR band λ_{max} shifted by 2nm from 559nm to 561nm and the SPR band also shifted and narrowed from 477-621nm to 481-621nm. Shifting and narrowing of the SPR band are also indicative of surface binding in the nanoparticle system.

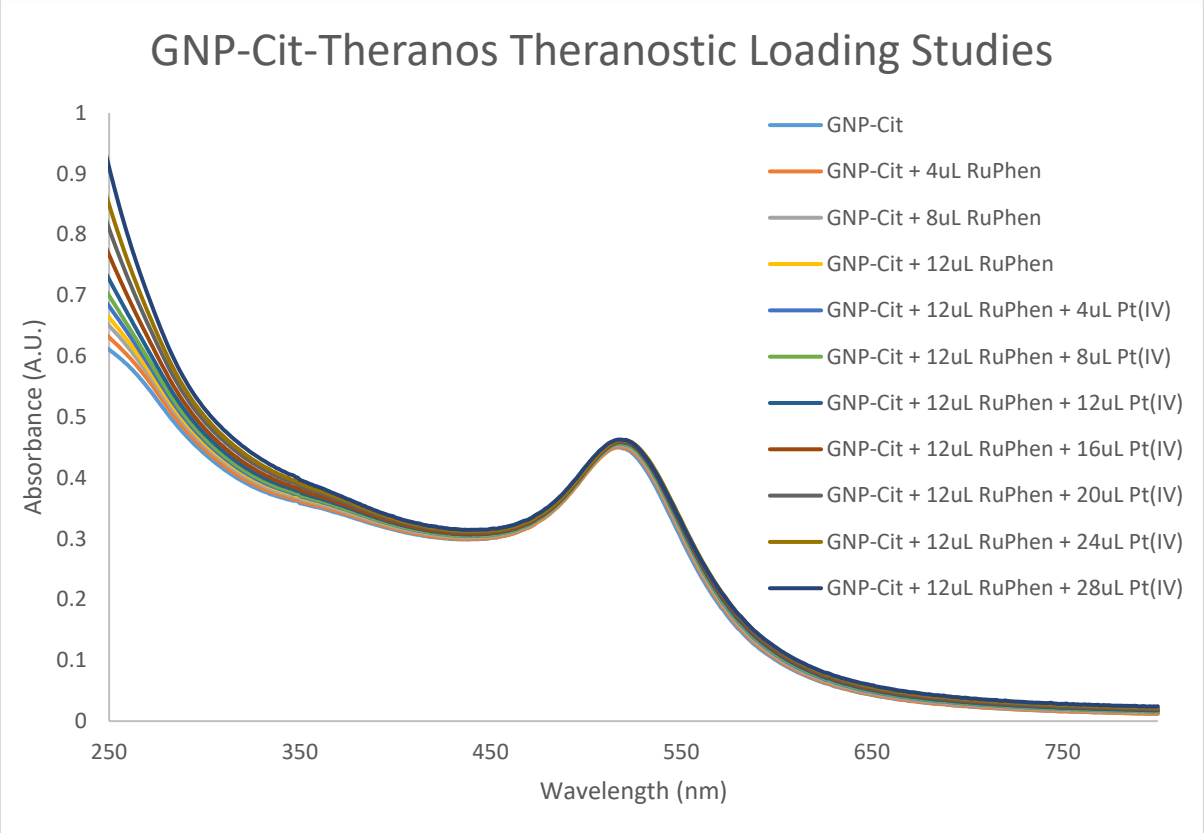

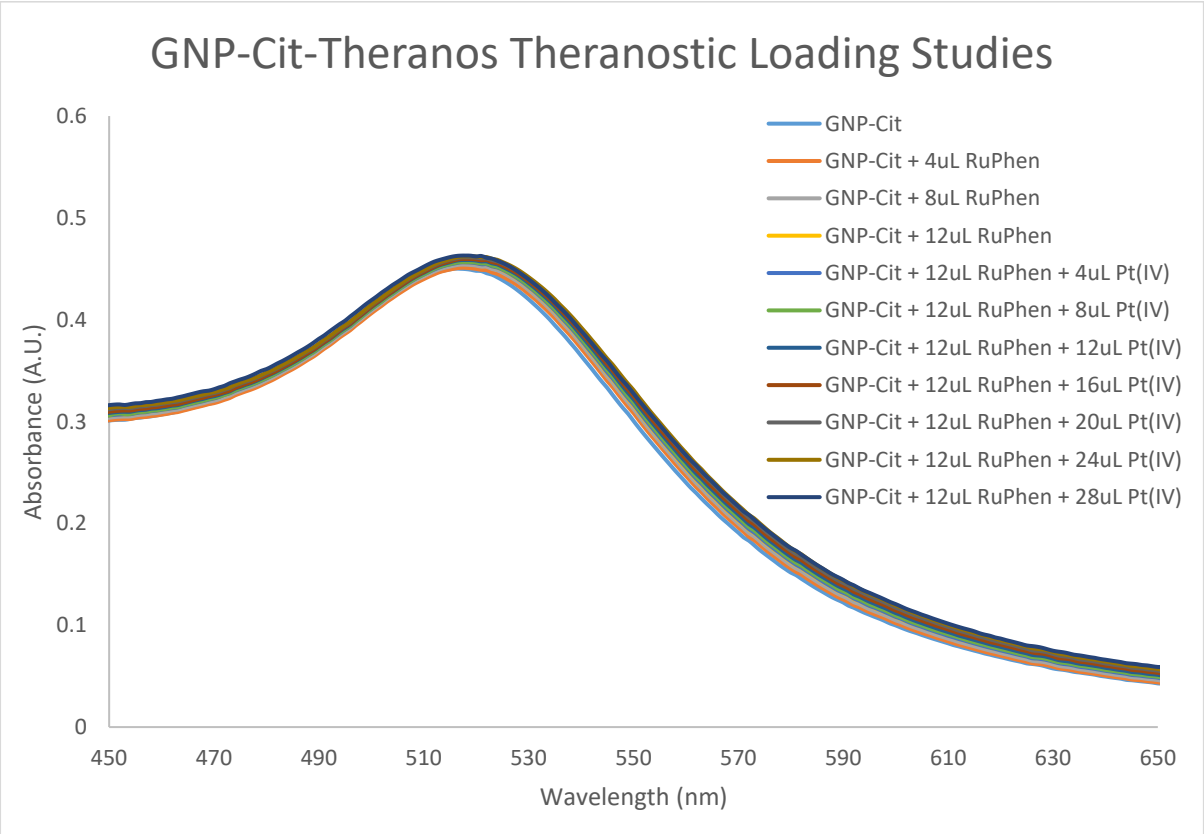

Figure 503: UV-Vis absorption spectrum data for titration of a 1mM RuPhen stock solution and a 1mg/mL Pt(IV)LipA stock solution into 1mL of 1nM GNP-Cit, affording GNP-Cit-

Theranos. The RuPhen solution was titrated into the nanoparticle suspension prior to the Pt(IV)LipA solution. The SPR band λ_{max} shifted by 2nm from 559nm to 561nm and the SPR band also shifted from 438-551nm to 439-552nm. Shifting of the SPR band is considered indicative of surface binding in the nanoparticle system.

The UV-Vis titration data of Figures 502 and 503 (GNP-Fol and GNP-Cit systems respectively) show similar effects of nanoparticle loading with RuPhen and Pt(IV)LipA solutions across the systems. In each system, the SPR band λ_{max} shifted by 2nm and the overall SPR band shifted upfield, which is typically representative of interaction of reagents with nanoparticle surfaces within the solutions. Unlike earlier loading studies, here the GNP-Fol system SPR band narrowed and the GNP-Cit system SPR band width was unchanged. These differences may be due to counteracting interactions of the two different reagents with the SPR band of the systems, but this shall require further research to ascertain.

The concentration and titration limit of the Pt(IV)LipA stock solution employed in these nanoparticle loading studies was selected to give a final concentration of 25µM Pt(IV)LipA within the respective system (GNP-Fol-Theranos and GNP-Cit-Theranos). 25µM of the Pt(IV)LipA complex was selected to theoretically give the greatest cellular damage signal within the subsequent immunocytochemical studies whilst not inducing significant cell death i.e. balancing induced signal with lost signal. The concentration and titration limit of the RuPhen stock solution was selected to give theranostic nanoparticle systems that would theoretically present sufficient fluorescence for cellular tracking and imaging studies whilst not overly straining the stability of the system (based on earlier results of section 3.6).

For continuity, the systems were dialysed for 24 hours in appropriately pH balanced deionised water (circa pH 9 for GNP-Fol and pH 7 for GNP-Cit) within microporous dialysis tubing to remove the majority of any unbound Pt(IV)LipA and RuPhen prior to investigating size and stability. Further research should be conducted following this stage of the particle preparation, using ICPMS to ascertain the quantities of the reagents which may now still be bounds to the particles. This data would also help to compliment the aforementioned surface loading studies conducted using UV-Vis spectroscopy.

The solutions were subsequently sonicated for 10 minutes and filtered through a cotton plug to remove precipitated material. It was not possible to record accurate particle sizing data via DLS studies due to some precipitation of the Pt(IV)LipA complex within the solutions. DLS sizing data for the GNP-Cit-Theranos system was particularly non-representative due to the surface surfactant Zonyl FSA, which is known within the Pikramenou group to cause sizing artefacts. Accordingly, the samples were sized by Transmission Electron Microscopy (TEM), these images are shown in Figures 504 and 505. These TEM samples were prepared as per section 5.5.2.

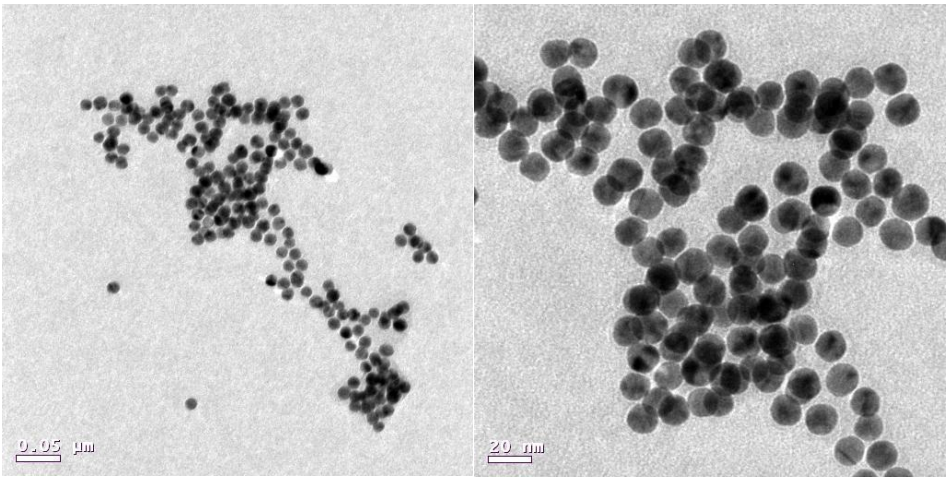

Figure 504: TEM images collected for the GNP-Fol-Theranos system later utilised for cellular studies. Size calculated as ~17nm ±2nm. Sample images recorded by Theresa Morris, Centre for Electron Microscopy, University of Birmingham.

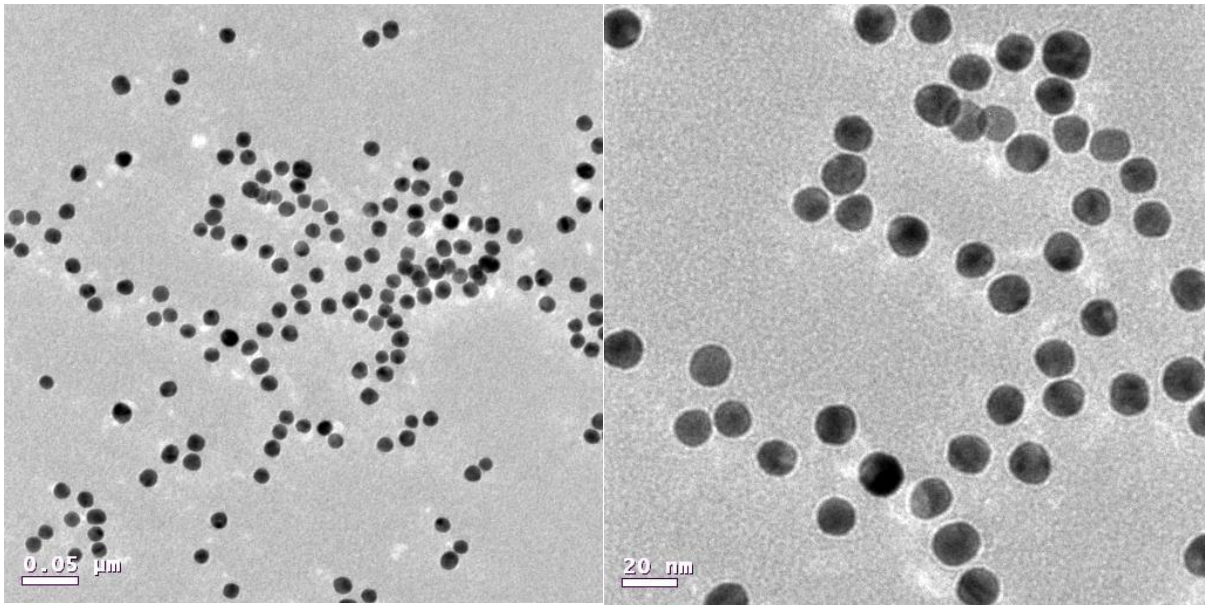

Figure 505: TEM images collected for the GNP-Cit-Theranos system later utilised for cellular studies. Size calculated as ~14nm ±2nm. Sample images recorded by Theresa Morris, Centre for Electron Microscopy, University of Birmingham.

The TEM images of Figures 504 and 505 show that the average size of the GNP-Fol-Theranos and GNP-Cit-Theranos systems were ~17nm ±2nm and ~14nm ±2nm respectively, which correlates with an approximately equal increase in size going from the respective original nanoparticle systems. It was also evident from the TEM images that the GNP-Fol-Theranos system appeared to show greater agglomeration of particles than the GNP-Cit-Theranos system, although this may be an artefact resulting from the TEM sample preparation.

After fresh formation of the above theranostic systems, the systems were qualitatively analysed for changes in stability over a 5 day period, observing changes in the colour of solution and presence of visible aggregates. It was noted that the systems displayed no visible change over four days, but on the fifth day the GNP-Fol-Theranos solution was starting to turn purple, which is considered to be an early indication of agglomeration / aggregation of the systems. These findings therefore suggest that the GNP-Fol-Theranos system is less stable than the GNP-Cit-

Theranos system and that said systems should be utilised within 1-2 days of formation. Accordingly, the theranostic systems were prepared as above and utilised within subsequent cellular studies within 12 hours of their formation to obviate complications associated with particle stability.

5.2. Fixed Cell Confocal Immunocytochemistry Studies

The therapeutic and tracking capabilities of the GNP-Fol-Theranos and GNP-Cit-Theranos systems were subsequently analysed by Immunocytochemical studies (qualitative analysis) and FACS analysis (quantitative). For continuity, the protocol employed for the immunocytochemical studies of the GNP-Fol-Pt(IV) and GNP-Cit-Pt(IV) systems was adapted and utilised (see experimental section 5.5.3).

In brief: high folate receptor α expressing A549 cells were seeded onto coverslips within 6 well plates and cultured for 24 hours; samples were then either incubated with appropriate solutions for 24 hours or had their media changed and incubated for a further 24 hours (as represented in Table 501) on a plate rocker; samples were subsequently washed, fixed and permeabilised, prior to staining with appropriate CP9/19 antibodies and Hoechst. As before, these immunocytochemistry studies were conducted on fixed cells that had been subsequently permeabilised to allow influx of the appropriate antibody.

The fixed cell confocal microscopy images for the samples of Table 501 are represented in Figures 506-511. Confocal images were collected as two separate z-stack profiles utilising the same z stack coordinates so as to ensure no bleed through of nuclear signal from the blue channel (Hoechst) into the green channel (DNA antibody). Accordingly, the brightfield, green (antibody signal, DNA adducts) and red (RuPhen signal, nanoparticle localisation) channels

were collected in one setting and the blue channel (Hoechst signal, nuclear stain) was collected in a separate setting, ensuring complete signal overlap and homogeneity across the z stack profile. The range of the z-stack profile was set using the brightfield channel, selecting the bottom and top of the cells within the focal field, ensuring collection of data across the entire cell. The blank and antibody only images were employed to calibrate the microscope to account for and obviate recording false-positive signal.

HIGH FOLATE RECEPTOR α EXPRESSING A549S DOSED WITH:	
No Blocking	**With Receptor α Blocking**
Blank (not shown)	-
Figure 506 - Secondary Antibody Only	-
Figure 507 – Pri + Sec Antibodies (AB)	-
Figure 508 - GNP-Fol-Theranos + AB	**Figure 510** - GNP-Fol-Theranos + AB
Figure 509 - GNP-Cit-Theranos + AB	**Figure 511** - GNP-Cit-Theranos + AB

Table 501: Overview of fixed cell confocal immunocytochemistry samples.

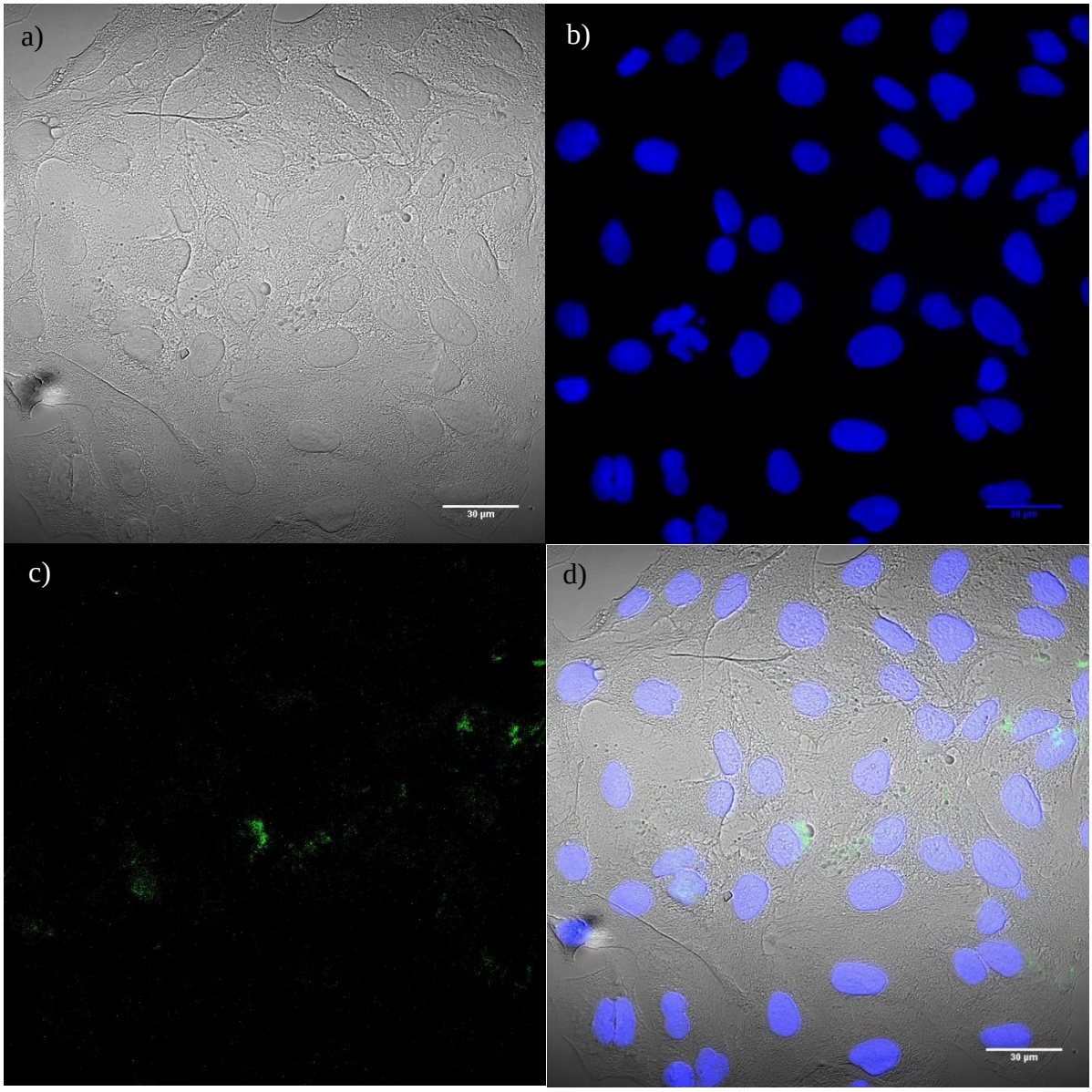

Figure 506: Fixed cell immunocytochemistry confocal studies of high folate receptor α expressing A549 cells that have been stained with the secondary antibody bearing Alexa-Fluor 488 only, illustrating false-positive fluorescence signal. A) in focus plane of the brightfield channel; B) average Hoechst signal across the Z stack; C) average DNA-damage antibody signal across the Z stack and D) overlay of all channels. No signal was observable within the red channel.

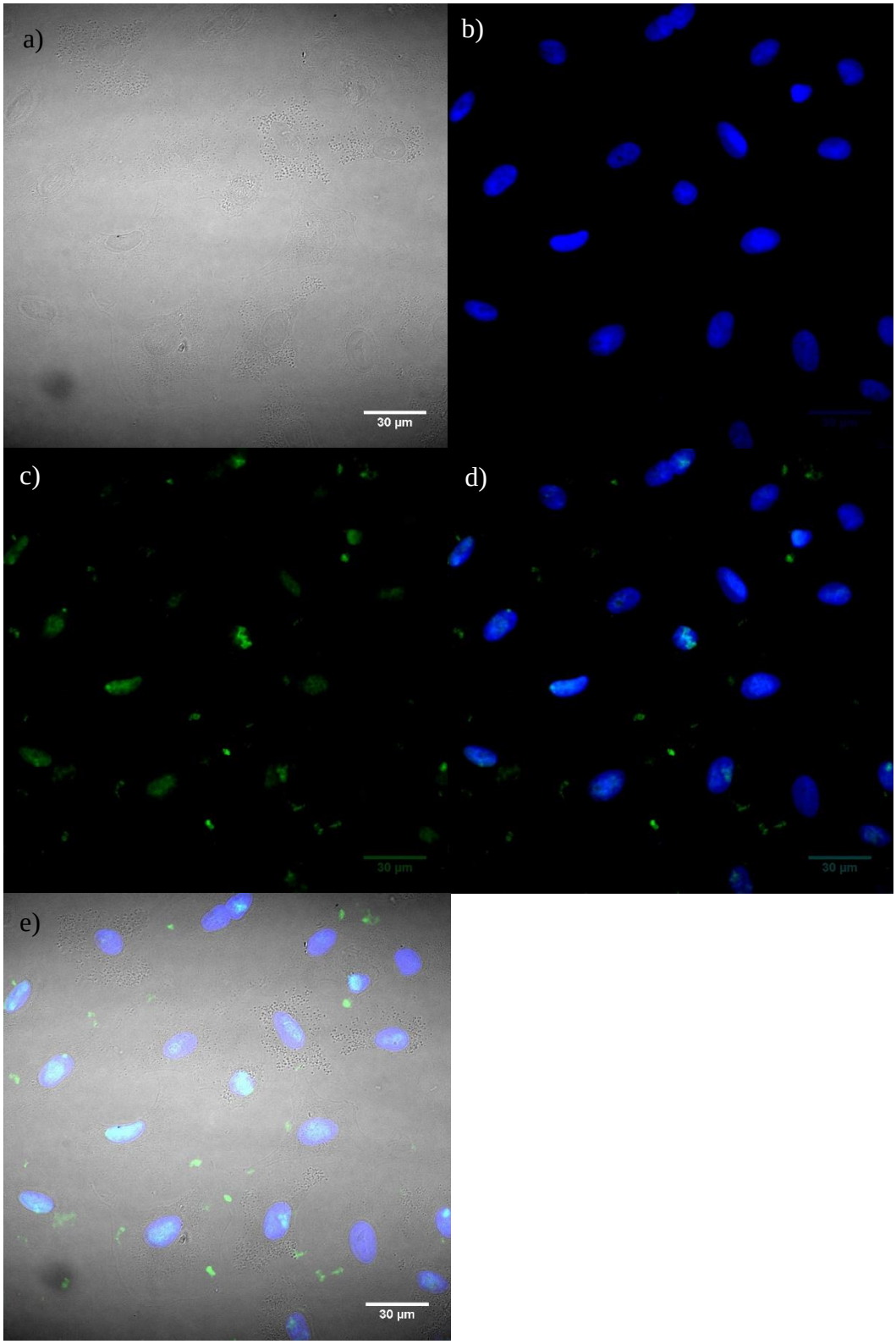

Figure 507: Immunocytochemical confocal studies of high folate receptor α expressing A549 cells that have been stained with primary and secondary antbodies, illustrating false-positive signal. A) in focus plane of brightfield channel; B) average Hoechst signal across Z stack; C) average DNA-damage antibody signal across Z stack, D) overlay of b and c and E) overlay of all channels. No signal was observable within the red channel.

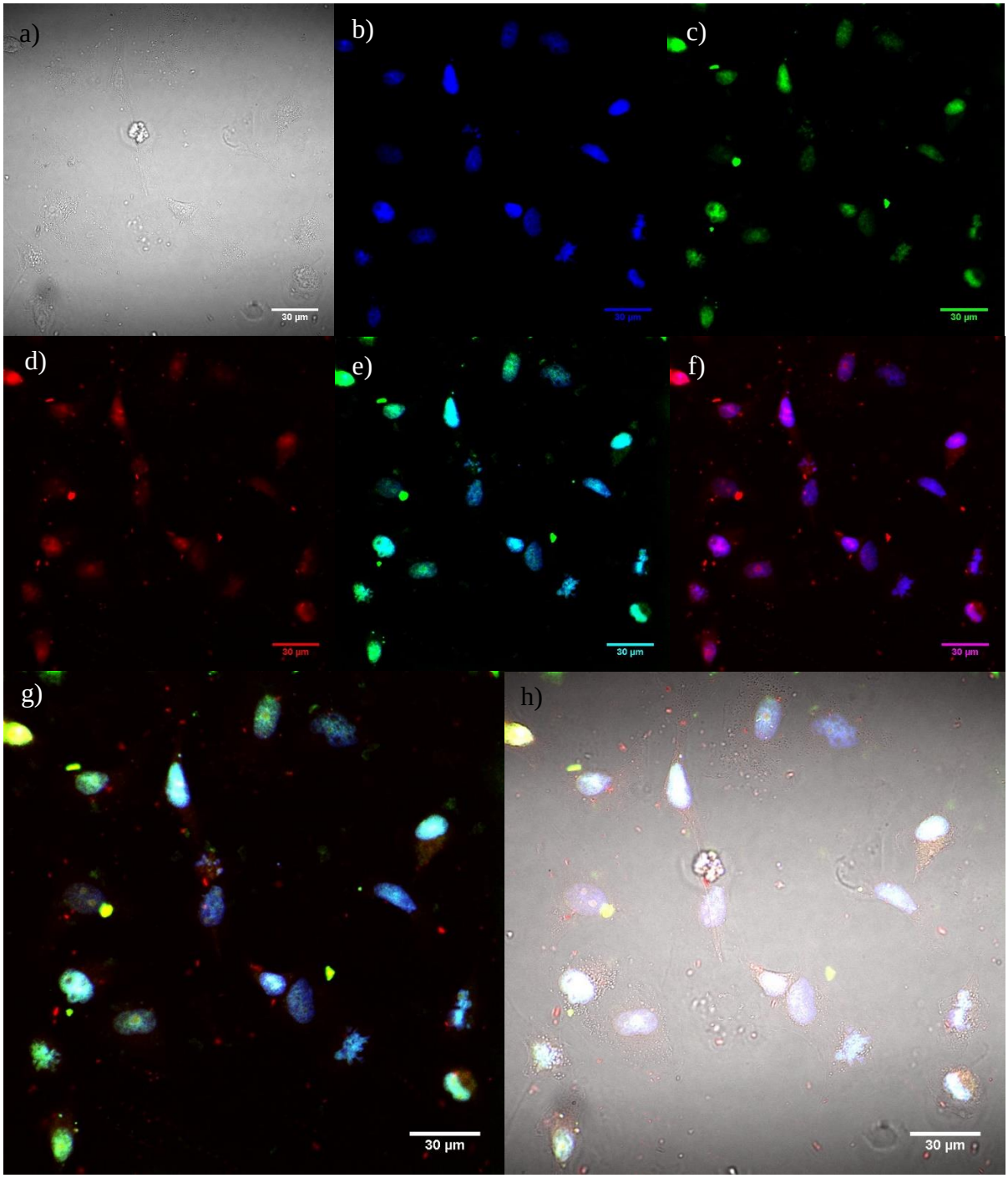

Figure 508: Immunocytochemistry confocal studies of high folate receptor α expressing A549 cells dosed with GNP-Fol-Theranos (1ml of ~1nM GNP-Fol loaded with 25µM Pt(IV)LipA and 12µL of 1mM RuPhen) for 24 hours and stained with CP9/19 / secondary antibody. A) in focus plane of brightfield channel; B) average Hoechst signal across Z stack; C) average DNA-damage signal across Z stack, D) average RuPhen signal across Z stack; E) overlay of b and c; F) overlay of b and d; G) overlay of b, c and d: H) overlay of all channels.

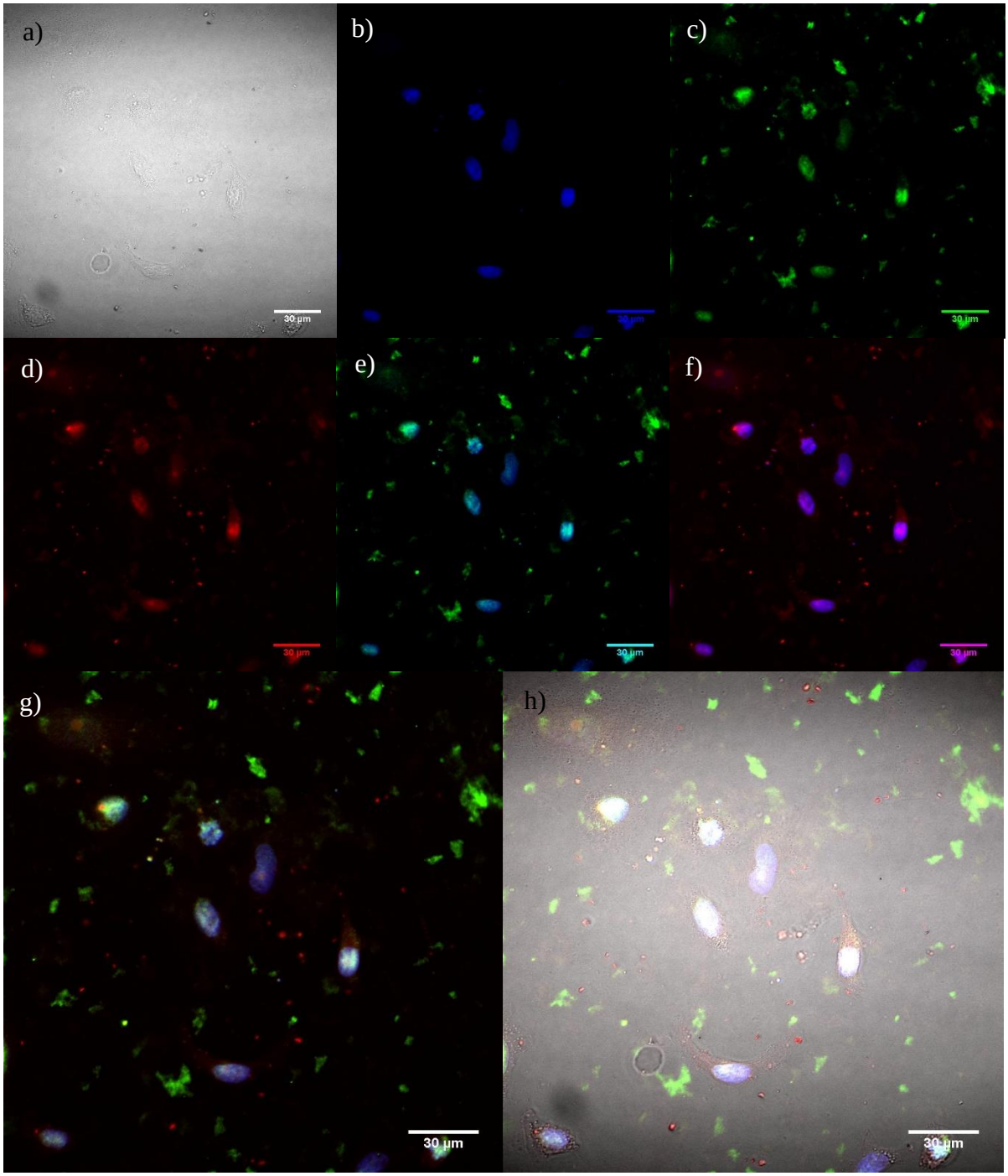

Figure 509: Immunocytochemistry confocal studies of high folate receptor α expressing A549 cells dosed with GNP-Cit-Theranos (1ml of ~1nM GNP-Cit loaded with 25µM Pt(IV)LipA and 12µL of 1mM RuPhen) for 24 hours and stained with CP9/19 / secondary antibody. A) in focus plane of brightfield channel; B) average Hoechst signal across Z stack; C) average DNA-damage signal across Z stack, D) average RuPhen signal across Z stack; E) overlay of b and c; F) overlay of b and d; G) overlay of b, c and d: H) overlay of all channels.

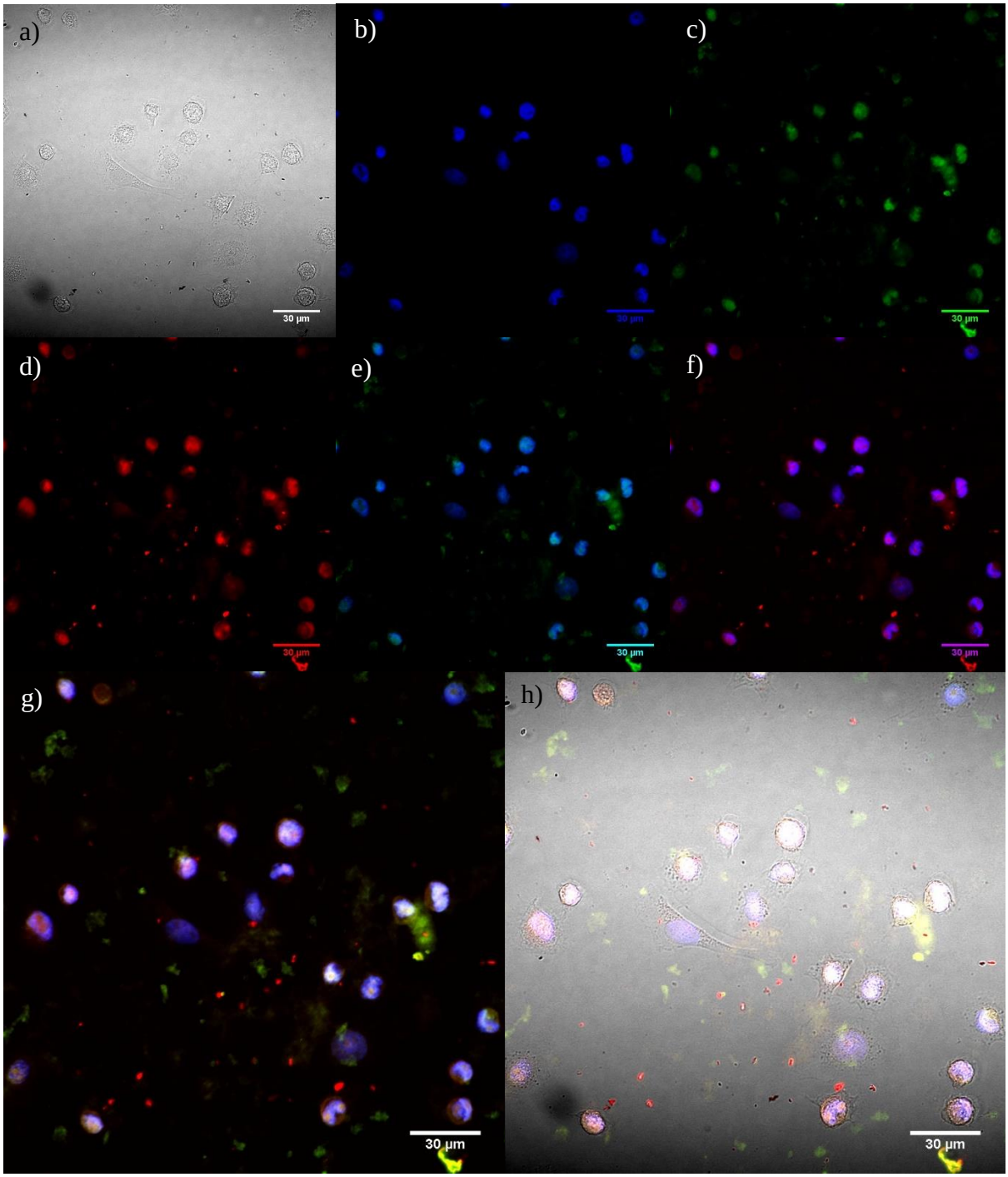

Figure 510: Immunocytochemistry confocal studies of high folate receptor α expressing A549 cells pre-dosed with folate receptor α primary antibody for receptor blocking and subsequently dosed with GNP-Fol-Theranos (1ml of ~1nM GNP-Fol loaded with 25µM Pt(IV)LipA and 12µL of 1mM RuPhen) for 24 hours and stained with CP9/19 / secondary antibody. A) in focus plane of brightfield channel; B) average Hoechst signal across Z stack; C) average DNA-damage signal across Z stack, D) average RuPhen signal across Z stack; E) overlay of b and c; F) overlay of b and d; G) overlay of b, c and d: H) overlay of all channels.

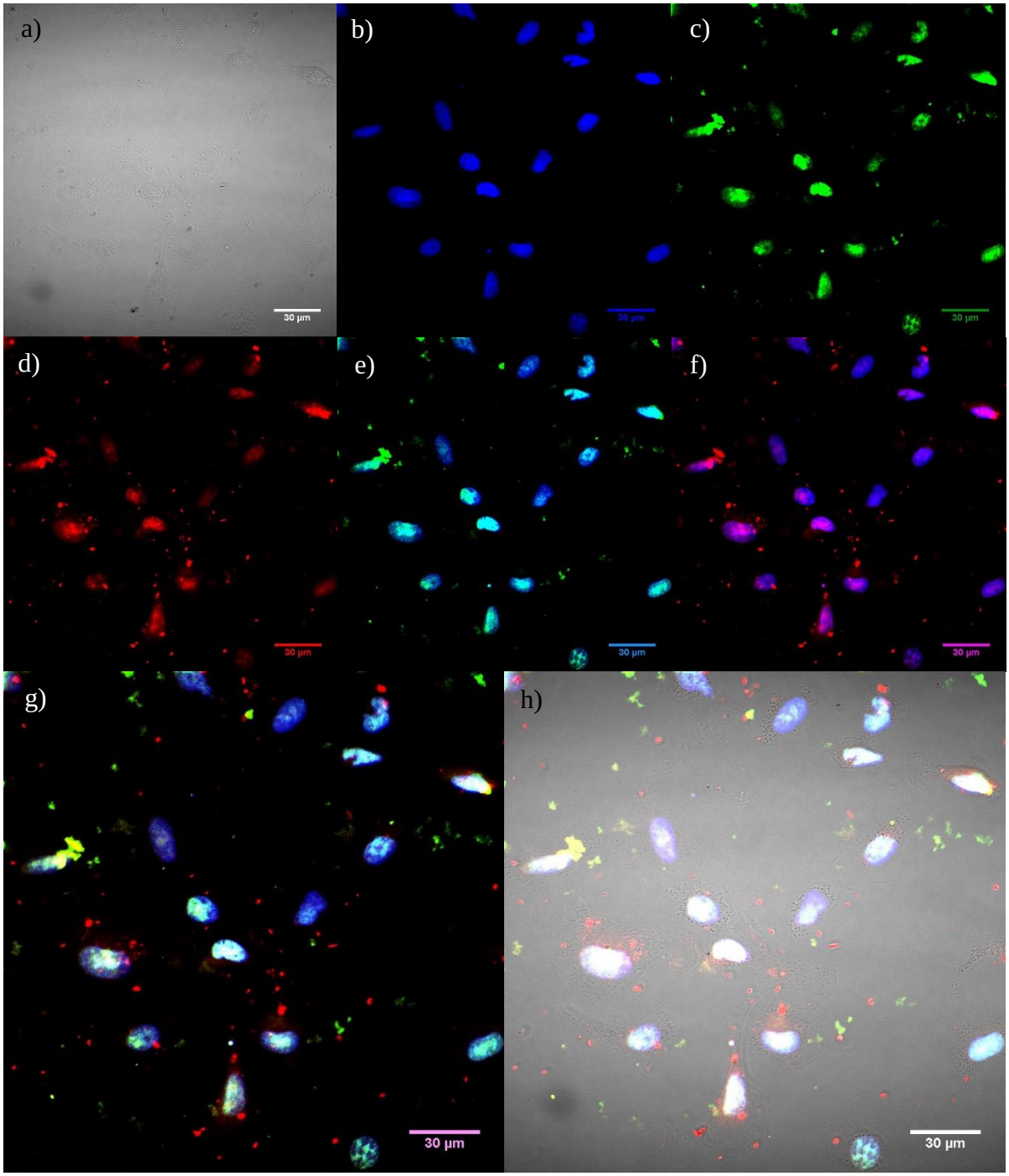

Figure 511: Immunocytochemistry confocal studies of high folate receptor α expressing A549 cells pre-dosed with folate receptor α primary antibody for receptor blocking and subsequently dosed with GNP-Cit-Theranos (1ml of ~1nM GNP-Cit loaded with 25µM Pt(IV)LipA and 12µL of 1mM RuPhen) for 24 hours and stained with CP9/19 / secondary antibody. A) in focus plane of brightfield channel; B) average Hoechst signal across Z stack; C) average DNA-damage signal across Z stack, D) average RuPhen signal across Z stack; E) overlay of b and c; F) overlay of b and d; G) overlay of b, c and d: H) overlay of all channels.

Confocal Microscopy Results Discussion

A number of comparisons can be drawn from these fixed cell immunocytochemical confocal microscopy studies by qualitative analysis of Figures 506 to 511. Firstly, it appears that pre-blocking folate receptors with folate receptor alpha monoclonal antibody leads to a decrease in RuPhen probe signal (red) and DNA-damage antibody signal (green) within high folate receptor α expressing A549 cells treated with GNP-Fol-Theranos (Figure 508 vs 510, unblocked vs blocked). For both signals (images c and d of the respective figures) there is a reduction in both fluorescence intensity and signal distribution. This agrees with the previous studies of sections 4.4.2. and 3.7, which indicate that pre-blocking folate receptors with the antibody leads to reduction in DNA damage and RuPhen signal respectively. Reduction in these signals is potentially indicative of reduced nanoparticle uptake and therefore reduced nanoparticle delivery of therapeutic (Pt(IV)LipA) and diagnostic (RuPhen) agents. Interestingly, the DNA-damage antibody signal of the GNP-Fol-Theranos system samples appears to be more localised to the nuclei of the cells than previous studies (GNP-Fol-Pt(IV), section 4.4.2.2), potentially with less mitochondrial DNA damage.

By comparison, there is no readily observable difference in DNA-damage antibody signal or RuPhen signal across the GNP-Cit-Theranos samples, irrespective of folate receptor blocking (Figures 509 and 511). This is in agreement with previous studies (sections 4.4.2.2 and 3.7) and is potentially the result of the lack of uptake of the citrate based nanoparticle system by folate receptor α. Accordingly, if the GNP-Cit-Theranos system is taken up independently of this folate receptor mediated pathway, minimal shift in uptake / induced signal is to be expected.

A second observation is that it is not readily apparent whether the GNP-Fol-Theranos system (unblocked, Figure 508) gives increased nanoparticle uptake and cellular delivery of reagents over the GNP-Cit-Theranos system (unblocked, Figure 509). In particular, there is no readily observable difference between the signal intensity or distribution of the DNA-damage antibody signal (images c, e, g and h) or the RuPhen signal (images d, f, g and h) for the two samples. This might therefore indicate that the folate receptor system does not provide an increased level of uptake of GNP-Fol-Thernaos over the other pathways afforded to the GNP-Cit-Theranos system, or that the difference between the uptake of the two systems is negligible over a concentrated 24 hour dosing period. This result is in contrast to the findings of sections 4.4.2. and 3.7, and was investigated further by FACS and ICPMS for quantitative analysis and review.

A third observation is that there appears to be a greater level of non-specific DNA-antibody binding within the GNP-Cit-Theranos samples (Figures 509 and 511) over the GNP-Fol-Theranos samples (Figures 508 and 510). In particular, images c, e, g and h of Figures 509 and 511 show that there is a lot of seemingly non-cellular based green fluorescence, which would imply that there was a greater amount of unbound fluorophore washed out of the cells or stuck to the cover slips. It is unknown why this would be more likely to happen for the GNP-Cit-Theranos system samples over the GNP-Fol-Thernos system samples, however, it would appear that the same is observable within the receptor blocking study GNP-Fol sample (Figure 510). This could be coincidental, and that it merely fortuitous that the non-receptor blocking GNP-Fol-Thernaos sample did not exhibit non-cellular based antibody signal. Alternatively, there could be a link between the folate receptor mediated endocytosis leading to more targeted delivery of reagents, which in turn leads to greater DNA damage, which increases the relative percentage of the antibodies used to stain the sample that bind appropriately, which therefore reduces the levels of free antibody available for non-specific binding.

A final observation is that there appears to be some nuclear localisation of the RuPhen probe across the theranostic particle samples. This is discussed further with respect to ICPMS studies later, however, RuPhen signal within the nuclei of the cells might indicate that the theranostic nanoparticular system is potentially unstable and might be releasing the probe within the cells upon uptake. This theory is somewhat reinforced by the studies of Chapter 3, wherein the cells were dosed with free RuPhen probe and no signal was readily apparent, indicating free probe does not get into the probe itself in sufficient concentrations to give a viewable signal. However, as part of a nanoparticular system, the probe may enter in larger quantities whilst bound and potentially subsequently dissociate from the particle surface. This theory shall of course require repeated studies of the above confocal microscopy experiments in collaboration with flow cytometry and ICPMS studies in order to fully ascertain the likelihood of particle degradation.

5.3. Flow Cytometry Studies

FACS analysis was utilised to quantitatively compare the induced antibody signal and associated RuPhen signal of the cell samples. For continuity, the same protocol and conditions were employed from the previously reported studies of Sections 3.7.2 and 4.5.3. The samples of the present FACS studies are represented in Table 502.

HIGH FOLATE RECEPTOR α EXPRESSING A549S DOSED WITH:	
No Blocking	**With Receptor α Blocking**
Blank	-
Pri + Sec Antibodies (AB)	-
Cisplatin + AB	-
Pt(IV)LipA + AB	-
GNP-Fol-Theranos + AB	GNP-Fol-Theranos + AB
GNP-Cit-Theranos + AB	GNP-Cit-Theranos + AB

Table 502: Overview of fixed cell Fluorescence-Activated Cell Sorting (FACS) samples.

The cell samples were identical to those of the confocal studies (section 5.2), with high folate receptor α expressing A549 cells seeded within 6 well plates (400,000 cells per well, no cover slips) and allowed to adhere overnight before being subjected to the appropriate conditions of table 502 for 24 hours (Experimental section 5.5.3). The cells were subsequently washed with PBS before being tripsinised and fixed in suspension ready for permeabilisation and immunocytochemical staining (See Experimental section 5.5.3 for full details). Post sample-staining, the samples were washed, centrifuged and re-suspended multiple times to remove free reagents and were subsequently analysed by FACS microscopy.

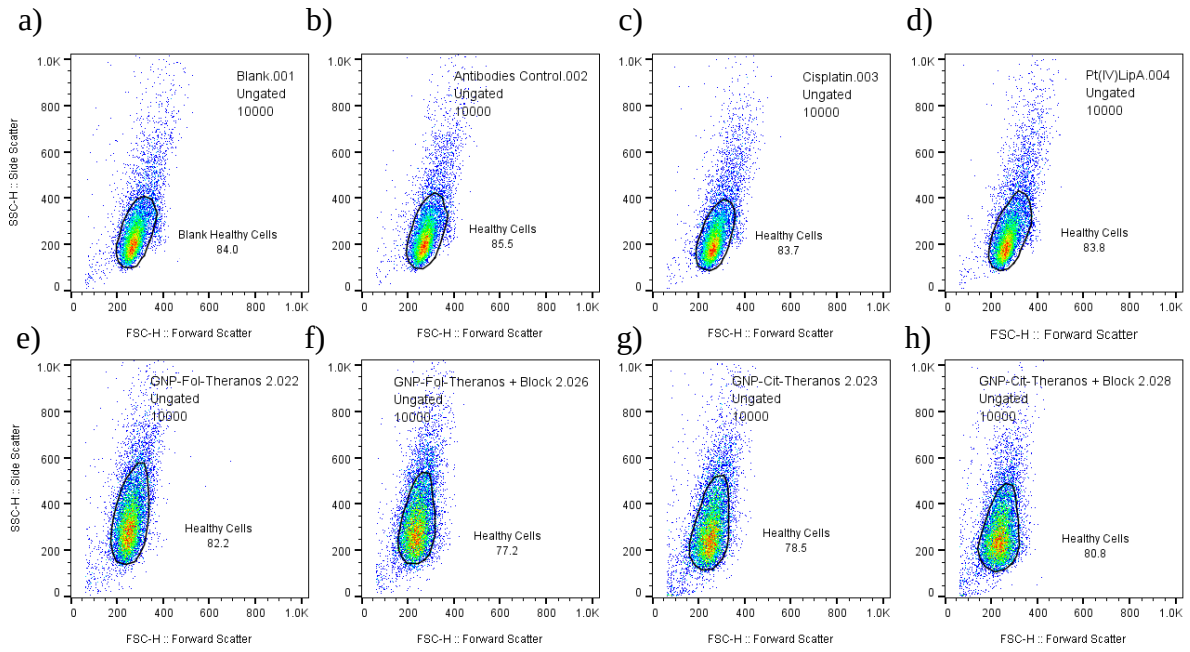

Figure 515: FACS dot-plot data of forward scatter (particle size) vs side scatter (particle granularity) for the samples of Table 502 in high folate receptor α expressing A549 cells. A) Blank sample, b) Antibody control, c) Cisplatin, d) Pt(IV)LipA, e) GNP-Fol-Theranos, f) GNP-Fol-Theranos-Block, g) GNP-Cit-Theranos and h) GNP-Cit-Theranos-Block. The circled population represents gating of fragments, with the cited number representing the percentage of the population corresponding to healthy cells.

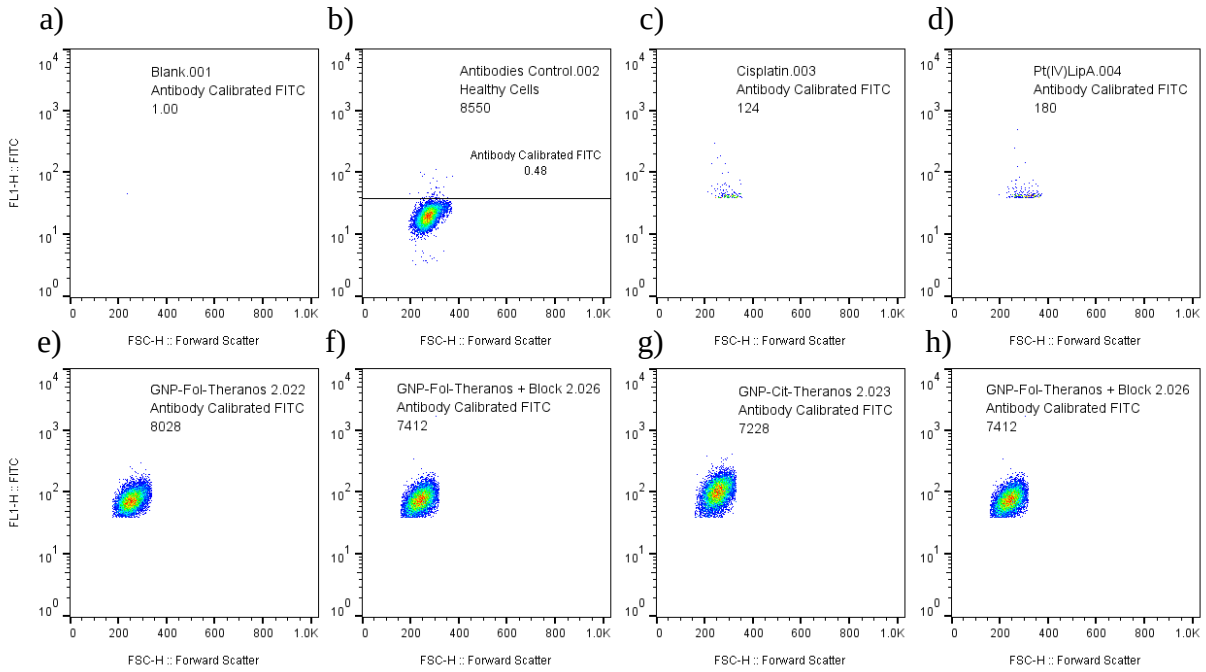

Subset Name with Gating Path	Count	Freq. of Total	Mean : FL1-H	Median : FL1-H
Blank.001/Blank Healthy Cells/Antibody Calibrated FITC	1.00	0.0100	45.6	45.6
Antibodies Control.002/Healthy Cells/Antibody Calibrated FITC	41.0	0.41	55.0	46.9
Cisplatin.003/Healthy Cells/Antibody Calibrated FITC	124	1.24	51.3	42.5
Pt(IV)LipA.004/Healthy Cells/Antibody Calibrated FITC	180	1.80	49.6	42.6
GNP-Fol-Theranos 2.022/Healthy Cells/Antibody Calibrated FITC	8028	80.3	76.6	72.7
GNP-Fol-Theranos + Block 2.026/Healthy Cells/Antibody Calibrated FITC	7412	74.1	78.6	74.3
GNP-Cit-Theranos 2.023/Healthy Cells/Antibody Calibrated FITC	7228	72.3	104	98.7
GNP-Cit-Theranos + Block 2.026/Healthy Cells/Antibody Calibrated FITC	7695	77.0	99.3	92.2

Figure 516: FACS dot-plot data of forward scatter (particle size) vs FITC channel signal intensity (antibody emission intensity) for the samples of Table 502 in high folate receptor α expressing A549 cells. A) Blank sample, b) Antibody control, c) Cisplatin, d) Pt(IV)LipA, e) GNP-Fol-Theranos, f) GNP-Fol-Theranos-Block, g) GNP-Cit-Theranos and h) GNP-Cit-Theranos-Block. "Antibody Calibrated FITC" represents cells with FITC channel fluorescence equal to or greater than the strongest emission of the antibody control sample (upper limit of non selective binding). Any signal therefore should represent cisplatin-DNA conjugate FITC fluorescence signal. Associated statistics are tabulated beneath within the FACS analysis software and are represented again later in Table 503.

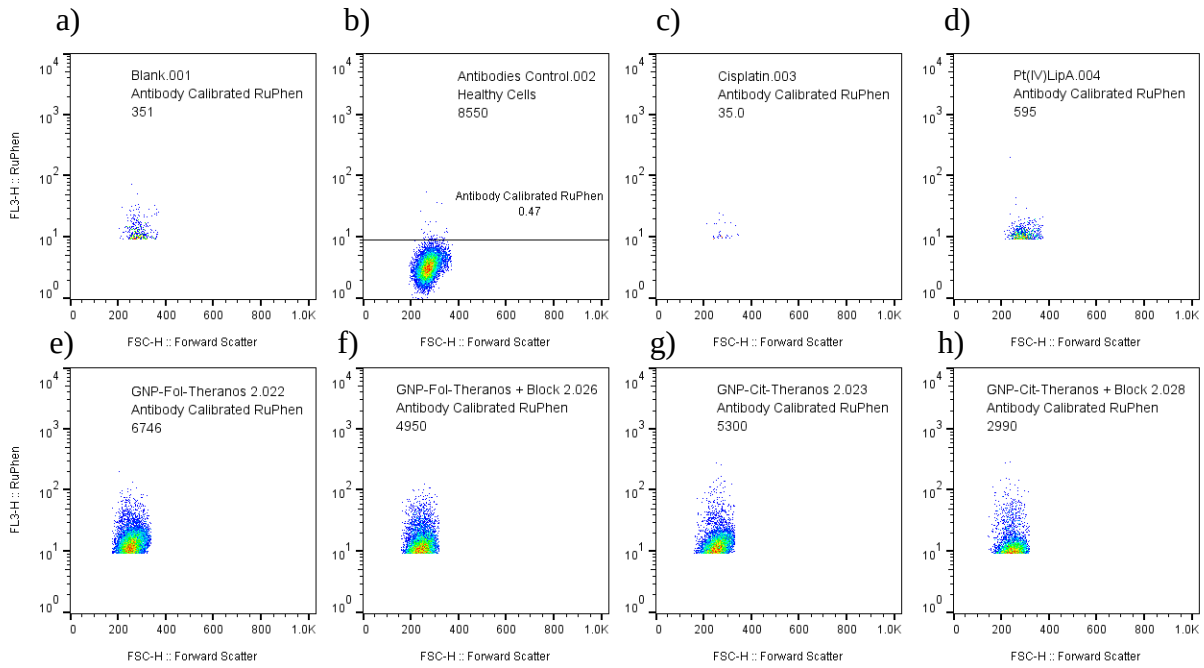

Subset Name with Gating Path	Count	Freq. of Total	Mean : FL3-H	Median : FL3-H
Blank.001/Blank Healthy Cells/Antibody Calibrated RuPhen	351	3.51	13.4	11.2
Antibodies Control.002/Healthy Cells/Antibody Calibrated RuPhen	40.0	0.40	14.1	10.5
Cisplatin.003/Healthy Cells/Antibody Calibrated RuPhen	35.0	0.35	12.4	10.4
Pt(IV)LipA.004/Healthy Cells/Antibody Calibrated RuPhen	595	5.95	11.9	10.8
GNP-Fol-Theranos 2.022/Healthy Cells/Antibody Calibrated RuPhen	6746	67.5	15.8	13.5
GNP-Fol-Theranos + Block 2.026/Healthy Cells/Antibody Calibrated RuPhen	4950	49.5	15.8	12.6
GNP-Cit-Theranos 2.023/Healthy Cells/Antibody Calibrated RuPhen	5300	53.0	15.2	12.6
GNP-Cit-Theranos + Block 2.028/Healthy Cells/Antibody Calibrated RuPhen	2990	29.9	15.4	11.3

Figure 517: FACS dot-plot data of forward scatter (particle size) vs red channel signal intensity (Ruphen emission intensity) for the samples of Table 502 in high folate receptor α expressing A549 cells. A) Blank sample, b) Antibody control, c) Cisplatin, d) Pt(IV)LipA, e) GNP-Fol-Theranos, f) GNP-Fol-Theranos-Block, g) GNP-Cit-Theranos and h) GNP-Cit-Theranos-Block. "Antibody Calibrated RuPhen" represents cells with RuPhen channel fluorescence equal to or greater than the strongest red channel emission of the antibody control sample (theoretically removing any potential signal bleedthrough). Any signal therefore should represent RuPhen induced fluorescence signal. Associated statistics are tabulated beneath within the FACS analysis software and are represented again later in Table 504.

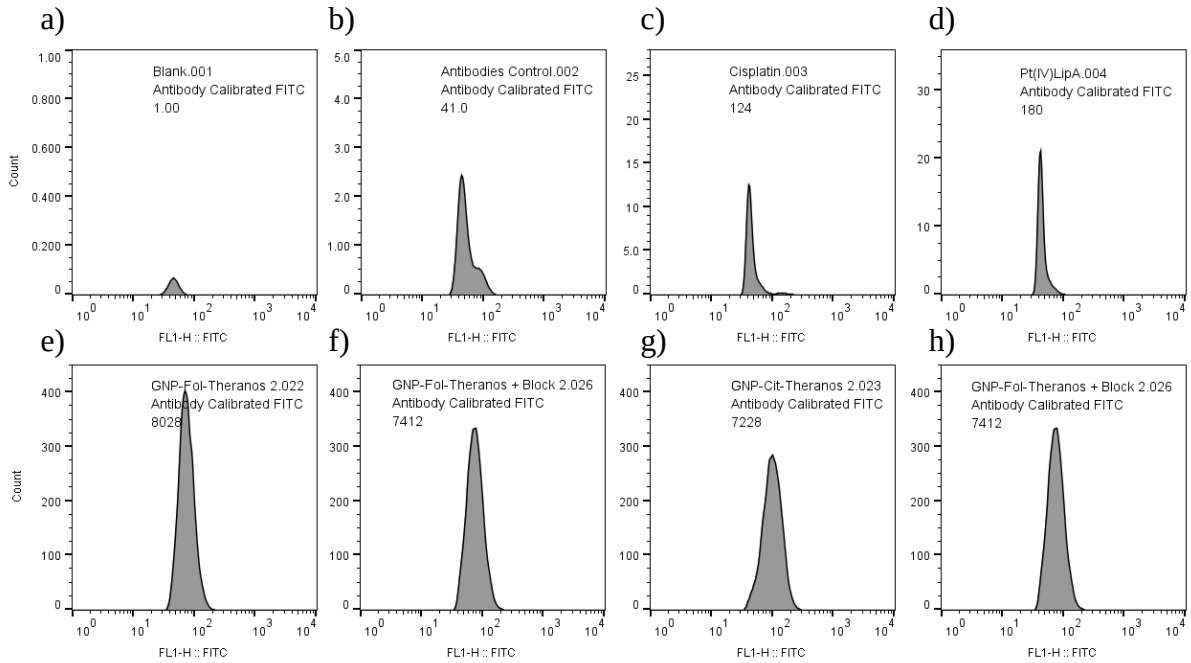

Figure 518: FACS Histogram data of FITC channel signal for the "Antibody Calibrated FITC" sub-population of the samples of Table 502 in high folate receptor α expressing A549 cells. A) Blank sample, b) Antibody control, c) Cisplatin, d) Pt(IV)LipA, e) GNP-Fol-Theranos, f) GNP-Fol-Theranos-Block, g) GNP-Cit-Theranos and h) GNP-Cit-Theranos-Block. The nanoparticle histograms (e-h) have been standardised to an intensity of 450 to allow for representative overlay.

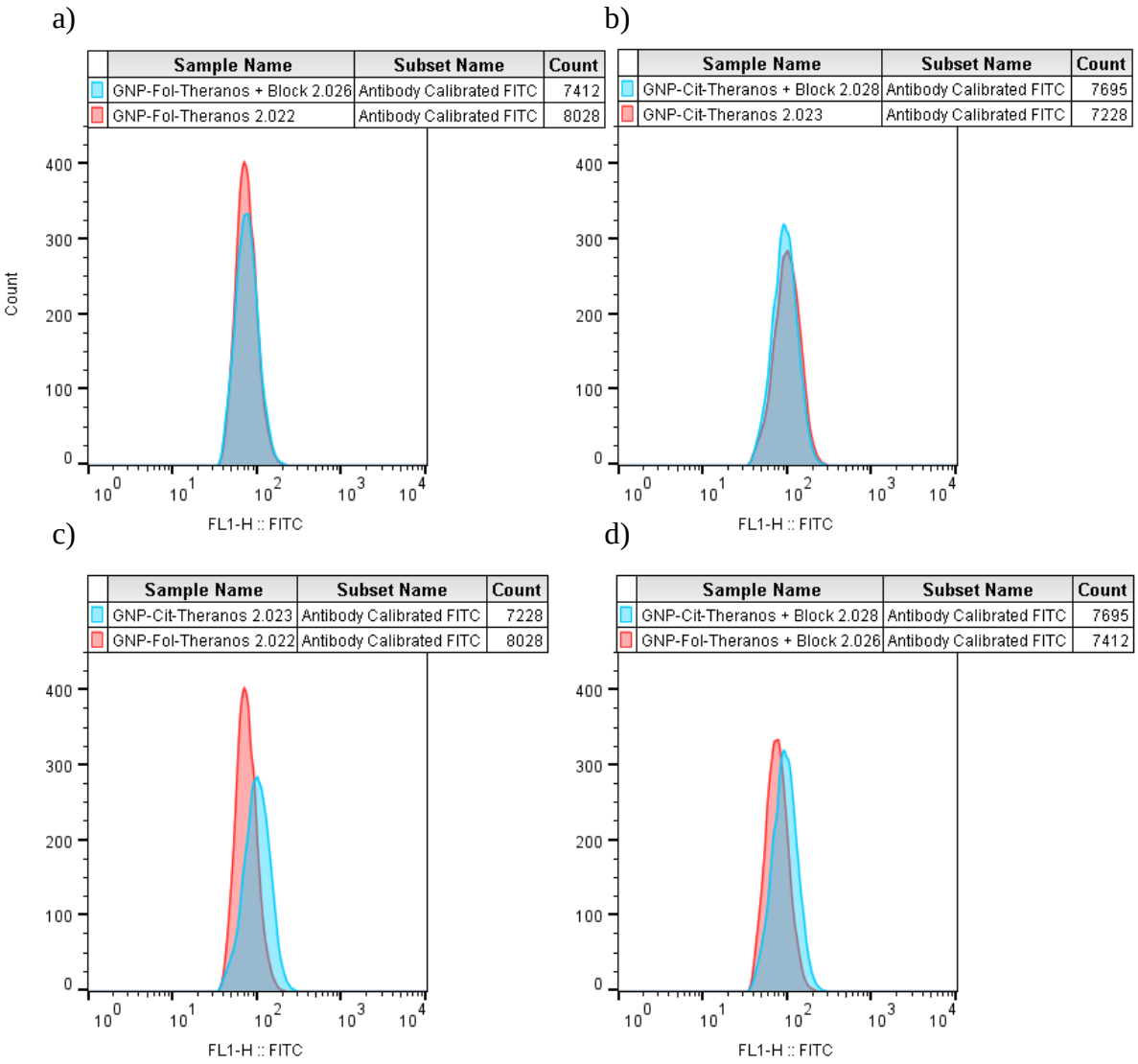

Figure 519: FACS Overlay histogram data of FITC channel signal for the "Antibody Calibrated FITC" sub-population of the samples of Table 502 in high folate receptor α expressing A549 cells. a) Overlay of GNP-Fol-Theranos and GNP-Fol-Theranos-Block; b) Overlay of GNP-Cit-Theranos and GNP-Cit-Theranos-Block; c) Overlay of GNP-Fol-Theranos and GNP-Cit-Theranos: and d) Overlay of GNP-Fol-Theranos-Block and GNP-Cit-Theranos-Block.

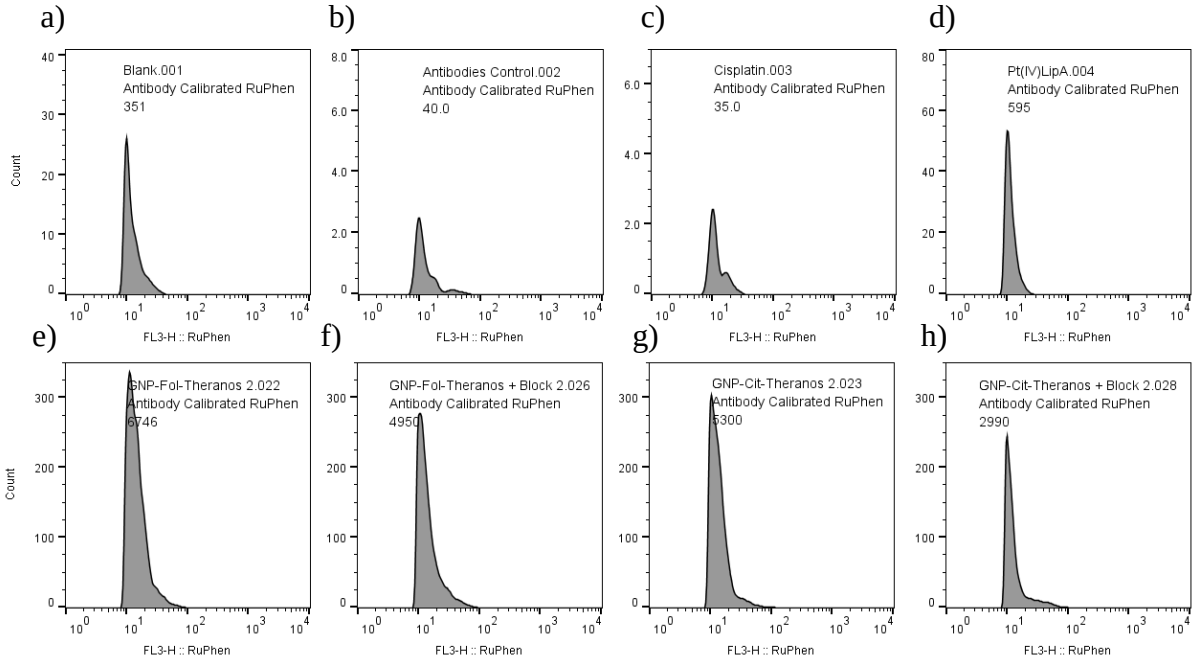

Figure 520: FACS Histogram data of RuPhen channel signal for the "Antibody Calibrated RuPhen" sub-population of the samples of Table 502 in high folate receptor α expressing A549 cells. A) Blank sample, b) Antibody control, c) Cisplatin, d) Pt(IV)LipA, e) GNP-Fol-Theranos, f) GNP-Fol-Theranos-Block, g) GNP-Cit-Theranos and h) GNP-Cit-Theranos-Block. The nanoparticle histograms (e-h) have been standardised to an intensity of 350 to allow for representative overlay.

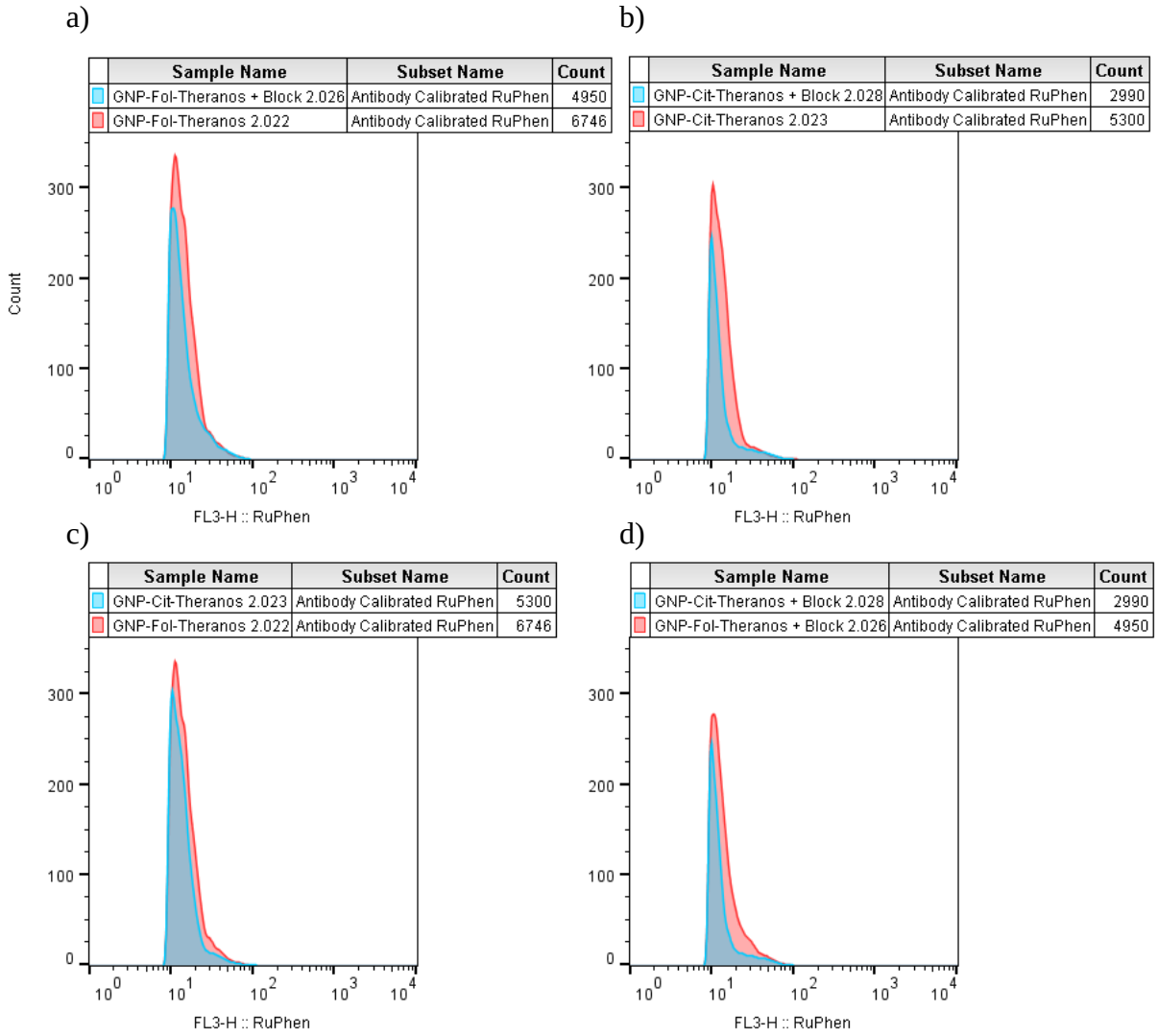

Figure 521: FACS Overlay histogram data of RuPhen channel signal for the "Antibody Calibrated RuPhen" sub-population of the samples of Table 502 in high folate receptor α expressing A549 cells. a) Overlay of GNP-Fol-Theranos and GNP-Fol-Theranos-Block; b) Overlay of GNP-Cit-Theranos and GNP-Cit-Theranos-Block; c) Overlay of GNP-Fol-Theranos and GNP-Cit-Theranos: and d) Overlay of GNP-Fol-Theranos-Block and GNP-Cit-Theranos-Block.

	Pt(IV)LipA Signal (Antibody Calibrated FITC Sub-Culture)			
Samples	**Events**	**% of Sample**	**Mean**	**Median**
Blank	1	0.01	45.6	45.6
Antibodies Control	41	0.41	55.0	46.9
Cisplatin	124	1.24	51.3	42.5
Pt(IV)LipA	180	1.80	49.6	42.6
GNP-Fol-Theranos	8028	80.3	76.6	72.7
GNP-Fol-Theranos-Block	7412	74.1	78.6	74.3
GNP-Cit-Theranos	7228	72.3	104	98.7
GNP-Cit-Theranos-Block	7695	77.0	99.3	92.2

Table 503: Statistical data from the FACS histogram plots of samples a)-h) of Figure 518, corresponding to the FITC channel measurements (Antibody Calibrated FITC signal).

	RuPhen Signal (Antibody Calibrated RuPhen Sub-Culture)			
Samples	**Events**	**% of Sample**	**Mean**	**Median**
Blank	351	3.51	13.4	11.2
Antibodies Control	40	0.4	14.1	10.5
Cisplatin	35	0.35	12.4	10.4
Pt(IV)LipA	595	5.95	11.9	10.8
GNP-Fol-Theranos	6746	67.5	15.8	13.5
GNP-Fol-Theranos-Block	4950	49.5	15.8	12.6
GNP-Cit-Theranos	5300	53.0	15.2	12.6
GNP-Cit-Theranos-Block	2990	29.9	15.4	11.3

Table 504: Statistical data from the FACS histogram plots of samples a)-h) of Figure 520, corresponding to the red channel measurements (RuPhen Signal) from the Antibody Calibrated RuPhen Sub-Culture.

DNA Damage Analysis (FITC Channel Data)

A number of observations can be made from the FACS data of Figures 515 to 519 and Table 503. In line with the Pt(IV) studies of Section 4.4.3, it appears upon review of Figures 515 and 518 that there is an increase in DNA damage induced FITC signal within the theranostic nanoparticle samples (e – h) over cisplatin (c) and Pt(IV)LipA alone (d). More particularly, Figure 516 represents dot-plot data for the samples of Table 502, plotting FITC channel signal (antibody fluorescence intensity) against forward scatter (cell size). The "Antibody Calibrated FITC" sub-population of the dot-plots represents the threshold for false positive fluorescence signal and therefore identifies the minimal fluorescence required of the subsequent samples to be considered representative of DNA-Cisplatin adduct induced antibody fluorescence signal. Accordingly, any particles displaying FITC intensity above this threshold fall within the "Antibody Calibrated FITC" sub-culture. Comparison of the plots shows that cisplatin (c) and Pt(IV)LipA (d) show less particles beyond the DNA damage antibody signal threshold vs each of the theranostic nanoparticle samples (e – h).

Figure 518 represents histogram plot data collected for samples a) – h), showing the distribution of particles displaying FITC channel fluorescence which exceeds the false-positive threshold (data points within the Antibody Calibrated FITC signal sub-culture). This data, in combination with the histogram-overlay data of Figure 519 and statistics of Table 503 better illustrate the relationship of DNA damage with the respective samples.

From review of overlay-histogram A) (overlap of plots e) and f) of Figure 518) there appears to be no significant change in the severity of induced DNA damage for samples treated with GNP-Fol-Theranos irrespective of folate receptor α blocking. Numerically, when A549 cells are treated with GNP-Fol-Theranos in the presence of folate receptor blocking there is an 8%

decrease in the number of events (8028 vs 7412), a 2% increase in the mean fluorescence intensity (76.6 vs 78.6) and a 2% increase in the median fluorescence intensity (72.7 vs 74.3). This data therefore contradicts the present assumption (and prior research detailed herein) that blocking folate receptor α leads to a much larger reduction in cellular damage induced by the nanoparticle system. Interestingly, whilst this data shows that there is a reduction in the uptake of GNP-Fol-Theranos system upon blocking α folate receptors (~8%), there is no readily observable equivalent reduction in the severity of the cytotoxic events (corresponding to signal intensity, which actually increases for the blocked sample).

One possible explanation for this observation is that the GNP-Fol-Theranos system might now be an unstable system (as previously discussed), and that the levels of Pt(IV)LipA bound to the particles within the system now vary. Accordingly, even if more particles are taken up, this may not subsequently lead to elevated levels of DNA adduct formation (FITC signal).

Upon review of overlay-histogram B) (overlap of plots g) and h) of Figure 518) it would also appear that there is no clear relationship between nanoparticle loading with the GNP-Cit-Theranos system irrespective of folate receptor α blocking in A549s. Numerically, when A549 cells are treated with GNP-Cit-Theranos in the presence of folate receptor blocking there is a 6% increase in the number of events (7228 vs 7695), a 5% reduction in the mean fluorescence intensity (104 vs 99.3) and a 7% reduction in the median fluorescence intensity (98.7 vs 92.2). This data therefore appears to agree with the hypothesis (and prior research detailed herein) that there is no induced trend in uptake of GNP-Cit-Theranos within high folate receptor α expressing A549s upon blocking the folate receptors. This might be because the citrate based system is more stable than the folate based system, or it might be a coincidence. Further experimental runs and repeats will therefore need to be performed across all of those reported

herein so as to appropriately explore whether these results are reproducible, especially with subsequent ICPMS studies to fully ascertain the stability of the folate and citrate systems.

Overlay histogram C) compares the uptake of GNP-Fol-Theranos vs GNP-Cit-Theranos and the induced DNA damage severity (FITC channel) within the Antibody Calibrated FITC sub-population (plots e) and g) of Figure 518). Upon review of this overlay histogram and the accompanying numerical data it would seem that the GNP-Fol-Theranos system displays 10% more events (8028 vs 7228 respectively), 35% lower mean fluorescence intensity (76.6 vs 104 respectively) and 35% lower median fluorescence intensity (72.7 vs 98.7 respectively) than the GNP-Cit-Theranos system within the high folate receptor α expressing A549 cells. As represented in overlay histogram D) (overlay of plots f) and h) of Figure 118), the same trend is observable for the folate receptor α blocked samples of the respective systems, with all numerical data being lower for the GNP-Fol-Theranos system.

It is proposed that this further potentially indicates a stability issue within the folate capped theranostic system over the citrate system. Again, this will need further research as triplicate experiments and sample replicates so as to allow for a more complete assessment of the results.

RuPhen Distribution Analysis (Red Channel Data)

Antibody Calibrated RuPhen Sub-Culture

The red channel signal data of the above studies is represented in Figures 520 to 523, with associated statistics represented in Table 504. Figures 520 and 521 represent red channel fluorescence data for cells within samples a)-h) of Table 502 which exhibit a fluorescence intensity beyond that of the antibody control sample, these data points fall within the "Antibody Calibrated RuPhen" sub-culture and the associated numerical data is recorded in

Table 504. This sub-culture was chosen for initial investigation so as to reduce the likelihood of signal bleed-through from the antibody fluorophore. It would appear upon review of the above data that there is little measurable signal within the red channel for samples a) to d) within this "Antibody Calibrated RuPhen" sub-culture (samples: blank, control, cisplatin and Pt(IV)LipA respectively). This result is anticipated, given that samples a) to d) contain no red channel emissive components. This data appears to confirm that the selection of the sub-culture was successful in minimising false positive recordings of cells that would display elevated red-channel signal due to signal bleed-through from the primarily green channel emissive secondary antibody, as opposed to elevated uptake of RuPhen bearing nanoparticles.

The overlay histogram data of Figure 521 and statistics of Table 504 for samples e) to h) are more comparable to the results reported for the FITC channel data as above. When A549 cells are treated with GNP-Fol-Theranos in the presence of folate receptor blocking, there is a 27% decrease in the number of events (6746 vs 4950), no change is observable in the mean fluorescence intensity (both 15.8) and a 7% reduction in the median fluorescence intensity (13.5 vs 12.6). This data therefore shows that the number of particles with fluorescence signal above the threshold is reduced upon blocking (indicative of less uptake), whilst the intensity is comparable. It would therefore appear that this data suggests that upon blocking, fewer particles do get taken up by the majority of the cells, but for the cells which do still take the particles up, there is a comparable RuPhen signal. This is somewhat different to the earlier studies, where reduction in events also lead to a reduction in signal intensity. This might then support the hypothesis that the folate based system is unstable.

Overlay-histogram B) (overlap of plots g) and h) of Figure 520) appears to show that a similar relationship exists for nanoparticle loading with the GNP-Cit-Theranos system. When A549

cells are treated with GNP-Cit-Theranos in the presence of folate receptor blocking there is a 43% decrease in the number of events (5300 vs 2990), a 1% increase in the mean fluorescence intensity (15.2 vs 15.4) and an 11% reduction in the median fluorescence intensity (12.6 vs 11.3). This data therefore appears to contradict the present hypothesis that folate receptor blocking has no significant effect on uptake of the citrate based nanoparticle system.

Moreover, overlay histogram C) compares the uptake of GNP-Fol-Theranos vs GNP-Cit-Theranos and the induced RuPhen signal (plots e) and g) of Figure 520). From this overlay histogram data and the accompanying numerical data, it appears that the GNP-Fol-Theranos system displays 22% more events (6746 vs 5300 respectively) than the GNP-Cit-Theranos system, with 4% higher mean fluorescence intensity (15.8 vs 15.2 respectively) and 7% higher median fluorescence intensity (13.5 vs 12.6 respectively), within the high folate receptor α expressing A549 cells. As represented in overlay histogram D) (overlay of plots f) and h) of Figure 520), the same trend is observable for the folate receptor α blocked samples of the respective systems.

This data therefore suggests that the GNP-Fol-Theranos system is more widely taken up by the A549 cells than the GNP-Cit-Theranos system, thus why there is a greater number of events (particles displaying fluorescence above the threshold). However, given that the intensity of the fluorescence within those cells is comparable, this would suggest a comparable level of uptake of the two systems within those cells which do display appropriate levels of probe emission. Alternatively, there could be different levels of uptake and therefore different levels of RuPhen probe present between the two samples / cultures, but this signal is not conveyed as there is no measurable difference in afforded signal intensity and number of RuPhen complexes present. Lastly, as hypothesised above, these results might come as a consequence of the GNP-

Fol system now being relatively unstable. As noted, further experiments will need conducting so as to fully explore this area of research.

Overview of Studies and Findings

From the above FACS studies it is hypothesised that the GNP-Fol-Theranos system displays increased cisplatin-DNA adduct formation over cisplatin and Pt(IV)LipA alone, but with comparable levels to the GNP-Cit-Theranos system in high folate receptor α expressing A549 cells. Contradicting data was retrieved for the RuPhen signal studies of the present FACS analysis. The data of this FACS analysis therefore contradicts the previous hypothesis and evidence set forth in confocal and cytotoxicity studies. The contradictory data might therefore indicate some inconsistencies with nanoparticle loading with reagents or that the folate capped theranostic system is now unstable. For more reliable quantitative data, ICPMS was conducted for the present theranostic systems to ascertain trends in nanoparticle uptake and cellular delivery of reagents. As noted, further experiments are essential within these studies so as to see if the results are reproducible and to fully ascertain the nature of the cellular loading.

5.4. ICPMS Studies

Following the immunocytochemical confocal and FACS microscopy studies detailed herein, subsequent research sought to quantify and assess the localisation of gold salt, ruthenium probe and platinum species within the whole cell, cytosol and nucleus of the A549 cells dosed with the GNP-Fol-Theranos and GNP-Cit-Theranos systems. Accordingly, ICPMS was conducted for samples of high folate receptor α expressing A549 cells that have been dosed as per Table 506 (for continuity, the same concentrations and dosing protocols were employed as per section 5.5.4). ICPMS data for these samples is represented in Figures 525 to 531 below.

HIGH FOLATE RECEPTOR α EXPRESSING A549S DOSED WITH:			
No Blocking		**With Receptor α Blocking**	
a)	Blank		-
b)	Cisplatin		-
c)	Pt(IV)LipA		-
d)	GNP-Fol-Theranos	f)	GNP-Fol-Theranos
e)	GNP-Cit-Theranos	g)	GNP-Cit-Theranos

Table 506: Overview of samples submitted for ICPMS. A549s were seeded onto 12 well plates (0.1 x 10^6 cells) and allowed to adhere overnight. Samples were then dosed with 25μM anti-cancer agent either alone (Cisplatin (b) and Pt(IV)LipA (c)) or with the theranostic nanoparticle systems, either 0.5mL of ~1nM GNP-Fol (samples d and f) loaded with Pt(IV)LipA (28μL of a 1mg/mL stock) and RuPhen (12μL of a 1mM stock) or 0.5mL of ~1nM GNP-Cit (samples e and g), loaded accordingly. Full details available in Experimental section 5.5.4.

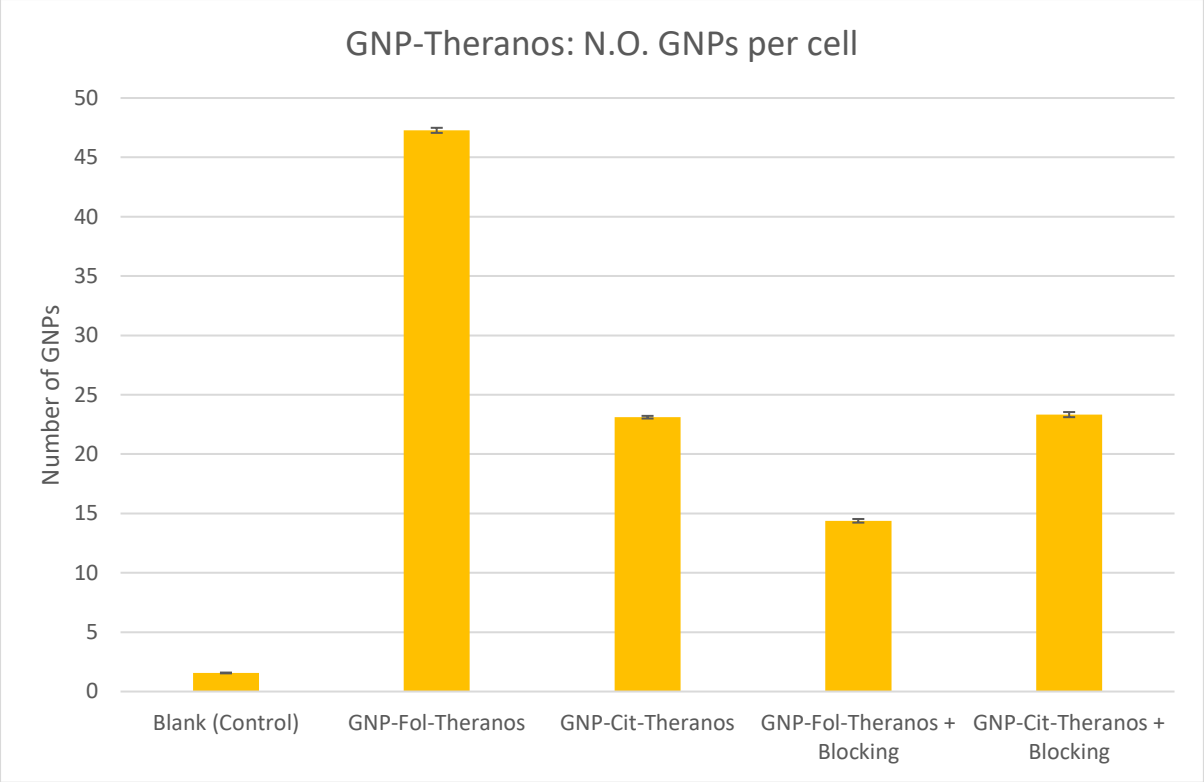

Figure 525: Graphical representation of the total number of gold nanoparticles on average per whole cell of samples d) to g) of Table 506. Expectedly, fewer GNP-Fol centres are present upon blocking the folate receptors (47 vs 13). Comparable levels of GNP-Cit cores were found on average in the presence of folate receptor blocking (23 vs 24).

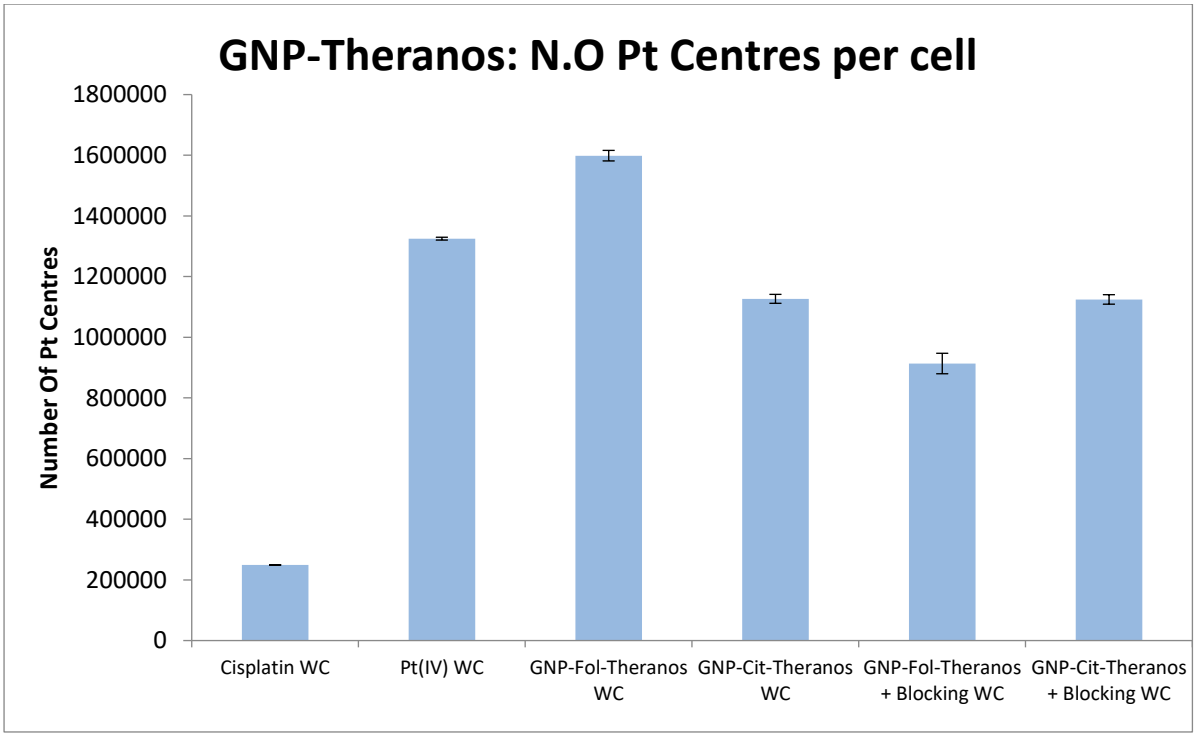

Figure 526: Graphical representation of the total number of platinum centres on average per whole cell of samples b) to g) of Table 506.

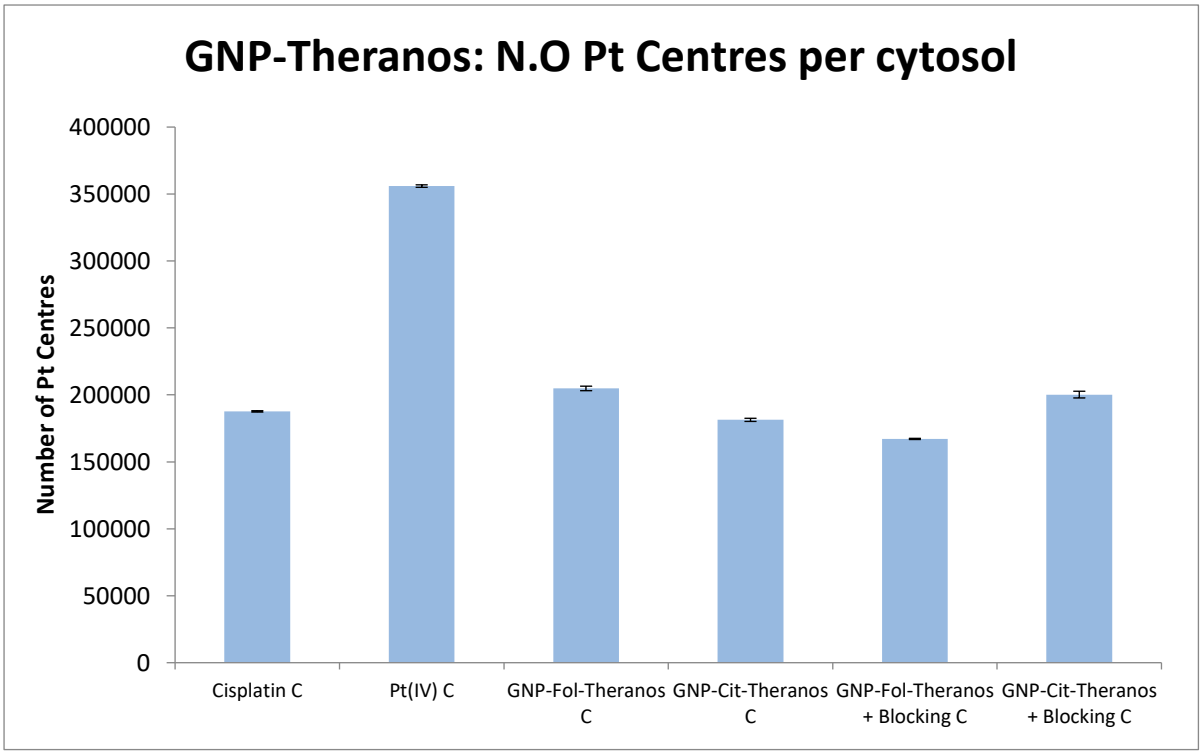

Figure 527: Graphical representation of the total number of platinum centres on average per cytosol of A549 cells dosed as per samples b) to g) of Table 506.

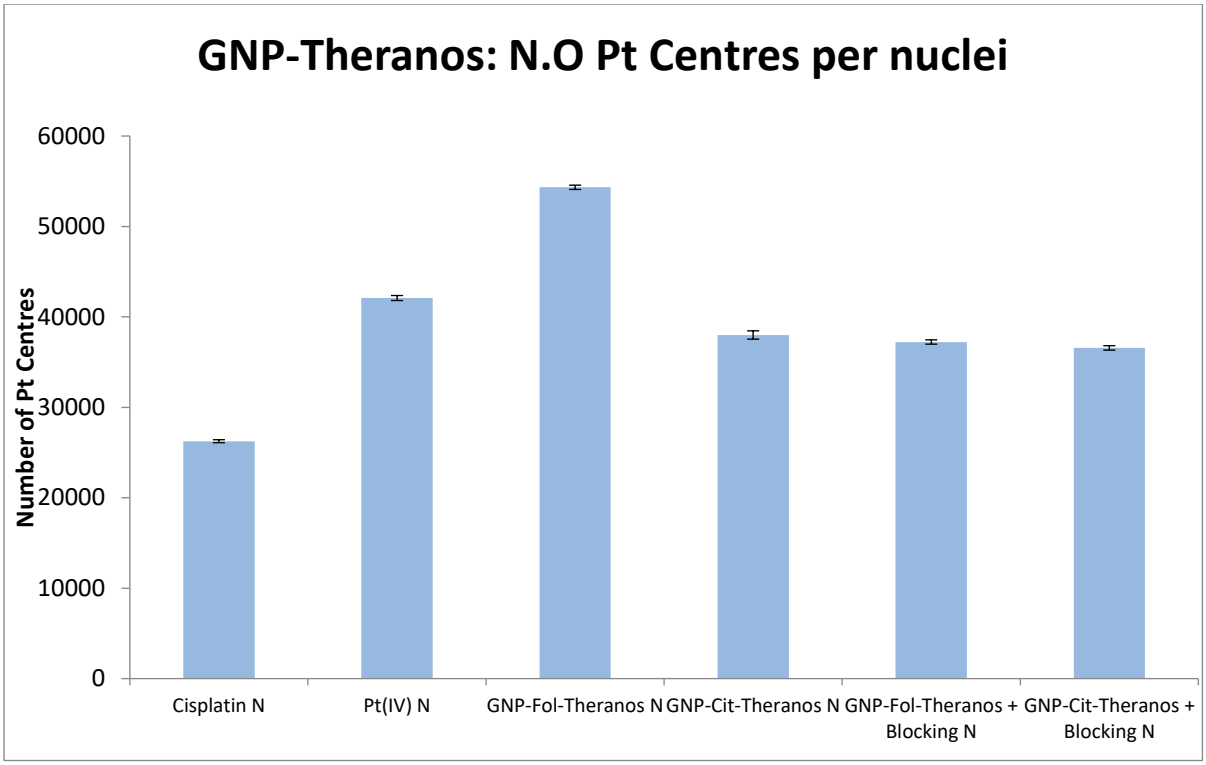

Figure 528: Graphical representation of the total number of platinum centres on average per nuclei of A549 cells dosed as per samples b) to g) of Table 506.

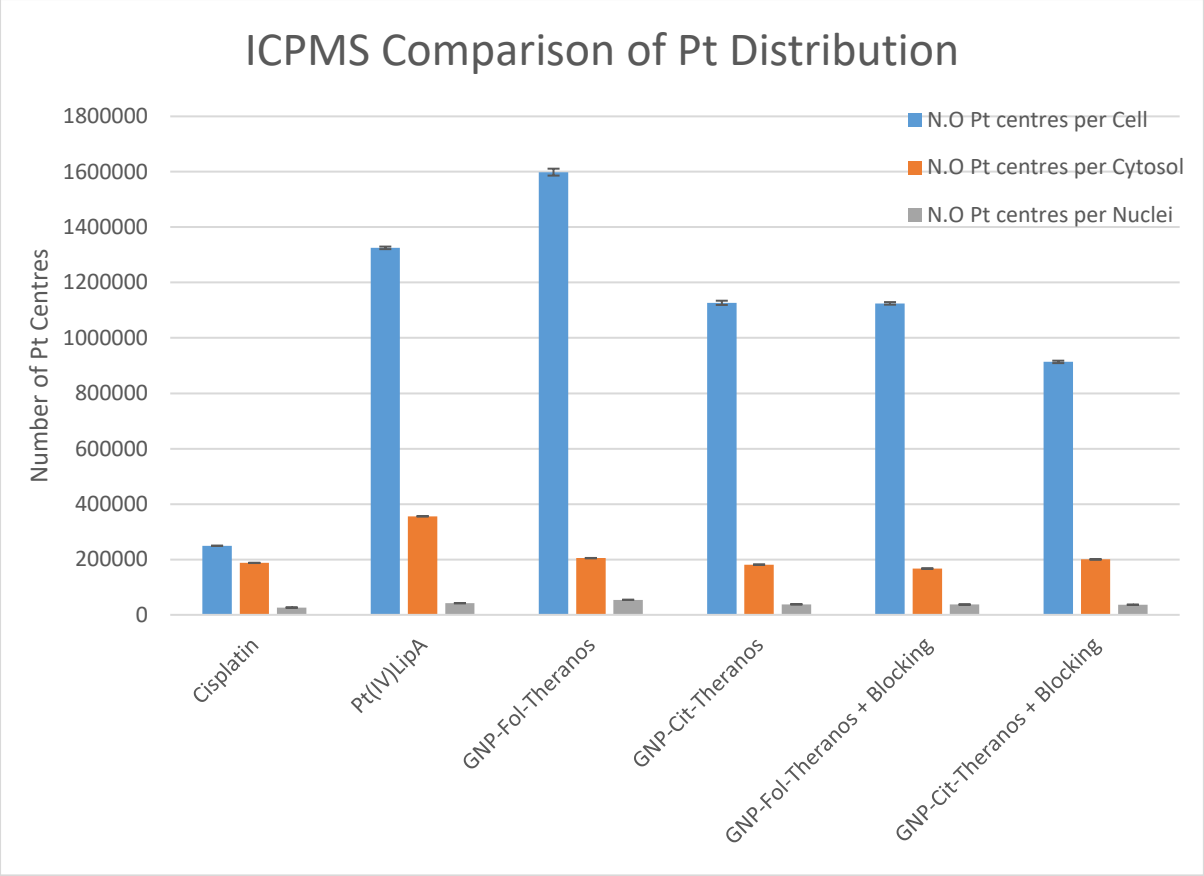

Figure 529: Graph comparing the Pt uptake statistics represented across Figures 526-528.

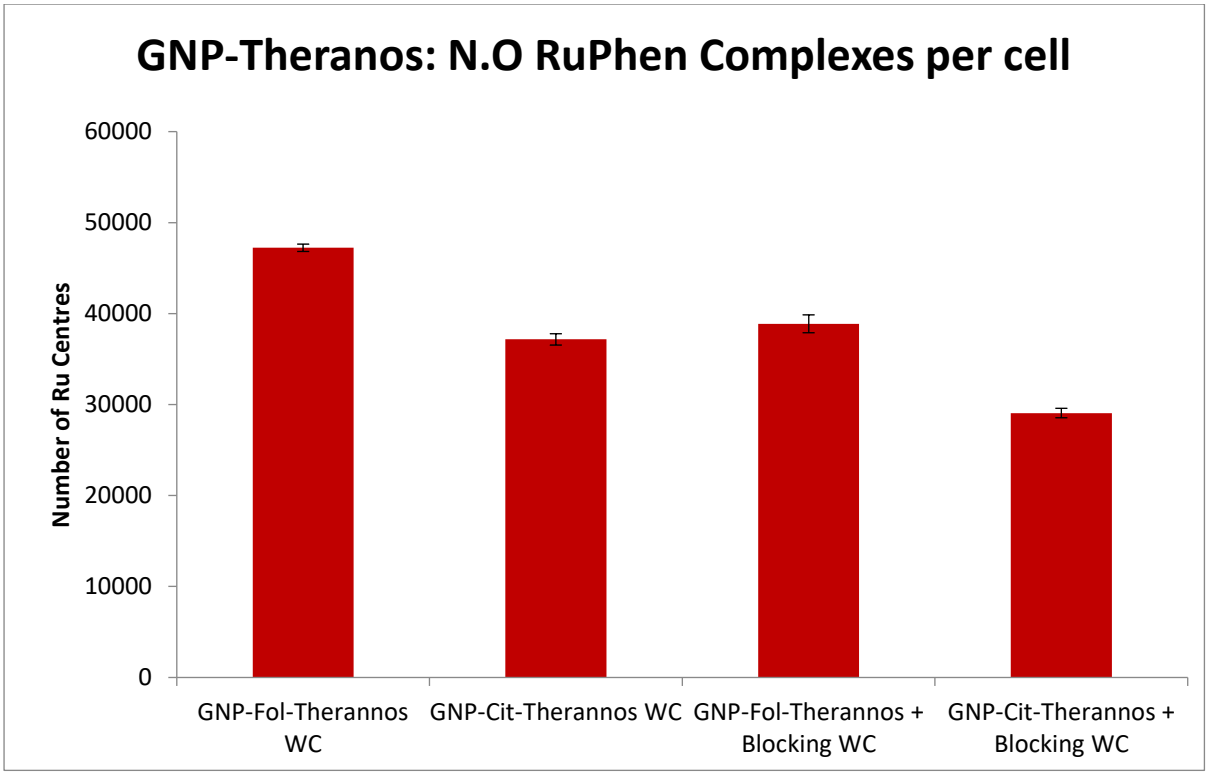

Figure 530: Graphical representation of the total number of ruthenium centres on average per whole cell of samples b) to g) of Table 506.

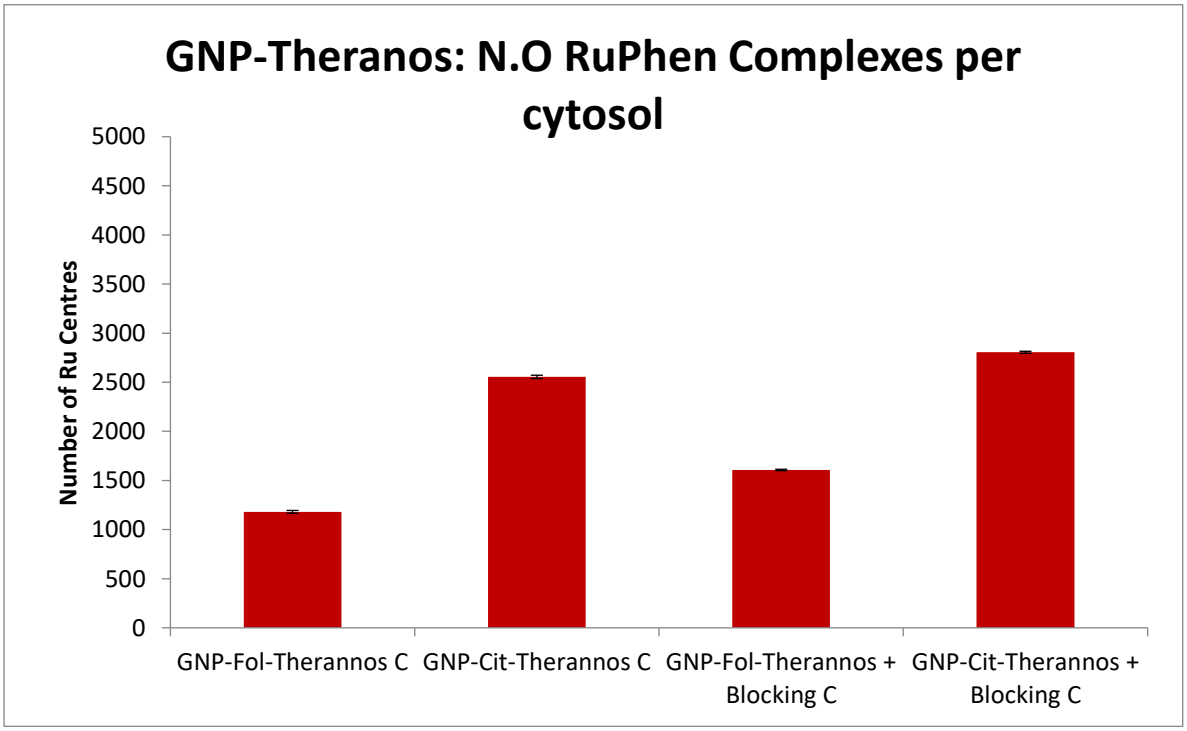

Figure 531: Graphical representation of the total number of ruthenium centres on average per cytosol of A549 cells dosed as per samples b) to g) of Table 506.

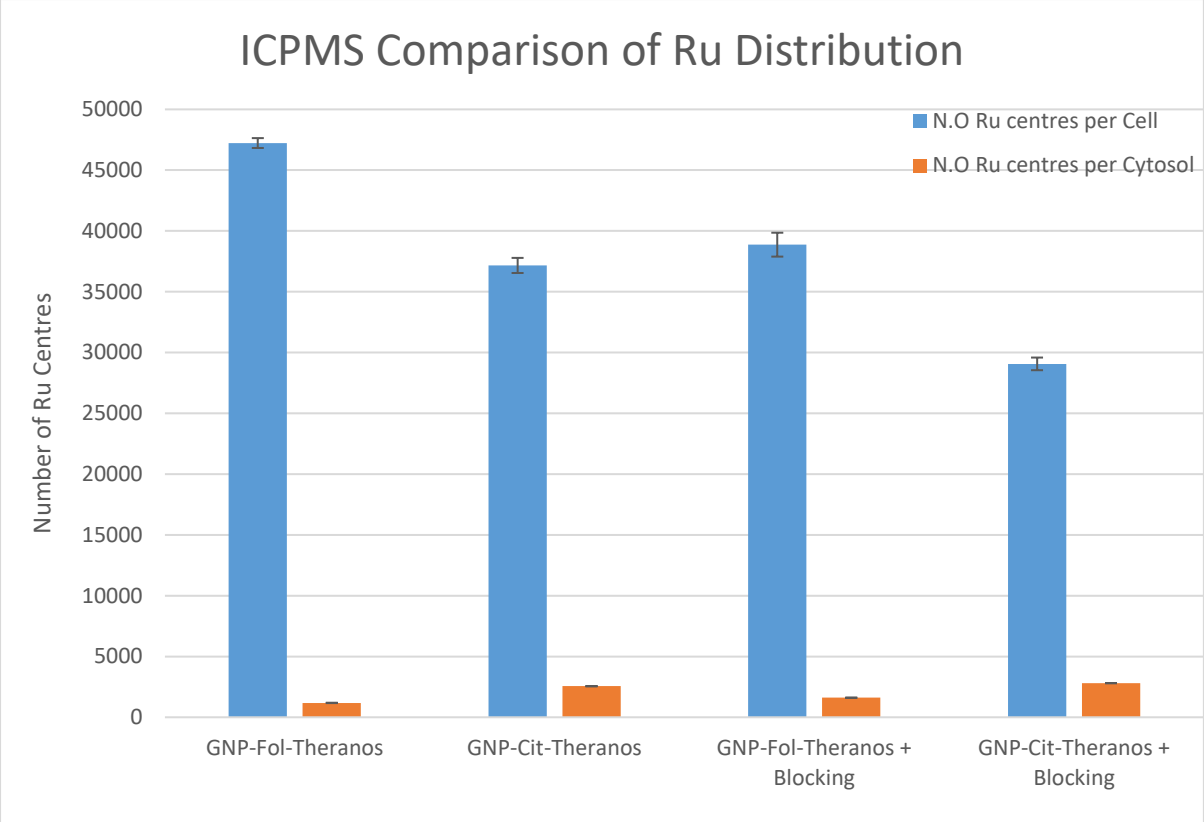

Figure 532: Graph comparing the Ru uptake statistics represented across Figures 530-531.

ICPMS Results Discussion

The data of Figure 525 suggests that, in line with prior data and present hypotheses, the blocking of folate receptor α with primary antibody leads to reduced levels of GNP-Fol uptake, with 73% less GNPs being delivered to the cell (47 GNPs per cell vs 13). In contradiction to the ICPMS studies of section 4.4.4, and in line with the present hypothesis, there appears to be no significant effect on uptake of GNP-Cit with receptor blocking (23 and 24 particles on average respectively). This supports the previous conclusion that the contradictory nanoparticle data of section 4.4.4 was likely as a result of a handling error.

Figure 526 represents the Pt centre data recorded by ICPMS for the average whole cell for samples b) to g) of Table 506. In line with prior cytotoxicity and immunocytochemical studies,

there is less Pt present per cell for the cisplatin sample (b) vs the Pt(IV)LipA sample (c) in the whole A549s, displaying 81% less Pt respectively. The unblocked GNP-Fol system was the only nanoparticle system to deliver more Pt to the whole cell than the free Pt(IV)LipA sample. The blocked GNP-Cit system displayed comparable levels of Pt within each cell, irrespective of blocking (varying by just 1%), which is in alignment with the nanoparticle uptake data. The blocked A549 cell sample dosed with GNP-Fol-Theranos shows 30% less Pt present within the whole cell than the unblocked sample.

The data of Figure 527 shows the same trend across the nanoparticle samples, with reduction in cytosolic Pt upon blocking for the GNP-Fol-Theranos system (19%) and comparable levels for the GNP-Cit-Theranos system (ranging by 8%). However, much the same as the ICPMS studies of 4.4.4, there is more cytosolic Pt for the free Pt(IV)LipA sample than for the nanoparticle samples (73% more in comparison to the closest nanoparticle system). As per section 4.4.4, it is hypothesised that the figure for Pt present in the cytosol of the sample for the nanoparticle samples is inherently low due to the method of fractioning the cellular samples prior to ICPMS analysis. In brief, it is likely that the Pt centre measurements for the nanoparticle samples of the cytosol are only representative of free Pt and not nanoparticlely bound Pt, thus, a large proportion of the Pt present is not recorded. The same can be said in this regard for the Ruthenium statistics of Figure 531.

The data of Figure 528 displays the same trend as the cytosolic data, with GNP-Fol-Theranos displaying more nuclear Pt centres than all other systems, but free Pt(IV)LipA displaying increased Pt than the remaining nanoparticular systems. The nanoparticle anomaly of the cytosolic Pt does not apply for this metric, as it would only ever be free Pt that is found within the nucleus. Thus, it is evident from the studies that there is more Pt delivered to the nuclei of

the cells via the unblocked GNP-Fol-Theranos system over all other systems. As per section 4.4.4, it is hypothesised that whilst the free Pt(IV)LipA system delivers more Pt to the nuclei of the cells, the nanoparticle systems still present with greater DNA damage as a result of their method of delivery. More particularly, it is assumed that the free Pt(IV)LipA complex has been modified and digested by the cell, reducing its toxicity or method of interaction with the DNA. In comparison, the nanoparticle systems might obviate these modifications and therefore potentially present less Pt as a whole, but more as effective complexes.

In contrast to the above Pt based studies, the Ru ICPMS data present with contradictory data. Figure 530 represents the Ru centre data recorded by ICPMS for the average whole cell for samples b) to g) of Table 506. In line with prior confocal and flow cytometry studies, there is less Ru present per cell for the blocked GNP-Fol-Theranos sample (f) in comparison to the unblocked GNP-Fol-Theranos syample (d) in A549s, displaying 18% less Ru respectively. This difference is however more marginal than for all other studies. Whilst the GNP-Fol-Theranos samples (d) did present with greater levels of Ru than the GNP-Cit-Theranos samples (e), this was again a smaller difference than observed across other studies, showing a 22% reduction. Another curious point is that the Ru data of the GNP-Cit-Theranos system appears to have been impacted by receptor blocking, with the blocked sample (g) giving 22% less Ru than the unblocked sample (e).

Moving on from this whole cell data, Figure 531 represents the Ru centre data recorded by ICPMS for the average cytosol for samples b) to g) of Table 506. Here, there is less Ru present for the GNP-Fol-Theranos samples (d) than all others. Moreover, the GNP-Cit-Theranos samples present with the greatest amount of Ru. Both systems display greater levels of Ru upon receptor blocking. This data therefore contradicts all hypothesis and the above data for the

whole cell Ru. Two theories are put forward in this regard. Firstly, this data might be erroneous and simply require repeats. Secondly, it might be possible that much the same as the Pt studies, the process of fractioning the cellular samples into the cytosolic and nuclear components could have played a role in this data. More particularly, as noted, it was observed that during centrifugation of the cellular components to give the suspended cytosolic fractions there was a nanoparticle pellet formed. This pellet likely comprised of nanoparticles that were still surface functionalised with Pt and Ru. Accordingly, the cytosolic measures for Ru might be a more accurate representation of dissociated Ru, as opposed to the number of nanoparticles that are present and have Ru bound. This second proposition would then account for the contradictory levels of Ru measured in the cytosol vs the whole cell for the samples. Moreover, this would then agree with the confocal and flow cytometry data, as well as the ICPMS data which indicates the greater presence of GNPs for the folate based system over the citrate system in the whole cell A549 samples. Lastly, as previously noted, it is possible that the folate capped nanoparticles are no longer stable as a theranostic system. This might then lead to differences in Ru and Pt in the fractionations depending upon the levels of the nanoparticle system degradation across the samples. Repeats shall be required across these studies to fully investigate this further, whilst also allowing for a statistical analysis of the data.

5.5. Conclusions

Theranostic folate capped and citrate capped gold nanoparticle systems were produced in the present studies by surface functionalisation with Pt(IV)LipA and RuPhenSS. These two theranostic systems were proven to be stable over a 5-day period in isolation and were carried forward for cellular uptake studies in A549 cells.

Confocal microscopy and flow cytometry studies showed that the GNP-Fol-Theranos system displayed comparable levels of induced cisplatin-DNA adducts than the GNP-Cit-Theranos system through immunocytochemistry studies. The folate capped gold nanoparticles also presented with comparable or less ruthenium probe emissions and a greater spread of the probe throughout the samples over the citrate capped gold nanoparticles. This trend was not readily apparent upon folate receptor competition / blocking with a folate receptor α polyclonal antibody within the GNP-Cit-Theranos samples. This is therefore potentially indicative of greater levels of GNP-Fol uptake over the GNP-Cit system as a result of folate receptor mediated endocytosis within A549 cells. Contradictory findings were therefore found and further experimentation is required, with triplicate experimental repeats as well as triplicate sample repeats.

ICPMS studies of these theranostic nanoparticle systems presented with some contradicting data. In agreement with previous studies, there was greater levels of Au found for the GNP-Fol-Theranos samples over GNP-Cit-Theranos, with this difference being reduced upon folate receptor blocking. The same trend was carried over for Pt studies, showing greater levels of Pt present in the whole cell, cytoplasm and nucleus for the GNP-Fol-Theranos system over the GNP-Cit-Theranos system. This data suggests that the GNP-Fol-Theranos system presents with greater levels of cellular uptake than the GNP-Cit-Theranos system in the absence of folate receptor blocking in A549s. However, there was no trend observable for Ru centres, with receptor blocking seemingly having no affect on levels present.

5.6. Experimental

5.6.1. Nanoparticle Loading Studies

The loading potential of RuPhen and Pt(IV)LipA onto the GNP-Fol and GNP-Cit systems was conducted as per the ruthenium probe titration experiments of section 2.3.2 and platinum agent loading experiments of section 4.6.3.

Fresh solutions of GNP-Fol and GNP-Cit were prepared as per section 2.3.2 and UV-Vis absorption spectra were collected for titration of a 1mM RuPhen solution followed by a 1mg/mL Pt(IV)LipA stock solution into 1mL of either ~1nM GNP-Fol or 1mL of ~1nM GNP-Cit. Each nanoparticle system was loaded with the RuPhen probe first in incrementl titrations, followed by the Pt(IV)LipA agent. Each system was dialysed overnight in a semi permeable membrane (Spectra-Por® Float-A-Lyzer® G2, 5 mL, MWCO 8-10 kDa) in deionised water to remove unbound reagents. The systems then had their concentrations roughly calculated via UV-Vis and the stronger system diluted to the same concentration as the weaker system (~1nM) before being carried forward for cellular studies.

5.6.2. TEM Sample Preparation

TEM samples were prepared via pipetting 10-20µL of the appropriate nanoparticle sample onto TEM grids and allowing to dry at room temperature underneath a glass petri dish to prevent dust accumulation. Care was taken not to touch the grids via utilisation of tweezers. Sample grids were transferred to a grid holder and immediately submitted to Theresa Morris of the Centre for Electron Microscopy, University of Birmingham, for storage and or imaging.

5.6.3. Fixed Cell Immunocytochemistry Studies

Cell Culture

High folate receptor α expressing A549s were cultured and maintained as per section 3.8.5.

Nanoparticle Preparation

Fresh batches of GNP-Fol and GNP-Cit were synthesised as per section 2.3.2, loaded with RuPhen (12µL of a 1mM solution) and 25µM YoungPt(IV) (14µL of a 1mg/mL stock solution) and were subsequently purified ready for cell culture experiments as per section 5.5.1.

Dosing Protocol

Cover slips were washed in 70% ethanol and rinsed with PBS before being stuck to the bottom of each well of 12 well plates. These dishes were allowed to dry for 1 hour before being seeded with high folate receptor α expressing A549s (400,000 cells per well) and incubated overnight to adhere. These coverslip samples were utilised for confocal microscopy studies, plain 6 well plates were utilised for flow cytometry studies.

The following samples were prepared:

HIGH FOLATE RECEPTOR α EXPRESSING A549S DOSED WITH:	
No Blocking	**With Receptor α Blocking**
Blank	-
Secondary Antibody Only	-
Pri + Sec Antibodies (AB)	-
Cisplatin + AB	-
Pt(IV)LipA + AB	-
GNP-Fol-Theranos + AB	GNP-Fol-Theranos + AB
GNP-Cit-Theranos + AB	GNP-Cit-Theranos + AB

Fixed Cell Confocal Immunocytochemical Studies

The fixation and mounting of samples was conducted via an adapted protocol provided by Dr Lucia Cardo on 29th March 2017 and as carried over from section 4.6.5.

The 12 well plates were removed from the incubator and the old media aspirated from the wells. The wells were washed with PBS (1mL) to remove dead cells and residual media. Each well was then treated with either 500µL of ~1nM GNP-Fol-Theranos or GNP-Cit-Theranos, 25µM Pt(IV)LipA alone or 25µM cisplatin alone, each of which made up to 1mL in fresh supplemented RPMI media. The folate receptor blocking samples were previously blocked for one hour with folate receptor α primary antibody as per section 3.8.7. The samples were subsequently returned to the incubator and incubated on a plate rocker for 18 hours. The plates were then removed, old media gently removed and the cells gently washed with PBS (2 x 1mL) to remove unbound reagents and free nanoparticles. The cells were subsequently fixed in formalin (500µL, 10% solution) for 10 minutes at room temperature. Formalin was removed and the cells washed with PBS (3 x 1mL), before being permeabilised with 0.1% Triton X-100 (0.5mL) for 10 minutes at room temperature. Triton was removed and the cells washed with PBS (3 x 1mL), before being blocked with 10% normal goat serum (0.5mL) at room temperature for 1 hour. Goat serum was removed and the cells were dosed with anti-cispltin modified antibody (CP9/19) at room temperature for two hours (500µL of a 2µg/mL solution in 10% normal goat serum). The primary antibody was removed and the coverslips washed with 1% goat serum (5 x 1mL). Cells were then dosed with secondary antibody (500µL of a 2µg/mL solution in 10% goat serum) for 1 hour at room temperature in the dark. Cells were rinsed with 1% goat serum (5 x 1mL) and the nuclei stained with Hoechst (500µL of a 5µg/mL solution in 1% goat serum) for 10 minutes at room temperature. The coverslips were washed

with 1% goat serum (1mL x 5), then dipped in PBS before being mounted onto microscope slides with a drop of mounting medium.

Fixed Cell Flow Cytometry Studies

The utilised fixed cell FACS protocol was adapted from the published protocol of Cell Signaling Technology[R417] and as carried over from section 4.6.5.

Cells were dosed with the appropriate samples as per the above confocal studies. The 6 well plates were then removed from the incubator, old media removed and the cells washed with PBS (1mL). The cells were then tripsinised (1mL tripsin 1X for 5 mins in an incubator) and collected with fresh RPMI media (1mL), cells were collected into 2mL Eppendorf's. The cells were pelleted at 1500rpm for 5 mins and the supernatant discarded. The cells were then re-suspended in 1mL 10% formalin, vortexed and fixed at 37°C for 10 minutes. The samples were chilled on ice for 1 minute, then centrifuged at 1500rpm for 5 minutes to remove formalin. The pellets were re-suspended in 1mL of 90% ice cold methanol and kept on ice for 30 minutes to permeabilise them. 1mL incubation buffer (0.5g Bovine Serum Albumin (BSA) in 100mL PBS) was added and the cells centrifuged. The supernatant was removed and the cells re-suspended in 1mL incubation buffer. This step was repeated three times. The cells were re-suspended in primary antibody (500µL of a 2µg/mL solution in incubation buffer) and dosed for one hour at room temperature. The cells were centrifuged, the supernatant removed and the pellets re-suspended in incubation buffer (1mL). This step was repeated three times. The cells were re-suspended in secondary antibody (500µL of a 2µg/mL solution in incubation buffer) for 30 minutes at room temperature in the dark. The cells were centrifuged, supernatant removed and re-suspended in incubation buffer (1mL). This step was repeated three times. The cells were then centrifuged, supernatant removed and re-suspended in 1mL PBS. The samples were then analysed by flow cytometry.

Confocal Microscope Settings

Blue Channel:	Excitation, 402nm	Emission, 450-490
Green Channel:	Excitation, 514nm	Emission, 500-570nm
Red Channel:	Excitation, 488nm	Emission, 580-680nm

5.6.4. ICPMS Studies

The below ICPMS protocol was adapted from protocols provided by Dr Lucia Cardo (Hannon research group, University of Birmingham) and Ms Siobhan King (Pikramenou research group, University of Birmingham) and carried over from section 4.6.6.

Cell Culture

High folate receptor alpha expressing A549 cells were seeded into seven T75 flasks (one flask per condition as per the below table) and cultured to 80% confluency as per section 3.8.5.

Dosing

The T75 flasks were dosed using the same protocol of 5.5.3, but with appropriately scaled reagents (approximately 7 x more cells present, therefore 7 x more nanoparticles / platinum agents used) and alternative sample work up.

HIGH FOLATE RECEPTOR α EXPRESSING A549S DOSED WITH:		
	No Blocking	**With Receptor α Blocking**
a)	Blank	-
b)	Cisplatin	-
c)	Pt(IV)LipA	-

d)	GNP-Fol-Theranos	f)	GNP-Fol-Theranos
e)	GNP-Cit-Theranos	g)	GNP-Cit-Theranos

Sample Work Up

Old media / media containing the reagents of the above table was removed from the T75 flasks and the cells gently washed with PBS (5mL x 3) to remove unbound reagents / particles and residual media. The cells were tripsinised and pelleted as per section 3.8.5. The cells were then re-suspended in 2mL of PBS and counted using a haemocytometer. 1mL of each sample was pipetted into fresh 2mL falcon tubes, pelleted at 1500rpm for 5 minutes and supernatant removed. The whole cell pellet samples were immediately stored at -80°C ready for whole cell ICPMS analysis.

Subsequent nuclear and cytosolic fractionation was conducted as per the protocol supplied with the BioVision Nuclear/Cytosol Fractionation Kit utilised.

The remaining 1mL of suspended cells were chilled on ice for 1 minute and subsequently centrifuged at 4°C for 5 minutes at 600G. The PBS was removed and 0.2mL of Cytosol Extraction Buffer A was added. The solutions were vortexed on the highest setting for 15 seconds and were incubated on ice for 10 minutes. 11µL of ice cold Cytosol Extraction Buffer B was added and the solution vortexed for 5 seconds. The solutions were then centrifuged at 4°C for 5 minutes at 16000G. The supernatant (cytoplasm fraction) was removed and immediately stored at -80°C ready for cytosolic ICPMS analysis.

The remaining pellet was re-suspended in 100µL ice cold Nuclear Extraction Buffer mix and vortexed on the maximum setting for 15 seconds. The samples were stored on ice for 10 minutes and this process was repeated four times. The samples were centrifuged at 16,000G,

4°C for 10 minutes. The supernatant (nuclear fraction) was transferred to a fresh Eppendorf and immediately stored at -80°C, ready for ICPMS analysis.

The resulting sample fractions (whole cell, nuclear and cytoplasm) were digested in a mixture of concentrated nitric acid (69%, 100µL) and freshly prepared aqua regia (3:1, HCl (32%) and HNO_3 (69%) 100 µL). Samples were transferred to screw cap vials and incubated overnight at 80 ºC in an oven to fully digest the metal particles and cells. Subsequently, the samples were diluted with milli-Q-water to a final acid concentration of ~2%. Samples were transferred to 15mL falcon tubes on ice and transported to the University of Warwick for sample analysis.

Chapter 6 – Conclusions & Future Work

The utilisation of folate receptor overexpression as a means for targeted delivery of therapeutic and diagnostic agents to select cancer cells was investigated in the research reported herein.

A novel synthetic protocol was developed for a more reliable and reproducible method of forming folate capped gold nanoparticles with comparable size and polydispersity to typical citrate capped gold nanoparticle systems that have been routinely developed and utilised within the field. As previously noted, further research must be done with regard to this novel protocol so as to better establish the intermediate species that is subsequerntly believed to be responsible for gold salt reduction and ultimately nanoparticle growth. This species might also have an impact on the specific folate moieties that are subsequently tethered to the outer surface of the nanoparticles and might ultimately play a key role in their ability to interact with folate receptors.

Subsequently, the potential for both folate and citrate capped gold nanoparticles to act as targeted imaging agents was investigated. More specifically, separate nanoparticular systems were surface functionalised with a ruthenium based polypyridyl probe (RuPhenSS) and their ability to be taken up into folate receptor positive A549s investigated. Efforts went beyond this to compare their uptake when the cells had been subjected to a folate receptor antibody solution so as to block folate receptor α and theoretically exacerbate the importance of the folate moieties on the outer surface of the folate capped nanoparticle system. Through confocal microscopy and flow cytometry studies it was found that folate receptors might indeed play a key role in the particle uptake, with the folate system displaying greater levels of uptake over the citrate system. This effect was further proven through folate receptor blocking leading to a much lesser extent of particle uptake.

Further research then developed a novel Pt(IV) complex (Pt(IV)LipA) that was fully characterised and possessed the potential to bind to the surface of nanoparticles via a thiol moiety of one of the axial ligands. Much the same as the ruthenium studies, the surface functionalisation was investigated and the subsequently Pt(IV) loaded folate and citrate capped systems were subjected to cellular studies. Through confocal microscopy, flow cytometry and ICPMS studies it was found that folate receptors might indeed play a key role in the particle uptake, with the folate system displaying greater levels of uptake over the citrate system. This effect was further proven through folate receptor blocking leading to a much lesser extent of particle uptake. Further research must be conducted in this area through experimental repeats so as to facilitate statistical analysis of the results.

Lastly, two theranostic gold nanoparticle systems were developed; a first utilising folate capped gold nanoparticles (for a folate receptor targeting system, GNP-Fol-Theranos) and a second utilising citrate capped gold nanoparticles (non-targeted system, GNP-Cit-Theranos). The gold nanoparticles of these respective systems were surface functionalised with the ruthenium based polypyridyl probe (RuPhenSS) and the novel Pt(IV) complex (Pt(IV)LipA), each utilising a lipoic acid based ligand for tethering means.

The uptake of these two theranostic nanoparticle systems was investigated in folate receptor positive A549 cells that had their levels of receptor modulated through media supplementation with excess folate. Folate receptor positive and negative uptake studies were conducted utilising A549s with and without folate receptor blocking with a polyclonal antibody. Confocal microscopy, flow cytometry and ICPMS studies all showed enhanced levels of Ru probe based emissions for the GNP-Fol-Theranos system over the GNP-Cit-Theranos system. The level of probe emission and particle uptake was decreased for GNP-Fol-Theranos upon folate receptor

blocking, whilst these parameters appeared relatively unchanged for the GNP-Cit-Theranos system, indicating a potentially high dependency and efficacy of folate receptor mediated endocytosis for the folate based particles.

The cytotoxicity and degree of DNA damage induced by Pt(IV)LipA was investigated through MTT studies as well as confocal and flow cytometry studies utilising a commercial antibody for cisplatin-DNA adducts. Pt(IV)LipA showed enhanced cytotoxicity over cisplatin in A549 cells both as a free agent and as part of the theranostic nanoparticle system. The GNP-Fol-Theranos system presented with the greatest cytotoxicity, closely followed by the GNP-Cit system. Confocal microscopy, flow cytometry and ICPMS studies all indicated an enhanced level of uptake of Pt for the GNP-Fol-Theranos system samples over GNP-Cit-Theranos system. These results again indicate a greater level of uptake as a result of folate receptor mediated endocytosis.

The confocal microscopy and ICP mass spectrometry results of the present research were not (and can not be) statistically analysed as only a single sample was analysed for each condition reported. This single sample experimental design was adopted since the synthetic experimental conditions were still being optimised in parallel, and repeat experiments require a larger batch of material. Now that the conditions for the experiment have been refined and the synthetic protocol finalised, future research efforts should look to repeat the experiments with triplicate samples per condition, as well as triplicate experimental runs as a whole, to allow for a full statistical analysis of the findings enabling quantitative rather than just qualitative conclusions.

Further studies should also re-visit cellular studies into competition for the GNP-Fol-Theranos system between a co-culture of folate receptor positive and negative cells. Alternatively, it

would be interesting to track the particles in a mouse model. The nanoparticle systems will likely benefit from further characterisation and optimisation in advance of any such studies. A further objective could also be the development of a variant of the Pt(IV)LipA agent bearing a folic acid motif, forming a novel Pt(IV) agent that itself comprises folate receptor targeting possibilities, much in the same way as Vintafolide.

Appendices

Figure 308 Fluorescence slices

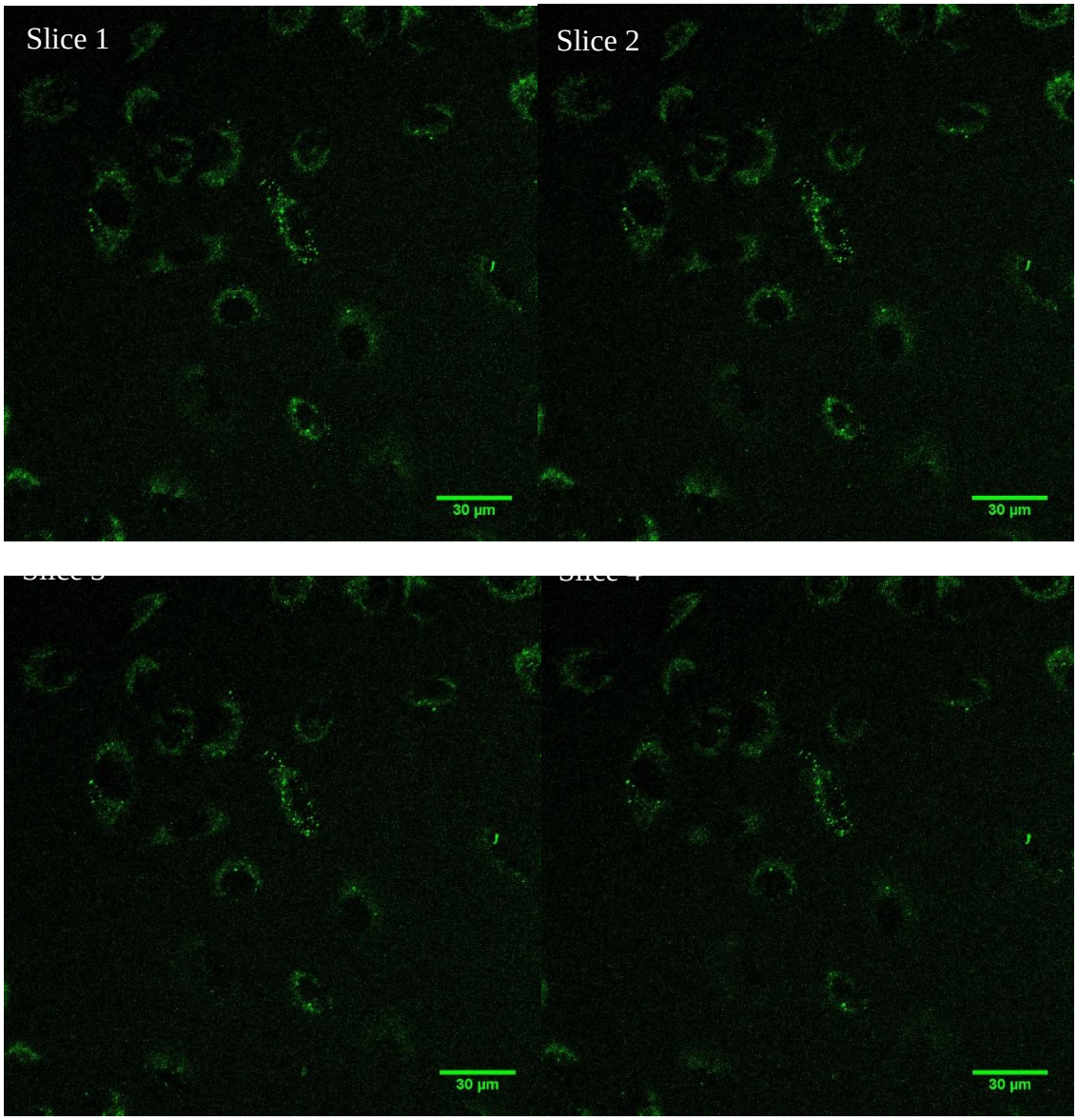

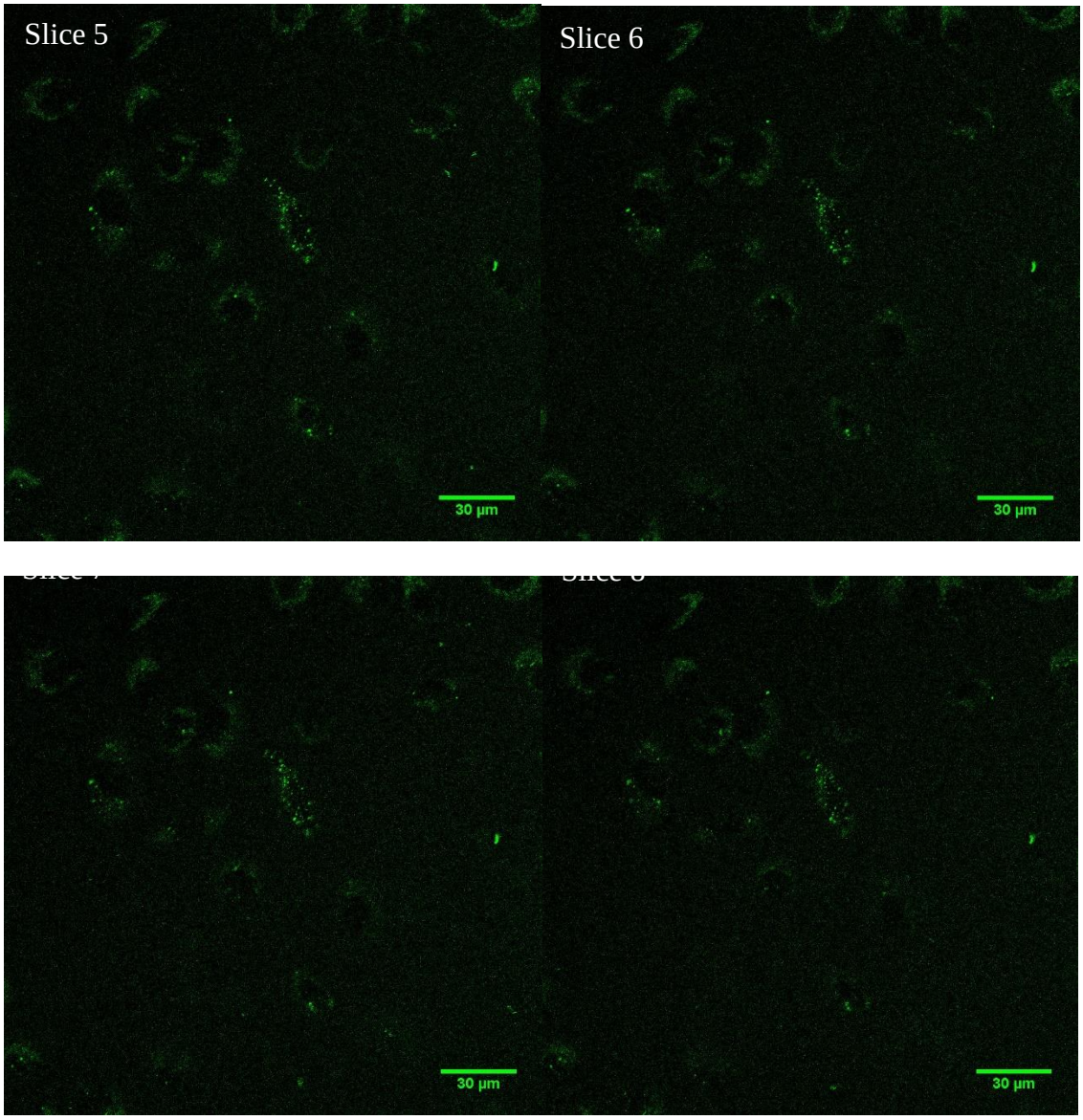
Slice 5
30 µm
Slice 6
30 µm
30 µm
30 µm

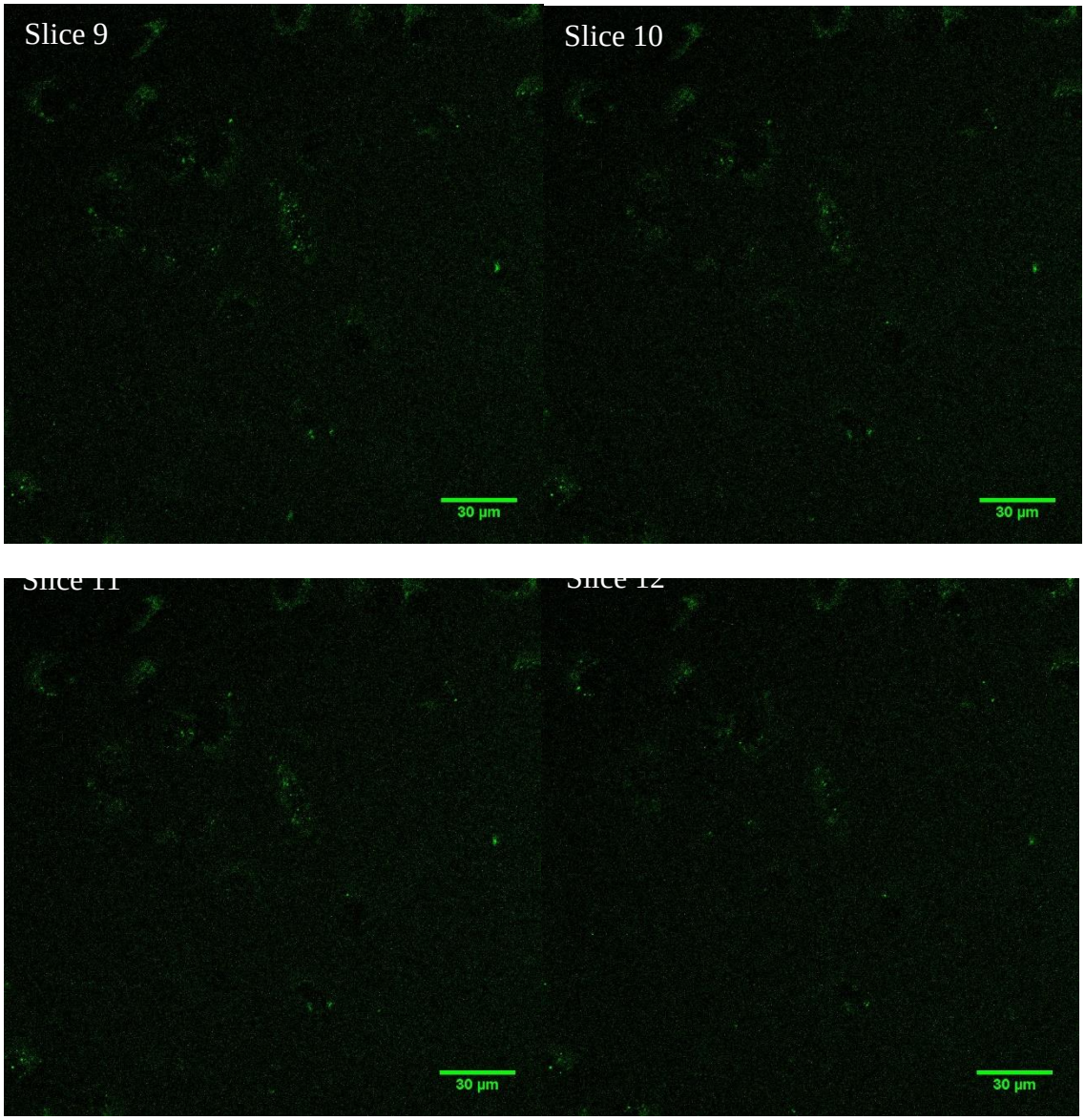

Blank A549s taken from zero folate RPMI media culture. Cells were seeded overnight onto MatTek dishes and subsequently treated with folate receptor alpha polyclonal antibody (2µg/mL in 2mL supplemented RPMI) for 45 minutes. Cultures were washed three times with PBS before being immersed in imaging media and immediately transferred to a live cell imaging chamber for confocal microscopy studies. Images 1 through 12 represent the gradual progression from the bottom of the cell culture to the top, through the collected z stack profile. The images show the peripheral localisation of the fluorescence signal, corresponding to surface bound antibody based fluorescence.

Pt(IV)LipA Data

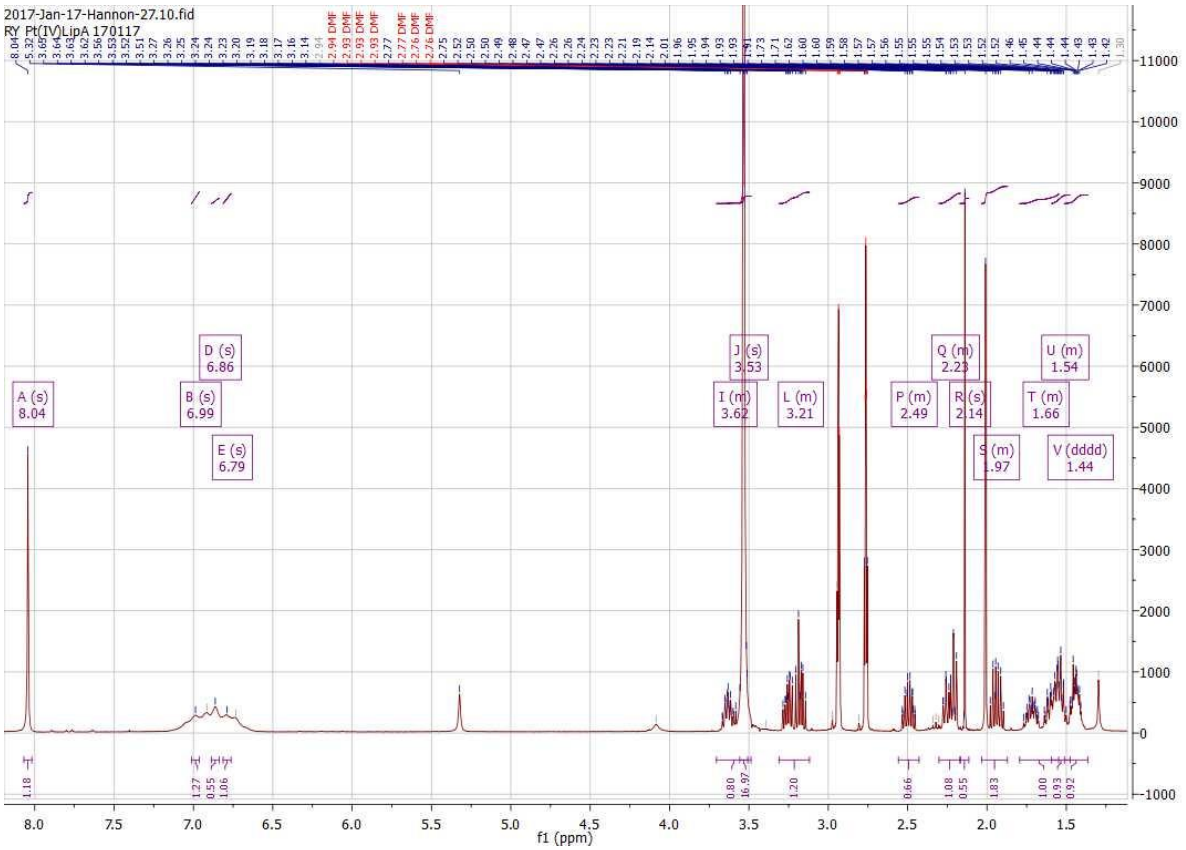

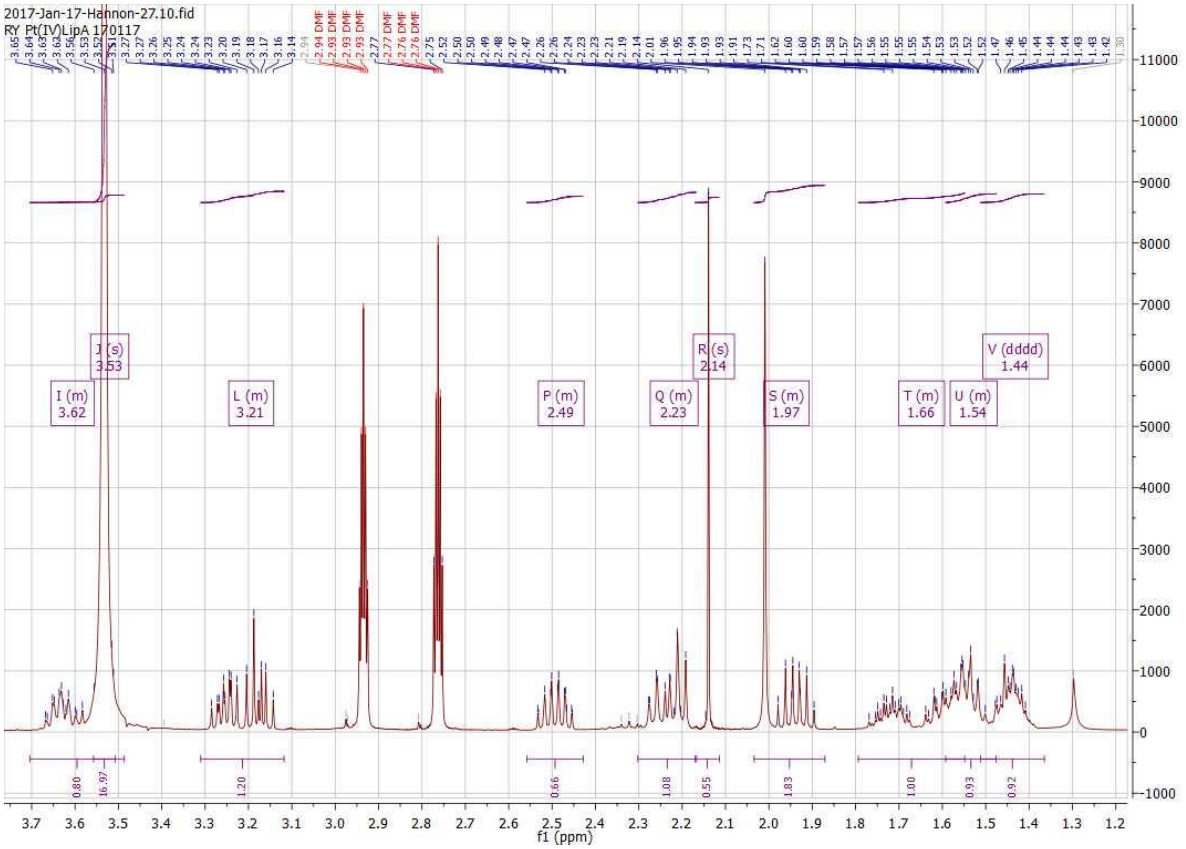

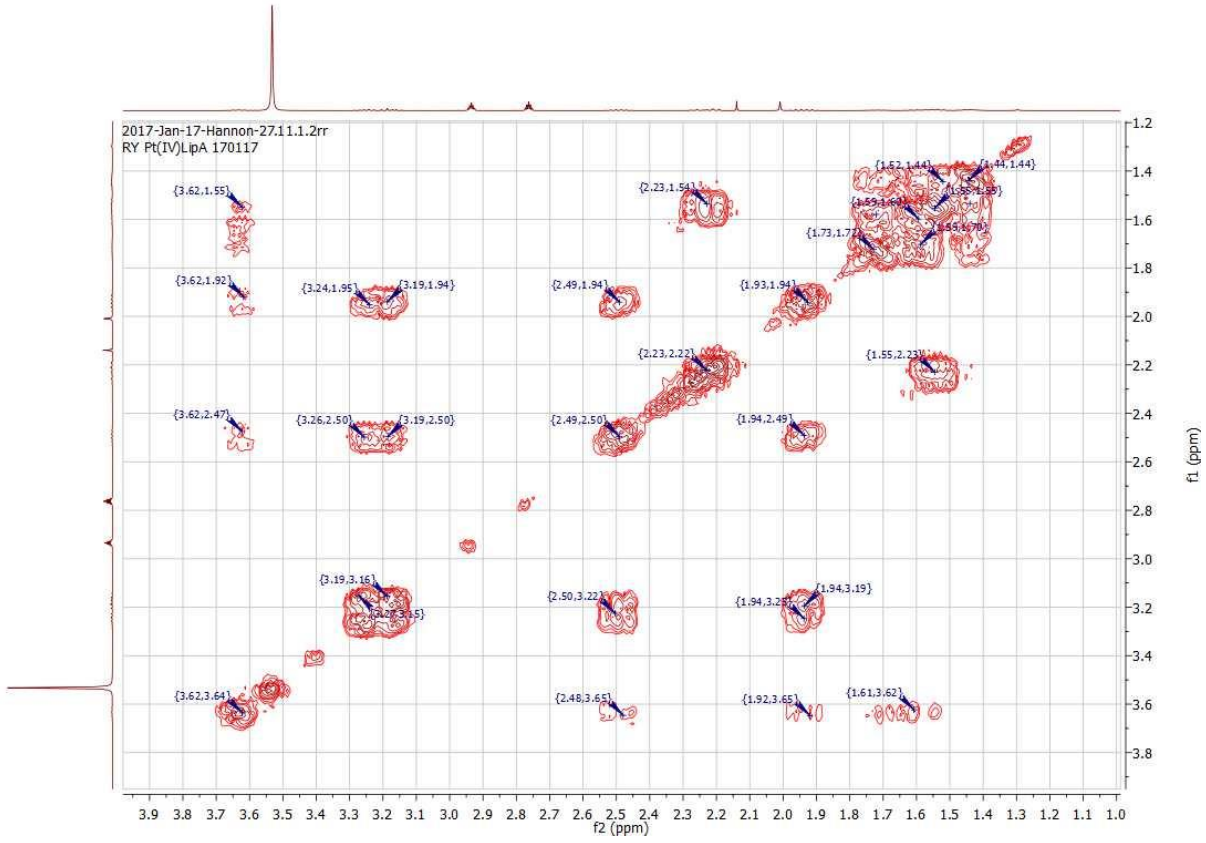
2017-Jan-17-Hannon-27.11.1.2rr
RY Pt(IV)LipA 170117
f2 (ppm)
f1 (ppm)

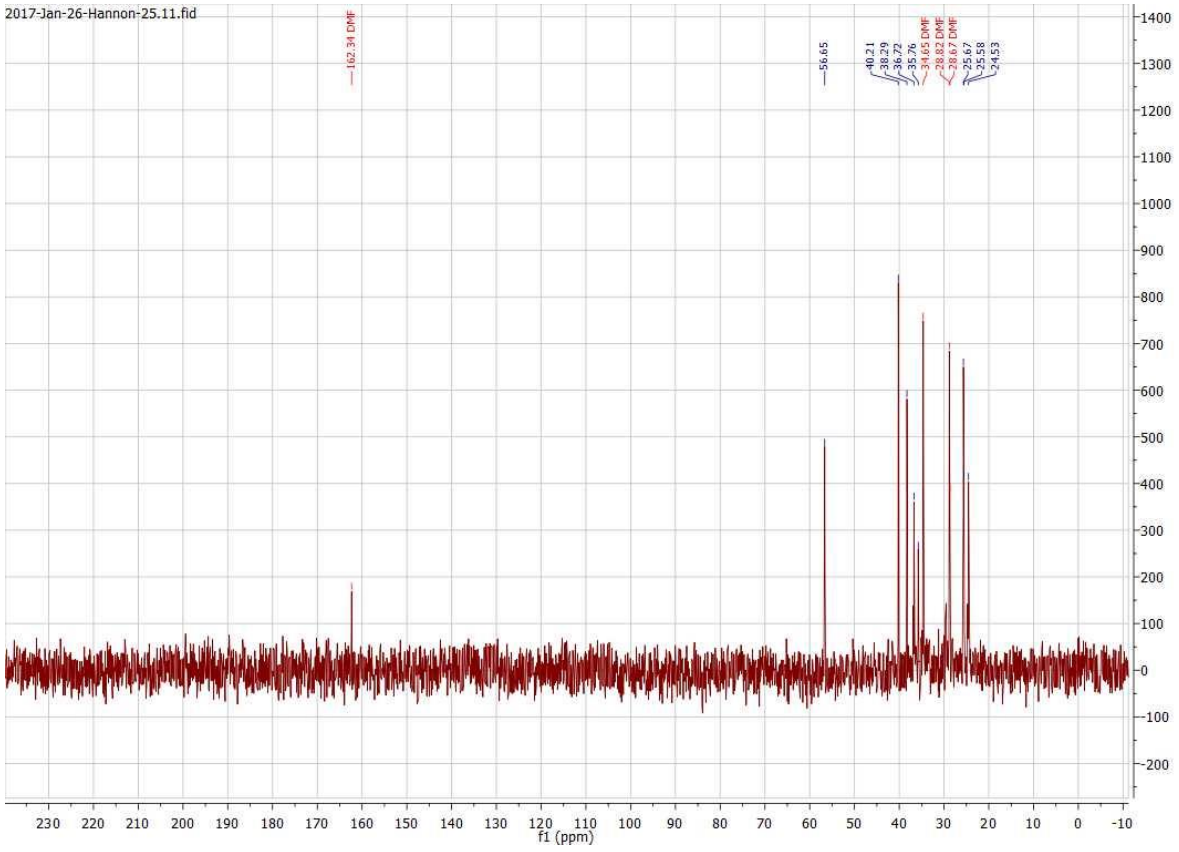
2017-Jan-26-Hannon-25.11.fid
162.34 DMF
56.65
40.21
38.29
36.72
35.76
34.65 DMF
28.82 DMF
28.67 DMF
25.67
25.58
24.53
f1 (ppm)

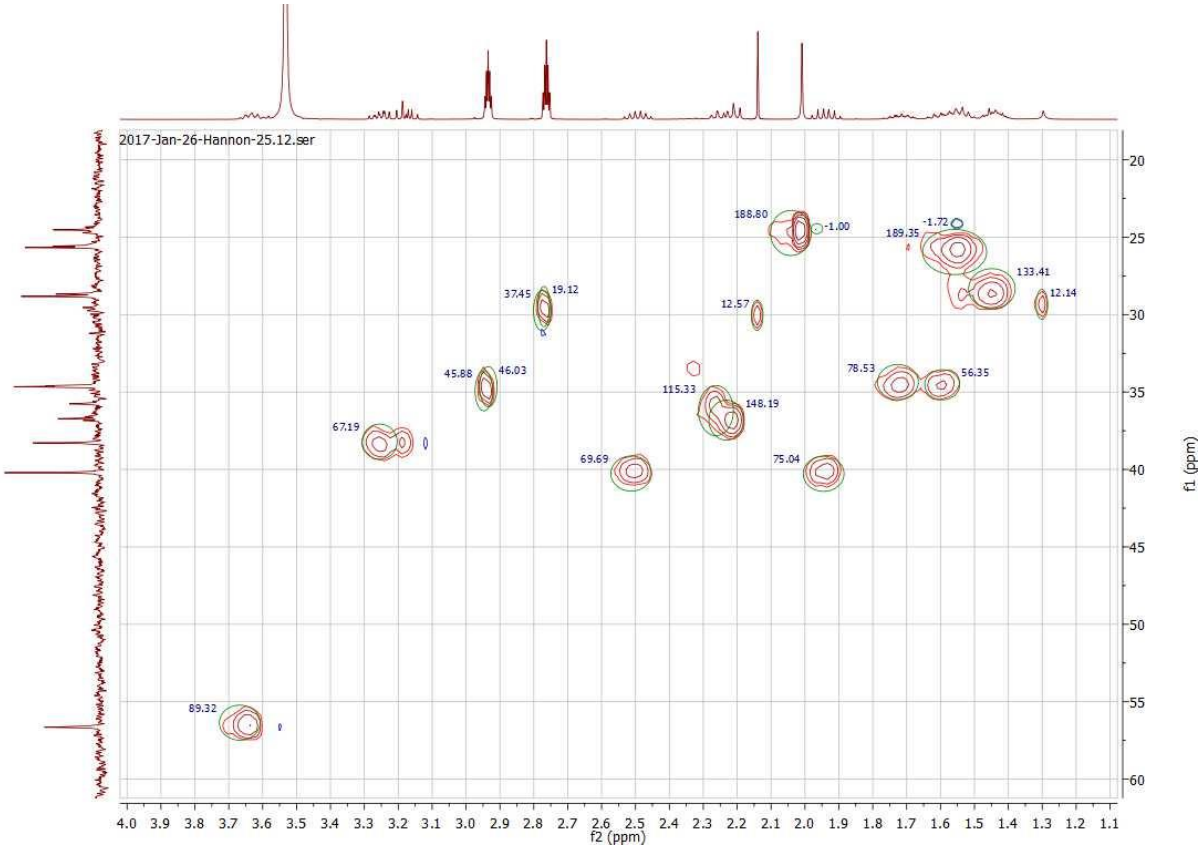
2017-Jan-26-Hannon-25.12.ser
188.80
-1.00
189.35
-1.72
133.41
12.14
37.45
19.12
12.57
45.88
46.03
115.33
148.19
78.53
56.35
67.19
69.69
75.04
89.32
f1 (ppm)
f2 (ppm)